





This is to certify that the

dissertation entitled

Non-Bound Contributions to the Propagation-Mode Spectrum of Open-Boundary Waveguides

presented by

Jerry Michael Grimm

has been accepted towards fulfillment of the requirements for

Ph.D. degree in Electrical Engineering

Demus P. Dyquist Major professor

Date 1/16/92

MSU is an Affirmative Action/Equal Opportunity Institution

0-12771

LIBRARY Michigan State University

PLACE IN RETURN BOX to remove this checkout from your record. TO AVOID FINES return on or before date due.

	DATE DUE	DATE DUE
Jno 8 10 8 2009		

MSU is An Affirmative Action/Equal Opportunity Institution ctcirc/detectus.pm3-p.1

NON-BOUND CONTRIBUTIONS TO THE PROPAGATION-MODE SPECTRUM OF OPEN-BOUNDARY WAVEGUIDES

Ву

Jerry Michael Grimm

A DISSERTATION

Submitted to
Michigan State University
in partial fulfillment of the requirements
for the degree of

DOCTOR OF PHILOSOPHY

Department of Electrical Engineering

1992

the nor

practica

continu

bounda integra:

implica

functio

comple

the ax.

superpo

with th

restrict

conver

with the

of \mathbf{w}_h

ABSTRACT

NON-BOUND CONTRIBUTIONS TO THE PROPAGATION-MODE SPECTRUM OF OPEN-BOUNDARY WAVEGUIDES

This dissertation advances an integral-operator formulation capable of determining the non-bounded contributions to the propagation-mode spectrum for a broad class of practical open-boundary waveguides. These non-bounded contributions consist of the continuous radiation spectrum and the discrete, non-spectral leaky-wave modes.

A transform-domain electric field integral equation (EFIE) is developed for open-boundary waveguides in a planar, tri-layered substrate/film/cover environment typical of integrated optics applications. Two complex (transform-variable) wavenumber planes are implicated through Sommerfeld-integral representations of the associated Green's functions and the axial inverse transform to recover the space-domain field, whose complete propagation-mode spectrum is recognized through a singularity expansion upon the axial wavenumber plane singularities. The radiation spectrum is the continuous superposition of solutions to the forced EFIE over a restricted spectral regime associated with the axial wavenumber plane branch cuts.

Branch cuts in the axial wavenumber plane are hyperbolic and are chosen to restrict migration of transverse wavenumber singularities, rendering forward transforms convergent. A new component of the radiation spectrum is identified as being associated with the surface-wave modes of the background structure.

The axial-wavenumber-plane branch cuts define a multi-sheeted Riemann surface of which the top sheet is proper. Leaky-wave modes are the solutions of the

homoge

cuts in

for a n

quantifi

integral

well.

transmi

Wavego

homogeneous EFIE on non-spectral Riemann sheets chosen by violating specific branch cuts in the axial-wavenumber plane.

The integral-operator formulation is validated, and its usefulness demonstrated, for a number of open-boundary waveguides. The continuous radiation spectrum is quantified for the canonical symmetric planar waveguide to confirm the validity of the integral-operator approach. Results are developed for asymmetric planar waveguides as well. The radiation spectral surface current distributions for a simple microstrip transmission line are determined. Finally, leaky modes of an integrated dielectric rib waveguide are determined.

Copyright • by Jerry Michael Grimm, 1992 All Rights Reserved To my loving parents, Bob and Sue Grimm

and

In memory of my grandmother Muriel Blauert, who would have been so proud

my effo

contribu graduat

assistan

taught c

Finally,

understa details v

assistan

Vincent

00-

comme

continu

years h

as well

fellow

Charles my c

my frie my stay

support

Acknowledgements

Great achievements are meaningless if no one shares in them. This pinnacle of my efforts is not possible without the assistance and contributions of friends.

Foremost among those whom I thank is Dr. Dennis Nyquist, my advisor, whose contributions are many. I will ever be grateful for his encouragement of my continuing graduate education. His thought-provoking questions and valuable insights were of great assistance during my research. He served as mentor to me, guiding my efforts as I taught classes, conducted research, and published papers at conferences and in journals. Finally, as a friend, he offered support throughout the entire process.

All who graciously served on my committee deserve thanks for their patience and understanding during this process. Dr. Byron Drachman's assistance on the mathematical details within was invaluable. Drs. Ed Rothwell and Kun-Mu Chen provided advice and assistance with both research and teaching efforts. Finally, I must thank Dr. Merv Vincent of Boeing for his wonderful patience with me and for his questions and comments.

I thank my family, parents Bob and Sue Grimm, and brother Brian, gave love and continual encouragement. I thank Sean Caughman, whose friendship for the last ten years has been one of the few constants in my life. I thank my extended family in Texas as well, Teresa Patterson and Scott Merritt, for their support and friendship.

I recognize those who made my life in Michigan enjoyable. These include my fellow grad students in the EM Lab, both old and new; my housemates Rob Butler and Charles Scripter; my friends over the years at Tau Beta Pi Michigan Alpha chapter; and my friends from science-fiction fandom. From these friends I take good memories of my stay at Michigan State University.

Finally, a last special thank-you to my colleagues at CNA, whose emotional support I enjoy as I finished publication of my dissertation.

Acknow

List of

List of

Chapter

Chapte:

Chapte

Table of Contents

Acknowledgements	V
List of Tables	,
List of Figures	x
Chapter 1 Introduction	1
Chapter 2 Electric-Field Integral Equation Description of Open-Boundary	
Waveguiding Systems	10
2.1 Development of an Electric-Field Integral Equation	
2.1.1 Equivalent currents	
2.1.2 Fields within layered media	14
2.1.3 Construction of the integral equation	16
2.2 Development of the Hertzian Potential Dyadic Green's Function 2.2.1 Two-dimensional Fourier transform	19
2.2.1 Two-dimensional Fourier transform	21 22
2.2.2 Finicipal Hertzian potentials	24
2.2.4 Dyadic Green's function for Hertzian potentials	26
2.2.5 Electric-field dyadic Green's function	28
2.3 Axial-Transform Domain Electric-Field Integral Equation	30
2.4 Development of a Transverse-Electric-Field Integral Equation for	
Integrated Dielectric Waveguides	33
Chapter 3	
Propagation-mode Spectrum for Open-Boundary Waveguides	43
3.1 The Fourier Transform in the Complex Plane	45
3.1.1 Fourier transform theory on the real-line	45
3.1.2 Theory of analytic functions	47
3.1.3 Regions of convergence for functions of exponential	
order	
3.2 Green's Function Singularities	5 3
3.2.1 Transverse wavenumber plane (complex ξ -plane)	
singularities	55
3.2.2 Considerations of forward transform convergence	59
3.2.3 Axial transform-domain (complex \(\zeta\)-plane) restrictions	63

Chapte Chapte Chapte Chap: Apper

3.3	Propagation-Mode Spectrum for Open-Boundary Waveguides	67
	3.3.1 Bound modes	
	3.3.2 Continuous radiation spectrum	
	Radiation Spectrum in the Low-loss Limit	
3.5	The Proper Role of Leaky-Wave Modes	
	3.5.1 Identification of leaky-wave modes via the EFIE	
	3.5.2 Usage of leaky-wave modes	
	3.5.3 Physical interpretation of leaky-wave modes	95
Chapter 4		
Cor	ntinuous Radiation Spectrum for Planar Waveguides	101
4.1	General Considerations for Planar Waveguides	102
	4.1.1 Transverse uniformity considerations	
	4.1.2 Uncoupled Transverse-Field EFIE	
4.2	TE Asymmetric Planar Waveguide Radiation Modes	
	Results	
~ 1 . ~		
Chapter 5	ntinuous Radiation Spectrum for Microstrip Transmission Line	125
	-	
5.1	Application of the EFIE	125
5.2	Method-of-Moments Solution	
	5.2.1 MoM expansions	
	5.2.2 Excitation considerations	
5.3	Results	137
Chapter 6		
	ky-wave Modes for the Dielectric Rib Waveguide	150
6.1	Application of the EFIE	150
0.2	6.1.1 Parity considerations	
	6.1.2 EFIE for integrated dielectric waveguide	
6.2	Method-of-Moments Solution	
0.2	6.2.1 MoM expansions	
	6.2.2 Special considerations for the MOM expansion	
63	Spectral Analysis Considerations	
	Results	
Chapter 7		100
Coi	nclusions and Recommendations	177
Appendix .		
	ctric Hertzian Potentials	185
A. 1	Electric Hertzian Potential	185
	2 Hertzian Potential Boundary Conditions	
	Interpretations and Considerations	

Apper

Apper

Biblic

Appendix B Spect	tral Representation of the Dyadic Green's Function	193
	Principal Dyadic Green's Function	
Appendix C Proof	f of the Analytic Function Definition Theorem of Chapter 3	204
C.1 C.2	Theorem and Definitions	
Bibliography	,	207

Table :

Table :

Table

List of Tables

Table 3.1	Effect of the coalesced transform-domain branch cut upon complex ξ-plane singularities	77
Table 3.2	Complex ξ-plane singularity arguments for ζ in the substrate radiation regime	80
Table 6.1	Table of space-wave leaky wave poles (sheet 3) and full leaky wave (sheet 4) for the dielectric rib waveguide where $b/a=1$	174

Figure

Figure

Figure

Figure

Figure

Figure

Figure

Figur

Figur

Figur

Figur

Figur

Figur

List of Figures

Figure 1.1	(a) Typical microstrip transmission line. (b) Typical integrated dielectric waveguide	5
Figure 2.1	(a) Typical configuration for integrated dielectric waveguide.(b) Typical configuration for microstrip transmission line	12
Figure 2.2	Hertzian potentials for a tri-layered environment	20
Figure 2.3	Configuration for axial-transform domain analysis of an integrated dielectric waveguide	31
Figure 2.4	Waveguide geometry for development of TEFIE	39
Figure 3.1	Regions of convergence for functions of exponential order. (a) Convergence in upper half-plane. (b) Convergence in lower half-plane	50
Figure 3.2	Strip of convergence in transform-domain for physically realizable functions of exponential order	51
Figure 3.3	Regions of convergence for exponentially increasing functions	54
Figure 3.4	Singularity locations in the transverse-transform domain (complex ξ -plane)	60
Figure 3.5	Strip of convergence in complex ξ -plane for forward transform on x . Arrows denote singularity migration directions	62
Figure 3.6	(a) Migration of a ξ-plane singularity across real-axis through contour of integration. (b) Migration of a ξ-plane singularity across real-axis, treated correctly	64
Figure 3.7	Branch cuts in axial-transform plane (complex ζ -plane) necessary to maintain convergence of forward Fourier transform on x	66
Figure 3.8	Contour deformation in complex ζ -plane used to identify the propagation-mode spectrum. Closure shown for $z < z'$	70

Figure Figure

Figure 3.9	Coalescing of complex ζ -plane branch cuts in low-loss limit. Closure for case of $z < z'$	76
Figure 3.10	Evaluation of complex-valued square roots	81
Figure 3.11	Complex ξ -plane singularity locations for the substrate radiation regime. (a) Interior side of branch cut S . (b) Exterior side of branch cut S	83
Figure 3.12	Complex ξ -plane singularity locations for the full (cover) radiation regime. (a) Interior side of branch cut B . (b) Exterior side of branch cut B	85
Figure 3.13	Complex ξ -plane singularity locations for transverse-only radiation regime. (a) Interior side of branch cut P . (b) Exterior side of branch cut P	87
Figure 3.14	(a) Four-sheeted axial wavenumber (complex-3) plane. (b) Nature of each Riemann sheet	89
Figure 3.15	Deformed inversion contour in complex ξ -plane used when upon a non-spectral Riemann sheet of the axial-transform plane	91
Figure 3.16	Typical steepest-descent plane	96
Figure 3.17	Physical interpretation of leaky-wave mode (plasma waveguide example from Shevchenko)	98
Figure 4.1	Configuration of asymmetric planar dielectric waveguide 1	l 03
Figure 4.2	Contour used for evaluation of TEFIE	05
Figure 4.3	TE excitation of planar waveguide by line source at $y=y_0$, $z=0$.	13
Figure 4.4	Spectral radiation mode amplitudes of a symmetric planar waveguide obtained by the integral-operator method compared to Rozzi's analytical closed-form results	18
Figure 4.5	Axial-wavenumber plane (complex \(\zeta\)-plane) branch cuts for a typical asymmetric planar waveguide	20
Figure 4.6	Spectral radiation modes in guiding region of asymmetric planar waveguide for both substrate and full radiation regimes	21

Figure

Figure

Figure

Figure

Figure

Figure

Figure

Figur

Figur

Figur

Figu

Figu

Figu

Figu

Figu

Figu

Figu

Figure 4.7	Effect of asymmetry $(n_s/n_c = 1.2)$ on the radiation mode field distributions, compared to the symmetric planar waveguide 122
Figure 4.8	Effect of small amount of asymmetry $(n_s/n_c = 1.05)$ on the radiation mode field distributions, compared to symmetric planar waveguide
	waveguide
Figure 5.1	Configuration of microstrip transmission line
Figure 5.2	Excitation of even radiation spectral modes for microstrip line 134
Figure 5.3	Excitation of odd radiation spectral modes for microstrip line 135
Figure 5.4	Axial wavenumber plane (complex ζ -plane) branch cuts for low-loss microstrip transmission line
Figure 5.5	Normalized radiation regime axial surface current density, even parity. Excitation is 5λ above microstrip line
Figure 5.6	Normalized radiation regime transverse surface current density, even parity. Excitation is 5λ above microstrip line 140
Figure 5.7	Effect of source excitation distance on radiation regime surface current amplitudes
Figure 5.8	Radiation regime axial surface current amplitude, even parity 143
Figure 5.9	Radiation regime transverse surface current amplitude, even parity
Figure 5.10	Radiation regime axial surface current amplitude, odd parity 145
Figure 5.11	Radiation regime axial surface current amplitude, odd parity 146
Figure 5.12	Typical surface current distribution within surface-wave radiation regime, even parity. Excitation source 5λ above microstrip, $\zeta = k_c$
Figure 5.13	Typical surface current distribution within surface-wave radiation regime, odd parity. Excitation source 5λ above microstrip, $\zeta = k_c$
Figure 6.1	Configuration of a rib dielectric optical waveguide
Figure 6.2	Complex ξ-plane singularities for surface-wave leakage 164

Figur Figur Figur Figur Figur Figur Figur Figur

Figure 6.3	Singularities in the complex ξ -plane for: (a) space-wave leakage (sheet 3). (b) full (space/surface wave) leakage (sheet 4)
Figure 6.4	Dispersion curve for integrated dielectric rib waveguide 168
Figure 6.5	Field distribution for dominant E_{11}^y waveguide mode for guide half-width of $a=1.788\lambda$
Figure 6.6	Field distribution for E_{11}^x waveguide mode for guide half-width of $a=1.788\lambda170$
Figure 6.7	Field distribution for E_{21}^x waveguide mode for guide half-width of $a=1.788\lambda$
Figure 6.8	Attenuation plot for E ₁₁ leaky-wave mode in surface-wave-leaky regime
Figure 6.9	Field distribution for E ^x ₁₁ leaky-wave of rib waveguide compared to a bound guiding mode
Figure 6.10	Comparison of field distributions of sheet 3 and sheet 4 leaky-wave modes

wav

use.

close

along

of be

integ

propa

total

its m

scatte

com

orthc

ponu

41,

Chapter 1

Introduction

Open-boundary waveguides, such as microstrip transmission lines or dielectric rib waveguides, are among the most fascinating type of waveguiding structures in common use. Open-boundary waveguides (OBWG) physically differ from their more conventional closed-pipe counterparts in one significant detail — electromagnetic waves are guided along a preferred axis essentially by the mechanism of total internal reflection, instead of being transversely confined by conducting walls. This characteristic makes open-boundary waveguides indispensable for integrated optics and millimeter/microwave integrated circuits (MMICs).

Of fundamental concern for waveguiding devices is a description of their propagation-mode spectrum. If the complete propagation-mode spectrum is known, the total electromagnetic field of an open-boundary waveguide can be expanded in terms of its modes; this modal expansion in turn is used in analysis of excitation, coupling and scattering problems [1,2]. Open-boundary waveguides have a significantly more complicated mode spectrum than their closed-pipe counterparts; it is well-known that the proper modal spectrum for open-boundary waveguides consists of a continuum of orthogonal radiation modes [3,4,5,6] in addition to a finite number of discrete, bound modes [7].

spectru

is conf

guiding

transm

modes

A radi

field p

infinit Sheve

an en:

While

all rad

mode

field,

effec:

propá

done

radia

for ti

the a

A bounded (or bound) mode is a component of the discrete propagation-mode spectrum, hence possessing a discrete propagation constant. The electromagnetic field is confined in near proximity to the guiding region; no power flows transverse to the guiding axis. Bound modes are the hybrid guided-wave modes used for signal transmission, and can be considered an analogue of conventional closed-pipe waveguide modes.

A radiation mode, however, has no analogue in closed-pipe waveguide theory. A radiation mode is not confined and bound to the guiding region; its electromagnetic field possesses a standing wave pattern of finite, non-vanishing amplitude as approaching infinity. This seems a non-physical solution, as no fields can exist at infinity. However, Shevchenko [8] observed that radiation modes can never occur singly, but occur over an entire continuum of propagation constants within a restricted spatial frequency regime. While each radiation mode individually is non-vanishing at infinity, the superposition of all radiation modes satisfies the radiation condition there. This superposition of radiation modes (or continuous spectrum) forms the spatial radiation field. This spatial radiation field, with non-vanishing transverse power flow, then models the loss due to radiation effects from the waveguiding structure.

While the continuous spectrum is an important component of the complete propagation-mode spectrum for open-boundary waveguides, very little work has been done in conceptualizing it save for the simplest of examples. Snyder has determined the radiation spectrum for the uniformly-clad circular fiber [9]. The radiation spectrum for the symmetric planar waveguide has been quantified by Rozzi [10], while that of the asymmetric planar waveguide has been presented in Marcuse [11]. The previous

a consequence, the regime of the p spectral components is obvious.

Recent work [12,13,14] trum of practical open-boundary arbitrary cross-section or structs surround cannot be analyzed wi inseparability of boundary conformulation, is instead used to versions [15,16,17,18] of the mon characteristic — for practic Bound-mode determination is technique; unfortunately, the probability with the integral-open characterization of the radiat

Another reason why
that leaky-wave modes prov
the continuous radiation m
confined mode whose fit
exponentially instead of va
proper spectrum, and is de
become useful when const
is not a modal decompo

corresponding to radiation

MICHIGAN STATE UNIVERSITY LIBRARIES
E31 Lansing, Michigan 46824-1048
NSV is an affirmative-scrion, equatopsis reference scriots and scriots are scriots and scriots and scriots and scriots are scriots are scriots and scriots are scriots and scriots are scriots are scriots and scriots are scriot

examples are actually two-dimensional problems and possess closed-form solutions; as

Having trouble finding what you are looking for? Go to the Reference Desk on the 1st floor, or pick up a red help phone.

Additional library information located at:

www.lib.msu.edu

1

O

ed is

a that

non-

crease

of the

modes

. which

 Michigan State University Archives and Historical Collections or Veterinary Medical Library - G201 Veterinary Medical Center, 17 · Math Library - 101D Wells Hall, 353-8852 Law Library - MSU Law College Building, 432-6860 · James Madison Library - South Case Hall Instructional Media Center – 126 Instructional Media Center, ly. • Engineering Library – 1515 Engineering Building, 355-8536 Business Library – 50 MSU Law College Building, 355-3380 Biomedical and Physical Sciences Bldg., 432-4900 x1990 itor Biomedical & Physical Sciences Library - 1440 (Displayed in the "Location" field of catalog records.) telv MSU Libraries' On-Campus Locations the

Step 4 - Locate the bookshelf where your call number range which she call number you are searching for to that on the spine of the item.

Step 3 - Go to the floor where the item is located. Where present, look at the board with call number ranges and colors. Find your call number. Look at the color next to it. Follow that color on the floor.

Step 2 - If the item is located in the Main Library, consult the front of the call number (DT4076) to determine the wing numbers of your call number (DT4076) to determine the wing and floor your item can be found on.

Step 1 - Look at the call number and the "Location" fields of the catalog record. Be sure of your item's location before proceeding. (Branch locations are listed below.)

Example: DT4076. A47 2007

parameter District of Congress call numbers:

exam

a con

specti

trum

arbitr SUITO

insep

formu

versio mon

Boun

techn

obvio

chara

that the ;

cont

exp∈

 $\text{pr}_{0; \tilde{l}}$ becq

is n

examples are actually two-dimensional problems and possess closed-form solutions; as a consequence, the regime of the propagation-mode spectrum corresponding to radiation spectral components is obvious.

Recent work [12,13,14] has focused on characterizing the radiation spectrum of practical open-boundary waveguiding devices. Uniformly-clad structures of arbitrary cross-section or structures of finite cross-sectional width in a multi-layered surround cannot be analyzed with conventional differential operator techniques due to inseparability of boundary conditions. An integral equation, or integral-operator formulation, is instead used to analyze practical open-boundary problems; the many versions [15,16,17,18] of these integral-operator formulations share one common characteristic — for practical problems, solutions must be developed numerically. Bound-mode determination is relatively straightforward using the integral-operator technique; unfortunately, the proper regime for the radiation spectrum is not immediately obvious with the integral-operator formulation. This is a major reason why the characterization of the radiation spectrum for these devices is non-existent.

Another reason why research into the continuous spectrum has been ignored is that leaky-wave modes provide a readily available approximation to the phenomena that the continuous radiation modes model. A leaky-wave mode [19] is a discrete, non-confined mode whose field distribution approaching infinity appears to increase exponentially instead of vanishing. The leaky-wave solution is obviously not part of the proper spectrum, and is denoted an improper or non-spectral mode. Leaky wave modes become useful when constructing the total field by the method of steepest descents, which is not a modal decomposition but an asymptotic technique to determine the scattered

field. After a suitable transformation of the propagation constant to the "steepest-descent plane" [20], the total field is constructed as the "steepest-descents" contribution evaluated at a "saddle-point", augmented where necessary by a number of other contributions [21]. The most significant of these other contributions is the leaky-wave mode. The leaky-wave mode contributes to the total field over a limited spatial regime; within this regime, the leaky wave accounts for power loss from the waveguiding structure. Consequently, much interest in the community is devoted to leaky-wave modes [22,23,24,25,26,27,28]. This is where the majority of research with open-boundary waveguides is being conducted.

The primary focus of this dissertation is on the characterization of the continuous radiation spectrum for open-boundary waveguides. It investigates those open-boundary waveguides operating in a planar, layered background environment, also known as a layered surround. The basic guiding structure for MMIC's (Millimeter/Microwave Integrated Circuit) is the strip transmission line (also known as microstrip), where a conducting strip serves as the waveguiding mechanism. This is depicted in Figure 1.1a. As the operational frequency increases, conductor loss becomes prohibitive. Replacing the strip with a dielectric guiding region forms an integrated dielectric waveguide (IDWG), as depicted in Figure 1.1b. Doing so can reduce losses dramatically, allowing usage at the intermediate microwave/optical frequencies. Most microstrip transmission lines are fabricated in a conductor/film/cover environment, while a typical IDWG is formed in a tri-layered substrate/film/cover environment.

Both waveguide types, integrated dielectric (IDWG) and microstrip (MS), are assumed to be invariant and of infinite extent along the waveguiding axis. The

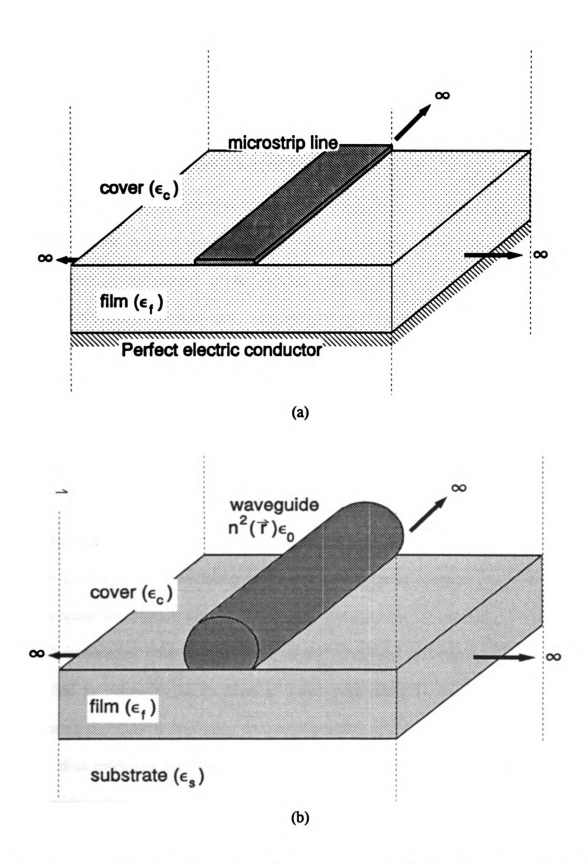


Figure 1.1 (a) Typical microstrip transmission line. (b) Typical integrated dielectric waveguide.

backg direc: that o to pe layer of se envir diele specti gene: Bagb terms boun due t whos spatia ident Posse mad_{e} wave this a EFIE

background region planar layers are assumed to be infinite in extent in the planar directions; practically, the transverse dimension of the planar layers is much greater than that of the waveguiding structure. Each of the background layers is uniform with respect to permittivity and permeability, but can possess dielectric and magnetic contrast from layer to layer. All the interior layers are of finite thickness; the two outermost layers are of semi-infinite vertical extent. It is apparent that the multi-layered background environment in the absence of the guiding region is itself an open-boundary, planar dielectric waveguide, consequently supporting its own guided wave modes and radiation spectrum.

The second chapter develops an integral-operator formulation used to analyze a general category of open-boundary waveguides. Based on the technique developed by Bagby and Nyquist [16,29], an electric field integral equation (EFIE) is formulated in terms of Hertzian potentials based upon equivalent sources that replace the open-boundary waveguide of interest. A dyadic Green's function for the Hertzian potentials due to a current source radiating in a layered background environment is developed, whose scalar components are two-dimensional spectral integrals on axial and transverse spatial frequencies (also denoted as axial and transverse wavenumbers). These are identified as belonging to the class of Sommerfeld integrals, highly oscillatory and possessing singularities depending upon both spatial frequencies. No approximations are made, thus rendering the dyadic Green's function exact. The axial invariance of the waveguiding system is exploited to reduce the dimensionality of the Green's functions; this allows an axial transform-domain EFIE to be developed. This transform-domain EFIE will be used throughout the dissertation. Finally, another form of the axial

transform-domain EFIE is developed for the specific case of integrated dielectric waveguides in terms of the transverse field components only.

In the third chapter, the complete propagation-mode spectrum of an openboundary waveguide is determined. First, a rationale to locate the branch cut singularities within the complex axial-transform plane is advanced, based upon observation of a subtle and usually ignored consequence of utilizing Fourier transforms for analysis. This is new, and a major contribution of this dissertation. This rationale is then applied to locate the desired singularities; a consequence of locating the singularities in the axial transform domain is that all the singularities associated with the dyadic Green's function are located as well. The propagation-mode spectrum for the open-boundary waveguide is then identified. The spectral components are found to be associated with the axial-transform domain singularities; the nature of each component of the propagation-mode spectrum is consequently discussed. A new component for the continuous radiation spectrum, a surface-wave radiation regime, arises from the presence of the integrated background environment. Lastly, the proper use of leaky-wave modes is addressed. Their relationship to the propagation-mode spectrum, in particular the radiation spectrum, will be discussed.

In the fourth chapter, the techniques developed in Chapter 3 will be applied to canonical planar structures to verify their validity and gain insights into their application. The transverse-field EFIE, developed at the end of Chapter 2, will be used to determine the spectral field components. A numerical method-of-moments solution will be implemented, and compared to the known canonical results.

transn

contin

by G

curre:

states

prese

diffe:

wave will

will

Resu

tions

dyad by a

 $den_{\mathbb{C}}$

mag:

Phys

The fifth chapter determines the continuous spectrum of the microstrip transmission line. This is a basic, practical structure, for which no results regarding the continuous radiation spectrum have been published. The appropriate EFIE will be solved by Galerkin's method-of-moments, using basis functions with the well-known edge current singularity built-in. Appropriate source excitation is chosen to exploit the parity states for microstrip surface current distributions. Surface current distributions will be presented and discussed for each different regime of the radiation spectrum.

As a final example, the sixth chapter sees the theory applied to determining the different types of discrete modes, both bound and leaky-wave, for a rib dielectric waveguide, a common structure in integrated optics. The axial-transform domain EFIE will be solved using method-of-moments techniques. Parity states for the rib waveguide will be taken into consideration to avoid the near-degeneracy of the bound modes. Results from this work will be presented and discussed.

Chapter 7 presents the conclusions of this dissertation, and provides recommendations as to the future of this research.

Throughout the dissertation, the following notational forms will be observed. All dyadics will be overstruck by a double-headed arrow, while vectors will be overstruck by an arrow. Also, with respect to any complex quantity z, the following holds: z', z_r denotes the real part of z, z_i denotes the imaginary part of z, while z'' denotes the magnitude of z_i . Consequently, z_i may have any sign, but z'' > 0. The following physical assumptions also hold throughout this dissertation:

Und

Cond

- (1) All media are linear and isotropic;
- (2) Inhomogeneities in conductance $\sigma(\vec{r})$ and permittivity $\vec{\epsilon}(\vec{r})$ are confined to localized regions, i.e., the guiding regions;
- (3) Harmonic time dependence $e^{j\omega t}$ is assumed and suppressed.

Under these assumptions, Maxwell's equations take the form

$$\nabla \times \vec{E}(\vec{t}) = -j\omega \mu \vec{H}(\vec{t}) \qquad \text{Faraday's Law}$$

$$\nabla \times \vec{H}(\vec{t}) = j\omega \vec{\epsilon}(\vec{t}) \vec{E}(\vec{t}) + \vec{J}(\vec{t}) \qquad \text{Ampere-Maxwell Law} \qquad (1.1)$$

$$\nabla \cdot (\vec{\epsilon}(\vec{t}) \vec{E}(\vec{t})) = \rho(\vec{t}) \qquad \text{Gauss's Law}$$

$$\nabla \cdot \vec{H}(\vec{t}) = 0 \qquad \text{Magnetic Source Law}$$

Conduction current density is $\vec{J}^{C}(\vec{r}) = \sigma(\vec{r})\vec{E}(\vec{r})$; consequently, a complex permittivity can be defined in the usual manner, $\epsilon(\vec{r}) = \overline{\epsilon}(\vec{r}) + \sigma(\vec{r})/j\omega$.

conv

the b

deve

Wav

and (30

gu

me

ati

e

Chapter 2

Electric-Field Integral Equation Description of Open-Boundary Waveguiding Systems

As observed in Chapter 1, practical open-boundary waveguides defy analysis by conventional differential operator techniques, primarily because of the inseparability of the boundary conditions imposed by the waveguide structure. This chapter describes the development of an integral-equation approach to the analysis of open-boundary waveguides. The work contained within this chapter has been advanced by other workers and is included for completeness. The notable contributions are by Johnson and Nyquist [30], which advances the usage of the polarization integral equation; Bagby, Nyquist and Drachman [16,29] which develops the approach for integrated background environments; and Viola and Nyquist [31], which clarifies source-point singularity considerations and advances a reduced-component integral equation for optical waveguides [32].

The key to this development is replacing the guiding region with equivalent sources. First, equivalent sources will be identified, and an electric field integral equation (EFIE) for arbitrary open-boundary devices, dielectric or microstrip, will be developed in terms of those sources. Secondly, the necessary Green's dyadic for electric-type Hertzian potentials supported by sources radiating in a planarly-layered background environment will be derived. This dyadic contains all the physical information about the background and makes no approximations; as a consequence, the

EFIE

Third

in axi
axial

wave

2.1

micr

the c

field

diela

laye

€] =

tran

the

becd

axis

syst

cur

₩a.

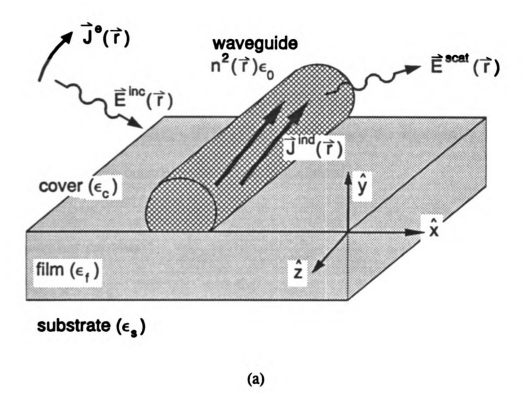
ele

EFIE is exact. The corresponding electric-field Green's dyadic will also be developed. Third, specific characteristics of waveguiding structures, in particular the infinite extent in axial direction, will be exploited to develop a computationally-simpler two-dimensional axial-transform-domain EFIE. Finally, a transverse-field EFIE for integrated dielectric waveguides will be developed from the two-dimensional axially-transformed EFIE.

2.1 Development of an Electric-Field Integral Equation

Both the integrated dielectric waveguide (IDWG) system in Figure 2.1a and the microstrip waveguide system in Figure 2.1b are open-boundary systems; that is, the fields are not confined strictly to the guiding regions. For problems in this dissertation, the open-boundary guiding structure is embedded within the cover layer of a tri-layered dielectric background environment, typically at the cover-film interface. The planar layers (cover, film or substrate) are homogeneous and uniform with permittivity of $\epsilon_l = n_l^2 \epsilon_0$ and free-space permeability $\mu_l = \mu_0$, and of infinite extent in axial and transverse directions. The film layer is of finite thickness in vertical extent, while both the cover and substrate layers are of semi-infinite vertical extent. The substrate layer becomes a perfect conductor for microstrip transmission-line problems. A coordinate system is chosen such that the x and z axes are tangential to the planar interfaces, the y-axis is normal to those interfaces, and the z-axis is specifically the guiding axis.

Consider the system depicted in Figure 2.1. Assume that a system of impressed current densities $\vec{J}^e(\vec{r})$ supports an electric field incident upon an open-boundary waveguide of arbitrary cross-section, permittivity and conductance. This impressed electric field $\vec{E}^i(\vec{r})$ is the field that would exist in the layered-background environment



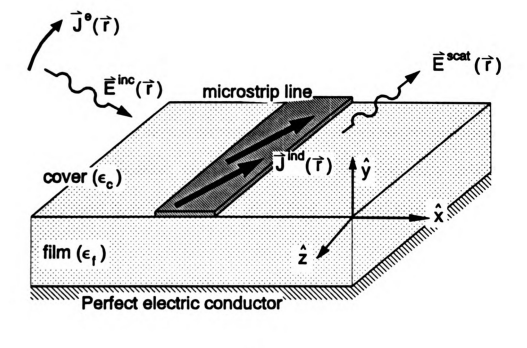


Figure 2.1 (a) Typical configuration for integrated dielectric waveguide.

(b) Typical configuration for microstrip transmission line.

(b)

with the

The su

condition

system

2.1.1

sources (more §

be repla

any poi

where 1

 $inhom_{\mathrm{O}}$

uniform in (2.1)

This is

with the waveguide absent. The impressed electric field induces currents within the waveguide; those induced currents in turn support a scattered or re-radiated field $\vec{E}^*(\vec{r})$. The sum of the impressed and scattered fields yields the total field anywhere within the system. This total field $\vec{E}(\vec{r}) = \vec{E}^i(\vec{r}) + \vec{E}^i(\vec{r})$ must satisfy the appropriate boundary conditions for the open-boundary waveguide in question.

2.1.1 Equivalent currents

Field equivalence principles state that an object can be replaced by its equivalent sources. If equivalent currents can be determined for an open-boundary waveguide (more generally, any open-boundary device, of which waveguides are a subset), it can be replaced by those equivalent currents.

Equivalent currents can be identified by considering Ampere-Maxwell's law at any point within the layer in which the open-boundary device is embedded, namely,

$$\nabla \times \vec{\mathbf{H}}(\vec{\mathbf{r}}) = \vec{\mathbf{J}}^{e}(\vec{\mathbf{r}}) + j\omega \epsilon(\vec{\mathbf{r}}) \vec{\mathbf{E}}(\vec{\mathbf{r}})$$
(2.1)

where \vec{J}^e is the impressed electric current density and ϵ is the complex permittivity. Any inhomogeneities are localized and correspond to the open-boundary devices. The uniform background layer with complex permittivity ϵ_l can be explicitly accounted for in (2.1), giving

$$\nabla \times \vec{\mathbf{H}} = \vec{\mathbf{J}}^{e} + j\omega [\epsilon(\vec{\mathbf{r}}) - \epsilon_{i}] \vec{\mathbf{E}} + j\omega \epsilon_{i} \vec{\mathbf{E}}.$$

This is easily recast into

$$\nabla \times \vec{\mathbf{H}} = \vec{\mathbf{J}}^{e} + j\omega \epsilon_{0} \delta n_{l}^{2}(\vec{\mathbf{r}}) \vec{\mathbf{E}} + j\omega \epsilon_{l} \vec{\mathbf{E}}$$

where definiti

from th

equival

the equ

through

sources

assume

of volu

(2.4) is

 $^{\text{device},}$

radiatir.

2.1.2

differer

 $type H_{\varepsilon}$

where $\delta n_l^2(\vec{r}) = n^2(\vec{r}) - n_l^2$ is the dielectric contrast (complex-valued). Based on its definition, the contrast factor is obviously non-zero only inside the open-boundary device; from this, equivalent polarization sources can be recognized as

$$\vec{P}_{eq}(\vec{r}) = \epsilon_0 \delta n_l^2(\vec{r}) \vec{E}(\vec{r}) . \qquad (2.2)$$

Inherent in the equivalent source definition (2.2) is the mechanism to define equivalent sources for any of the open-boundary waveguides of interest. For IDWGs, the equivalent sources are exactly as developed in equation (2.2), or

$$\vec{P}_{eq}(\vec{r}) = \epsilon_0 \delta n_l^2(\vec{r}) \vec{E}(\vec{r}) = \epsilon_0 [n^2(\vec{r}) - n_l^2] \vec{E}(\vec{r})$$
 (2.3)

throughout the volume of the IDWG. For microstrip devices, the device conductivity is assumed to be infinite, hence the internal field vanishes. The appropriate equivalent sources are then surface currents, denoted as $\vec{K}(\vec{r})$, which are the surface specializations of volume equivalent polarization currents, where

$$\vec{J}_{pol}(\vec{r}) = j \omega \vec{P}_{eq}(\vec{r}). \tag{2.4}$$

The net effect of developing equivalent sources as given in relations (2.3) and (2.4) is to remove the inseparable boundary conditions imposed by the open-boundary device, leaving the much simpler problem of determining the fields supported by sources radiating into a multi-layered planar environment.

2.1.2 Fields within layered media

The planar layered environment problem has much simpler boundary conditions; differential operator techniques can be applied to obtain an exact solution. The electric-type Hertzian vector potential (or Hertzian potential) will be introduced as an auxiliary

potentia

used b

earth.

polariz

electric

where a

current

bounda

in term

then be

of the 1

where

effects

be four

potential. This choice is prompted by historical considerations, as these potentials were used by Sommerfeld [33] in his classic analysis of a Hertzian dipole over a lossy earth. Additionally, the electric-type Hertzian vector potential is supported directly by polarization currents which, as demonstrated in (2.3), have a simple relationship to the electric field.

As developed in Appendix A, the Hertzian potential satisfies Helmholtz's equation

$$\nabla^2 \vec{\Pi} + k^2 \vec{\Pi} = \frac{-\vec{P}}{\epsilon}$$
 (2.5)

where the polarization source current in (2.5) is the sum of the impressed polarization current ($\vec{P}^e = \vec{J}^e/j\omega$) and the equivalent polarization currents induced in the open-boundary devices of interest. The sources in equation (2.5) can be alternatively written in terms of electric current densities, as $\vec{P} = \vec{J}/j\omega$. The electric and magnetic fields can then be represented in terms of the Hertzian potential as

$$\vec{\mathbf{E}} = k^2 \vec{\mathbf{I}} + \nabla \nabla \cdot \vec{\mathbf{I}}$$

$$\vec{\mathbf{H}} = j\omega \epsilon \nabla \times \vec{\mathbf{I}}$$
(2.6)

The solution to Helmholtz's equation in (2.5) must satisfy the boundary conditions of the layered background environment. It can be written in the general form

$$\vec{\Pi}(\vec{r}) = \frac{1}{\epsilon} \int_{V} \vec{G}(\vec{r} | \vec{r}') \cdot \vec{P}(\vec{r}') dV' \qquad (2.7)$$

where $\ddot{\mathbf{G}}(\vec{\mathbf{r}}|\vec{\mathbf{r}}')$ is a Hertzian potential dyadic green's function which accounts for all the effects associated with the layered background environment. The total electric field can be found as

is sup

suppo

for so

as Ē(i

2.1.3

support the tota

to dete

everyw

Once t

known determ

for $d\mathrm{i}_{\theta}$

$$\vec{E}(\vec{r}) = (k^2 + \nabla \nabla \cdot) \int_{V} \vec{G}(\vec{r} | \vec{r}') \cdot \frac{[\vec{P}^e(\vec{r}) + \vec{P}_{eq}(\vec{r}')]}{\epsilon} dV'$$
 (2.8)

for sources within the cover region. As defined previously, the impressed electric field is supported by impressed polarization currents \vec{P}^e , while the scattered electric field is supported by the induced polarization currents \vec{P}_{eq} . The total field is then constructed as $\vec{E}(\vec{r}) = \vec{E}^i(\vec{r}) + \vec{E}^s(\vec{r})$, where

$$\vec{E}^{i}(\vec{r}) = (k^{2} + \nabla \nabla \cdot) \int_{V} \vec{G}(\vec{r} | \vec{r}') \cdot \frac{\vec{P}^{o}(\vec{r})}{\epsilon} dV'$$

$$\vec{E}^{o}(\vec{r}) = (k^{2} + \nabla \nabla \cdot) \int_{V} \vec{G}(\vec{r} | \vec{r}') \cdot \frac{\vec{P}_{oq}(\vec{r})}{\epsilon} dV'.$$
(2.9)

2.1.3 Construction of the integral equation

For the integrated dielectric waveguide, the total field as given in (2.9) is partially supported by the equivalent sources in the guiding region. These sources depend upon the total electric field within that region, which is unknown. Thus, an integral equation to determine the unknown guiding region electric field is constructed by enforcing (2.8) everywhere within the waveguiding region, or

$$\vec{\mathbf{E}}(\vec{\mathbf{r}}) - (k_c^2 + \nabla \nabla \cdot) \int_{V} \vec{\mathbf{G}}(\vec{\mathbf{r}} | \vec{\mathbf{r}}) \cdot \frac{\delta n^2(\vec{\mathbf{r}}') \vec{\mathbf{E}}(\vec{\mathbf{r}}')}{n_c^2} dV' = \vec{\mathbf{E}}^{i}(\vec{\mathbf{r}}); \ \forall \vec{\mathbf{r}} \in V.$$
 (2.10)

Once the guiding region electric field is known, the equivalent polarization currents are known as well, and the electric and magnetic fields elsewhere is space can then be determined. Even though constructed for waveguide analysis, the EFIE in (2.10) is valid for dielectric devices occupying arbitrary volume regions.

of the i

where densitie

device,

the ele

different The EI

integral

.

is an in EFIE's

while t

operato

to excl

([2.4])

For microstrip transmission-line systems, the boundary condition upon the surface of the microstrip device must be satisfied, viz., $\hat{\mathbf{t}} \cdot (\vec{\mathbf{E}}^i + \vec{\mathbf{E}}^s) = 0$. Enforcing this boundary condition upon the total field as given in (2.9) results in

$$\hat{\mathbf{t}} \cdot (k_c^2 + \nabla \nabla \cdot) \int_{\mathbf{r}} \vec{\mathbf{G}}(\vec{\mathbf{r}} | \vec{\mathbf{r}}') \cdot \frac{\vec{\mathbf{K}}(\vec{\mathbf{r}}')}{j\omega \epsilon_c} ds' = -\hat{\mathbf{t}} \cdot \vec{\mathbf{E}}^{inc}(\vec{\mathbf{r}}); \ \forall \vec{\mathbf{r}} \in S$$
 (2.11)

where electric current densities have been used, as opposed to polarization current densities. Integral equation (2.11) is valid over the entire surface of the microstrip device, and can be solved for the unknown surface currents $\vec{K}(\vec{r})$. Once $\vec{K}(\vec{r})$ is known, the electric and magnetic fields elsewhere in space can be determined.

The integral equations developed in (2.10) and (2.11) are technically integrodifferential equations, yet will be referred to as electric field integral equations (EFIE's). The EFIE for microstrip transmission line in (2.11) is an inhomogeneous Fredholm integral equation of the first kind; the EFIE for integrated dielectric waveguides in (2.10) is an inhomogeneous Fredholm integral equation of the second kind. Additionally, both EFIE's (2.10) and (2.11) are of the Wiener-Hopf type, in which the range is semi-infinite while the domain is finite.

A true integral-equation representation can be developed by passing the $(k_c^2 + \nabla \nabla \cdot)$ operator through the integration over the source region. In doing so, care must be taken to exclude the source-point, as the integrable singularity there will become non-integrable ([2.4]). As a consequence, integral equation (2.10) becomes

$$\vec{\mathbf{E}}(\vec{\mathbf{r}}) - \int_{V} \vec{\mathbf{G}}^{c}(\vec{\mathbf{r}} \mid \vec{\mathbf{r}}) \cdot \frac{\delta n^{2}(\vec{\mathbf{r}}') \vec{\mathbf{E}}(\vec{\mathbf{r}}')}{n_{c}^{2}} dV' = \vec{\mathbf{E}}^{i}(\vec{\mathbf{r}}); \ \forall \vec{\mathbf{r}} \in V,$$
 (2.12)

with si

where .

sources

detail is

device

represen

conditio

(2.11) b

Only m

in this c

of whic

In that

total sc.

equival extensi

but is 1

with similar results for integral equation (2.11). The electric-field dyadic Green's function is defined as

$$\ddot{\mathbf{G}}^{\bullet}(\vec{\mathbf{r}}|\vec{\mathbf{r}}') = \mathbf{P.V.}\left\{ (k_c^2 + \nabla\nabla\cdot)\ddot{\mathbf{G}}(\vec{\mathbf{r}}|\vec{\mathbf{r}}') \right\} + \ddot{\mathbf{L}}\delta(\vec{\mathbf{r}}-\vec{\mathbf{r}}')$$
(2.13)

where P.V. implies that integration of (2.12) is in the Cauchy principal value sense, excluding the source point, while \tilde{L} is a depolarizing dyad that corrects for any artificial sources introduced by the exclusion of the source point [34]. This is given more detail in Section 2.2.5.

If the microstrip device has finite conductivity, an electric field internal to the device exists, and can be simply modeled as $\vec{E}^{int} = Z^i \vec{K}(\vec{t})$, assuming a simple representation for the surface impedance Z^i can be found. The appropriate boundary condition is $\hat{t} \cdot (\vec{E}^i + \vec{E}^a) = \hat{t} \cdot \vec{E}^{int}$ on the microstrip surface, and the integral equation in (2.11) becomes

$$\hat{\mathbf{t}} \cdot (k_c^2 + \nabla \nabla \cdot) \int_{s'} \vec{\mathbf{G}}(\vec{\mathbf{r}} | \vec{\mathbf{r}}') \cdot \frac{\vec{\mathbf{K}}(\vec{\mathbf{r}}')}{j\omega \epsilon_c} ds' - \hat{\mathbf{t}} \cdot [Z^i \vec{\mathbf{K}}(\vec{\mathbf{r}})] = -\hat{\mathbf{t}} \cdot \vec{\mathbf{E}}^{inc}(\vec{\mathbf{r}}); \ \forall \vec{\mathbf{r}} \in S. \ (2.14)$$

Only microstrip transmission-lines with infinite conductivity ($Z^{i} = 0$) will be considered in this dissertation, but (2.14) is included for completeness.

This technique can be extended to include many open-boundary devices, not all of which need be waveguides, or even a mixture of dielectric and microstrip devices. In that case, each open-boundary device is represented by an equivalent source. The total scattered field is a superposition of the scattered fields supported by each individual equivalent source; the resulting EFIE is enforced with each such individual device. This extension, of value for coupled-device problems, is not of interest for this dissertation, but is mentioned for completeness.

being

potent

This se

2.2 Development of the Hertzian Potential Dyadic Green's Function

Consider the tri-layered situation in Figure 2.2, with the source in the cover layer being either equivalent or impressed currents, denoted generally as \vec{J} . These currents support a principal Hertzian potential radiating outward from the source in apparently unbounded space. This potential propagates until it encounters a planar boundary, where the wave is partially transmitted and partially reflected. The total Hertzian potential in the source layer is the sum of that principal potential plus the scattered potential from the interface. For other layers, the Hertzian potential is that portion of the principal potential transmitted through the planar interface boundary.

As a consequence of the above analysis, Helmholtz's equation can be written as

$$(\nabla^2 + k_i^2) \begin{cases} \vec{\Pi}_i^p \\ \vec{\Pi}_i^s \end{cases} = \begin{cases} -\vec{J}/j\omega \epsilon_i & i=c \\ 0 & all i. \end{cases}$$
 (2.15)

where $\vec{\Pi}_i^P$ is a principal Hertzian potential directly supported by current sources \vec{J} (or polarization current sources since $\vec{P} = \vec{J}/j\omega$) radiating in an unbounded medium, and $\vec{\Pi}_i^s$ are the scattered Hertzian potentials from the planar interfaces indirectly supported by the sources in the i^{th} (cover) layer. The total potential in any layer is the superposition of principal and scattered Hertzian potentials in that layer; this total potential must satisfy the boundary conditions on Hertzian potentials developed in Appendix A. A solution for the total potential of the form (2.7) is sought, namely,

$$\vec{\Pi}(\vec{r}) = \frac{1}{j\omega\epsilon} \int_{V} \vec{G}(\vec{r} | \vec{r}') \cdot \vec{J}(\vec{r}') dV'.$$

This section addresses the determination of the desired dyadic Green's function.

E

€,

J

Figure

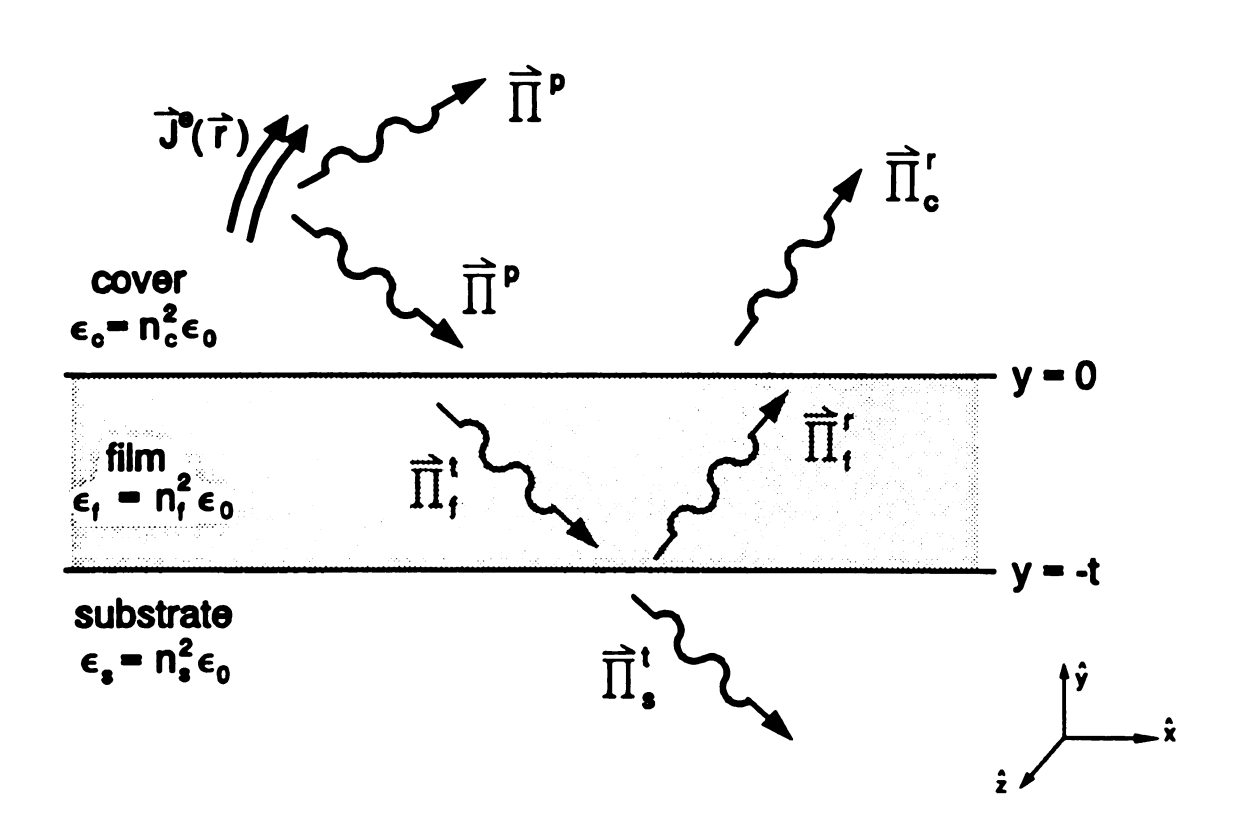


Figure 2.2 Hertzian potentials for a tri-layered environment.

conditi

Recogn

directio

and z.

where

be writ

product

The int

t. App

the trai

numbe:

2.2.1 Two-dimensional Fourier transform

Solving the Helmholtz equations as given in (2.15) subject to the boundary conditions developed in Appendix A is still difficult, but an exact solution does exist. Recognition that the interface is infinite in extent in the transverse (x) and axial (z) directions prompts a two-dimensional Fourier transform on those spatial coordinates x and z. This transform pair is given as

$$\vec{\Pi}(\vec{r}) = \frac{1}{(2\pi)^2} \int_{-\infty}^{\infty} \int_{-\infty}^{\infty} \vec{\Pi}(\vec{\lambda}; y) e^{j\vec{\lambda} \cdot \vec{r}} d^2 \lambda$$

$$\vec{\Pi}(\vec{\lambda}; y) = \int_{-\infty}^{\infty} \int_{-\infty}^{\infty} \vec{\Pi}(\vec{r}) e^{-j\vec{\lambda} \cdot \vec{r}} d^2 r$$
(2.16)

where $\vec{\lambda} = \xi \hat{x} + \zeta \hat{z}$ is a two-dimensional spectral frequency. This transform pair can also be written as an iterated set of one-dimensional transforms; this is apparent if the dot product in (2.16) is explicitly carried out, and takes the form

$$\vec{\Pi}(\vec{r}) = \frac{1}{2\pi} \int_{-\infty}^{\infty} \left[\frac{1}{2\pi} \int_{-\infty}^{\infty} \vec{\Pi}(\xi, \zeta; y) e^{j\xi x} d\xi \right] e^{j\zeta z} d\zeta$$

$$\vec{\Pi}(\xi, \zeta; y) = \int_{-\infty}^{\infty} \left[\int_{-\infty}^{\infty} \vec{\Pi}(\vec{r}) e^{-j\xi x} dx \right] e^{-j\zeta z} dz$$

The inner, bracketed quantities form a transform pair on x and transverse spatial frequency ξ ; while the outer transform pair is obviously on z and axial spatial frequency ζ . Application of this transform pair to the Helmholtz equations in (2.15) yields

$$\left(\frac{\partial^2}{\partial y^2} - p_i^2\right) \begin{bmatrix} \tilde{\Pi}^p(\vec{\lambda}; y) \\ \tilde{\Pi}^s(\vec{\lambda}; y) \end{bmatrix} = \begin{bmatrix} \tilde{J}_i(\vec{\lambda}; y)/j\omega \epsilon_i \\ 0 \end{bmatrix},$$
(2.17)

the transform-domain Helmholtz equations. The quantity p_i is a transformed wavenumber parameter, and given as

$$p_i = \sqrt{\lambda^2 - k_i^2} = \sqrt{\xi^2 + \zeta^2 - k_i^2}. \tag{2.18}$$

The squa

pair (2.1

different

solutions

condition

2.2.2 P

by pola

obeying

the solu for $\vec{\Pi}_i^P$

where t

Unfort

problei

interfac

 $transf_{O}$

The square root in (2.18) will be chosen to enforce $\Re\{p_i\} > 0$. Usage of transform pair (2.16) converts partial differential equations in the space-domain to ordinary differential equations in the spatial-frequency domain which possess relatively simple solutions, while retaining the spatial y-dependence necessary for implementing boundary conditions.

2.2.2 Principal Hertzian potentials

As defined, the principal Hertzian potential $\vec{\Pi}_i^p$ is the potential directly supported by polarization currents radiating in unbounded space, in this case the cover medium, obeying the forced space-domain Helmholtz equation in (2.15). For unbounded space, the solution of the forced Helmholtz equation is well-known; consequently, the solution for $\vec{\Pi}_i^p$ is simply

$$\vec{\Pi}^{p}(\vec{r}) = \int_{V} G^{p}(\vec{r} | \vec{r}') \frac{\vec{J}(\vec{r}')}{j\omega\epsilon_{c}} dV', \qquad (2.19)$$

where the principal Green's function $G^{p}(\vec{r}|\vec{r}')$ is the usual free-space Green's function

$$G^{p}(\vec{r}\,|\vec{r}') = \frac{e^{-jk_{c}|\vec{r}-\vec{r}'|}}{4\pi\,|\vec{r}-\vec{r}'|}.$$
 (2.20)

Unfortunately, the spatial form given in (2.20) is not terribly useful in waveguiding problems, nor for matching the boundary conditions for the total potential at a planar interface.

A more tractable form of (2.20) can be developed by first solving for the transform-domain principal Green's function $\tilde{G}^{P}(\vec{\lambda}; y-y')$, then constructing $G^{P}(\vec{r}|\vec{r}')$

in the sp

in the tv

the solu

where

inverse function

By unic

 $\vec{l} = \vec{l}'$

the spe

due to

 e_{xpone}

in the space-domain via the inverse transform as defined in (2.16). The Green's function in the two-dimensional Fourier transform domain solves the equation

$$\left(\frac{\partial^2}{\partial y^2} - p_c^2\right) \tilde{G}^{P}(\vec{\lambda}; y | y') = -\delta(y - y'),$$

the solution of which is

$$\tilde{G}^{p}(\vec{\lambda}; y - y') = \frac{e^{-p_{c}|y-y'|}}{2p_{c}}. \tag{2.21}$$

where $\Re\{p_c\} > 0$ is required to satisfy the radiation condition. Application of the inverse transform to (2.21) then recovers the desired space-domain principal Green's function in a spectral representation of

$$G^{p}(\vec{r}-\vec{r}') = \frac{1}{(2\pi)^{2}} \int_{-\pi}^{\pi} \frac{e^{-p_{c}|y-y'|}}{2p_{c}} e^{j\vec{\lambda}\cdot(\vec{r}-\vec{r}')} d^{2}\lambda. \qquad (2.22)$$

By uniqueness, the spatial form (2.20) and spectral form (2.22) of the free-space Green's function are equivalent; this relationship is the Weyl identity [35], i.e.,

$$\frac{e^{-jk_c|\vec{r}-\vec{r}'|}}{4\pi |\vec{r}-\vec{r}'|} = \int_{-\infty}^{\infty} \frac{e^{j\vec{\lambda}\cdot(\vec{r}-\vec{r}')} e^{-p_c|y-y'|}}{2(2\pi)^2 p_c} d^2\lambda.$$

It is obvious from (2.20) that a singularity occurs at the source point, when $\vec{\mathbf{r}} = \vec{\mathbf{r}}'$. This singularity is contained in (2.22) as well, albeit not obviously. As $\vec{\mathbf{r}} \rightarrow \vec{\mathbf{r}}'$, the spectral form is slowly convergent. The obvious exponential decay in the integrand due to $\exp(|y-y'|)$ vanishes, as do the destructive oscillations of the complex exponentials as $x \rightarrow x'$, $z \rightarrow z'$. At $\vec{\mathbf{r}} = \vec{\mathbf{r}}'$, the integrand takes the asymptotic form

$$\frac{1}{2(2\pi)^2}\int_{-\pi}^{\pi}\int_{-\pi}^{d^2\lambda} d^2\lambda$$

which is

manifest

2.2.3 5

each pla

is not d

and is e

 \vec{W}_{i}^{z} are

in Appe

inverse

surrou

this se

nature

open-

withir

source

in Fig

which is obviously divergent. The singularity of order $O(|\vec{r}-\vec{r}'|^{-1})$ in (2.20) thus manifests itself as a divergent integral for (2.22).

2.2.3 Scattered Hertzian potentials

The scattered Hertzian potentials obey the homogeneous Helmholtz equation in each planar layer. Solving the homogeneous transform-domain Helmholtz equation (2.17) is not difficult; a general solution in the ith layer takes the form

$$\vec{\Pi}_{i}^{s}(\vec{\lambda},y) = \vec{W}_{i}^{\dagger}(\vec{\lambda})e^{-p_{i}y} + \vec{W}_{i}^{\dagger}(\vec{\lambda})e^{+p_{i}y}, \qquad (2.23)$$

and is easily recognized as a plane-wave type solution traveling in the $\pm y$ direction. The \vec{W}_i^{\pm} are vector constants that satisfy the Hertzian potential boundary conditions developed in Appendix A. The space-domain scattered Hertzian potential follows naturally via the inverse transform of (2.16),

$$\vec{\Pi}_{i}^{a}(\vec{r}) = \iiint_{-\infty} \left[\vec{W}_{i}^{*}(\vec{\lambda}) e^{-p_{i}y} + \vec{W}_{i}^{-}(\vec{\lambda}) e^{*p_{i}y} \right] \frac{e^{j\vec{\lambda}\cdot\vec{r}}}{(2\pi)^{2}} d^{2}\lambda . \qquad (2.24)$$

Determination of the vector constants \vec{W}_i^* appropriate for the layered-background surround is a rather tedious process. The complete details can be found in Appendix B; this section summarizes the major considerations, in order to provide insight as to the nature of \vec{W}_i^* .

Designate the cover, film and substrate as regions 1, 2, and 3 respectively. For open-boundary waveguides of interest in this dissertation, the guiding region is entirely within the cover; consequently, only the total potential in the cover is of interest. Any sources are assumed to be entirely in the cover region as well. This is the case depicted in Figure 2.2. In the transform domain, the scattered Hertzian potentials are

traveling

by the

(assume

the sup

 $\vec{\mathbb{I}}_{i}(\vec{r})$

Here,

prac

sou

Te.

St

a

`

$$\tilde{\Pi}_{1}^{s}(\vec{\lambda}, y) = \tilde{W}_{1}^{r}(\vec{\lambda})e^{-p_{1}y}$$

$$\tilde{\Pi}_{2}^{s}(\vec{\lambda}, y) = \tilde{W}_{2}^{t}(\vec{\lambda})e^{+p_{2}y} + \tilde{W}_{2}^{r}(\vec{\lambda})e^{-p_{2}y}$$

$$\tilde{\Pi}_{3}^{s}(\vec{\lambda}, y) = \tilde{W}_{3}^{t}(\vec{\lambda})e^{+p_{3}y}$$
(2.25)

The cover (region 1) is unbounded as $y \to +\infty$; consequently, only outward traveling potentials $\vec{W}_1^r(\vec{\lambda})e^{-p_1y}$ in +y exist in region 1 ($\Re e\{p_1\} > 0$ required), supported by the reflection of the principal potential off the interface between regions 1 and 2 (assumed to be y=0). The total space-domain Hertzian potential in region 1 is then

$$\vec{\Pi}_{1}(\vec{r}) = \vec{\Pi}_{1}^{P}(\vec{r}) + \vec{\Pi}_{1}^{r}(\vec{r}), \qquad (2.26)$$

the superposition of the principal and scattered Hertzian potentials. By using the spectral form of the principal Green's function, the total space domain Hertzian potential becomes

$$\vec{\Pi}_{1}(\vec{r}) = \frac{1}{(2\pi)^{2}} \int_{-\infty}^{\infty} e^{j\vec{\lambda}\cdot\vec{r}} \left(e^{\frac{2p_{1}(\lambda)y}{\hbar}} \left[\int_{V} \frac{\vec{J}}{j\omega\epsilon_{1}} \frac{e^{-j\vec{\lambda}\cdot\vec{r}'}e^{\frac{2p_{1}(\lambda)y'}{\hbar}} dV'}{2p_{1}(\lambda)} \right] + \vec{W}_{1}^{r}(\vec{\lambda}) e^{-p_{1}(\lambda)y} \right] d^{2}\lambda \quad (2.27)$$

Here, the relation $e^{p_1(\lambda)|y-y'|} = e^{-p_1(\lambda)y'}e^{*p_1(\lambda)y}$ if y' > y is exploited, since the interface is below any source currents in the cover (if y' < y, $e^{p_1(\lambda)|y-y'|} = e^{*p_1(\lambda)y'}e^{-p_1(\lambda)y}$). The bracketed quantity in (2.26) is denoted as $\vec{V}(\vec{r}')$, and depends upon the location of the source currents.

The total potential in other regions is just the scattered Hertzian potential in those regions. The film layer (region 2) is bounded in y; the scattered potential therein is the sum of a transmitted potential from region 1, $\vec{W}_2^t(\vec{\lambda})e^{-p_2y}$, traveling in the -y direction, and a reflected potential off the lower boundary, $\vec{W}_2^t(\vec{\lambda})e^{-p_2y}$, traveling in the +y direction. The substrate (region 3) is unbounded as $y \to -\infty$; it sees only a transmitted

poten

poten

applic tediou

enviro

condi

compo

potent

obser.

2.2.4

cover

potential, $\vec{W}_3^t(\vec{\lambda})e^{-p_3y}$, from region 2 traveling in the -y direction. The space-domain potentials in regions 2 and 3 are then

$$\vec{\Pi}_{2}(\vec{r}) = \frac{1}{(2\pi)^{2}} \int_{-\pi}^{\pi} e^{j\vec{\lambda}\cdot\vec{r}} \left[\vec{W}_{2}^{t}(\vec{\lambda})e^{p_{2}(\lambda)y} + \vec{W}_{2}^{r}(\vec{\lambda})e^{-p_{2}(\lambda)y} \right] d^{2}\lambda. \tag{2.28}$$

$$\vec{\Pi}_{3}(\vec{r}) = \frac{1}{(2\pi)^{2}} \int_{-\infty}^{\infty} e^{j\vec{\lambda}\cdot\vec{r}} \left[\vec{W}_{3}^{t}(\vec{\lambda})e^{p_{3}(\lambda)y} \right] d^{2}\lambda. \tag{2.29}$$

The boundary conditions on Hertzian potentials are given by (A.14); their application to the potentials of (2.27) - (2.29) at each interface is straightforward though tedious; details are given in Appendix B for a number of different background environments. In brief, inspection of (A.14) reveals that, at a planar interface, the conditions for continuity of tangential Hertzian potentials ($\alpha = x, z$) involve only tangential components; while the conditions matching the normal (9) component of Hertzian potential couples the normal and tangential Hertzian potential components. Based on this observation, it is clear that the scatted potential in the cover takes on the form

$$\Pi_{1\alpha} = \iiint_{\vec{r}} R_{t}(\vec{\lambda}) V_{\alpha}(\vec{r}') \frac{e^{-p_{1}y} e^{j\vec{\lambda} \cdot \vec{r}}}{(2\pi)^{2}} d^{2}\lambda; \quad \alpha = x, z$$

$$\Pi_{1y} = \iiint_{\vec{r}} R_{n}(\vec{\lambda}) V_{y}(\vec{r}') \frac{e^{-p_{1}y} e^{j\vec{\lambda} \cdot \vec{r}}}{(2\pi)^{2}} d^{2}\lambda$$

$$+ \left(\frac{\partial}{\partial x} \hat{x} + \frac{\partial}{\partial z} \hat{z}\right) \cdot \iint_{\vec{r}} C(\vec{\lambda}) \vec{V}(\vec{r}') \frac{e^{-p_{1}y} e^{j\vec{\lambda} \cdot \vec{r}}}{(2\pi)^{2}} d^{2}\lambda$$
(2.30)

2.2.4 Dyadic Green's function for Hertzian potentials

With the recognition that $\vec{V}(\vec{r}')$ involves the sources, the resulting potential in the cover region can now be written as

where th

The prin

while th

The sca

spectra

These

Somn typify

coup]

funct

the w

ing to

$$\vec{\Pi}_1(\vec{r}) = \frac{1}{j\omega\epsilon_c} \int_V \vec{G}(\vec{r}|\vec{r}') \cdot \vec{J}(\vec{r}') dV' \qquad (2.31)$$

where the Green's dyad can be decomposed as

$$\ddot{G}(\vec{r}|\vec{r}') = \ddot{G}^{P}(\vec{r}|\vec{r}') + \ddot{G}^{r}(\vec{r}|\vec{r}'). \tag{2.32}$$

The principal Green's dyadic is

$$\ddot{G}^{p}(\vec{r}|\vec{r}') = \ddot{I}G^{p}(\vec{r}|\vec{r}') \tag{2.33}$$

while the reflected Green's dyadic takes the form

$$\vec{G}'(\vec{r}|\vec{r}') = \hat{x} G_t^r \hat{x} + \hat{y} \left[\frac{\partial G_c^r}{\partial x} \hat{x} + G_n^r \hat{y} + \frac{\partial G_c^r}{\partial z} \hat{z} \right] + \hat{z} G_t^r \hat{z}. \tag{2.34}$$

The scalar components of the Green's dyadic are two-dimensional inverse transforms on spectral frequency $\vec{\lambda}$, and are given as

$$G^{p}(\vec{r}|\vec{r}') = \int_{-\pi}^{\pi} \frac{e^{j\vec{\lambda}\cdot(\vec{r}-\vec{r}')} e^{-p_{c}|y-y'|}}{2(2\pi)^{2}p_{c}} d^{2}\lambda$$
 (2.35)

$$\begin{cases}
G_t'(\vec{r}|\vec{r}') \\
G_n'(\vec{r}|\vec{r}') \\
G_c''(\vec{r}|\vec{r}')
\end{cases} = \int_{-\infty}^{\infty} \begin{cases}
R_t(\lambda) \\
R_n(\lambda) \\
C(\lambda)
\end{cases} \frac{e^{j\vec{\lambda}\cdot(\vec{r}-\vec{r}')}e^{-p_c(y+y')}}{2(2\pi)^2 p_c} d^2\lambda. \tag{2.36}$$

These scalar components of the dyadic Green's function are of the form of the notorious Sommerfeld integrals, and possess the rapid oscillation for large spatial distances that typify these integrals. The coefficients $R_t(\lambda)$, $R_n(\lambda)$ and $C(\lambda)$ are reflection and coupling coefficients specific to a given layered background surround. They are functions of the *magnitude* of spectral frequency $\vec{\lambda}$ ($\lambda = \sqrt{\xi^2 + \zeta^2}$) as implicated through the wavenumber parameter p_i given in (2.18), and possess pole singularities corresponding to the surface-wave behavior of that background structure, which itself is a planar,

open-

backg

waves

respor

within

relates

maint influe

Finall

norma

2.2.5

develo

develo

integr

where

 dy_{adi}

the el

open-boundary waveguide. Appendix B lists the forms for a number of typical background environments.

This dyadic Green's function can be interpreted as the superposition of plane waves propagating transversely with spectral frequency λ (= $\sqrt{\xi^2 + \zeta^2}$) and normally in the $\pm y$ directions with propagation constant p_c . The dyadic Green's function is the total response in the cover region to a unit dyadic point source current $\ddot{I} \delta(\vec{r} - \vec{r}')$ radiating within the planar layered background surround. The reflected Green's component G_t^r relates the influence of the background structure on the tangential Hertzian potential maintained by a tangential point source. Likewise, G_n^r relates the background structure's influence upon the normal Hertzian potential maintained by a normal point source. Finally, G_c^r relates the background-induced coupling of tangential point sources to normal components of Hertzian potential.

2.2.5 Electric-field dyadic Green's function

Even though the dyadic Green's function for the Hertzian potential has been developed, the electric field in the cover region is needed to satisfy the EFIE's as developed in (2.10)-(2.11). Passage of the operator $(k_c^2 + \nabla \nabla \cdot)$ through the source-point integration is desirable, to obtain an electric field representation of the form

$$\vec{E}(\vec{r}) = \frac{1}{j\omega\epsilon_c} \int_{V} \vec{G}^{\epsilon}(\vec{r}|\vec{r}') \cdot \vec{J}(\vec{r}') dV' \qquad (2.37)$$

where $\vec{G}''(\vec{r}|\vec{r}')$ is the electric-field dyadic Green's function, also called the electric dyadic Green's function. This representation in (2.37) provides a compact notation for the electric field amenable to algebraic manipulations. Passage of the spatial derivatives

through

A very

key poir

quires

reflecte

not. Th

arising

can be

incorpo

The th

invoki source

-10

where

through the source-point integral requires special care, in particular the $\nabla\nabla$ operator. A very comprehensive discussion of this procedure is carried out by Viola [31,36]; the key points are reviewed here.

Passage of the operator $\nabla \nabla \cdot$ on field points through the source-point integral requires that the integrand be uniformly convergent. The scalar components of the reflected dyadic Green's function possess this property; the principal component does not. The presence of the absolute value function |y-y'| gives rise to a singularity at y=y' arising from derivatives with respect to the normal coordinate variable y. This situation can be handled by defining the spatial integral in a principal value (P.V.) sense, and incorporating an appropriate correction term [37].

The electric field in the cover region can be rewritten as

$$j\omega\epsilon_{c}\vec{E}(\vec{r}) = (k_{c}^{2} + \nabla\nabla\cdot)\int_{V} \vec{G}'\cdot\vec{J}(\vec{r}')dV'$$

$$+ k_{c}^{2}\int_{V} \vec{I}G^{P}\cdot\vec{J}(\vec{r}')dV'$$

$$+ \nabla\nabla\cdot\int_{V} \vec{I}G^{P}\cdot\vec{J}(\vec{r}')dV'.$$
(2.38)

The third term in (2.38) demands careful attention. It can be properly evaluated by invoking Leibnitz's rule, and excluding a shape-dependent principal volume about the source point, ie.

$$\nabla\nabla\cdot\int_{V}\vec{G}^{P}\cdot\vec{J}(\vec{r}')dV' = P.V.\int_{V}\nabla\nabla\cdot\vec{G}^{P}\cdot\vec{J}(\vec{r}')dV' + \vec{L}\delta(\vec{r}-\vec{r}')$$

where P.V. designates evaluating the integration in a principal value sense, that is

whe dyad

natu

2.3

inclu

fields

by a typica

usuall

Sugge

domai

spatial

guidin

Waveg (-∞<

that of

(2.10

$$P.V.\int_{V} \{\cdots\} dV' = \lim_{V_{\delta} \to 0} \int_{V-V_{\delta}} \{\cdots\} dV'$$

where V_0 is the shape-dependent excluded principal volume and $\vec{\mathbf{L}}$ is a depolarizing dyad. For the planar layered background environment, a slice principal volume is naturally assumed [2.4]; for this principal volume, $\vec{\mathbf{L}} = \hat{y}\hat{y}$.

2.3 Axial-Transform Domain Electric-Field Integral Equation

The EFIE's developed in (2.10)-(2.11) are in terms of three-dimensional spatial fields, and are of use for any arbitrary-shaped obstacle. The dyadic Green's function includes the effect of the environment upon the obstacle; for spatial fields, it is defined by a two-dimensional inverse transform over the spectral frequency $\vec{\lambda} = \pounds\xi + \pounds\zeta$. The typical waveguiding system of interest, microstrip or integrated dielectric waveguide, is usually axially uniform and of infinite extent along the guiding axis. This symmetry suggests that advantages might be obtained by solving the EFIE in the axial-transform domain, and then recovering the spatial fields via an inverse transform on the axial spatial frequency ζ .

Consider the situation depicted in Figure 2.3. Let CS be the cross-section of the guiding region of an integrated dielectric waveguide. Then the volume integral for the waveguide is an integral over the guide cross-section and the entire guiding axis $(-\infty < z < \infty)$. Inspection of the dyadic Green's function as given by (2.32)-(2.36) shows that $\ddot{G}(\vec{r}|\vec{r}') = \ddot{G}(\vec{\rho}|\vec{\rho}';z-z')$. Taking explicit account of these observations in EFIE (2.10) gives

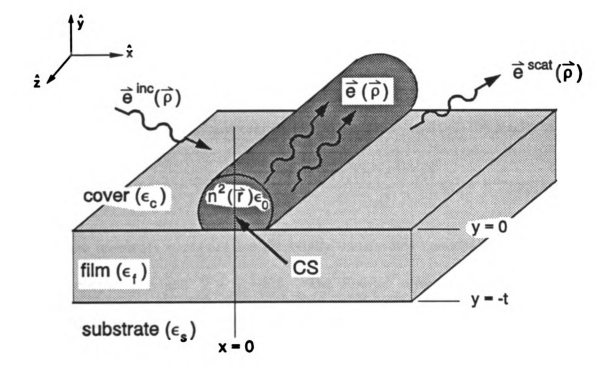


Figure 2.3 Configuration for axial-transform domain analysis of an integrated dielectric waveguide.

Ē(

The EF

Applica

where

spatial

theore:

(2.11)

domai

where

pansu

$$\vec{\mathbf{E}}(\vec{\mathbf{r}}) - (k_c^2 + \nabla \nabla \cdot) \int_{CS} \left[\int_{-\infty}^{\infty} \vec{\mathbf{G}}(\vec{\mathbf{r}} - \vec{\mathbf{r}}') \cdot \frac{\delta n_i^2(\vec{\mathbf{r}}') \vec{\mathbf{E}}(\vec{\mathbf{r}}')}{n_i^2} dz' \right] ds' = \vec{\mathbf{E}}^{inc}(\vec{\mathbf{r}}); \ \forall \vec{\mathbf{r}} \in V.$$

The EFIE possesses an easily recognized convolutional kernel over the infinite extent of the guiding axis, suggesting an application of a Fourier transform on axial variable z.

The axial transform pair is defined as

$$\vec{E}(\vec{\rho},z) = \frac{1}{2\pi} \int_{-\infty}^{\infty} \vec{e}(\vec{\rho},\zeta) e^{j\zeta z} d\zeta$$

$$\vec{e}(\vec{\rho},\zeta) = \int_{-\infty}^{\infty} \vec{E}(\vec{\rho},z) e^{-j\zeta z} dz$$
(2.39)

Application of the Fourier transform defined in (2.39) to EFIE (2.10) results in

$$\vec{e}(\vec{\rho},\zeta) - (k_c^2 + \tilde{\nabla}\tilde{\nabla}\cdot) \int_{CS'} \vec{g}(\vec{\rho}|\vec{\rho}';\zeta) \cdot \frac{\delta n_i^2(\vec{\rho}') \vec{e}(\vec{\rho}';\zeta)}{n_i^2} ds' = \vec{e}^{inc}(\vec{\rho};\zeta) \quad (2.40)$$

where the lowercase quantities are the axially-transformed versions of their respective spatial counterparts and $\tilde{\nabla} = \nabla_t + j\zeta\hat{z}$. The Fourier convolution theorem (Faltung theorem) allows the convolutional kernel on z to be replaced by the product of the transformed Green's dyad and the axial-transform-domain field. A similar analysis upon (2.11) reveals that the EFIE for microstrip transmission lines in the axial-transform domain is

$$\hat{\mathbf{t}} \cdot (\mathbf{k}_c^2 + \nabla \nabla \cdot) \oint_C \vec{\mathbf{g}}(\vec{\rho} \mid \vec{\rho}'; \zeta) \cdot \frac{\vec{\mathbf{k}}(\vec{\rho}'; \zeta)}{j\omega \epsilon_c} dl' = -\hat{\mathbf{t}} \cdot \vec{\mathbf{e}}^{inc}(\vec{\rho}; \zeta)$$
 (2.41)

where C is the cross-sectional contour bounding the surface of the microstrip transmission line.

The dyadic Green's function in the axial-transform domain becomes

where

and th

The G

backg

 λ as π

functi

2.4

descr

by (2

regio

$$\vec{g}(\vec{\rho}|\vec{\rho}',\zeta) = \vec{g}^{p}(\vec{\rho}|\vec{\rho}',\zeta) + \vec{g}'(\vec{\rho}|\vec{\rho}',\zeta) \tag{2.42}$$

where

$$\vec{g}^{p}(\vec{o}|\vec{o}',\zeta) = \vec{I}g^{p}(\vec{o}|\vec{o}',\zeta) \tag{2.43}$$

$$\vec{g}^{r}(\vec{\rho}\,|\,\vec{\rho}^{\prime},\zeta) = \hat{x}\,g_{t}^{r}\hat{x} + \hat{y}\left[\frac{\partial g_{c}^{r}}{\partial x}\hat{x} + g_{n}^{r}\hat{y} + j\zeta g_{c}^{r}\hat{z}\right] + \hat{z}\,g_{t}^{r}\,\hat{z} \qquad (2.44)$$

and the scalar components are

$$g^{p}(\vec{\rho} | \vec{\rho}'; \zeta) = \int_{-\pi}^{\pi} \frac{e^{j\xi(x-x')} e^{-p_{c}|y-y'|}}{4\pi p_{c}} d\xi$$
 (2.45)

$$\begin{cases}
g_t''(\vec{\rho} | \vec{\rho}'; \zeta) \\
g_n''(\vec{\rho} | \vec{\rho}'; \zeta)
\end{cases} = \int_{-\infty}^{\infty} \begin{cases}
R_t(\lambda) \\
R_n(\lambda) \\
C(\lambda)
\end{cases} \frac{e^{j\xi(x-x')}e^{-p_c(y+y')}}{4\pi p_c} d\xi \tag{2.46}$$

The Green's function scalar components are still Sommerfeld integrals, but are now one-dimensional inverse transforms on transverse spatial frequency ξ . Note that the background reflection and coupling coefficients R_i , R_n , and C are the same functions of λ as mentioned previously; consequently, the Green's function scalar components are still functions of the axial spatial frequency ζ .

2.4 Development of a Transverse-Electric-Field Integral Equation for Integrated Dielectric Waveguides

In the previous section, an axial-transform domain EFIE was developed to describe the fields associated with integrated dielectric waveguides. This EFIE as given by (2.40) utilizes all three electric-field components, $\vec{e} = \hat{x}e_x + \hat{y}e_y + \hat{z}e_z$. In a source-free region, however, only two of the three electric-field components are independent, since

the electronside

only tw

domain

exampl

by det

equatio

One cap $(\vec{e}_t = \dot{x})$

waveg

field b

obser,

and ur

to rec

obvio

for, e

obvio

electri

origin

and t

the electric field must satisfy Gauss's Law, $\nabla \cdot (n^2 \epsilon_0 \vec{e}) = 0$. An appropriate question to consider is whether the EFIE developed in (2.40) can be recast into an EFIE utilizing only two independent electric-field components?

There is well-established precedence for this consideration. In the axial-transform domain, only two of six field components $(e_x, e_y, e_z, h_x, h_y, h_z)$ are independent. For example, any waveguiding problem in a homogeneous, source-free region can be solved by determining the axial fields (e_z, h_z) independently, then satisfying the "Magic equations",

$$\begin{cases} \vec{\mathbf{e}}_{t} \\ \vec{\mathbf{h}}_{t} \end{cases} = \frac{1}{(k^{2} - \zeta^{2})} \left[j \zeta \nabla_{t} \begin{cases} e_{z} \\ h_{z} \end{cases} + j \omega \hat{z} \times \nabla_{t} \begin{cases} \mu h_{z} \\ -\epsilon e_{z} \end{cases} \right].$$

One can just as easily proceed to work with electric fields transverse to the guiding axis $(\vec{e}_t = \hat{x}e_x + \hat{y}e_y)$ as the independent field components. It is well known from closed-pipe waveguide theory that knowledge of the transverse fields is sufficient to characterize all field behavior for a closed-pipe waveguide in a source-free region. Likewise, the same observation about transverse electric fields can be made for planar dielectric waveguides and uniformly-clad dielectric waveguides like the circular dielectric rod. It is desirable to recast EFIE (2.40) into a form involving only the transverse electric fields. The obvious advantage of doing so is a reduction in the number of unknowns to be solved for, especially with MoM techniques. The other advantage, which is not as readily obvious, is a reduction in the order of the source-point singularity that occurs in the electric dyadic Green's function kernel. This section presents that development, originally performed by Viola [2.5]. Within this development, explicit dependence on $\vec{\rho}$ and $\vec{\zeta}$ is suppressed, unless necessary for clarity.

(TEFIE

electric

 $\vec{e} = \vec{e}_{t}$

Solvin

where.

compd

ĉż·,

Subtr

∇, =

ĕ,(p

The fundamental step in deriving the Transverse Electric Field Integral Equation (TEFIE) is invoking Gauss's Law in the axial transform domain to determine the axial electric field in terms of the transverse electric fields. The electric field decomposes as $\vec{e} = \vec{e}_t + \hat{z}e_z$, and considering that the operator $\nabla = \nabla_t + j\zeta\hat{z}$, Gauss's Law becomes

$$\nabla_{t} \cdot (n^{2}\vec{e}_{t}) + j\zeta n^{2}e_{z} = 0.$$

Solving to find the axial electric field e, gives

$$j\zeta e_z = -\nabla_t \cdot \vec{e}_t - \vec{d}_n \cdot \vec{e}_t \qquad (2.47)$$

where, to simplify notation, the vector quantity $\vec{d}_{\mathbf{a}}$ is defined as

$$\vec{d}_n = \frac{\nabla_i n^2}{n^2} = \nabla_i \ln n^2. \qquad (2.48)$$

The next step is to remove the axial component from the EFIE. First, the axial component of (2.40) is recognized by premultiplying the EFIE in (2.40) with the dyadic 22, resulting in

$$\hat{z}e_{z}(\vec{\rho}) = \hat{z}e_{z}^{inc}(\vec{\rho}) + \hat{z}k_{c}^{2}\int_{cs} \frac{\delta n^{2}(\vec{\rho}')}{n_{c}^{2}} \left[\hat{z}\cdot\vec{g}(\vec{\rho}|\vec{\rho}')\cdot\vec{e}(\vec{\rho}')\right]ds' \\
+ \hat{z}j\zeta\,\tilde{\nabla}\cdot\int_{cs} \frac{\delta n^{2}(\vec{\rho}')}{n_{c}^{2}}\,\vec{g}(\vec{\rho}|\vec{\rho}')\cdot\vec{e}(\vec{\rho}')ds'.$$
(2.49)

Subtracting (2.49) from the original EFIE (2.40) and exploiting the decompositions $\nabla_{r} = \nabla - j\zeta\hat{z}$ and $\vec{e}_{t} = \vec{e} - \hat{z}e_{z}$ gives

$$\vec{e}_{t}(\vec{\rho}) = \vec{e}_{t}^{i}(\vec{\rho}) + k_{c}^{2} \int_{CS} \frac{\delta n^{2}(\vec{\rho}')}{n_{c}^{2}} [\vec{g}(\vec{\rho}|\vec{\rho}') - \hat{z}\hat{z} \cdot \vec{g}(\vec{\rho}|\vec{\rho}')] \cdot \vec{e}(\vec{\rho}') ds'$$

$$+ \nabla_{t} \int_{CS} \frac{\delta n^{2}(\vec{\rho}')}{n_{c}^{2}} \tilde{\nabla} \cdot \vec{g}(\vec{\rho}|\vec{\rho}') \cdot \vec{e}(\vec{\rho}') ds'$$
(2.50)

by t

when

nota

trans

The a

this $_{
m i}$

Next, the dyadic reductions that occur within (2.50) are expanded and grouped by transverse and axial electric field components to reveal that

$$\vec{g} \cdot \vec{e} = \vec{g} \cdot \vec{e}_t + \left[\hat{y} j \zeta g_c^r + \hat{z} (g^p + g_t^r) \right] e_z$$

$$\hat{z} \hat{z} \cdot \vec{g} \cdot \vec{e} = \hat{z} (g^p + g_t^r) e_z = \hat{z} g^H e_z$$

$$\vec{g} \cdot \vec{e} - \hat{z} \hat{z} \cdot \vec{g} \cdot \vec{e} = \vec{g} \cdot \vec{e}_t + \hat{y} j \zeta g_c^r e_z$$
(2.51)

$$\tilde{\nabla} \cdot \vec{\mathbf{g}} \cdot \vec{\mathbf{e}} = (\nabla_t + j\zeta \hat{\mathbf{z}}) \cdot \left\{ \vec{\mathbf{g}} \cdot \vec{\mathbf{e}}_t + \left[\hat{y} j\zeta g_c' + \hat{z} (g^p + g_t') \right] e_z \right\}$$

$$= \nabla_t \cdot \vec{\mathbf{g}} \cdot \vec{\mathbf{e}}_t + \left(\frac{\partial g_c'}{\partial y} + g^p + g_c' \right) (j\zeta e_z) = \nabla_t \cdot \vec{\mathbf{g}} \cdot \vec{\mathbf{e}}_t + g_{zl} j\zeta e_z$$
(2.52)

where the terms $g^H = g^P + g_c^P$ and $g_{zl} = g^P + g_c^P + \frac{\partial g_c^P}{\partial y}$ have been defined to simplify notation. Substitution of (2.51) and (2.52) into (2.50) and separating integrals on transverse and axial electric field components gives

$$\vec{e}_{t}(\vec{\rho}) = \vec{e}_{t}^{i}(\vec{\rho}) + k_{c}^{2} \int_{CS} \frac{\delta n^{2}(\vec{\rho}')}{n_{c}^{2}} \vec{g}(\vec{\rho}|\vec{\rho}') \cdot \vec{e}_{t}(\vec{\rho}') ds'$$

$$+ \nabla_{t} \int_{CS} \frac{\delta n^{2}(\vec{\rho}')}{n_{c}^{2}} \nabla_{t} \cdot \vec{g}(\vec{\rho}|\vec{\rho}') \cdot \vec{e}_{t}(\vec{\rho}') ds'$$

$$+ k_{c}^{2} \int_{CS} \frac{\delta n^{2}(\vec{\rho}')}{n_{c}^{2}} \hat{y} g_{c}^{r}(\vec{\rho}|\vec{\rho}') [j\zeta e_{z}(\vec{\rho}')] ds'$$

$$+ \nabla_{t} \int_{CS} \frac{\delta n^{2}(\vec{\rho}')}{n_{c}^{2}} g_{zl}(\vec{\rho}|\vec{\rho}') [j\zeta e_{z}(\vec{\rho}')] ds' .$$

$$(2.53)$$

The axial electric field component e_z occurs explicitly in the last two integrals of (2.52); this is removed by substituting (2.47) into (2.52), thus yielding

an E

unde

parts

where

 $\nabla_{i}\delta_{n}$

the 8

Take:

(2.54

$$\vec{e}_{t}(\vec{\rho}) = \vec{e}_{t}^{1}(\vec{\rho}) + k_{c}^{2} \int_{CS} \frac{\delta n^{2}(\vec{\rho}')}{n_{c}^{2}} \vec{g}(\vec{\rho}|\vec{\rho}') \cdot \vec{e}_{t}(\vec{\rho}') ds'$$

$$+ \nabla_{t} \int_{CS} \frac{\delta n^{2}(\vec{\rho}')}{n_{c}^{2}} \nabla_{t} \cdot \vec{g}(\vec{\rho}|\vec{\rho}') \cdot \vec{e}(\vec{\rho}') ds'$$

$$- \hat{y}k_{c}^{2} \int_{CS} \frac{\delta n^{2}(\vec{\rho}')}{n_{c}^{2}} g_{c}'(\vec{\rho}|\vec{\rho}') \left[\nabla_{t}' \cdot \vec{e}_{t}(\vec{\rho}') + \vec{d}_{n}(\vec{\rho}') \cdot \vec{e}_{t}(\vec{\rho}')\right] ds'$$

$$- \nabla_{t} \int_{CS} \frac{\delta n^{2}(\vec{\rho}')}{n_{c}^{2}} g_{zt}(\vec{\rho}|\vec{\rho}') \left[\nabla_{t}' \cdot \vec{e}_{t}(\vec{\rho}') + \vec{d}_{n}(\vec{\rho}') \cdot \vec{e}_{t}(\vec{\rho}')\right] ds'$$

an EFIE for transverse electric fields only in terms of transverse electric fields.

In this formulation, the derivatives of \vec{e}_t inside the last two integrals are undesired. Removal of these derivatives (the $\nabla'_t \cdot \vec{e}_t$ term) is effected by integration by parts. Using the vector identity $\nabla \cdot (\phi \vec{A}) = \nabla \phi \cdot \vec{A} + \phi \nabla \cdot \vec{A}$ shows that

$$\delta n^{2}(\vec{\rho}') g_{\alpha}(\vec{\rho} | \vec{\rho}') \nabla_{t}' \cdot \vec{e}_{t}(\vec{\rho}') =$$

$$\nabla_{t}' \cdot \left\{ \delta n^{2}(\vec{\rho}') g_{\alpha}(\vec{\rho} | \vec{\rho}') \vec{e}_{t}(\vec{\rho}') \right\} - \delta n^{2}(\vec{\rho}') \left[\nabla_{t}' g_{\alpha}(\vec{\rho} | \vec{\rho}') \cdot \vec{e}(\vec{\rho}') \right]$$

$$- g_{\alpha}(\vec{\rho} | \vec{\rho}') \left[\nabla_{t}' n^{2}(\vec{\rho}') \cdot \vec{e}_{t}(\vec{\rho}') \right]$$

$$(2.55)$$

where g_a is either g_c^r or g_{cl} , and where the observation

 $\nabla_t \delta n^2(\vec{\rho}) = \nabla_t \{n^2(\vec{\rho}) - n_c^2\} = \nabla_t n^2(\vec{\rho})$ has been invoked to simplify results. Furthermore, the $\delta n^2(\vec{\rho}') \, \bar{d}_{\rm m} / n_c^2$ product associated with the last two integrals of (2.54) reduces to

$$\frac{\delta n^2(\vec{\rho}') \vec{d}_n}{n_c^2} = \frac{n^2(\vec{\rho}') - n_c^2}{n_c^2} \frac{\nabla_i n^2(\vec{\rho}')}{n^2(\vec{\rho}')} = \left(\frac{1}{n_c^2} - \frac{1}{n^2(\vec{\rho}')}\right) \nabla_i n^2(\vec{\rho}').$$

Taken together with (2.55) and the above result, the last two integrals of the EFIE in (2.54) take the generic form of

 $\int_{CS} \frac{\delta n^2}{n}$

one te

(Greer

2 ∆'.

where

and n

gathe

The

simp

opv

 Δ^{G}

$$\int_{CS} \frac{\delta n^{2}(\vec{\rho}')}{n_{c}^{2}} g_{\alpha}(\vec{\rho} | \vec{\rho}') \left[\nabla_{t}' \cdot \vec{e}_{t}(\vec{\rho}') + \vec{d}_{\alpha}(\vec{\rho}') \cdot \vec{e}_{t}(\vec{\rho}') \right] ds'$$

$$= \int_{CS} \nabla_{t}' \cdot \left\{ \frac{\delta n^{2}(\vec{\rho}')}{n_{c}^{2}} g_{\alpha}(\vec{\rho} | \vec{\rho}') \vec{e}_{t}(\vec{\rho}') \right\} ds'$$

$$- \int_{CS} \frac{\delta n^{2}(\vec{\rho}')}{n_{c}^{2}} \nabla_{t}' g_{\alpha}(\vec{\rho} | \vec{\rho}') \cdot \vec{e}_{t}(\vec{\rho}') ds' - \int_{CS} g_{\alpha}(\vec{\rho} | \vec{\rho}') \vec{d}_{\alpha} \cdot \vec{e}_{t}(\vec{\rho}') ds'$$
(2.56)

one term of which is amenable to application of the two-dimensional divergence theorem (Green's Theorem in the Plane). The explicit result for that integral is

$$\int_{CS} \nabla_t' \cdot \left\{ \frac{\delta n^2(\vec{\rho}')}{n_c^2} g_{\alpha}(\vec{\rho} | \vec{\rho}') \vec{e}_t(\vec{\rho}') \right\} ds' = \oint_{\Gamma} \frac{\delta n^2(\vec{\rho}')}{n_c^2} g_{\alpha}(\vec{\rho} | \vec{\rho}') \left[\hat{n}' \cdot \vec{e}_t(\vec{\rho}') \right] dl' \qquad (2.57)$$

where Γ is the contour bounding the cross-sectional surface of the dielectric waveguide, and \Re is the outward directed normal from contour Γ , as seen in Figure 2.4.

After all the manipulations mentioned in (2.55) through (2.57), terms can be gathered to generate a nice form for a TEFIE of

$$\vec{e}_{t}(\vec{\rho}) = \vec{e}_{t}^{i}(\vec{\rho}) + k_{c}^{2} \int_{CS} \frac{\delta n^{2}(\vec{\rho}')}{n_{c}^{2}} \left[\vec{g} + \hat{y} \nabla_{t}' g_{c}' \right] \cdot \vec{e}_{t}(\vec{\rho}') ds'$$

$$+ \nabla_{t} \int_{CS} \frac{\delta n^{2}(\vec{\rho}')}{n_{c}^{2}} \left[\nabla_{t} \cdot \vec{g} + \nabla_{t}' g_{zl} \right] \cdot \vec{e}_{t}(\vec{\rho}') ds'$$

$$+ \int_{CS} \left[\hat{y} k_{c}^{2} g_{c}' + \nabla_{t} g_{1z} \right] \vec{d}_{n}(\vec{\rho}') \cdot \vec{e}_{t}(\vec{\rho}') ds'$$

$$- \oint_{\Gamma} \frac{\delta n^{2}(\vec{\rho}')}{n_{c}^{2}} \left[\hat{y} k_{c}^{2} g_{c}' + \nabla_{t} g_{zl} \right] (\hat{n}' \cdot \vec{e}_{t}(\vec{\rho}')) dl'$$

The bracketed quantities are new Green's functions, but are not represented in their simplest form, as certain derivatives will cancel out. It is well-known (and equally obvious by inspection of (2.45) that the principal Green's function behaves as $\nabla_t g^p = -\nabla_t' g^p$. The reflected Green's functions are subtly different. While the

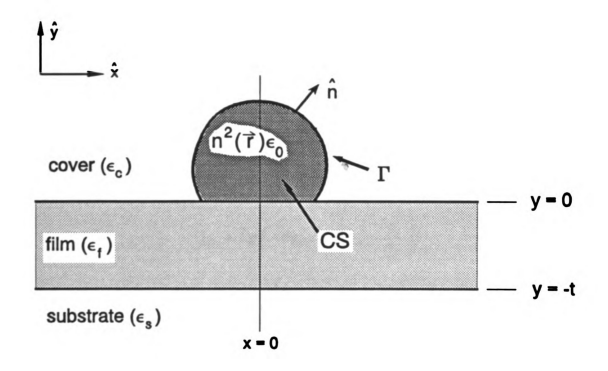


Figure 2.4 Waveguide geometry for development of TEFIE.

trai

∂g,

as

elec

whe

Note

quan

(2.6)

elec

 \vec{p}_{i}

transverse behavior is the same as that of the principal Green's function (ie, $\partial g_a'/\partial x = -\partial g_a'/\partial x'$), inspection of (2.46) reveals that the normal derivatives will behave as $\partial g_a'/\partial y = \partial g_a'/\partial y'$. Under these considerations, the desired form of the transverse electric field integral equation (TEFIE) is

$$\vec{e}_{t}(\vec{\rho}) = \vec{e}_{t}^{i}(\vec{\rho}) + k_{e}^{2} \int_{CS} \frac{\delta n^{2}(\vec{\rho}')}{n_{e}^{2}} \vec{g}_{t1}(\vec{\rho}|\vec{\rho}') \cdot \vec{e}_{t}(\vec{\rho}') ds'$$

$$+ \nabla_{t} \int_{CS} \frac{\delta n^{2}(\vec{\rho}')}{n_{e}^{2}} \vec{g}_{tv}(\vec{\rho}|\vec{\rho}') \cdot \vec{e}_{t}(\vec{\rho}') ds'$$

$$+ \int_{CS} \vec{g}_{\phi}(\vec{\rho}|\vec{\rho}') \vec{d}_{n}(\vec{\rho}') \cdot \vec{e}_{t}(\vec{\rho}') ds'$$

$$- \oint_{\Gamma} \frac{\delta n^{2}(\vec{\rho}')}{n_{e}^{2}} \vec{g}_{\phi}(\vec{\rho}|\vec{\rho}') (\hat{n}' \cdot \vec{e}_{t}(\vec{\rho}')) dl'$$

$$(2.58)$$

where the following Green's function quantities have been defined:

$$\vec{\mathbf{g}}_{t1} = \vec{\mathbf{I}} g^{p} + \hat{\mathbf{x}} g_{t}^{r} \hat{\mathbf{x}} + \hat{\mathbf{y}} \left(g_{n}^{r} + \frac{\partial g_{c}^{r}}{\partial y} \right) \hat{\mathbf{y}}$$
 (2.59)

$$\vec{g}_{tv} = \nabla_t \left[\left(g_A^r + g_t^r + \frac{\partial g_c^r}{\partial y} \right) \hat{y} \right]$$
 (2.60)

$$\vec{g}_{\phi} = \hat{y}k_c^2 g_c^r + \nabla_t \left[g^p + g_t^r + \frac{\partial g_c^r}{\partial y} \right]$$
 (2.61)

Note that both Green's functions \ddot{g}_{t1} and \ddot{g}_{ty} are dyadic, while \ddot{g}_{ϕ} is simply a vector quantity.

A physical interpretation of the newly developed Green's functions in (2.59) to (2.61) is possible by identifying the nature of the sources induced by the transverse electric field. Transverse polarization current density is easily recognized as $\vec{p}_t = \delta n^2(\vec{\rho}) \epsilon_0 \vec{e}_t$. It is readily apparent from considering (2.58) that both \vec{g}_{t1} and \vec{g}_{tv}

relate funct wave

induc

kerne

gradie

is rea

comp

well-t

Sumn

integr

ment

syster

trans:

integ

transy

relate the polarization current density to the electric field. The vector \mathbf{g}_{ϕ} is a Green's function that relates the electric field to the polarization charge densities throughout the waveguide cross-section and the waveguide boundary. From this consideration, the induced polarization charge densities can be recognized as

$$\rho_{\nu} = -\epsilon_0 n_c^2 \, \vec{\mathbf{d}}_{\mathbf{a}} \cdot \vec{\mathbf{e}}_{\mathbf{t}}$$

$$\rho_{\mu} = \epsilon_0 \delta n^2 \, \hat{n} \cdot \vec{\mathbf{e}}_{\mathbf{t}}$$
(2.62)

The final form of the TEFIE as given in (2.58) is devoid of a highly singular kernel, as desired. This is because the operator upon the principal Green's function that introduced the source-point singularity $(\nabla_t \nabla_t \cdot \vec{g}^p)$ has been manipulated into only a gradient operation $(\nabla_t g^p)$. This term is now on the order of $|\vec{p} - \vec{p}'|^{-1}$ as $y \rightarrow y'$, which is readily integrable. As noted previously, there never was a problem with the scalar components of the reflected Green's dyadic. Consequently, all Green's functions are well-behaved and independent of the shape of the excluded source-region.

Summary

An electric-field integral equation for open-boundary waveguiding systems, integrated dielectric waveguide or microstrip, in a planar-layered background environment has been developed. Exploitation of the axial uniformity of these waveguiding systems allows the appropriate electric field integral equation to be solved in the axial-transform domain. The necessary Green's functions are one-dimensional integrals on ξ , the transverse spatial frequency, and given by (2.42)-(2.46). Finally, for the case of integrated dielectric waveguide, an electric field integral equation based solely on transverse field components can be developed. Regardless of which EFIE is used, the

spati

to th

spatial electric fields can then be constructed as the inverse transforms of the solutions to the axial-transform domain EFIE's.

bou

an don

of t

wav

spec

the a

of th

vital

 $\frac{depe}{depe}$

deve!

(Cot

Chapter 3

Propagation-mode Spectrum for Open-Boundary Waveguides

In Chapter 2, an integral equation for the axial transform-domain fields of open-boundary waveguides was developed. Subsequent to solution of that integral equation, an inverse transform on axial spatial frequency ζ is necessary to recover the space-domain fields. One possible representation of the space-domain fields¹ is a superposition of the spectral modes of the open-boundary waveguide, where a spectral mode is any waveguide mode that satisfies the Sommerfeld radiation condition. This chapter exposes a method to recover the space-domain fields and recognize the propagation-mode spectrum (axial eigenspectrum) of open-boundary waveguides.

The propagation-mode spectrum is found to be associated with the singularities of the transform-domain field² in the axial transform (complex- ζ) plane; hence, locating the appropriate axial transform-domain singularities and determining their nature is of vital importance. This task is non-trivial, as the Green's function integrands are dependent upon axial spectral frequency ζ and transverse spectral frequency ξ through the relationship $\lambda^2 = \xi^2 + \zeta^2$. It is not a priori obvious how singularities of the Green's

¹The development in this chapter is performed for the electric field of the IDWG structure. This development is equally valid for the surface current of microstrip transmission lines.

²Throughout Chapter 3, transform-domain without any qualification refers to the axial transform domain (Complex \(\zeta - plane \)).

functi

singu'.

transf

In Sec

The a

trans:

transv comp

restri

ion zi

probl

field defo

expa

radi

zbe par

ope

re

 q_{J}

function in the *transverse* spectral frequency (complex- ξ) plane impact the location of singularities in the *axial transform* plane, or vice versa.

Section 3.1 provides a necessary first step, developing conditions for a Fourier transform pair to exist in the complex plane by consideration of analytic function theory. In Section 3.2, these conditions are applied to the analysis of open-boundary waveguides. The axial transform-domain Green's function scalar components are inverse Fourier transforms on transverse spectral frequency ξ . Requiring that the forward transform on transverse position x converge serves to restrict the location of the singularities in the complex ξ -plane; this restriction on the complex ξ -plane singularities locates and restricts the singularities in the complex ξ -plane. The criterion developed in Section 3.1 is not new, just subtle; the application of this criterion to the open-boundary waveguiding problem is new, and the major contribution of this dissertation.

Section 3.3 of this chapter develops a spectral representation for the space-domain fields by evaluating the inverse Fourier transform on axial spectral frequency by contour deformation into the complex ξ -plane. This propagation-mode spectrum is a singularity expansion of the transform-domain fields from which the radiation field and continuous radiation spectrum can be conceptualized. For open-boundary waveguides of finite transverse extent in a layered background environment, a new regime of the radiation spectrum will be identified. Section 3.4 is a discussion of the radiation spectrum for open-boundary waveguides with limitingly low-loss. The specific character of each regime of the radiation spectrum, and the effect upon the complex ξ -plane, will be discussed.

leaky-

treme

why t

3.5.

3.1

for n

physi

Most

trans

comp

3.1.1

engir math

[3.1]

be of

Finally, Section 3.5 addresses a related topic — the usage of the non-spectral or leaky-wave modes in the representation of the space-domain fields. Leaky-waves are of tremendous interest to the research community, yet almost no one adequately discusses why they are of interest and importance; hence, this will be explicitly detailed in Section 3.5. Section 3.5 will also comment on their relationship to the radiation field.

3.1 The Fourier Transform in the Complex Plane

Little consideration outside the inclusion of generalized function theory is needed for most typical applications of Fourier transform analysis that occur in electrical engineering. Engineering problems analyzed via the Fourier transform usually possess physical requirements that easily satisfy the existence conditions for the transform pair. Most typical applications of the Fourier transform also deal with strictly real-valued transform variables as well. As a consequence, when the transform variable becomes complex, little, if any, extra consideration is given to the now complex-valued problem.

3.1.1 Fourier transform theory on the real-line

There is a great body of literature on the Fourier integral, from the basic engineering-oriented considerations of Papoulis [38] and LePage [39] to in-depth mathematical treatments [40,41]. The important conclusions, taken from Papoulis [3.1], are summarized below. In this basic treatment, all functions f(x) are assumed to be of bounded variation.

The familiar version of the Fourier transform pair, in this case on x and ξ , is

A

be

Cer

Con beh

toni

abs(

inte

shou

Inve

Whi

by s

$$f(x) = \frac{1}{2\pi} \int_{-\pi}^{\pi} F(\xi) e^{j\xi x} d\xi$$
 (3.1)

$$F(\xi) = \int_{-\infty}^{\infty} f(x) e^{-j\xi x} dx \qquad (3.2)$$

A sufficient condition for the Fourier integral (3.2) to converge is that the function f(x) be absolutely integrable, that is

$$\int_{-\infty}^{\infty} |f(x)| dx < \infty \tag{3.3}$$

Certain functions, such as $\sin(\alpha x)/x$, do not obey (3.3) yet possess a Fourier transform. Consequently, a second condition for the convergence of (3.2) is that the function f(x) behave as $f(x) = g(x)\sin(\alpha x + \phi)$, where α and ϕ are arbitrary constants, g(x) monotonically decreases as $|x| \to \infty$, and that $\int_{-\infty}^{\infty} |f(x)x^{-1}| dx$ exists, that is, f(x)/x is absolutely integrable. Under this condition, the Fourier integral in (3.2) should be interpreted in the Cauchy Principal value sense, namely,

$$\int_{-T}^{T} f(x) dx = \lim_{T \to \infty} \int_{-T}^{T} f(x) dx$$

One can refer to Titchmarsh [3.3] for more discussion on the above topics. It should be noted that the starting point in Titchmarsh is actually Fourier's Single Inversion Integral (SII),

$$f(x) = \lim_{\xi \to \infty} \int_{-\pi}^{\pi} \frac{f(t)}{\pi} \frac{\sin \xi(x-t)}{(x-t)} dt$$

which can be formally developed from the Fourier transform pair given in (3.2) and (3.1) by substituting (3.2) into (3.1) and exchanging the integration order.

3.1.2 Theory of analytic functions

With open-boundary waveguide problems, the spectral frequencies are often times complex-valued. Of necessity, the theory of complex variables is involved, in particular the theory of analytic functions. Certain key observations and theorems are presented below. In the following discussion, z, w, and α are all complex variables unless otherwise noted.

The definition of an analytic function is a complex function f(z) of a complex variable z is analytic at a point z_0 if it is differentiable at every point within a neighborhood of z_0 . A function is analytic in a region D if it is analytic at all points of the region D (also denoted as regular in D); herein, the term analytic refers to functions analytic in a region unless otherwise explicitly stated. Obviously, no singularities of function f(z) exist in region D.

Application of analytic function theory to the Fourier transform pair requires a theorem that allows for analytic functions to be defined by means of integration.

Theorem I: Let D be the region. Let f(z, w) be continuous in z and w where $z \in D$ and w lies on a smooth contour C, possibly unbounded. Let f(z, w) be an analytic function of z in D for each w on C. Let $\int_C f(z, w) dw$ be uniformly convergent. Then

$$F(z) = \int_C f(z, w) dw$$
 (3.4)

is an analytic function of z in D.

This elegant theorem is stated in slightly different form in [42]. A proof of Theorem I is developed in Appendix C.

3

t

0

it P

w] fu

Als

un

the

rea the

ļ

3.1.3 Regions of convergence for functions of exponential order

The Fourier transform is used as a tool to solve the Helmholtz equation subject to the boundary conditions of a planarly layered background environment. The solutions to the Helmholtz equation are exponential functions. It is necessary, then, to determine the region of convergence for the Fourier transform pair of a function of exponential order. This follows the development from Mittra and Lee [43].

Let f(x) be a function of exponential order with a finite number of discontinuities. These discontinuities are not of concern, and can be handled in the Cauchy Principle Value sense. A function f(x) of exponential order has the general behavior

$$|f(x)| < \begin{cases} Ae^{\tau_{-}x}; & x \to \infty \\ Be^{\tau_{-}x}; & x \to -\infty \end{cases}$$
 (3.5)

where A>0, B>0. To analyze the convergence properties of exponential order functions, the forward transform in (3.2) will be decomposed as the sum of two parts,

$$F(\xi) = \int_{-\infty}^{0} f(x)e^{-j\xi x}dx + \int_{0}^{\infty} f(x)e^{-j\xi x}dx$$

$$= F_{-}(\xi) + F_{+}(\xi)$$
(3.6)

Also, the following analysis assumes that $\xi = \sigma + j\tau$.

Consider where $F_{\bullet}(\xi)$, the integral from 0 to ∞ , is analytic. By Theorem 1, the integral defining $F_{\bullet}(\xi)$ is analytic wherever it converges uniformly. To show uniform convergence, choose some $\tau_0 > \tau_-$. Consider now an x = T for T > R. It is readily apparent that, if $|f(x)| < Ae^{\tau_+ x} \ \forall x > R$ where A and R are positive real numbers, then the following

is tr

inde

Nov

regi that

of f

that is a

nor

the

co

of

is

$$\int_{R}^{T} f(x)e^{j(\sigma+j\tau)x}dx < \int_{R}^{T} Ae^{(\tau_{-}-\tau)x}e^{j\sigma x}dx = I_{1}$$

is true. Since e^{jex} has a magnitude of 1, and that $\tau > \tau_0 > \tau_-$, it is also obvious that

$$\int_{R}^{T} A e^{(\tau_{-}-\tau)x} e^{j\sigma x} dx < \int_{R}^{T} A e^{-(\tau_{0}-\tau_{-})x} dx = I_{2}$$

Now, integral I_2 exists independently of $\xi = \sigma + j\tau$ in the region $\tau > \tau_-$. Since this independent upper limit exists, the entire integral for $F_*(\xi)$ converges uniformly in that region; within that region then, $F_*(\xi)$ is analytic. This is shown in Figure 3.1a. Note that if f(x) is non-zero for x>0, and zero for x<0, then $F_*(\xi)$ is the Fourier transform of f(x). The required inversion contour on ξ must then lie within the region $\tau > \tau_-$.

A similar analysis can be conducted for $F_{-}(\xi)$. It takes but little effort to show that $F_{-}(\xi)$ is uniformly convergent for ξ in the region $\tau < \tau_{+}$. Within this region, $F_{-}(\xi)$ is analytic. This situation is shown in Figure 3.1b. It should be noted that if f(x) is non-zero for x < 0, and zero for x > 0, then $F_{+}(\xi)$ is the Fourier transform of f(x), and the appropriate inversion contour lies within the region $\tau < \tau_{+}$.

Returning now to the decomposition in (3.6) reveals that the regions of convergence for $F_{\bullet}(\xi)$ and $F_{-}(\xi)$ must overlap if $F(\xi)$ is to be the Fourier transform of a function of exponential order, as demonstrated in Figure 3.2. This overlap region is a strip in the complex ξ -plane, parallel to the real-axis, where

$$\tau_{-} < \tau < \tau_{+} \tag{3.7}$$

 $F(\xi)$ is analytic in this strip and the Fourier inversion contour lies within it. The Fourier transform of f(x) exists only if this common strip of convergence in ξ exists.

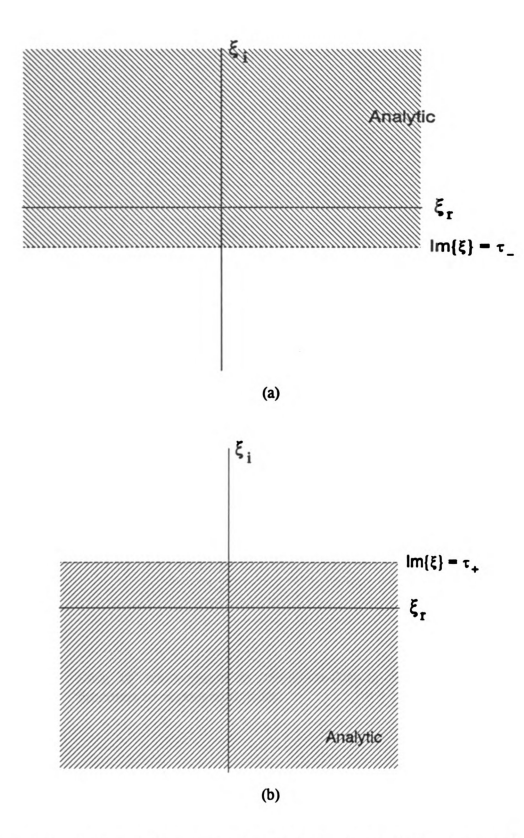


Figure 3.1 Regions of convergence for functions of exponential order. (a) Convergence in upper half-plane. (b) Convergence in lower half-plane.

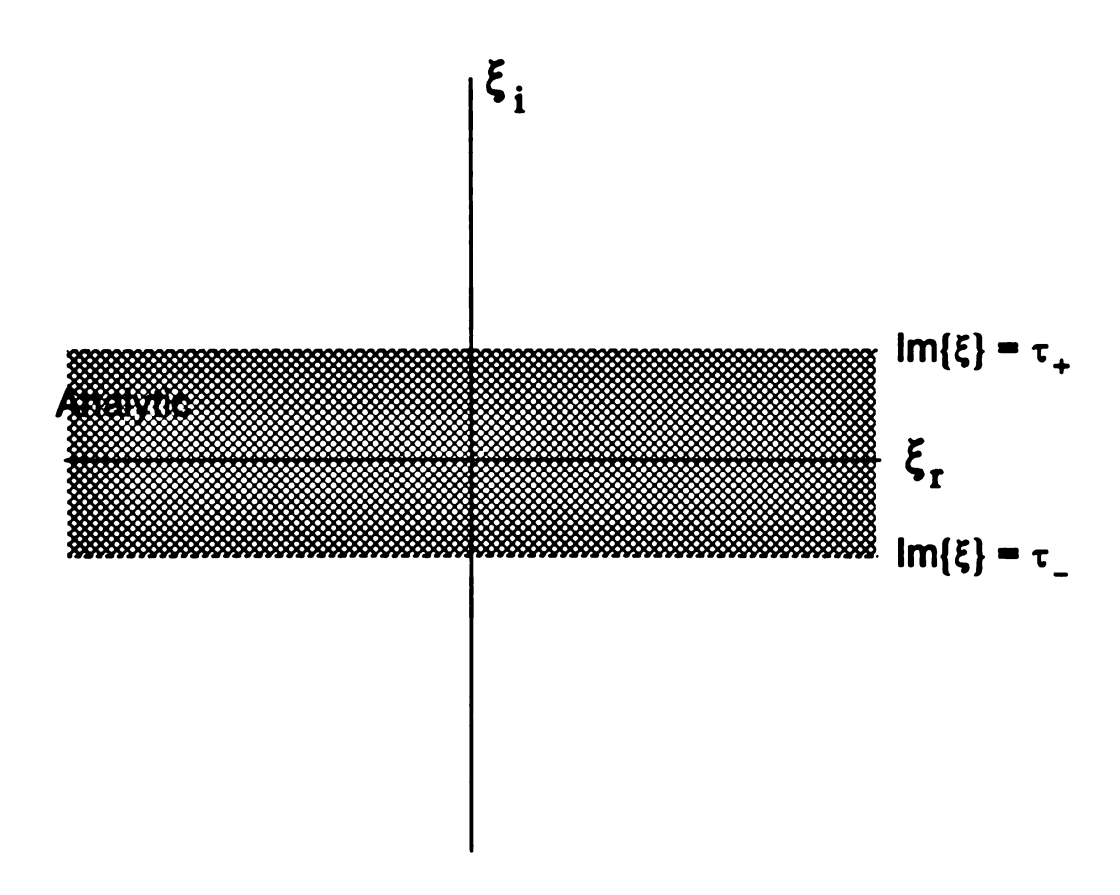


Figure 3.2 Strip of convergence in transform-domain for physically realizable functions of exponential order.

th m ex 01 T tr of As mentioned previously, the Fourier transform is used in the process of solving the Helmholtz equation. A typical solution to the Helmholtz equation takes the form

$$f(x) = e^{j\alpha|x|} \tag{3.8}$$

where $\alpha = \alpha_r + j\alpha_t$. For these solutions to be physically realizable over all space, they must be bounded as $|x| \to \infty$. This will be true if f(x) is either: (1) a decaying exponential function in x, requiring that

$$\alpha_i > 0 \tag{3.9}$$

or (2), an purely oscillatory function in x, which requires

$$\alpha_i = 0 \tag{3.10}$$

The effects of each of these cases on the region of convergence within the Fourier transform plane will be investigated.

For case (1), $f(x) \rightarrow e^{-\alpha_i x}$ as $x \rightarrow \infty$. Comparison with (3.5) reveals that $\tau_{-} = -\alpha_i$. As $x \rightarrow -\infty$, $f(x) \rightarrow e^{\alpha_i x}$; it is apparent that $\tau_{+} = \alpha_i$. The Fourier transform of (3.8) exists, and converges in a strip of finite width in ξ ,

$$-\alpha_i < \Im m\{\xi\} < \alpha_i \tag{3.11}$$

This convergence strip in particular contains the real axis of ξ , upon which the inverse transform to recover f(x) would be taken.

With case (2), $|f(x)| \to 1$ as $x \to \pm \infty$. The asymptotic behavior in case (2) can be viewed as the limiting case of a decaying exponential function, i.e.,

$$f(x) = \lim_{\nu \to 0} e^{j\alpha_{\nu}x} e^{-\nu|x|}, \quad \nu > 0$$

The region of convergence for case (2) is the limit of case (1) as $v = \alpha_i$ approaches zero. In this limit, the strip of convergence of the Fourier transform contains only the real axis, upon which the inversion contour lies.

Of course, it is possible for $\alpha_i < 0$ in (3.8), which leads to growing exponential functions in x; these are obviously not physically realizable as they are unbounded as $|x| \to \infty$. Another consequence is that there is no common strip of convergence in the Fourier transform plane, as $\tau_- > 0$ and $\tau_+ < 0$. This is demonstrated in Figure 3.3. By previous considerations, no Fourier transform for this type of exponential function exists.

The conditions for the existence of the Fourier transform in the complex-plane for functions of exponential order have been established. Assuming that these functions obey the standard requirements for Fourier transformable functions, as stated in Section 3.1.1, then the Fourier transform pair exists if the forward transform converges in a strip of finite width in the transform plane. This strip is parallel to the real axis, and must minimally include the real axis in the transform plane if the transformed function is to be physically realizable, that is, bounded at infinity. Finally, this strip of convergence is analytic and consequently, devoid of any singularity.

3.2 Green's Function Singularities

As observed at the beginning of this chapter, the transform-domain (axially-transformed) Green's function singularities have a complicated and interrelated dependence upon ξ and ζ . As the Green's functions are complex integrals, knowing the location and nature of the singularities is vital to guarantee an answer exists. Application of basic complex variables theory is sufficient to identify and determine the nature of the

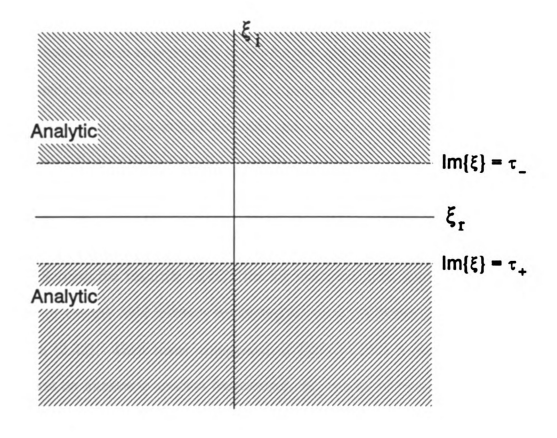


Figure 3.3 Regions of convergence for exponentially increasing functions.

singularities.

The Green's function is physically interpreted as the response of the background environment to a point source excitation. It is desired that the Green's function be a spectral quantity; that is, it must satisfy the radiation condition at infinity. Imposing the physical requirements upon the transform-domain Green's function determines the location of the singularities. Based on the development in Section 3.1, it is clear that one of those physical requirements is that the forward transform on x, used to determine the Green's function, must converge. This last requirement is the key to resolving and locating the singularities in both the axial and transverse transform domains unambiguously, regardless of the relationship between ξ and ζ .

3.2.1 Transverse wavenumber plane (complex ξ -plane) singularities

Solving the requisite EFIE's for the unknown axial transform-domain surface current or electric field involves computing the axial transform-domain dyadic Green's function (2.42). Each scalar component of $\vec{g}(\vec{\rho} \mid \vec{\rho}'; \zeta)$ is a one-dimensional inverse transform on transverse spectral frequency ξ , and can be represented generally as

$$g_{\alpha}^{\beta}(\vec{\rho}\,|\,\vec{\rho}';\zeta) = \frac{1}{2\pi} \int_{-\pi}^{\pi} \left[F_{\alpha}^{\beta}(p_i,y,y') e^{-j\xi x'} \right] e^{j\xi x} d\xi \tag{3.12}$$

where $p_i = \sqrt{\xi^2 + \zeta^2 - k_i^2}$ and $F_a^{\beta}(p_i, y, y')$ is the appropriate function involving background reflection coefficients and the exponential behavior in y. Since ξ is potentially a complex variable, pole and branch point singularities are possible; the locations of the singularities in the transverse spectral frequency plane (complex ξ -plane)

must be known to guarantee that the integrands are single-valued and non-singular, i.e, the integrals exist.

Specifically, the axially-transformed Green's functions are given by (2.45) and (2.46), namely

$$g^{p}(\vec{\rho} | \vec{\rho}'; \zeta) = \int_{-\infty}^{\infty} \frac{e^{j\xi(x-x')} e^{-p_{c}|y-y'|}}{4\pi p_{c}} d\xi$$
 (3.13)

$$\begin{cases}
g_t''(\vec{\rho} | \vec{\rho}'; \zeta) \\
g_n''(\vec{\rho} | \vec{\rho}'; \zeta) \\
g_c''(\vec{\rho} | \vec{\rho}'; \zeta)
\end{cases} = \int_{-\infty}^{\infty} \begin{cases}
R_t(\lambda) \\
R_n(\lambda) \\
C(\lambda)
\end{cases} \frac{e^{j\xi(x-x')}e^{-p_c(y+y')}}{4\pi p_c} d\xi \tag{3.14}$$

Reflection coefficients R_l , R_n , and C relate the background environment effects, including the surface-wave behavior, through wavenumber parameter $p_l = \sqrt{\xi^2 + \zeta^2 - k_l^2}$ in each layer, where $l = c_n f$, s (denoting cover, film or substrate respectively). These coefficients are detailed in Appendix B; for reference purposes, the coefficients for the conductor-/film/cover background are reproduced here as

$$R_{t}(\lambda) = \frac{p_{c} - p_{f} \coth(p_{f} t)}{Z^{h}(\lambda)}$$

$$R_{n}(\lambda) = \frac{N_{fc}^{2} p_{c} - p_{f} \tanh(p_{f} t)}{Z^{e}(\lambda)}$$

$$C(\lambda) = \frac{2(N_{fc}^{2} - 1) p_{c}}{Z^{h}(\lambda) Z^{e}(\lambda)}$$
(3.15)

where

$$Z^{e}(\lambda) = N_{fc}^{2} p_{c} + p_{f} \tanh(p_{f}t)$$

$$Z^{h}(\lambda) = p_{c} + p_{f} \coth(p_{f}t).$$
(3.16)

The following development assumes small losses in the background media, namely, $k_i = k_{i,j} + jk_{i,j}$, $k_{i,j} < 0$.

The wavenumber parameters p_l are multi-valued functions of complex spectral frequency ξ , implying the existence of branch points and branch cuts in the complex ξ -plane. The wavenumber parameters become multi-valued around the point where $Arg\{p_l\} = 0$, or where $p_l^2 = \xi^2 + \zeta^2 - k_l^2 = 0$. A branch-point singularity in the complex ξ -plane is thus located at

$$\xi_{kl} = \sqrt{k_l^2 - \zeta^2} \tag{3.17}$$

It is obvious by inspection of equation (3.17) that the branch point locations in the complex ξ -plane directly depend upon the value of axial wavenumber ζ and migrate as ζ varies; furthermore, the branch point locations are related to ζ through a square-root in the complex ζ -plane. This is a very important observation, and will be dealt with later.

A branch cut emanating from the branch point ξ_{N} in the complex ξ -plane is necessary to define a single-valued function. This branch cut indicates the joining of Riemann sheets, upon which the wavenumber parameters are single-valued. Mathematically, any arbitrary curve in the complex ξ -plane approaching a complex ξ_{N} will serve to render the wavenumber parameters single-valued. However, the Green's functions were developed under the assumption that $\Re\{p_i\} > 0$; this must be enforced if the Green's functions are to have any physical meaning. Enforcing spectral behavior on the Green's function results in the more restrictive criteria of

$$\Re\{p_l\} = \Re\{\sqrt{\xi^2 - \xi_M^2}\} > 0$$
 (3.18)

being used to define branch cuts in the complex ξ -plane and enforce spectral behavior on the top Riemann sheet upon which the inversion contour must lie. This is the

equivalent of enforcing the Sommerfeld radiation condition on y, that is, the Green's functions vanish as $|y| \rightarrow 0$. Criteria (3.18) implies that

$$-\frac{\pi}{2} < Arg \left\{ \sqrt{\xi^2 - \xi_{kl}^2} \right\} \le \frac{\pi}{2}. \tag{3.19}$$

for the top Riemann sheet of the complex ξ -plane. The branch cut is the limiting case of inequality (3.19), where $\Re \{p_l\} = 0$; this results in the relations

$$\Re\{\xi^{2} - \xi_{bl}^{2}\} = (\xi_{r}^{2} - \xi_{bl,r}^{2}) + (\xi_{bl,i}^{2} - \xi_{i}^{2}) < 0$$

$$\Im\{\xi^{2} - \xi_{bl}^{2}\} = \xi_{r}\xi_{i} - \xi_{bl,r}\xi_{bl,i} = 0$$
(3.20)

(the negative real axis in the complex ξ^2 -plane) which lead to a hyperbolic branch cut in the complex ξ -plane, initiating at the branch points of $\xi = \pm \xi_M$, and extending asymptotically to infinity along the imaginary axis, such that

$$\xi = \frac{\Im m\{\xi_{bl}^2\}}{2\xi_i} + j\xi_i \; ; \quad |\xi_i| > |\Im m\{\xi_{bl}\}| \; . \tag{3.21}$$

Each wavenumber parameter p_l (where $l=c_s f$ and s) obeys a branch cut of this form. But, since the branch cut emanates from the branch point ξ_{kl} , they are also dependent upon ζ in the same manner as the branch point. This is illustrated in Figure 3.4.

Inspection of the coefficients R_i , R_n , and C, as given in (3.15)-(3.16), reveals that they are even with respect to p_f , the wavenumber parameter for the film layer. Consequently, the branch cut associated with p_f is removable. This behavior also occurs in the substrate/film/cover background as well; it generalizes for an N-layer structure, where the branch cuts for all interior layers are removable [44]. It should also be observed that the principal Green's function, as given in (3.13), implicates only the branch cut associated with the cover layer.

There are also pole singularities in the complex ξ -plane where the denominators in the reflection coefficients vanish. These denominators are functions of the wavenumber parameter p_i which itself must obey the branch cuts defined in (3.21). As a result, location of any pole singularity in the complex ξ -plane is implicitly dependent upon the value of ζ . Observations in Appendix B reveal that the reflection coefficient singularities are physically associated with the (possibly many) surface-wave modes λ_p^n of the background structure. Consequently, the pole locations are seen to be explicitly dependent upon the value of ζ , since

$$\xi_p^n = \sqrt{(\lambda_p^n)^2 - \zeta^2} \tag{3.22}$$

As observed with the branch points in (3.17), this pole location in the complex ξ -plane is dependent upon ζ through a square root. There can be any number of pole singularities depending upon the background structure; for clarity, only one is shown in Figure 3.4. This is the situation for an electrically-thin film layer in a substrate/film-/cover environment.

3.2.2 Considerations of forward transform convergence

Figure 3.4 shows the location of the complex ξ -plane singularities, save for the removable branch cut for p_f . The singularities are fixed for the integration over spatial frequency ξ , but will migrate as axial wavenumber ζ varies, denoted by the arrows in Figure 3.4. Furthermore, the sign convention for the square root on ζ is chosen to locate poles and branch points in the lower half of the complex ξ -plane, that is

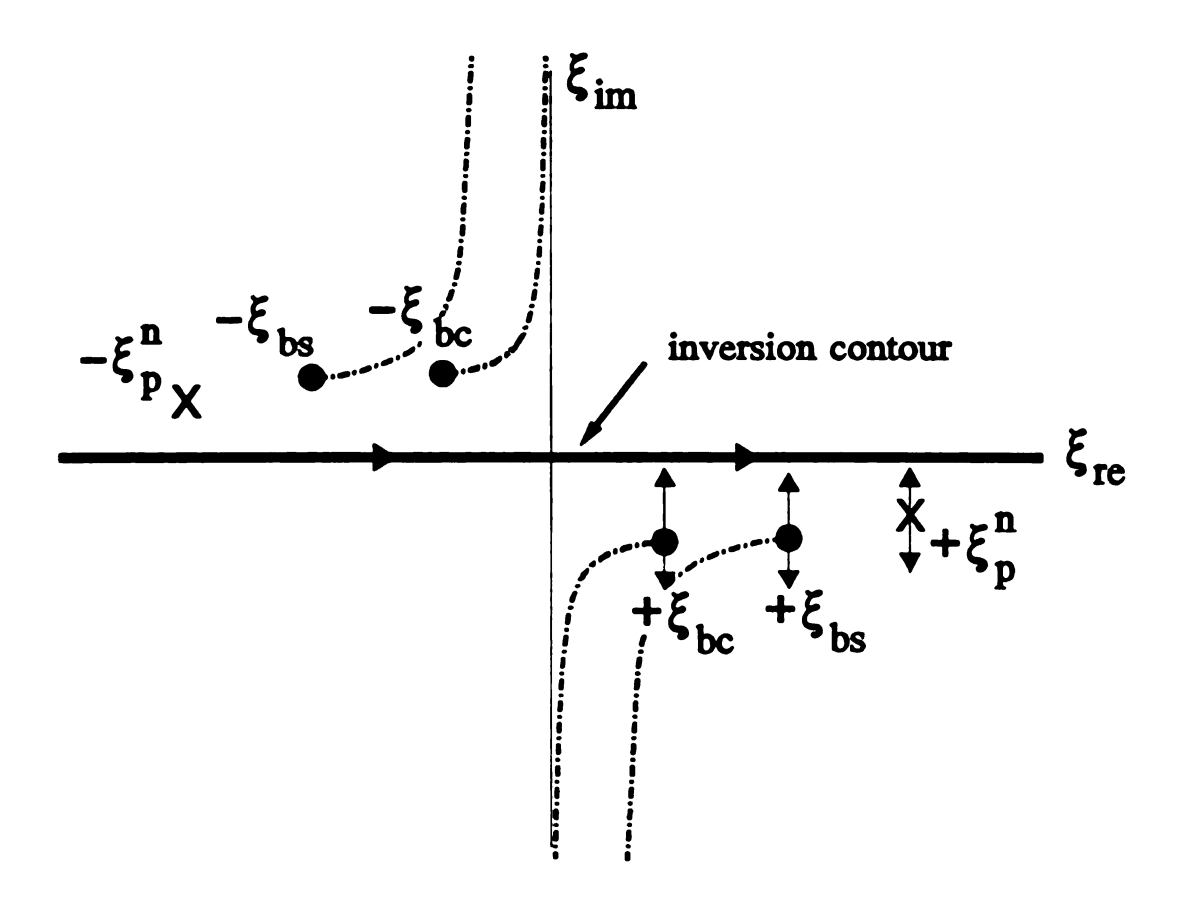


Figure 3.4 Singularity locations in the transverse-transform domain (complex ξ -plane).

$$\xi_{M} = -jX_{M}, \quad X_{M} = \sqrt{\zeta^{2} - k_{l}^{2}}$$

$$\xi_{p}^{n} = -jX_{p}^{n}, \quad X_{p}^{n} = \sqrt{\zeta^{2} - (\lambda_{p}^{n})^{2}}$$
(3.23)

It is obvious from (3.23) that branch cuts in the complex ζ -plane are necessary if ζ is complex valued; it is not obvious how the branch cuts are to be chosen.

As stated previously, a spectral representation for the Green's functions (and the subsequent waveguide fields) is desired. The Green's functions are solutions to the Helmholtz equation with a point source excitation and *must* vanish as the observation point becomes distant; a spectral representation for the Green's functions obeys that boundary condition. From the analysis in Section 3.1, the forward Fourier transform on x converges within a horizontal strip in the complex ξ -plane. Also, the Fourier transform is regular in this strip. Since the strip of convergence is regular, no singularities can reside within it; the strip width is thus limited by the singularity nearest the real axis in the complex ξ -plane, as shown in Figure 3.5. It is obvious that as the axial wavenumber ζ varies, the ξ -plane singularities migrate, possibly narrowing or widening the necessary strip of convergence. Yet, regardless of the ξ -plane singularity location, the analysis requires that the forward transform converge. This transform is to represent a spectral Green's function; the forward transform on x must converge in a strip minimally containing the real axis in the complex ξ -plane.

This requirement of convergence of the forward Fourier transform in x restricts the migration of the complex ξ -plane singularities. As long as any ξ -plane singularity does not migrate across the real axis, the forward transform on x converges and defines a spectral mode. The transform converges even in the case where the ξ -plane singularities reside on the real-axis, since traditional real-line Fourier theory allows for

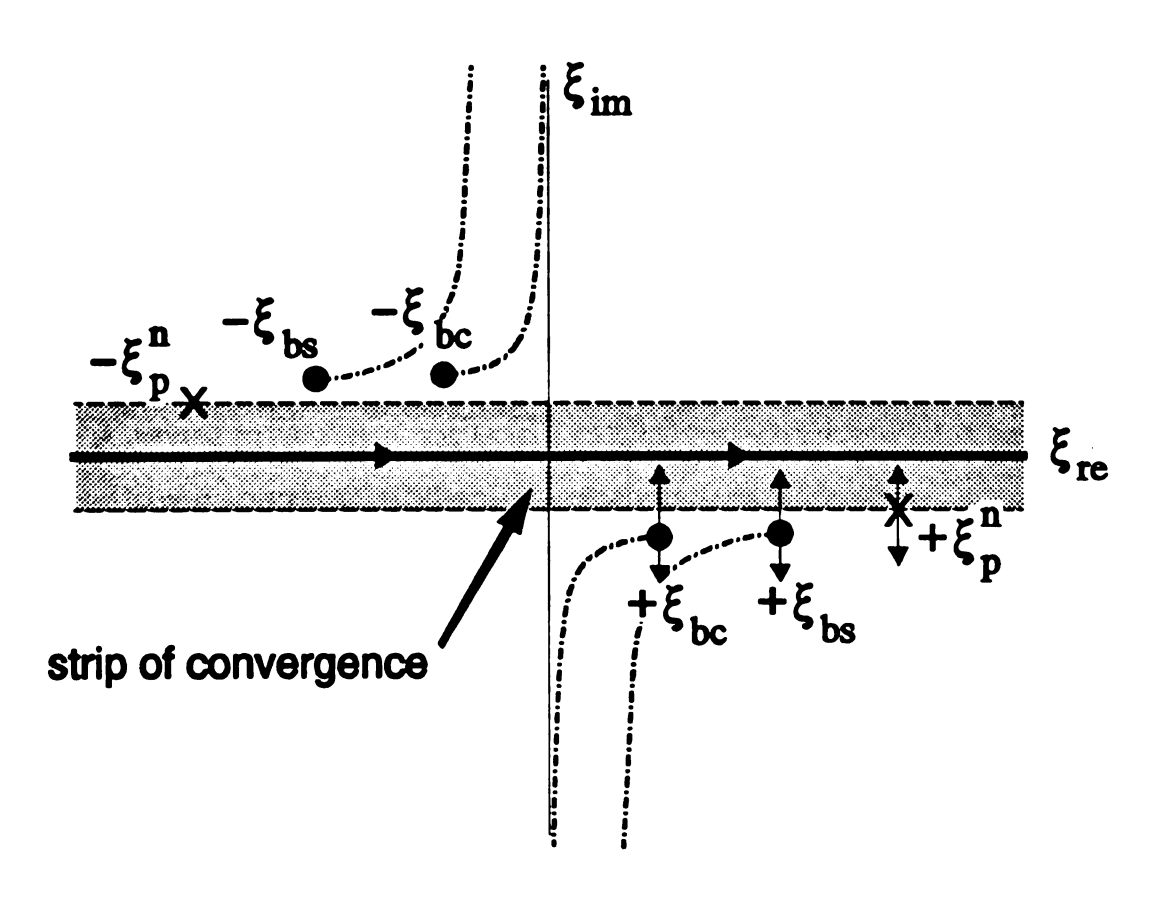


Figure 3.5 Strip of convergence in complex ξ -plane for forward transform on x. Arrows denote singularity migration directions.

this possibility. Obviously, none of the ξ -plane singularities can migrate across the real axis in the ξ -plane; this is the criterion that defines branch cuts in the complex ζ -plane.

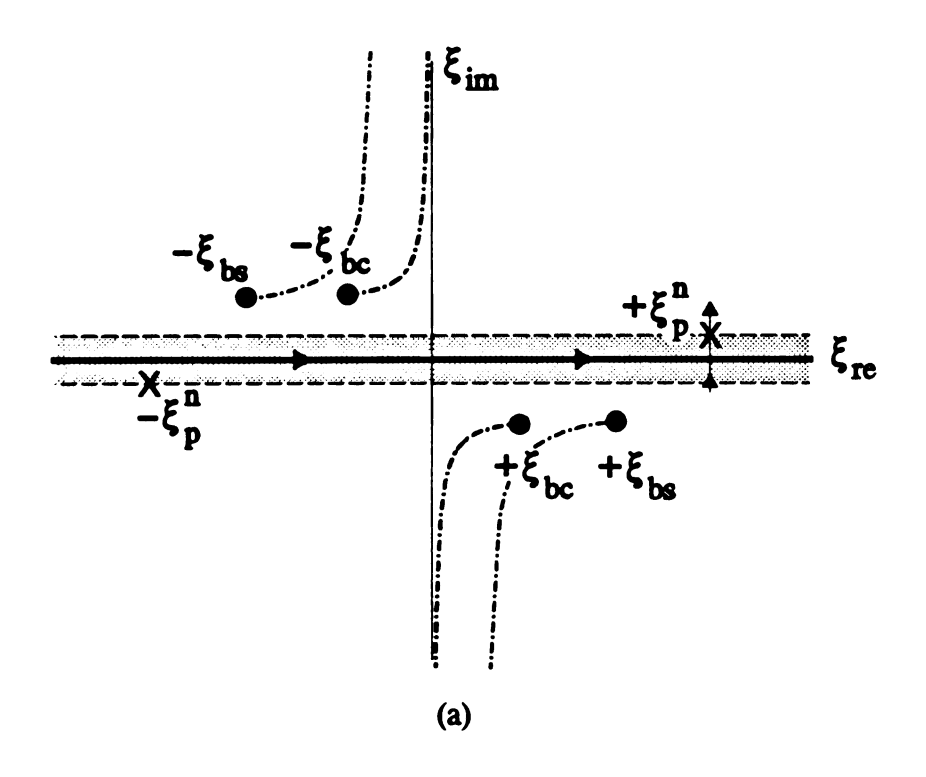
What can occur if a ξ -plane singularity migrates across the real axis when ξ varies continuously (no discontinuous steps). The first possibility is that a strip of analyticity in the ξ -plane, which includes the real-axis as an inversion contour, can be determined, as seen in Figure 3.6a. For this case, the singularity passes from below the inversion contour to above the inversion contour; the inverse transform changes discontinuously while ξ changes smoothly. This is undesirable; when considering the Green's functions, this is an equivalent to the physical problem changing discontinuously [45].

A second possibility arises by not passing through the inversion contour on the real axis in the complex ξ -plane. Viewing the forward transform on x in the sense of the decomposition (3.6) leads to Figure 3.6b; in which the Fourier integral $F_{\bullet}(\xi)$ converges for all $\mathfrak{Sm}\{\xi\} > \mathfrak{Sm}\{+\xi_{sing}\}$, while $F_{-}(\xi)$ is convergent for all $\mathfrak{Sm}\{\xi\} < \mathfrak{Sm}\{-\xi_{sing}\}$. There can be no common strip in which the Fourier transform (sum of $F_{\bullet}(\xi)$ and $F_{-}(\xi)$) converges; in this case, a spectral representation cannot be obtained.

3.2.3 Axial transform-domain (complex \zeta-plane) restrictions

Considering the definition for pole and branch point singularities in (3.23), it is observed that these singularities must remain in the lower-half of the complex ξ -plane, regardless of the value that ζ takes. Based on that definition, then, it is obvious that

$$\Re e\{X_{\nu}\} > 0 \tag{3.24}$$



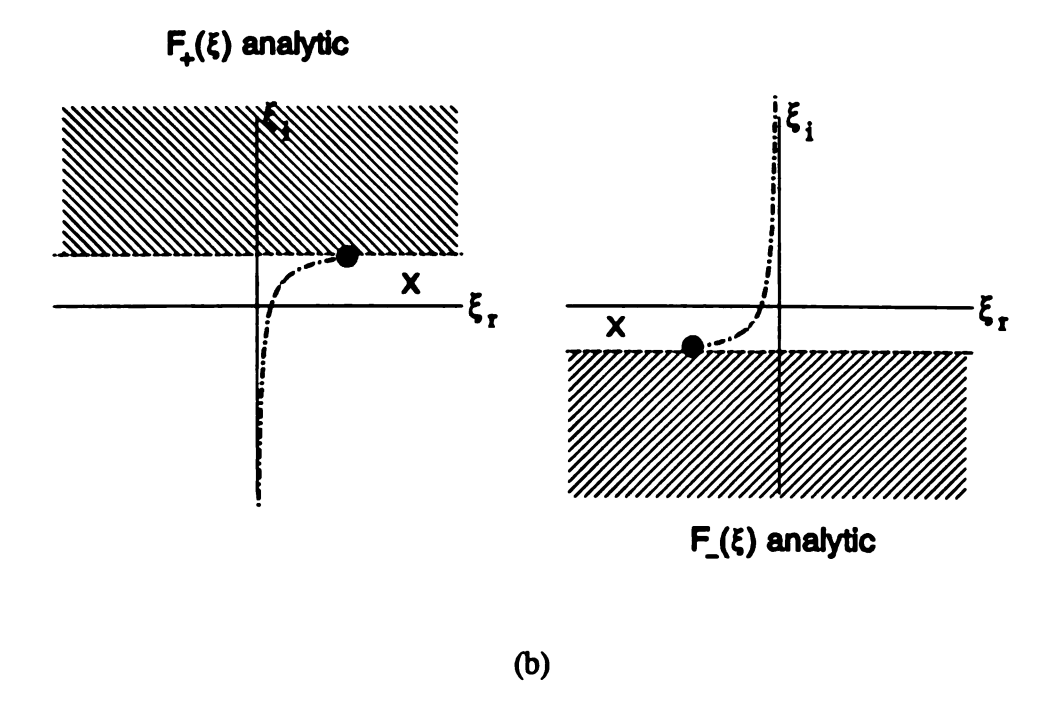


Figure 3.6 (a) Migration of a ξ -plane singularity across real-axis through contour of integration. (b) Migration of a ξ -plane singularity across real-axis, treated correctly.

is required to restrict the branch points in the complex ξ -plane to the lower half-plane;

$$\Re e\{X_n^n\} > 0 \tag{3.25}$$

is required to restrict the pole singularities in the ξ -plane to the lower half-plane. Since X_{kl} and X_{p}^{n} are multi-valued functions of ζ , these requirements lead to branch cuts in the axial transform plane. Inspection of (3.23) indicates that branch points in the complex ζ -plane occur at $\zeta = \pm k_{l}$ and at $\zeta = \pm \lambda_{p}^{n}$. Requirements (3.24) and (3.25) are similar to the requirement of (3.18); consequently, little work is necessary to show that the hyperbolic branch cut of

$$\zeta_{l} = \frac{Im\{k_{l}^{2}\}}{2\zeta_{i}} + j\zeta_{i}; \quad |\zeta_{l}| > |Im\{k_{l}\}|$$
 (3.26)

restricts the complex ξ -plane branch points (ξ_{H}) appropriately, while the hyperbolic branch cut

$$\zeta_n = \frac{Im\{(\lambda_p^n)^2\}}{2\zeta_i} + j\zeta_i; \quad |\zeta_i| > |Im\{\lambda_p^n\}|$$
 (3.27)

restricts the complex ξ -plane poles (ξ_p^n). This is illustrated in Figure 3.7, where only one branch cut arising from the complex ξ -plane pole singularities is shown for clarity (case depicted for a thin-film background environment).

It is curious to note that while the Green's function possesses both pole and branch point singularities in the transverse spectral frequency (ξ) plane, it possesses only branch point singularities in the axial wavenumber (ζ) plane. It should be explicitly observed that a *pole* in the transverse spectral frequency plane (complex ξ -plane) leads to a *branch point and branch cut* in the axial transform-domain (complex ζ -plane). This

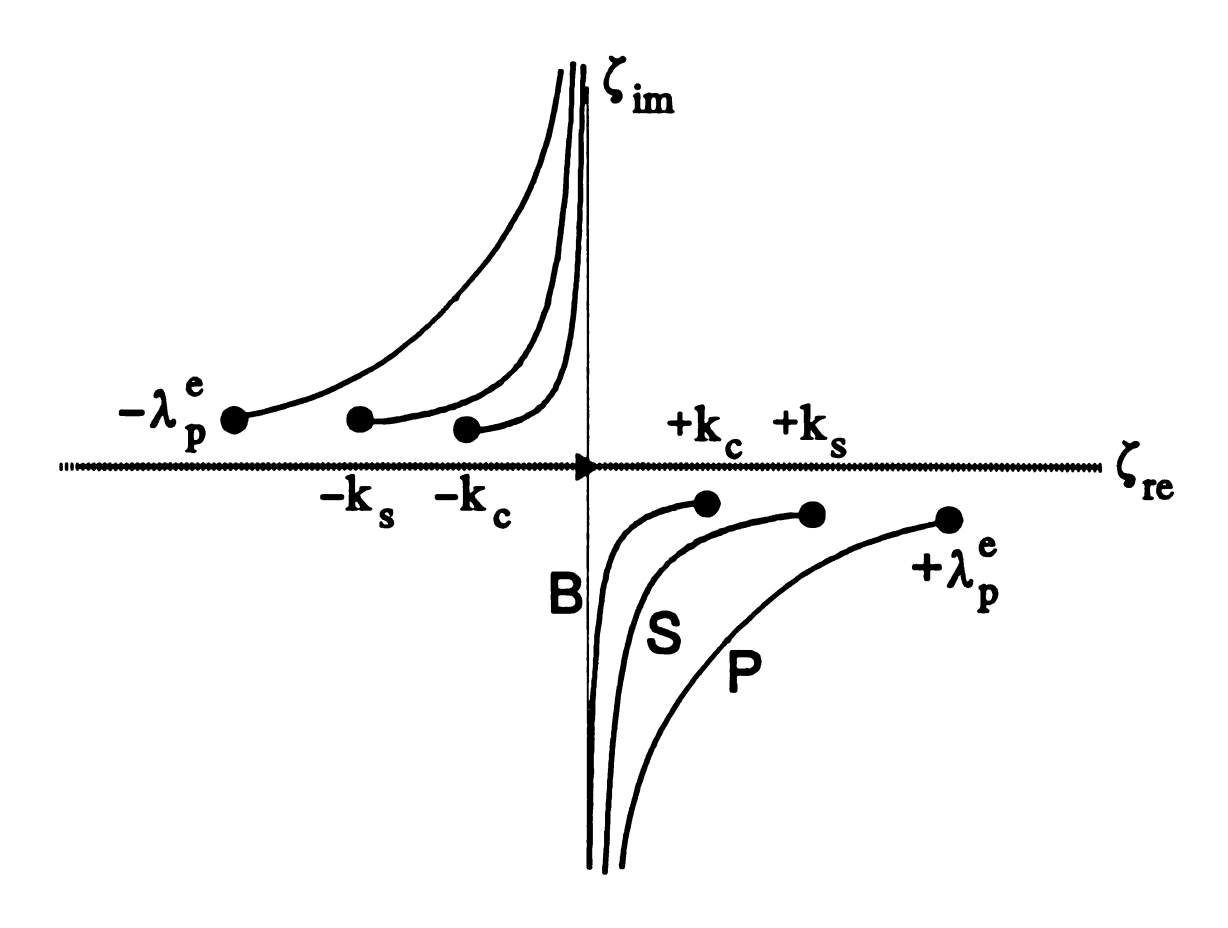


Figure 3.7 Branch cuts in axial-transform plane (complex ζ -plane) necessary to maintain convergence of forward Fourier transform on x.

is a new observation, and difficult to accept at face value; only when the propagationmode spectrum is recognized in the next section does this observation make sense.

By defining branch cuts in the axial transform plane (Figure 3.7) as per (3.26) and (3.27), the locations of the singularities of the Green's function in the transverse spectral frequency plane are fixed, and their migration is restricted such that the forward transform on x converges. The axial transform-plane branch cuts emanating from $\zeta = \pm k_e$, the wavenumber in the cover, locates transverse spectral frequency branch point ξ_{ke} ; similarly for the branch cuts from $\zeta = \pm k_g$. If the substrate becomes a perfect conductor $(n_g \to -j\infty)$, this branch point is unnecessary. The axial transform-plane branch cuts emanating from $\zeta = \pm \lambda_g^n$ locate and restrict the transverse spectral frequency poles. These branch cuts are associated with the surface-wave modes on the background structure; a branch cut is needed for each individual surface-wave mode. Obviously, if no surface-wave behavior in the background structure is possible, none of those branch cuts are necessary. Finally, these branch cuts define a multi-sheeted Riemann surface in the axial transform-domain, separating the spectral (top Riemann sheet) sheet from the non-spectral (all other Riemann sheets) sheets.

3.3 Propagation-Mode Spectrum for Open-Boundary Waveguides

Solutions to the axial transform domain EFIE (2.40) can now be obtained, since the axial transform-plane branch cuts guarantee that the Green's function comprising the kernel of (2.40) exists. For convenience sake, the EFIE is reproduced here

$$\vec{e}(\vec{\rho}) - \int_{CS} \vec{g}^{e}(\vec{\rho} | \vec{\rho}'; \zeta) \cdot \frac{\delta n_{c}^{2}(\vec{\rho}') \vec{e}(\vec{\rho}'; \zeta)}{n_{c}^{2}} ds' = \vec{e}^{i}(\vec{\rho}; \zeta), \quad ... \forall \vec{\rho} \in CS \quad (3.28)$$

using the transform-domain electric dyadic Green's function

$$\ddot{\mathbf{g}}^{\bullet}(\vec{\rho}\,|\vec{\rho}';\zeta) = (k_e^2 + \tilde{\nabla}\tilde{\nabla}\cdot)\ddot{\mathbf{g}}(\vec{\rho}\,|\vec{\rho}';\zeta) + \tilde{\ell}\delta(\vec{\rho}-\vec{\rho}')$$

where $\xi(\vec{\rho}|\vec{\rho}';\zeta)$ is defined by (2.42)-(2.46). The space-domain electric field is recovered from the solutions of EFIE (2.40) via the application of the inverse Fourier transform on axial wavenumber ζ , that is,

$$\vec{E}(\vec{r}) = \frac{1}{2\pi} \int_{-\infty}^{\infty} \vec{e}(\vec{\rho}, \zeta) e^{j\zeta z} d\zeta$$
 (3.29)

A number of approaches are available to evaluate the inverse transform (3.29). A pure numerical solution would utilize a fast Fourier transform (FFT) on the real-line inversion contour in the complex ζ -plane to obtain the total space-domain field at each spatial point of interest. This approach offers no insight into the modal spectrum or the waveguide physics. As spatial coordinate z grows large, the complex exponential becomes very oscillatory, and amenable to asymptotic evaluation techniques like the method of steepest descents. This approach, detailed in the next section, is not a modal expansion but does offer insights into the waveguide physics.

The inverse transform can also be evaluated by contour deformation into the complex ζ -plane; this is a singularity expansion of the waveguide field. This singularity expansion determines the entire propagation-mode spectrum of the device; the bound hybrid guided-wave modes are associated with ζ -plane poles, while the continuous radiation spectrum field is associated with the ζ -plane branch cuts.

That the transform-domain field $\vec{e}(\vec{\rho},\zeta)$ can possess a finite number of isolated singularities (poles of order m) is not difficult to accept. Yet, any branch cuts within the axial transform-plane arise only from the Green's functions. If these complex ζ -plane

branch cuts are to be used in a modal expansion, then $\vec{e}(\vec{\rho}, \zeta)$ should share the branch points of the Green's functions. This is intuitively obvious when considering the physical interpretation of the Green's functions as a point source response within the layered background environment. A waveguide field $\vec{e}(\vec{\rho}, \zeta)$ in this environment is thus assembled as the superposition of equivalent point source responses; naturally, this field shares the branch points of the Green's functions. This can also be demonstrated by an indirect proof [46].

The details of performing the inverse transform (3.29) by contour closure are now presented. Without loss of generality, a space-domain current source can be decomposed as $\vec{J}^e = \vec{J}_o(\vec{\rho}) \delta(z-z')$, which becomes $\vec{J}_o(\vec{\rho}) e^{-j\zeta z'}$ in the transform-domain. It is apparent that the Fourier kernel in (3.29) takes the form $e^{j\zeta(z-z')}$. Closure in the ζ -plane will be performed such that the integrand vanishes upon the contour at infinity. This implies closure in the lower half-plane for z < z' and the upper half-plane for z > z'; the integrand and complex exponential vanish on the infinite semicircle by consideration of Jordan's lemma. This closure is shown in Figure 3.8 for the case of z < z'.

Application of Cauchy's residue theorem states that the closed contour integral of an analytic function is proportional to the sum of the residues at the enclosed pole singularities, namely,

$$\oint_C \vec{e}(\vec{\rho},\zeta)e^{j\zeta z}d\zeta = 2\pi j\sum_{\mathbf{m}} \operatorname{Res}_{\mathbf{m}} \{\vec{e}(\vec{\rho},\zeta)e^{j\zeta z}\}$$
 (3.30)

This closed contour is the sum of the real-line inversion contour, the contour at infinity, and all the deformed contours around the branch cuts; consequently, Cauchy's residue theorem allows the inverse transform in (3.29) to be written as

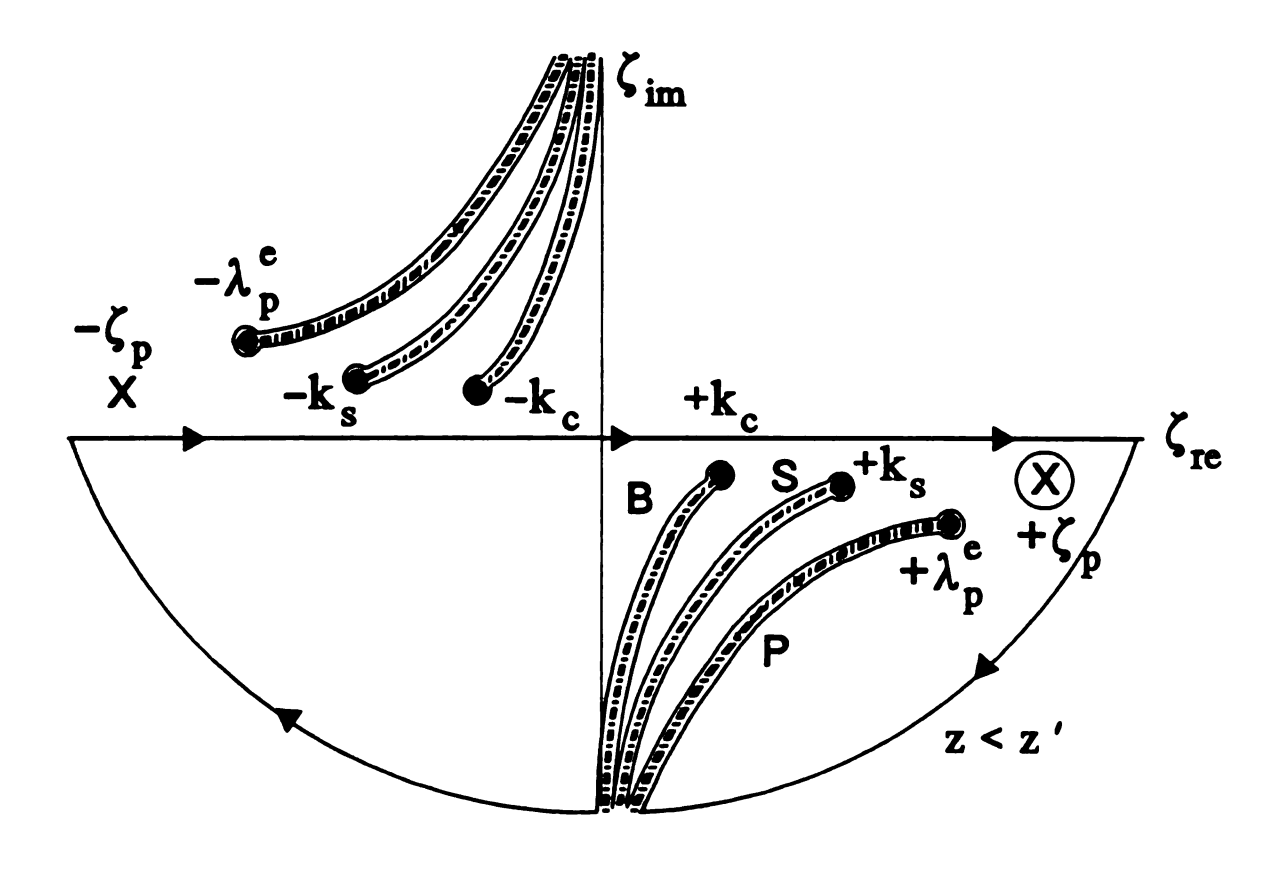


Figure 3.8 Contour deformation in complex ζ -plane used to identify the propagation-mode spectrum. Closure shown for z < z'.

$$\vec{E}(\vec{r}) = j \sum_{m} \text{Res}_{m} \{ \vec{e}(\vec{\rho}, \zeta) e^{j\zeta z} \} - \frac{1}{2\pi} \int_{C_{nm}} \vec{e}(\vec{\rho}, \zeta) e^{j\zeta z} d\zeta$$
 (3.31)

where the contribution from the contour at infinity vanishes by Jordan's Lemma. For the case of Figure 3.8, the space-domain field's singularity expansion is

$$\vec{E}(\vec{r}) = \mp j \sum_{n=0}^{N} \vec{e}_{res}(\vec{\rho}, \pm \zeta_{p}^{n}) e^{-j\zeta_{p}^{n}|z-z'|} - \frac{1}{2\pi} \int_{C_{g}} \vec{e}(\vec{\rho}, \zeta) e^{-j\zeta|z-z'|} d\zeta$$

$$- \frac{1}{2\pi} \int_{C_{p}} \vec{e}(\vec{\rho}, \zeta) e^{-j\zeta|z-z'|} d\zeta - \frac{1}{2\pi} \int_{C_{g}} \vec{e}(\vec{\rho}, \zeta) e^{-j\zeta|z-z'|} d\zeta$$
(3.32)

3.3.1 Bound modes

The pole singularities of \vec{e} comprise the discrete spectrum of the waveguide field.

The axial transform-domain field \vec{e} takes on the behavior

$$\vec{e}(\vec{\rho},\zeta) = \frac{a_p \vec{e}_{-n}(\vec{\rho},\zeta_p)}{(\zeta - \zeta_p)^n}$$
 (3.33)

for ζ very near a pole of order m. At this time, assume m=1; under this assumption, \vec{e}_{-1} is the residue, denoted \vec{e}_{res} . Substitution of this field into the EFIE results in

$$\frac{a_p}{(\zeta - \zeta_p)} \left[\vec{e}_{res}(\vec{\rho}; \zeta) - \int_{CS} \frac{\delta n^2(\vec{\rho}')}{n_c^2} \vec{g}^{\circ}(\vec{\rho} | \vec{\rho}'; \zeta) \cdot \vec{e}_{res}(\vec{\rho}'; \zeta) ds' \right] = \vec{e}^{i}(\vec{\rho}, \zeta) \quad (3.34)$$

The impressed field $\vec{e}^i(\vec{\rho}, \zeta)$ supported by independent source currents is regular for $\zeta = \zeta_p$, the pole of the waveguide field. The left-hand-side of (3.34) must be indeterminate if the EFIE is to be satisfied; the bracketed quantity in (3.34) must vanish for $\zeta = \zeta_p$. In this situation, \vec{e}_{res} satisfies the homogeneous form of EFIE (3.28),

$$\vec{\mathbf{e}}_{res}(\vec{\rho};\zeta_p) - \int_{CS} \frac{\delta n^2(\vec{\rho}')}{n_c^2} \, \vec{\mathbf{g}}^{\,\circ}(\vec{\rho} \,|\, \vec{\rho}';\zeta_p) \cdot \vec{\mathbf{e}}_{res}(\vec{\rho}';\zeta_p) \, ds' = 0 \qquad (3.35)$$

It is obvious that for $\zeta = \zeta_p$, the residue field is a natural mode of the waveguide.

Any poles used in the modal expansion of the waveguide fields are located on the top sheet of the axial transform plane. On the top sheet, all modes are spectral and satisfy the radiation condition; this implies that the natural-mode fields exponentially decay outside the waveguide. It has thus been established that poles in the transform-domain waveguide field lead to the guided-wave modes of the open-boundary waveguide.

If the electric field pole is of a higher order, the previous analysis does not arrive at the correct residue field for that pole. An iterative technique for poles of higher order is presented in [3.46]; also presented is a methodology for determining the order of the pole. This is not necessary for any waveguiding problem in this dissertation.

The field excited on the waveguide can be expanded in terms of the hybrid guided-wave modes [47]. The excitation coefficient is

$$a_{p} = \frac{-1}{C_{p}} \int_{CS} \frac{\delta n^{2}(\vec{\rho}')}{n_{c}^{2}} \vec{e}_{p}(\vec{\rho}, \zeta) \cdot \vec{e}^{i}(\vec{\rho}, \zeta) ds \qquad (3.36)$$

an overlap integral of the impressed field with the guided-wave mode $\vec{e}_p(\vec{\rho}, \zeta_p)$ weighted by an appropriate normalization coefficient given by

$$C_{p} = \int_{CS} \int_{CS} \left(\frac{\delta n^{2}(\vec{\rho}')}{n_{c}^{2}} \vec{e}_{p}(\vec{\rho}, \zeta_{p}) \right) \cdot \frac{\partial}{\partial \zeta} \vec{g}^{o}(\vec{\rho} | \vec{\rho}', \zeta) \bigg|_{-\zeta_{p}} \cdot \left(\frac{\delta n^{2}(\vec{\rho}')}{n_{c}^{2}} \vec{e}_{p}(\vec{\rho}', \zeta_{p}) \right) ds ds' \quad (3.37)$$

Details of this development can be found in [16] or [48].

Finally, it should be noted that the transform-domain field $\vec{e}(\vec{\rho}, \zeta)$ has poles that occur on the other non-spectral Riemann sheets. This possibility, and the leaky-wave modes associated with these non-spectral poles, will be discussed in Section 3.5.

3.3.2 Continuous radiation spectrum

The sum of the contour integrations along the branch cuts comprises the total continuous spectrum of the waveguide radiation field. The transform-domain waveguide field at any point along the branch cut is the solution of EFIE (3.28) for a given excitation.

To recognize that the continuous superposition along the branch cut determines a radiation spectrum, consider that these branch cuts represent the limiting values of acceptable f defining a spectral mode. Recall that a spectral mode satisfies the radiation condition at infinity. In this limiting case, the behavior at infinity is bounded and oscillatory but non-zero; this is obviously a radiation spectral component. As observed by Shevchenko [49], the superposition of these modes vanishes at infinity; hence, this superposition of solutions along the branch cut represents the radiation field of the open-boundary waveguide.

There are a number of branch cuts defined in the axial transform plane. Up to two of these cuts are associated with the wavenumbers of the semi-infinite in y background layers (cover and substrate), and control the spectral behavior in those layers via control of the complex ξ -plane branch point singularity migration. For those two branch cuts, the limiting acceptable spectral behavior is bounded oscillation in y. Consequently, the branch cut from $\zeta = k_c$ defines the cover radiation spectrum while the branch cut from $\zeta = k_c$ defines the substrate radiation spectrum.

The remaining branch cuts in the transform-domain control the spectral behavior of the background surface-wave modes by controlling the location of the complex ξ -plane pole singularities. A branch cut is needed for each surface wave mode the waveguide

can support. The radiation spectrum associated with these branch cuts is called a transverse radiation spectrum; as it arises from the existence of surface wave modes, it will possess the same field structure. These transverse radiation modes thus are exponentially decaying in y like surface waves but possess the characteristic radiation-mode standing-wave pattern in x. This transverse-radiation regime is believed to constitute the observation of a new physical wave phenomena.

The continuous spectrum solution is directly dependent upon the impressed electric field. It is desirable to not re-evaluate the forced EFIE in (3.28) for each separate excitation. A conceptual dyadic Green's function of the radiation modes can be advanced to construct a formulation for the radiation field which is useful for arbitrary excitation.

Let $\vec{j}^i(\vec{\rho}_0) = \hat{x}_e \delta(\vec{\rho} - \vec{\rho}_0)$, a unit-amplitude point source excitation current at $\vec{\rho}_0$ directed along \hat{x}_e restricted to spectral frequency ζ along any of the branch cuts. This excitation supports an impressed field upon the waveguide of $-j(\eta_c/k_c)\vec{g}^e(\vec{\rho}|\vec{\rho}_0;\zeta)\cdot\hat{x}_e$, which in turn induces a elementary spectral field component $\vec{E}_e(\vec{\rho}|\vec{\rho}_0;\zeta)$ which satisfies

$$\vec{E}_{\alpha}(\vec{\rho} \mid \vec{\rho}_{0}; \zeta) - \int_{CS} \frac{\delta n^{2}(\vec{\rho}')}{n_{c}^{2}} \vec{g}^{\circ}(\vec{\rho} \mid \vec{\rho}'; \zeta) \cdot \vec{E}_{\alpha}(\vec{\rho}' \mid \vec{\rho}_{0}) ds' = \frac{-j\eta_{c}}{k_{c}} \vec{g}^{\circ}(\vec{\rho} \mid \vec{\rho}_{0}; \zeta) \cdot \hat{x}_{\alpha} \quad (3.38)$$

If a radiation spectral dyad is defined as

$$\vec{E}(\vec{\rho}'|\vec{\rho}_0;\zeta) = \sum_{\alpha=x,y,z} \vec{E}_{\alpha}(\vec{\rho}'|\vec{\rho}_0)\hat{x}_{\alpha}$$
 (3.39)

then the radiation field is the continuous superposition of all spectral field components

$$\vec{\mathbf{E}}_{\mathbf{R}}(\vec{\rho},z) = \frac{-1}{2\pi} \int_{C_{RAD}} d\zeta \, e^{j\zeta z} \int_{CS} \left[\sum_{\alpha = x,y,z} \vec{\mathbf{E}}_{\zeta,\alpha}(\vec{\rho} \,|\, \vec{\rho}^{\,\prime}) \right] \cdot \vec{\mathbf{j}}^{\,i}(\vec{\rho}^{\,\prime}) \, ds^{\,\prime} \tag{3.40}$$

where the contour C_{RAD} is any or all of the appropriate branch cuts. Expressing the excitation current in (3.40) as the forward transform of space-domain current \vec{J}^i yields

$$\vec{E}_{R}(\vec{r}) = \int_{V} \vec{G}_{R}(\vec{r}|\vec{r}') \cdot \vec{J}(\vec{r}') dV' \qquad (3.41)$$

in which the radiation Green's dyad is identified as

$$\ddot{\mathbf{G}}_{\mathbf{R}}(\vec{\mathbf{r}}|\vec{\mathbf{r}}') = \frac{-1}{2\pi} \int_{C_{\mathbf{R},\mathbf{D}}} \left[\sum_{\alpha = x,y,z} \vec{\mathbf{E}}_{\alpha}(\vec{\rho}|\vec{\rho}';\zeta) \hat{x}_{\alpha} \right] e^{j\zeta(z-z')} d\zeta$$
 (3.42)

This is clearly a continuous superposition of the elementary spectral field components as defined by (3.38).

3.4 Radiation Spectrum in the Low-loss Limit

Specialization to a limitingly low-loss ($\Im \{k_l\} \to 0$; $l = c_s f_s$) waveguide facilitates identification of the physical characteristics of each regime of the radiation spectrum. Furthermore, many practical structures are fabricated from low-loss materials. In the low-loss limit, the hyperbolic branch cuts in the axial wavenumber plane coalesce and become "dog-leg" branch cuts, as depicted in Figure 3.9. Throughout this analysis, only one surface wave mode will be assumed to propagate; more surface wave modes could easily be included.

There are subsequently three regions of interest upon the coalesced branch cut. The first region is denoted P; this branch cut only affects the location of ξ_p^e , the background surface-wave pole singularities. The second region is denoted by S; this branch cut affects the location of the substrate ξ -plane branch point ξ_{be} . Branch cut S also affects the location of ξ_p^e as well, as branch cut S is a continuance of branch cut P. The last region is denoted B and controls the location of the cover ξ -plane branch point

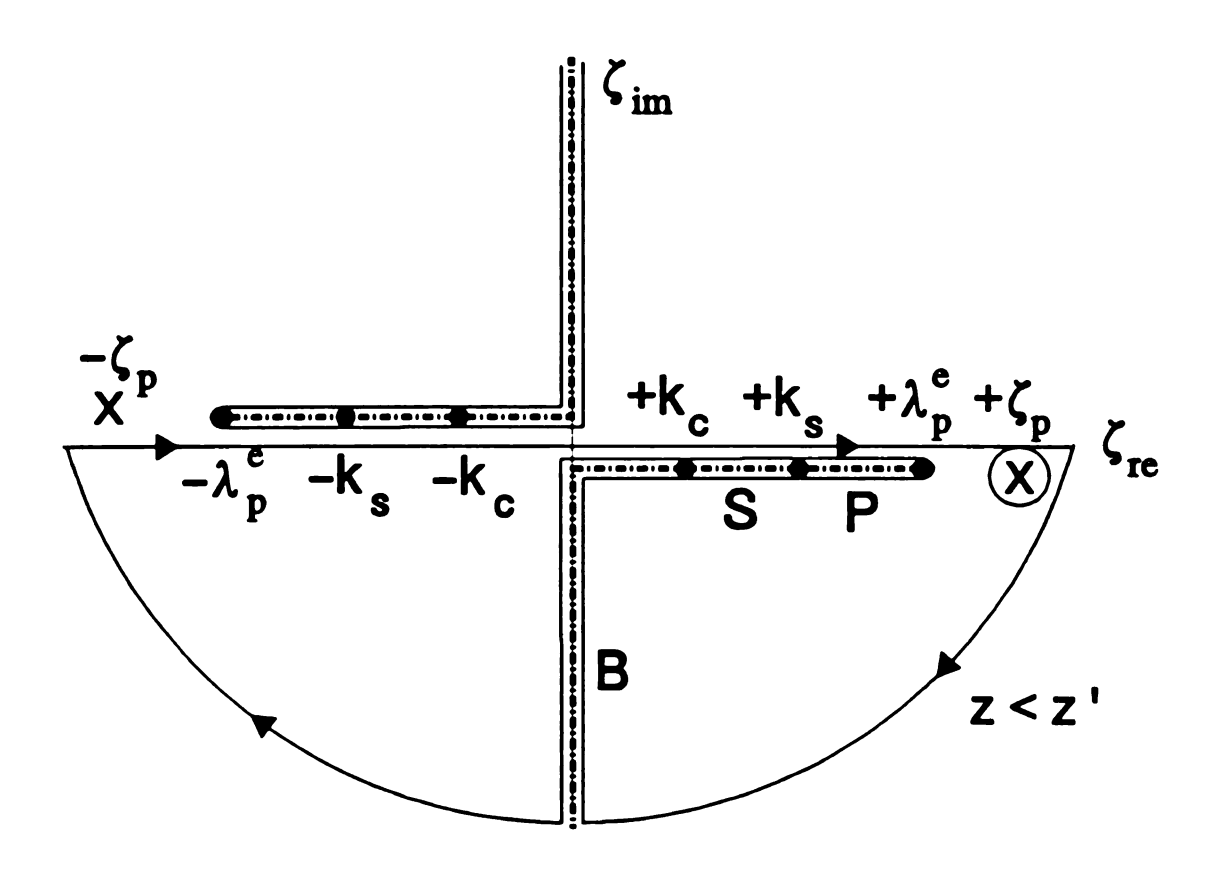


Figure 3.9 Coalescing of complex ζ -plane branch cuts in low-loss limit. Closure for case of z < z'.

 ξ_{bc} ; branch cut B also affects the locations of both ξ_{bc} and ξ_{p}^{e} . Table 3.1 summarizes the effect of different portions of the coalesced transform-domain branch cut upon the ξ -plane singularities.

Table 3.1 Effect of the coalesced transform-domain branch cut upon complex ξ -plane singularities

Restricted By:

Singularity	Formula	P	S	В
surface-wave pole	$\xi_p^e = -j\sqrt{\zeta^2 - (\lambda_p^e)^2}$	Yes	Yes	Yes
substrate branch point	$\xi_{bs} = -j\sqrt{\zeta^2 - k_s^2}$	No	Yes	Yes
cover branch point	$\xi_{bc} = -j\sqrt{\zeta^2 - k_c^2}$	No	No	Yes

Based upon Figure 3.9, the total field for this specific case is constructed in terms of its propagation-mode spectrum as

$$\vec{E}(\vec{r}) = \sum_{k=0}^{N} \vec{E}_{k}(\vec{r}) + \vec{E}_{R}^{SW}(\vec{r}) + \vec{E}_{R}^{S}(\vec{r}) + \vec{E}_{R}^{C}(\vec{r})$$
 (3.43)

The first term in the representation (3.43) is the sum of the discrete modes (pole residues) of the waveguide structure, where each discrete mode is specifically

$$\vec{E}_{k}(\vec{r}) = \mp j \vec{e}_{res}(\vec{\rho}, \pm \zeta_{p,k}) e^{-j\zeta_{p,k}|z-z'|}$$
(3.44)

Closure in the lower half-plane for z < z' encloses $+\zeta_{p,k}$ clockwise, giving rise to -j weighting the residue at $+\zeta_{p,k}$; upper half-plane closure for z < z' encloses $+\zeta_{p,k}$ counterclockwise, etc. The absolute value on z - z' arises from the consideration that in the lower half-plane, (z - z') = -|z - z'| while in the upper half-plane (z - z') = |z - z'|.

The remainder of the terms in (3.43) comprise the total radiation field arising from the branch cut integration. The total radiation field is composed of three components, each with a different modal characteristics. The first component is denoted a surface-wave radiation field, given as

$$\vec{E}_{RAD}^{SW}(\vec{r}) = -\frac{1}{2\pi} \int_{\lambda_{\rho}^{\bullet}}^{k_{\rho}} \left[\vec{e}(\vec{\rho}, \zeta^{i}) - \vec{e}(\vec{\rho}, \zeta^{\circ}) \right] e^{-j\zeta|z-z'|} d\zeta$$
 (3.45)

and consisting of the superposition of continuous radiation modes in the regime $k_{p} < \zeta_{p} < \lambda_{p}^{e}$. The second component is the substrate radiation field,

$$\vec{E}_{\text{RAD}}^{\text{S}}(\vec{r}) = -\frac{1}{2\pi} \int_{k_{c}}^{k_{c}} \left[\vec{e}(\vec{\rho}, \zeta^{i}) - \vec{e}(\vec{\rho}, \zeta^{o}) \right] e^{-j\zeta|z-z'|} d\zeta$$
(3.46)

and is a superposition of radiation modes in the regime $k_c < \zeta_r < k_s$. The final component is the cover radiation field,

$$\vec{E}_{RAD}^{C}(\vec{r}) = -\frac{1}{2\pi} \int_{k_{c}}^{-j\infty} \left[\vec{e}(\vec{\rho}, \zeta^{i}) - \vec{e}(\vec{\rho}, \zeta^{o}) \right] e^{-j\zeta|z-z'|} d\zeta$$
 (3.47)

and is the superposition of radiation modes in the regimes $0 < \zeta_r < k_c$ and $-\infty < \zeta_i < 0$.

In (3.45)-(3.47), the notation ζ^i denotes a axial wavenumber ζ located on the interior of the transform-domain branch cut; the interior being defined as the side nearest the origin of the complex ζ -plane; likewise, ζ^o denotes values of ζ on the branch cut

exterior (outside), where the exterior side is not the interior side. The integration contour is then parameterized along the interior side of the branch cut from $\zeta = \lambda_p^e$ to $\zeta = -j\infty$; the branch cut integrand then becomes $\vec{\epsilon}(\vec{\rho}, \zeta^{\dagger}) - \vec{\epsilon}(\vec{\rho}, \zeta^{\circ})$, as given in (3.45)-(3.47), which then explicitly accounts for the exterior branch cut contribution. This difference will be denoted

$$\vec{e}_{R}(\vec{\rho},\zeta) = \vec{e}(\vec{\rho},\zeta^{\dagger}) - \vec{e}(\vec{\rho},\zeta^{\circ}) \tag{3.48}$$

and is the spectral radiation mode for axial wavenumber ζ .

The characteristics of each of these three radiation field components depend upon the behavior of the Green's functions in each of the three regimes. For ease of reference, the general form (3.12) is reproduced here

$$g_{\alpha}^{\beta}(\vec{\rho}\,|\vec{\rho}';\zeta) = \frac{1}{2\pi} \int_{-\infty}^{\infty} R_{\alpha}^{\beta}(p_i,y',x')e^{-p_iy}e^{j\xi x}d\xi$$
 (3.49)

slightly modified to show explicit exponential dependence upon y. Consequently, the spectral mode characteristics are highly dependent upon the location of the singularities in the complex ξ -plane. Locating these singularities and determining their effects involves evaluating a complex square root quantity of the generic form $-j[z^2-z_0^2]^{-1/2}$; this evaluation is achieved by factoring the square root as

$$Q = \sqrt{z^2 - z_0^2} = \sqrt{z - z_0} \sqrt{z + z_0}$$
 (3.50)

and considering the argument of each individual square root as influenced by the respective branch cut and branch point. The total argument for the singularity locations will then be simply

$$-\frac{\pi}{2} + \text{Arg}\{Q\} = -\frac{\pi}{2} + \frac{1}{2}(\theta^* + \theta^-)$$

where θ^* is the argument about the branch point at $z = +z_0$, θ^- is the argument about $z = -z_0$, and $-\pi/2$ arises from -j. This method is depicted in Figure 3.10.

Application of this technique is similar in each radiation regime; details will be presented for the substrate radiation regime, while general conclusions will be discussed for the remaining regimes. The substrate radiation regime is $k_c < \zeta_r < k_s$, in which ζ lies along the portion of the transform-domain branch cut denoted S. This portion of the branch cut restricts the migration of the substrate branch point ξ_{bs} and the background surface-wave pole singularity ξ_p^s . The complex ξ -plane singularity locations will be computed as per (3.50); the appropriate branch-cut arguments are summarized below.

Table 3.2 Complex ξ -plane singularity arguments for ζ in the substrate radiation regime

	0 +	в	$Arg\{\xi_{sing}\}$
ξ°	π	0	0
ξbe	π	0	0
ξ _{bc}	0	0	-π/2

Arguments for ζ^i

	θ+	0 -	$Arg\{\xi_{sing}\}$
ξ°	-π	0	-π
ξbe	-π	0	-π
ξ _{bc}	0	0	-π/2

Arguments for ζ^o

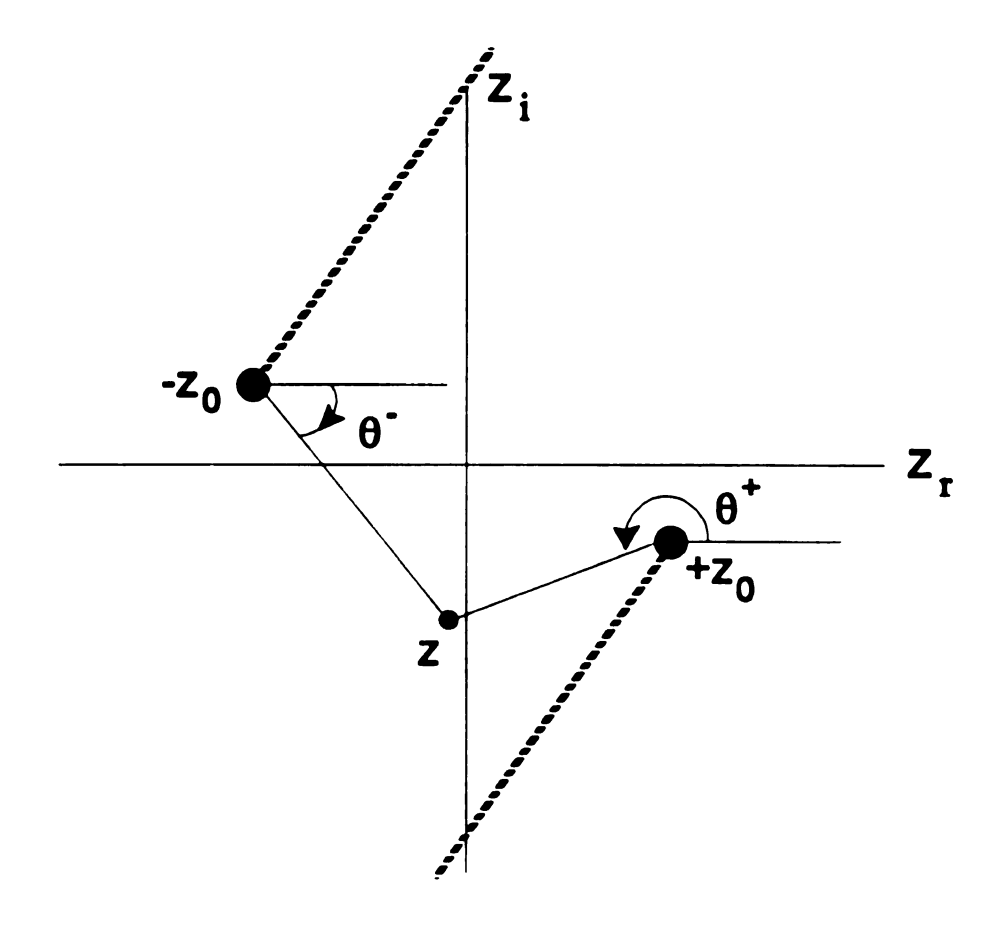


Figure 3.10 Evaluation of complex-valued square roots.

Figure 3.11 shows the location of the complex ξ -plane singularities for this regime, where the region about the real axis has been exaggerated. Based on the table, it is apparent that as ζ switches sides of branch cut S, both ξ_p^{ℓ} and ξ_{be} switch location in the complex ξ -plane. For a ζ^{ℓ} on S, both the pole ξ_p^{ℓ} and branch cut ξ_{be} are located on the positive real axis; the inversion contour should remain above both these singularities, as shown in Figure 3.11a, since choice of sign was made to locate the pole in the lower half-plane. Enforcing the radiation condition on p_{ℓ} for values of ξ results in another "dog-leg" branch cut, this time in the complex ξ -plane. This branch cut associated with p_{ℓ} runs parallel to the real axis towards the origin, then heads towards $-j\infty$. For a ζ^{0} on S, the behavior is reversed; in particular, the p_{ℓ} branch cut still runs parallel to the real axis towards the origin in ξ but then heads towards $+j\infty$, as shown in Figure 3.11b. Meanwhile, for ξ_{bc} , its argument does not change as ζ switches sides.; consequently, it stays in the same location. The branch cut enforcing the radiation condition on p_{ℓ} is easily determined, and coincides with the branch cut for p_{ℓ} along the imaginary axis.

The Green's functions can be evaluated as the sum of the real-line integral along the branch cut from $-\xi_{be} < \xi_r < \xi_{be}$, the real-line integral from $\pm \xi_{be}$ to infinity, and the small deformation around the poles at $\pm \xi_p^e$. For a ζ^i (Figure 3.11a), the argument of p_r is $+\pi/2$ along the branch cut in ξ and 0 beyond the branch point, on the real-line contour to $\pm \infty$. For a ζ^e (Figure 3.11b), the argument of p_r is $-\pi/2$ along the branch cut but still 0 beyond the branch point. Constructing the radiation spectral mode as per (3.48) indicates that there will be an standing wave pattern in p_r within the substrate, arising from that portion of the integration path along the branch cut. A similar analysis indicates that p_e has an argument of 0 upon the real-line contour.

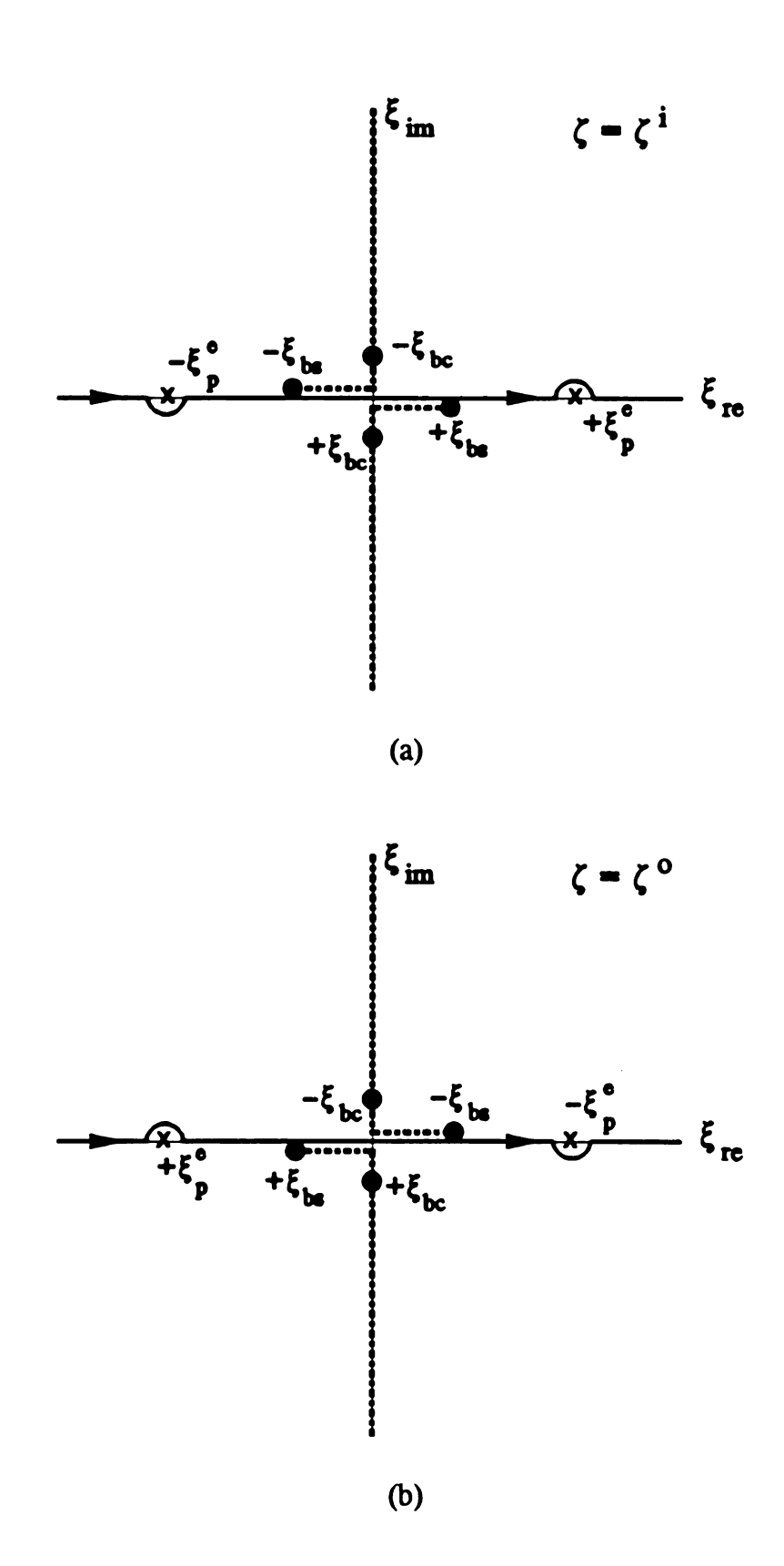
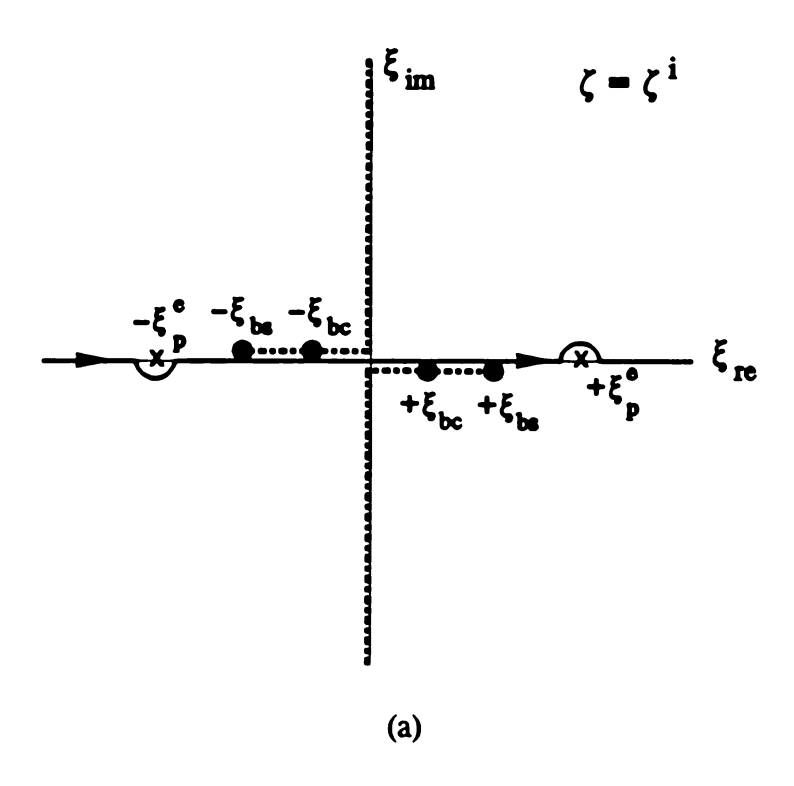


Figure 3.11 Complex ξ -plane singularity locations for the substrate radiation regime. (a) Interior side of branch cut S. (b) Exterior side of branch cut S.

The pole deformation integral is proportional to the residue at that surface-wave pole. Consider the deformation along the positive real axis in the ξ -plane. For a ξ^i on the interior side of S, that portion of the Green's function is proportional to $e^{-i\xi_p x}$, a phase front propagating in the -x direction. As ξ switches sides of the S branch cut, the pole locations switch and the inversion contour deforms about $-\xi_p^e$ as in Figure 3.11b. The contribution of this pole is now proportional to $e^{-i\xi_p x}$. The superposition of both sides of branch cut S indicates a standing wave pattern in x. Naturally, the same applies for the pole on the negative real axis.

For any value of ζ upon S within the substrate radiation regime, the Green's functions, and consequently the electric field, are oscillatory in x and in y for y < 0 but exponentially decaying in y for y > 0. This corresponds to a radiation mode that can carry energy away into the substrate and transversely away from the waveguide by an excited surface-wave mode of the background structure. Also, as the value of ζ is real, each of the radiation spectral components are propagating radiation modes.

The second regime of interest is the cover radiation regime defined by the portion of the branch cut denoted B. Radiation modes in this regime are either propagating, with axial wavenumbers $0 < \zeta_r < k_c$, or evanescent for $-j \approx < \zeta_i < 0$. The effect of branch cut B upon the complex ξ -plane is shown in Figure 3.12; notably, all the types of singularities are affected. Based on the previous analysis, it is observed that a standing wave pattern in y will occur for y in either the cover or substrate. The background surface-wave pole is still intercepted, and consequently, a standing wave pattern in x occurs as well. These cover, or full, radiation modes carry energy away from the waveguide into the cover and substrate regions.



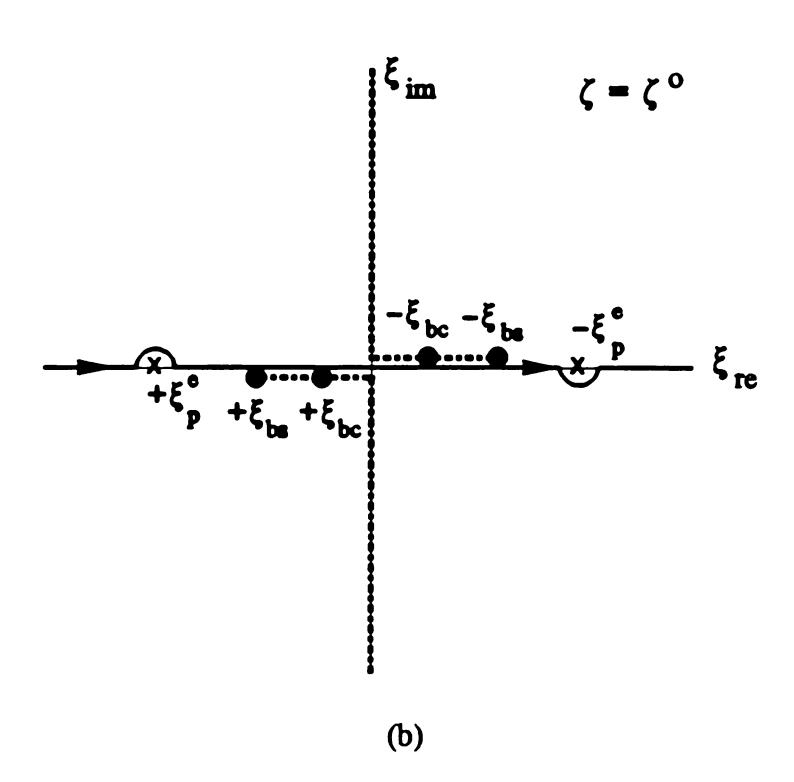


Figure 3.12 Complex ξ -plane singularity locations for the full (cover) radiation regime. (a) Interior side of branch cut B. (b) Exterior side of branch cut B.

The last regime of interest is the surface-wave radiation regime. This is characterized by $k_s < \zeta_r < \lambda_p^e$; the effect of the transform-domain branch cut P upon the complex ξ -plane is shown in Figure 3.13. Radiation modes in this regime are propagating modes, possessing evanescent behavior in y for y in both the cover and substrate regions, but still possessing oscillatory behavior in x. This radiation mode will then carry energy transversely away from the waveguide within an excited background surface wave mode. Note that in this case, the energy is confined to the film layer of the background structure. Whether this portion of the radiation spectrum is a significant contribution depends upon the background structure. For thin-film structures, it is expected that this radiation component will be small.

3.5 The Proper Role of Leaky-Wave Modes

A leaky-wave mode is a discrete mode of the waveguide that possesses non-spectral behavior. A leaky-wave mode is a solution of (3.35) whose field distribution exhibits exponential growth transverse to the waveguiding structure in either x or y. Obviously, these modes cannot physically exist over all of space; consequently, these modes certainly are not part of any proper eigenmode expansion of the waveguide field. Yet, these leaky-wave modes are of tremendous interest to the research community, and much effort is expended to determine the leaky-wave mode solutions.

3.5.1 Identification of leaky-wave modes via the EFIE

For the discussion in Section 3.5, the background environment is assumed to be a conductor/film/cover configuration. The film is assumed to be thin and hence only one

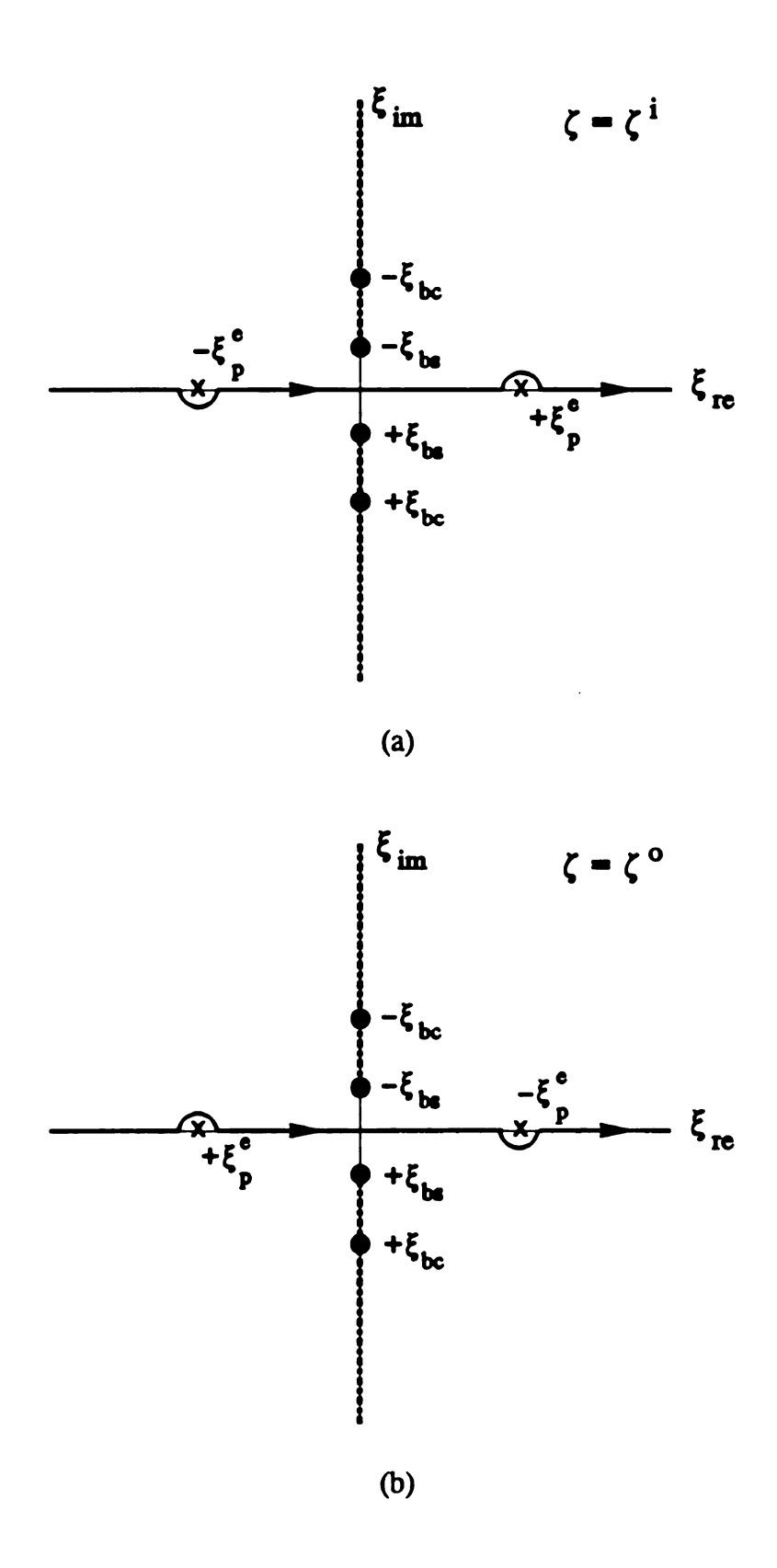


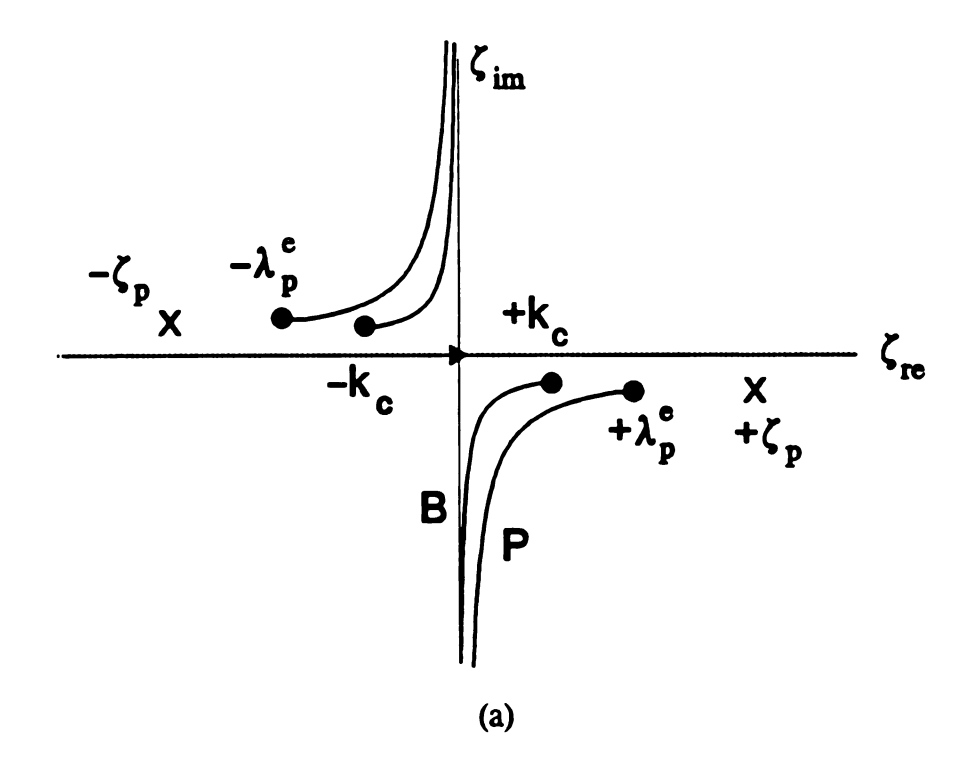
Figure 3.13 Complex ξ -plane singularity locations for transverse-only radiation regime. (a) Interior side of branch cut P. (b) Exterior side of branch cut P.

surface-wave background mode (TM₀) is supported. This is the situation depicted in Figure 3.14a, where the axial transform-plane branch cuts are defined to enforce spectral behavior. This section addresses finding leaky-wave solutions to the EFIE (3.35).

The branch cuts in the axial transform plane serve to define a four-sheeted Riemann surface, as depicted in Figure 3.14b. The branch cuts are the limiting case of spectral behavior. The top sheet, denoted (1), is the spectral sheet. Upon this sheet lies the inversion contour and the bound guiding modes (proper modes) of the waveguide.

The second sheet is reached by intentionally passing through the branch cut P. When this branch cut is violated, the background surface wave pole in ξ migrates above the real axis and introduces non-spectral behavior (exponential growth) in x. The branch cut B is still obeyed and exponential decay in y is still maintained. Solutions on this sheet are called surface-wave leaky modes, as the non-spectral behavior is confined to the background planar interface.

The third sheet is reached by intentionally passing through branch cut B from the top sheet. In this case, the ξ -plane branch point migrates above the real axis and introduces non-spectral behavior in y. The branch cut P is still obeyed, and the background surface wave is not excited. Solutions on sheet (3) are called space-wave leaky modes, as the leakage effect is directly into the cover region but not into the surface wave. Sheet (3) cannot be directly reached from locations on sheet (2). This implies that a surface-wave leaky mode cannot evolve into a space-wave leaky mode. The last sheet, sheet (4), is reached by violating both the P and B branch cuts. On sheet (4), energy leaks into both the cover and the background surface wave. Sheet (4) can be reached from either sheet (3) or sheet (2).



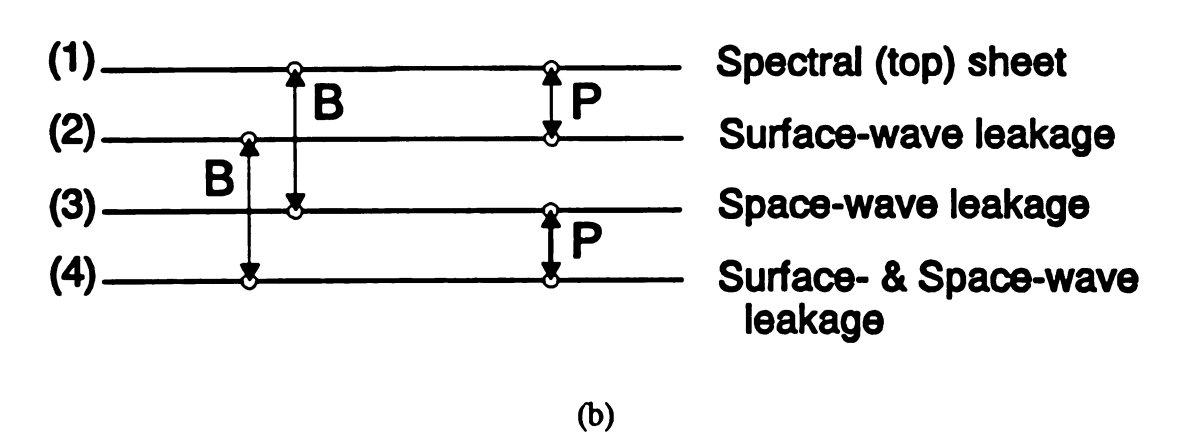


Figure 3.14 (a) Four-sheeted axial wavenumber (complex-3) plane. (b) Nature of each Riemann sheet.

Unfortunately, by allowing the ξ -plane singularities to migrate above the real-axis, the original Fourier transform on x becomes non-convergent on the real axis. The inversion contour must be deformed to stay within an analytic region in the ξ -plane. Complicating matters is that the analytic regions do not overlap (Figure 3.6b). To maintain convergence of the forward transform, the integral needs to be considered in the sense of (3.6), with a contour lying within each convergent half-plane. By using analytic continuation, the analytic function defined where each Fourier integral in (3.6) converges can be extended uniquely (Monodromy theorem, [50]) until a singularity is encountered. An analytic continuation can therefore be defined for each region of convergence from (3.6); within this analytic continuation lies the deformed inversion contour, as shown in Figure 3.15. By the process of analytic continuation, the forward transform on x remains convergent for leaky-wave modes.

The above discussion suggests the method in which to use the EFIE of (3.35) to find leaky-wave modes. First, a choice of sheet is made, which chooses the nature of mode leakage that is to be of interest. The appropriate branch cuts are violated depending upon the nature of the leaky-wave mode of interest, and their associated singularities are allowed to migrate across the real axis. The inversion contour must be deformed and kept above these singularities. Once the ξ -plane singularities and inversion contour are known, the Green's functions are evaluated, and a solution to the homogeneous EFIE is then determined. More specific details on this topic will be dealt with in Chapter 6.

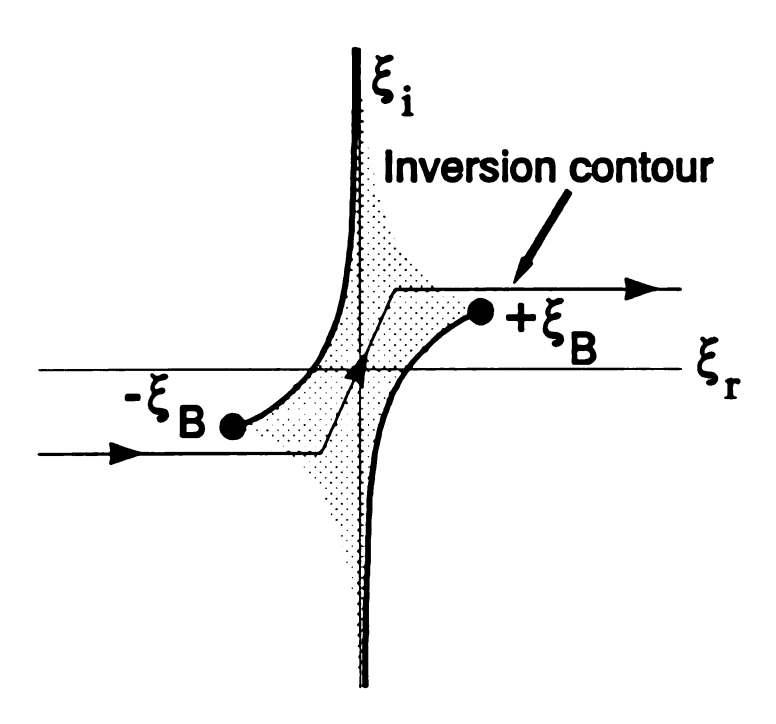


Figure 3.15 Deformed inversion contour in complex ξ -plane used when upon a non-spectral Riemann sheet of the axial-transform plane.

3.5.2 Usage of leaky-wave modes

Up to this point, this dissertation has followed the traditional presentation of leaky-wave modes within the literature, namely, how to find these solutions. It now departs from tradition and explains how to use the leaky-wave mode solutions. It should be stated that a number of good references are available that treat this topic [20,51, 52]; however, these references restrict analysis to a two-dimensional problem.

The total field of the waveguide is often times desired, especially for determining the radiation patterns of open-boundary devices. The Green's functions have the form (3.49), from which it is clear that as x becomes large the Green's functions are highly oscillatory and very difficult to compute numerically. This nature, while rendering numerical integration techniques useless, is readily amenable to an asymptotic expansion evaluation via the method of Steepest Descents. Briefly, the method of Steepest Descents (SD) is a saddle-point method applied to evaluate integrals of the type

$$\int_{0}^{z} F(z)e^{zf(z)} dz \tag{3.51}$$

where α is a large parameter. General details can be found in Matthews and Walker [53]. In brief, Cauchy's theorem allows the original inversion contour to be deformed to one upon which the exponential in the integrand has constant phase and rapidly vanishes (the Steepest Descent Contour or SDC), which allows the infinite contour to be approximated by a contour of finite length. This SDC is defined by the relationship

$$\mathfrak{I}m\{f(z)\} = \mathfrak{I}m\{f(z_0)\} \tag{3.52}$$

where the SDC passes through the saddle point z_0 , the point where $f'(z_0) = 0$; this saddle point region is the dominant contribution to the integral.

Application of the method of steepest descents to this problem allows the determination of the scattered field from the open-boundary waveguide at large distances. The space-domain scattered field is an inverse-transform on ζ of the transform-domain scattered field. In the transform domain, the scattered field is

$$\vec{e}^{s}(\vec{\rho},\zeta) = \int_{CS} \frac{\delta n^{2}(\vec{\rho})}{n_{\epsilon}^{2}} \vec{g}^{\epsilon}(\vec{\rho}|\vec{\rho}',\zeta) \cdot \vec{e}_{g}(\vec{\rho}',\zeta) ds'$$

where \vec{e}_g is the field in the guiding region that serves as the equivalent source supporting that scattered field. Obtaining the space-domain field means that it is necessary to evaluate integrals of the type

$$E_{\alpha}(r) = \int_{-\infty}^{\infty} e_{\alpha}(\rho, \zeta) e^{j\zeta z} d\zeta$$
 (3.53)

where e_a is a scattered field component. In two-dimensional problems, this scattered field integral is converted into polar coordinates in both space coordinates and in spatial frequency, which allows for identification of a saddle-point with specific physical interpretation. For a three-dimensional problem of the waveguide, a transformation into a spherical coordinate system should be effected.

Observe first that the Green's function is an inverse transform on ξ . Also note that the waveguide field is a function of $\vec{\rho}'$ and ζ , but not of ξ . An interchange of the spectral integral on ξ with the spatial integral over the waveguide cross-section gives

$$e_{\alpha}(x,y,\zeta) = \int_{-\infty}^{\infty} F_{\alpha}(\xi) \prod_{g}(\xi,\zeta) e^{j\xi x} e^{-p_{\xi}y} d\xi$$
 (3.54)

where Π is the source field integrated over the waveguide cross-section and F is a Green's function coefficient. Depending upon $p_l = [\xi^2 - \xi_{kl}^2]^{(1/2)}$, and the appropriate F,

equation (3.54) can represent the field component anywhere in the layered background. This formulation is explicitly a function of ξ and ζ , in which the spectral integral on ξ can now be evaluated asymptotically. A change of variables is made to polar coordinates, namely,

$$\xi = \xi_{kl} \sin \phi'$$
 $x = \rho \sin \phi$
 $p_l = j\xi_{kl} \cos \phi'$ $y = \rho \cos \phi$

after which the square root upon ξ for p_l is no longer implicated. Equation (3.54) becomes

$$R_{\alpha}(\rho,\zeta) = \int_{-\infty}^{\infty} F_{\alpha}(\xi_{bP}\phi') \Pi_{\alpha}(\xi_{bP}\phi',\zeta) e^{-j\xi_{bP}\cos(\phi-\phi')} d\phi'$$

An asymptotic evaluation of the integral upon ϕ' shows that the saddle point occurs when $\phi = \phi'$; consequently, equation (3.54) takes the form

$$R_{\sigma}(\rho,\zeta) = \tilde{R}_{\sigma}(\rho,\phi;\xi_{M},\zeta)e^{-j\xi_{M}\rho}$$
 (3.55)

When (3.55) is used in the inverse transform on ζ of (3.53); equation (3.53) becomes

$$I_{\alpha}(r) = \int_{-\infty}^{\infty} \tilde{R}_{\alpha}(\rho, \phi; \xi_{bh}, \zeta) e^{-j\xi_{bh}\rho} e^{j\zeta z} d\zeta$$
 (3.56)

This form is again amenable to evaluation by the method of steepest descents, using another set of polar variable transformations on complex angle $\theta' = \sigma + j\eta$,

$$\zeta = k_i \sin \theta' \tag{3.57}$$

$$\xi_{bl} = \sqrt{k_l^2 - \zeta^2} = k_l \cos \theta' \tag{3.58}$$

The transformation in (3.57) is similar to the traditional SDC mapping for twodimensional problems. Evaluating (3.56) using (3.57) and deforming into the steepest descent contour gives insight into the usage of leaky-wave modes.

3.5.3 Physical interpretation of leaky-wave modes

The "Steepest-descents" plane in Figure 3.16 is a mapping of ζ through (3.57) and (3.58) which removes a branch cut in ζ ; in this case, there is no mechanism to separate spectral from non-spectral sheets. There are 8 quadrants in the steepest-descent plane; their relation to the original axial transform domain depends upon (3.57) and (3.58). Finishing the spherical coordinate transformation by using $z = r\sin\theta$, $\rho = r\cos\theta$ results in

$$I_{\alpha}(r) = \int_{-\infty}^{\infty} \tilde{R}_{\alpha}(r, \phi, \theta') e^{-jk_{l}r\cos(\theta-\theta')} d\theta'$$

The saddle point is at $\theta = \theta'$; when the inversion contour is deformed to the SDC as defined by (3.52), the final asymptotic form is

$$I_{\alpha}(r,\theta,\phi) = e^{-jk_{\parallel}r} \int_{SDC} \tilde{R}_{\alpha}(r,\phi,z) e^{-rz^2} dz \qquad (3.59)$$

As the observation angle θ changes, the saddle point moves along the real axis in the steepest-descents plane. The SDC naturally follows the saddle point movement; a portion of the SDC now lies upon a non-spectral portion of the steepest-descents plane. A leaky mode then contributes to the waveguide radiation field only if it is intercepted by the steepest-descent contour. This is the only situation for which a leaky-wave mode is useful. The contour only intercepts the leaky-wave pole over a restricted spatial regime; in this restricted spatial regime, the leaky-wave mode now possesses propagating

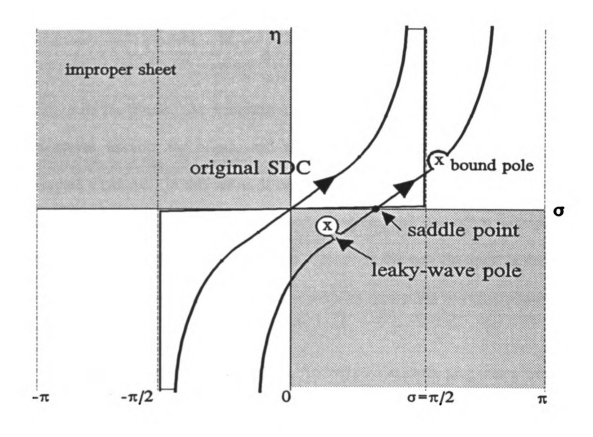


Figure 3.16 Typical steepest-descent plane.

exponential behavior away from the waveguide as r becomes large. In that regime, the leaky wave mode augments the scattered field. Once out of the contributing regime of the leaky waves, the scattered field is just the saddle-point contribution.

A nice physical picture of the leaky-wave effect is given in Shevchenko, and is reproduced in Figure 3.17. Based on (3.57), the spatial observation angle θ can be written as

$$\theta = \tan^{-1}(\frac{z}{y})$$

for any ρ on the y-axis. As y increases, z/y decreases, and θ decreases. The saddle point moves towards the origin, and at some point then leaky-wave pole is not intercepted anymore. In this sense, it can be seen that leaky modes contribute to the waveguide radiation field in a restricted spatial regime, and shut off at an angle of θ . This angle is often called the leakage angle. Based on the way the angle is defined, it is rather obvious that the leaky-wave mode is useful only near the waveguide-background interface.

As observed before, in this regime, the leaky-wave mode propagates away from the waveguide, thus it is used to model the waveguide radiation and transverse power flow away from the waveguide. It is through this interpretation of the leaky-wave pole, in the method-of-steepest descents, that the leaky-wave relates to the radiation spectrum.

Because of its field structure, a leaky-wave mode is never part of the proper eigenvalue spectrum and cannot be used in a modal expansion of the waveguide field. Rather, the leaky-wave mode is useful in the excitation problem of determining scattered fields.

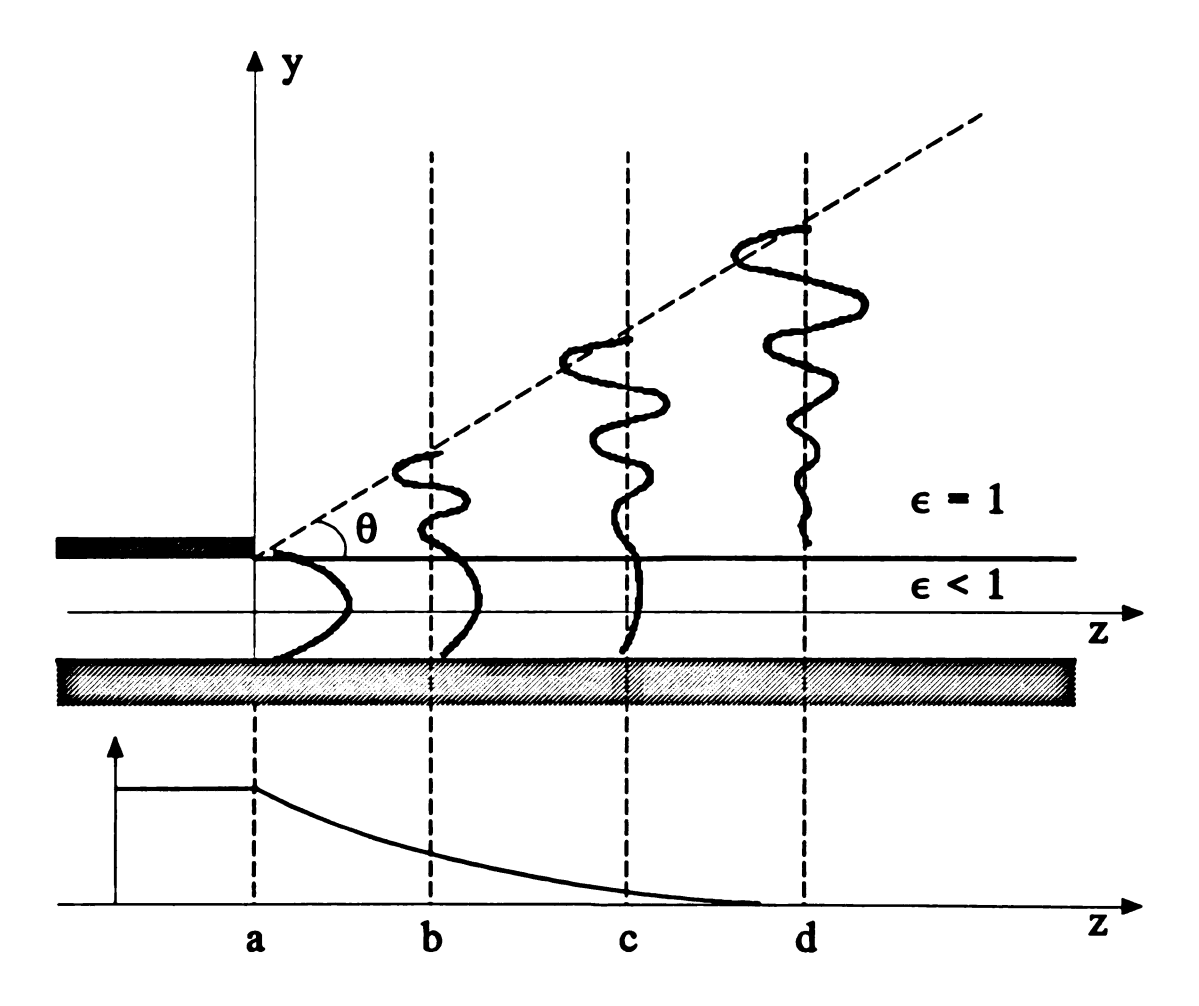


Figure 3.17 Physical interpretation of leaky-wave mode (plasma waveguide example from Shevchenko).

Summary

This chapter has presented a formulation for the complete propagation-mode spectrum of a general open-boundary waveguide. The discrete spectral components correspond to bound, hybrid guiding modes and are associated with first-order pole singularities of the axial transform-domain fields. The continuous spectral components correspond to the radiation modes of the guiding structure and are associated with hyperbolic branch cuts in the axial transform domain. The branch cuts in the axial transform domain are chosen to restrict the migration of singularities in the transverse transform (complex ξ) plane and guarantee that the forward transform on x converges. Branch cuts in the complex ξ -plane are chosen to satisfy the Sommerfeld radiation condition, while poles in the complex ξ -plane incorporate the surface-wave behavior of the layered background environment.

A new component of the continuous radiation spectrum is identified as being associated with the surface-wave modes of the background structure. These radiation spectral components have a standing wave pattern in x but remain bound to the surface of the background; this will account for energy carried away by excited surface wave modes in the background structure. In the limiting low-loss case, this surface-wave radiation spectrum is confined to a finite range of axial wavenumbers.

Finally, the use of leaky-wave modes was addressed. Leaky-wave modes are discrete modes with non-spectral behavior, and are associated with poles of the transform-domain field located on all non-spectral, improper 5-plane sheets. These poles are not part of the proper eigenvalue spectrum, as they possess exponential growth

transverse to the guiding axis. Their importance is linked to the evaluation of the scattered field in a waveguide excitation problem via asymptotic steepest-descent-contour techniques. In this case, leaky-wave modes characterize the scattered radiation field of the waveguide in a limited spatial regime near the waveguide surface, when they are captured by the steepest-descents contour.

Chapter 4

Continuous Radiation Spectrum for Planar Waveguides

In Chapter 3, a method for using an integral-operator formulation to identify an open-boundary waveguide's continuous radiation spectrum was advanced. Central to this method is the criterion for cutting the axial transform plane; the continuous radiation spectrum is the superposition of all spectral modes along those branch cuts. Confirmation of this theory is desirable, but few canonical examples exist to compare with. For waveguides in a planarly-layered background, only the simple planar waveguide possesses a closed-form, canonical solution for its radiation modes [10].

This chapter uses the integral-operator method to identify the continuous radiation spectrum for a planar waveguide structure, and to determine the individual spectral components of the radiation field. The planar waveguide supports either TE fields (where $\vec{e} = \hat{x}e_x$) or TM fields (where $\vec{e} = \hat{y}e_y + \hat{z}e_z$). This simplified set of electric-field components is particularly amenable to analysis by the transverse-field EFIE as advanced in (2.58); in each case, the TEFIE (2.58) reduces to a single, uncoupled integral equation, easily solved using the Method of Moments and expanding the unknown field in terms of subsectional-domain pulse basis functions.

4.1 General Considerations for Planar Waveguides

A typical planar waveguide considered in this dissertation is depicted in Figure 4.1. It is comprised of three planar layers, of infinite extent in the transverse (x) and axial (z) directions. The substrate and cover layers are semi-infinite in extent in the normal y direction, while the film layer is of finite thickness t. The film layer is the guiding region, with refractive index of n(y) uniform in x; consequently, the background environment is a simple two-layer interface. Canonical solutions exist for a planar waveguide with a homogeneous film layer; for this case, the film layer refractive index is denoted n_f . The cover refractive index is n_c and substrate refractive index is n_s . Guided waves are assumed to propagate in the $\pm z$ directions; hence, the waveguide fields are invariant in the transverse x direction.

From chapter 2, the Transverse-field EFIE (TEFIE) is given as

$$\vec{e}_{t}(\vec{\rho}) = \vec{e}_{t}^{i}(\vec{\rho}) + k_{c}^{2} \int_{CS} \frac{\delta n^{2}(\vec{\rho}')}{n_{c}^{2}} \vec{g}_{t1}(\vec{\rho}|\vec{\rho}') \cdot \vec{e}_{t}(\vec{\rho}') ds'$$

$$+ \int_{CS} \frac{\delta n^{2}(\vec{\rho}')}{n_{c}^{2}} \vec{g}_{tv}(\vec{\rho}|\vec{\rho}') \cdot \vec{e}_{t}(\vec{\rho}') ds'$$

$$+ \int_{CS} \vec{g}_{\phi}(\vec{\rho}|\vec{\rho}') \vec{d}_{a}(\vec{\rho}') \cdot \vec{e}_{t}(\vec{\rho}') ds'$$

$$- \oint_{\Gamma} \frac{\delta n^{2}(\vec{\rho}')}{n_{c}^{2}} \vec{g}_{\phi}(\vec{\rho}|\vec{\rho}') (\hat{n}' \cdot \vec{e}_{t}(\vec{\rho}')) dl'$$

$$(4.1)$$

where the Green's functions are defined by

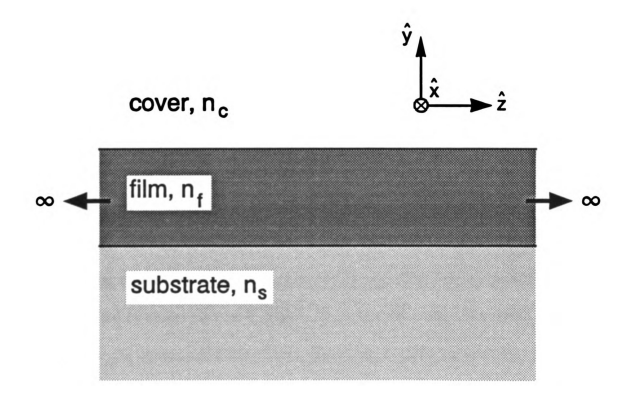


Figure 4.1 Configuration of asymmetric planar dielectric waveguide.

$$\vec{g}_{t1} = \vec{I} g^{p} + \hat{x} g_{t}^{r} \hat{x} + \hat{y} \left(g_{n}^{r} + \frac{\partial g_{c}^{r}}{\partial y} \right) \hat{y}$$

$$\vec{g}_{tv} = \nabla_{t} \left(g_{n}^{r} + g_{t}^{r} + \frac{\partial g_{c}^{r}}{\partial y} \right) \hat{y}$$

$$\vec{g}_{\varphi} = \hat{y} k_{c}^{2} g_{c}^{r} + \nabla_{t} \left(g^{p} + g_{t}^{r} + \frac{\partial g_{c}^{r}}{\partial y} \right)$$

$$(4.2)$$

and $\vec{d}_n = \nabla_t \ln n^2(y')$. The scalar components for the above Green's functions are defined in (2.45) to (2.46) and take the general form of

$$g_{\alpha}^{\beta}(x|x';y|y') = \int_{-\infty}^{\infty} f_{\alpha}^{\beta}(\xi,y,y') \frac{e^{j\xi(x-x')}}{2\pi} d\xi$$
 (4.3)

4.1.1 Transverse uniformity considerations

As observed before, the waveguide fields are x-invariant, making the planar waveguide essentially a two-dimensional problem. An obvious specialization in this case is any spatial derivatives on x vanish, i.e., $\partial/\partial x = 0$. The Green's functions in (4.2) are specialized by observing that $\nabla_t = \Im \frac{\partial}{\partial y}$. Invariance in x also corresponds to a spatial frequency in the complex ξ -plane of zero; hence, the ξ -plane behavior is simply $\delta(\xi)$. The scalar components can be a priori specialized by taking the Dirac delta function behavior into account when performing the integration over ξ , which produces the integrand $f_{\pi}^{\beta}(\xi,y,y')$ evaluated at $\xi=0$. Since effectively a two-dimensional problem, the cross-section surface integral reduces to an integral over the guide thickness in y, and the contour integral reduces to point contributions at the edges of guiding region.

The intuitive conclusions will now be developed rigorously. The EFIE in (4.1) is applied to the planar waveguide as shown in Figure 4.2. There are two types of integrals in (4.1) to consider when the waveguide cross-section becomes infinite in

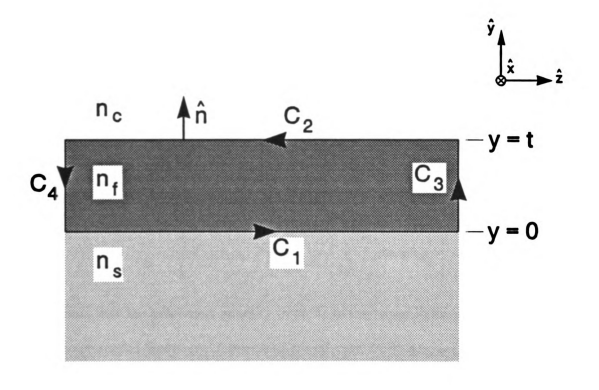


Figure 4.2 Contour used for evaluation of TEFIE.

transverse extent - the two-dimensional surface integral over the now-infinite waveguide cross-section and the contour integral around the waveguide cross-section as edges 3 and 4, as defined in Figure 4.2, approach infinity.

First consider a typical cross-section integral, of the form

$$I_{CS} = \int_{CS} g_{\alpha}^{\beta}(x|x';y|y')\vec{j}_{\sigma}(y')ds'$$
 (4.4)

where $\vec{j}_{s}(y')$ is any of the equivalent current sources in (4.1). Substitution of the Green's function general form (4.3) into (4.4) and allowing the cross-section to approach infinity along x results in

$$I_{CS} = \lim_{R \to \infty} \int_{-R}^{R} \int_{0}^{t} \left(\int_{-\infty}^{\infty} f_{\alpha}^{\beta}(\xi, y, y') \frac{e^{j\xi(x-x')}}{2\pi} d\xi \right) j_{\alpha}(y') dx' dy'$$

and a simple exchange of integration order gives

$$I_{CS} = \int_{0}^{\xi} \vec{j}_{e}(y')dy' \int_{-\infty}^{\xi} f_{a}^{\beta}(\xi,y,y') \left[\frac{1}{2\pi} \int_{-\infty}^{\infty} e^{j\xi(x-x')} dx' \right] d\xi$$
 (4.5)

It is obvious that the bracketed quantity in (4.5) is the Dirac delta function $\delta(\xi)$. The integral over spatial frequency ξ becomes trivial, and (4.5) becomes

$$I_{CS} = \int_{0}^{t} \vec{j}_{s}(y')g_{\alpha}^{\beta}(y|y')dy'$$
 (4.6)

where

$$g_{\sigma}^{\beta}(y|y') = f_{\sigma}^{\beta}(\xi=0,y,y')$$
 (4.7)

by the sifting property of the delta function. In this chapter, a Green's function which is explicitly written as $g_{\alpha}^{\beta}(y|y')$ is independent of x or x' and is evaluated as per (4.7); that is, at $\xi = 0$.

The contour integral presents more challenges in its handling. It takes the general form of

$$I_{\Gamma} = \oint_{\Gamma} g_{\alpha}^{\beta}(x|x';y|y') \left[\vec{j}_{\sigma}(y') \cdot \hat{n}'_{\text{out}} \right] dl'$$
 (4.8)

where \hat{n}'_{out} is the outward normal to the contour, and in which the vector nature of g_a^{β} (since only g_{ϕ} involves the contour integral) is suppressed for clarity. This contour integral decomposes into 4 components as suggested by Figure 4.2, namely,

$$I_{\Gamma} = I_1 + I_2 + I_3 + I_4 \tag{4.9}$$

where the various components take the form

$$I_{1} = \lim_{R \to \infty} \int_{-R}^{R} g_{\alpha}^{\beta}(x|x';y|0) [\vec{j}_{\epsilon}(0) \cdot (-\hat{y})] dx'$$
 (4.10)

$$I_2 = \lim_{R \to \infty} \int_{-R}^{R} g_{\alpha}^{\beta}(x|x';y|t) \left[\vec{j}_{\alpha}(t) \cdot \hat{y} \right] dx'$$
 (4.11)

$$I_{3} = \lim_{R \to \infty} \int_{0}^{r} g_{\alpha}^{\beta}(x|R;y|y') [\vec{j}_{\alpha}(y') \cdot \hat{x}] dy'$$
 (4.12)

$$I_{4} = \lim_{R \to \infty} \int_{a}^{b} g_{a}^{\beta}(x|-R;y|y') [\vec{j}_{e}(y') \cdot (-\hat{x})] dy'$$
 (4.13)

Integrals I_1 and I_2 are similar and will be dealt with first. Substitution of the Green's function general form (4.3) results in

$$I_{1,2} = \mp \hat{y} \cdot \vec{j}_{e}(y_{1,2}) \int_{-\infty}^{\infty} f_{a}^{\beta}(\xi, y, y_{1,2}) \left[\frac{1}{2\pi} \int_{-\infty}^{\infty} e^{j\xi(x-x')} dx' \right] d\xi$$

where $y_{1,2}$ denotes the location of contour I or contour I. From the previous evaluation of the cross-section integral, it is easily recognized that I_1 and I_2 become

$$I_{1,2} = \mp \hat{y} \cdot \vec{j}_{s}(y_{1,2}) g_{s}^{\beta}(y|y_{1,2}). \tag{4.14}$$

The remaining two contour integrals I_3 and I_4 are trickier to handle. Since the field and sources are x-invariant, it is expected that the contribution from each of the two sides at infinity should cancel each other out; as written in (4.12) and (4.13), the sum of I_3 and I_4 should vanish. The sum is then just

$$I_{3} + I_{4} = \lim_{R \to \infty} \int_{0}^{t} (\vec{j}_{e}(y') \cdot \hat{x}) \left[g_{\alpha}^{\beta}(x|R;y|y') - g_{\alpha}^{\beta}(x|-R;y|y') \right] dy'$$

$$= \lim_{R \to \infty} \int_{0}^{t} (\vec{j}_{e}(y') \cdot \hat{x}) \int_{-\infty}^{\infty} \left[f_{\alpha}^{\beta}(\xi,y,y') \frac{e^{j\xi x}e^{-j\xi R}}{2\pi} - f_{\alpha}^{\beta}(\xi,y,y') \frac{e^{j\xi x}e^{j\xi R}}{2\pi} \right] d\xi dy$$

where, as before, (4.3) has been substituted for the Green's function of interest. This becomes, after interchanging the order of integration and algebraic manipulation,

$$I_3 + I_4 = \int_0^t (\vec{j}_e(y') \cdot \hat{x}) \left[\lim_{R \to \infty} \int_{-\infty}^{\infty} 2f_{\alpha}^{\beta}(\xi, y, y') \sin(\xi x) \sin(R\xi) d\xi \right]$$

If $F(\xi) = 2f_{\alpha}^{\beta}(\xi, y, y')\sin(\xi x)$, then the bracketed spectral integral on ξ is simply

$$\lim_{R\to\infty}\int_{-\infty}^{\infty}F(\xi)\sin(R\xi)\,d\xi$$

which vanishes because of the Riemann-Lebesgue lemma. The conjecture is correct, and

$$I_{3} + I_{A} = 0$$
 (4.15)

A final representation for I_{Γ} can be given as

$$I_{\Gamma} = \hat{y} \cdot \vec{j}_{e}(t) g_{\alpha,\xi=0}^{\beta}(y|t) - \hat{y} \cdot \vec{j}_{e}(0) g_{\alpha,\xi=0}^{\beta}(y|0)$$
 (4.16)

From this point onwards, any time a Green's function is referred to, it will be assumed to be of the form $g_{\alpha}^{\beta}(y|y')$ unless explicitly stated otherwise.

4.1.2 Uncoupled Transverse-Field EFIE

The transverse-field EFIE can now be specialized to explicitly account for the xinvariance of the planar waveguide structure. In this case, (4.1) becomes

$$\vec{e}_{t}(\vec{\rho}) = \vec{e}_{t}^{i}(\vec{\rho}) + k_{0}^{2} \int_{0}^{t} \delta n^{2}(y') \vec{g}_{t1}(y|y') \cdot \vec{e}_{t}(y') dy'$$

$$+ \int_{0}^{t} \frac{\delta n^{2}(y')}{n_{c}^{2}} \vec{g}_{tv}(y|y') \cdot \vec{e}_{t}(y') dy'$$

$$+ \int_{0}^{t} \vec{g}_{\phi}(y|y') [\vec{d}_{a}(y') \cdot \vec{e}_{t}(y')] dy'$$

$$- \frac{1}{n_{c}^{2}} [\delta n^{2}(t) (\hat{y} \cdot \vec{e}_{t}(t)) \vec{g}_{\phi}(y|t) - \delta n^{2}(0) (\hat{y} \cdot \vec{e}_{t}(0)) \vec{g}_{\phi}(y|0)]$$
(4.17)

where the Green's functions are now

$$\vec{g}_{t1} = \vec{I} g^{p} + \hat{x} g_{t}^{r} \hat{x} + \hat{y} \left(g_{n}^{r} + \frac{\partial g_{c}^{r}}{\partial y} \right) \hat{y}$$
 (4.18)

$$\vec{g}_{rv} = \hat{y} \frac{\partial}{\partial y} \left(g_t^r + g_n^r + \frac{\partial g_c^r}{\partial y} \right) \hat{y}$$
 (4.19)

$$\vec{g}_{\phi} = \hat{y} \left(k_c^2 g_c^r + \frac{\partial}{\partial y} \left(g_t^r + g_n^r + \frac{\partial g_c^r}{\partial y} \right) \right)$$
 (4.20)

and $\vec{d}_n = y \frac{\partial \ln n^2(y')}{\partial y'}$. Under close scrutiny, the dyadic Green's functions in (4.18)-

(4.19) are observed to be diagonal, and (4.17) can be written as

$$\vec{e}_{t}^{i}(y) = \vec{e}_{t}(y) - \int_{0}^{t} \delta n^{2}(y') \vec{g}_{x}(y|y') \cdot \vec{e}_{t}(y') dy'$$

$$- \int_{0}^{t} \delta n^{2}(y') \vec{g}_{y}(y|y') \cdot \vec{e}_{t}(y') dy'$$

$$- \int_{0}^{t} \vec{g}_{\phi}(y|y') \left[\vec{d}_{n}(y') \cdot \vec{e}_{t}(y') \right] dy'$$

$$+ \frac{1}{n^{2}} \left[\delta n^{2}(t) \vec{g}_{\phi}(y|t) \hat{y} \cdot \vec{e}_{t}(t) - \delta n^{2}(0) \vec{g}_{\phi}(y|0) \hat{y} \cdot \vec{e}_{t}(0) \right]$$
(4.21)

where

$$\frac{1}{n_c^2} \left(k_c^2 \vec{g}_{t1} + \vec{g}_{tv} \right) = \vec{g}_x + \vec{g}_y = \hat{x} \hat{x} g_{xx} + \hat{y} \hat{y} g_{yy}$$
 (4.22)

The contribution from the edges at y=0 and y=t involve as source terms only normal electric-field components (e_y) . Also note that $\overline{d}_n(y') \cdot \overline{e}_t(y') = d_{ny}(y')e_y(y')$ and that \overline{g}_{ϕ} is normally directed. This behavior, taken together with the diagonal dyadic Green's function, indicates that (4.17) decouples into two independent scalar integral equations.

The first scalar integral equation involves only the \hat{x} component of the electric field, and is given as

$$e_x^i(y) = e_x(y) - \int_0^t \frac{\delta n^2(y')}{n_c^2} g_{TE}(y|y') e_x(y') dy'$$
 (4.23)

where

$$g_{TE}(y|y') = k_c^2 [g^p(y|y') + g_t'(y|y')]$$
 (4.24)

This is the integral equation for TE waves on an asymmetric planar waveguide.

The second scalar integral equation involves only the e_y component of the electric field, and is

$$e_{y}^{i}(y) = e_{y}(y) - \int_{0}^{t} \frac{\delta n^{2}(y')}{n_{c}^{2}} g_{TM}(y|y') e_{y}(y') dy - \int_{0}^{t} g_{\phi y}(y|y') d_{y}(y') e_{y}(y') dy' + \frac{1}{n_{c}^{2}} \left[\delta n^{2}(t) g_{\phi y}(y|t) e_{y}(t) - \delta n^{2}(0) g_{\phi y}(y|0) e_{y}(0) \right]$$

where

$$g_{TM} = k_c^2 \left(g^p + g_n^r \right) + \frac{\partial}{\partial y} \left[\frac{\partial g_n^r}{\partial y} + \frac{\partial g_t^r}{\partial y} + \left(\frac{\partial^2}{\partial y^2} + k_c^2 \right) g_c^r \right]$$
(4.26)

$$g_{\phi y} = \frac{\partial g^{P}}{\partial y} + \left[\frac{\partial g_{t}^{r}}{\partial y} + \left(\frac{\partial^{2}}{\partial y^{2}} + k_{c}^{2} \right) g_{c}^{r} \right]$$
 (4.27)

This is the integral equation for TM waves on an asymmetric planar waveguide.

The EFIE for TM modal behavior is much more complicated than that for the TE modes. The extra terms are fields due to induced charge distributions within the waveguide. As observed in Chapter 2, $d_{ny}e_y$ is a volume polarization charge; this arises from an inhomogeneous film layer. Also, $\delta n^2(y_0)e_y(y_0)$ is a surface charge arising from the discontinuous jump in dielectric constant at the waveguide-cover and waveguide-substrate interfaces.

Finally, the Green's function scalar components appropriate to (4.24), (4.26) and (4.27) take the form

$$g^{p}(y|y') = \frac{e^{-\gamma_{c}|y-y'|}}{2\gamma_{c}} ; \begin{cases} g'_{t}(y|y') \\ g'_{c}(y|y') \\ g''_{n}(y|y') \end{cases} = \begin{cases} R_{T} \\ R_{N} \\ C \end{cases} \frac{e^{-\gamma_{c}(y+y')}}{2\gamma_{c}}$$
(4.28)

$$\gamma_{l} = \sqrt{\zeta^{2} - k_{l}^{2}}$$
; $l = s, c$ (4.29)

where the following coefficients are specifically for the two-layer interface

$$R_T = \frac{\gamma_c - \gamma_s}{\gamma_c + \gamma_s} \tag{4.30}$$

$$R_N = \frac{N_{sc}^2 \gamma_c - \gamma_s}{N_{sc}^2 \gamma_v + \gamma_s}$$
 (4.31)

$$C = \frac{2(N_{sc}^2 - 1)\gamma_c}{(\gamma_c + \gamma_c)(N_{sc}^2 \gamma_c + \gamma_c)}$$
(4.32)

4.2 TE Asymmetric Planar Waveguide Radiation Modes

There are two major considerations in determining the radiation spectrum of the planar waveguide. The first is choosing a method to solve for the unknown field distribution within the film guiding region. The second is choosing an appropriately located and directed source to maintain the impressed field upon the planar waveguide. It should be noted at the outset that the TEFIE as presented in (4.1) is not applicable to determining the impressed field upon the planar waveguide; for this, the definition of the electric field via the Hertzian potential (A.11) is used in conjunction with the original dyadic Green's function (2.42) with scalar components as developed in (4.28)–(4.32).

Consider the configuration of Figure 4.3. The appropriate EFIE for analysis is (4.23). The unknown field e_x will be determined by a method-of-moments expansion. The unknown field will be expanded in terms of pulse functions, namely

$$e_{x}(y) = \sum_{n=1}^{N} e_{xn} p_{n}(y) ; p_{n}(y) = \begin{cases} 1; & |y-y_{n}| < \frac{\Delta y}{2} \\ 0; & elsewhere \end{cases}$$
 (4.33)

where $y_n = (n - \frac{1}{2}) \Delta y$; $\Delta y = t/N$. The film layer will be assumed to be homogeneous, consequently, $n^2(y') = n_f^2$ and $\delta n^2(y') = n_f^2 - n_c^2 = \Delta N_{fc}^2$. Under these considerations,

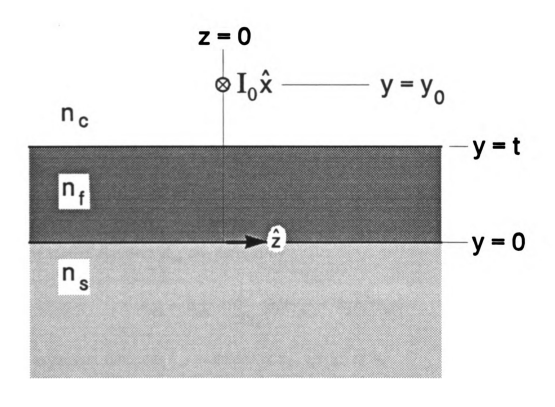


Figure 4.3 TE excitation of planar waveguide by line source at $y=y_0$, z=0.

the scalar EFIE for TE modes becomes

$$\sum_{n=1}^{N} e_{xn} \left[p_{n}(y) - \frac{\Delta k^{2}}{2\gamma_{c}} \left[h_{n}^{p}(y) + R_{T} h_{n}^{r}(y) \right] \right] = e_{x}^{inc}(y)$$
 (4.34)

where $\Delta k^2 = \Delta N_{fe}^2 k_0^2$ and the expansion functions are

Point match (4.34) at the center of each basis function by employing the testing operator

$$\int_{0}^{t} \delta(y - y_{m}) \cdots dy \; ; \quad m = 1, 2, \dots N$$
 (4.36)

The result can be written as

$$[A_{mn}][e_{xn}] = [e^{inc}(y_m)]$$
 (4.37)

where the matrix elements A_{ma} are defined by

$$A_{mn} = \delta_{mn} - \frac{\Delta k^2}{2\gamma_c} [h_n^P(y_m) + R_T h_n^r(y_m)]$$
 (4.38)

and the expansion functions h_n , evaluated at x_m , are given as

$$h_n^p(y_m) = \frac{2}{\gamma_c} \begin{cases} e^{-\gamma_c |y_m - y_n|} \sinh(\gamma_c \frac{\Delta y}{2}) ; y_m \neq y_n \\ 1 - e^{-\gamma_c \frac{\Delta y}{2}} ; y_m = y_n \end{cases}$$

$$h_n^p(y_m) = \frac{2}{\gamma_c} e^{-\gamma_c (y_m + y_n)} \sinh(\gamma_c \frac{\Delta y}{2})$$

$$(4.39)$$

The selection of an impressed field has yet to be considered. From Appendix A, the impressed field necessary in (4.37) can be calculated from

$$e_x^i = \hat{x} \cdot (k_c^2 + \tilde{\nabla} \tilde{\nabla} \cdot) \vec{\pi}^i$$

where, of course,

$$\vec{\pi}^{i}(y) = \frac{1}{j\omega\epsilon_{\epsilon}} \int \vec{g}(y|y') \cdot \vec{j}^{\epsilon}(y) dy'$$

All sources for the impressed field must be x-invariant; furthermore, the $\mathcal{L} \cdot \nabla$ operator vanishes. Thus, the impressed field for TE excitation is

$$e_x^i(y) = k_c^2 \pi_x(y)$$
 (4.40)

The only source able to support the impressed TE field (4.40) is an \hat{x} -directed current of $\vec{j}^{e}(y) = \hat{x}j_{x}^{e}(y)$, as depicted in Figure 4.3. The specific form of the impressed TE field supported by the line current is then

$$e_x^{inc}(y_m) = \frac{-j\eta_c k_c}{2\gamma_c} \int_0^t \left[e^{-\gamma_c |y_m - y'|} + R_T e^{-\gamma_c (y_m + y')} \right] j_x^e(y') dy'$$
 (4.41)

4.3 Results

A method-of-moments code was implemented for a symmetric planar dielectric waveguide of thickness t located within 0 < y < t. This is shown in Figure 4.3. The guiding region (film layer) is uniform and homogeneous with a refractive index n_f , the cover refractive index is n_c , and the substrate refractive index $n_s = n_c$.

It is desirable to compare to known results. From Rozzi [10], the radiation eigenmodes of a symmetric planar waveguide of guiding refractive index n_f , cover refractive index n_c and thickness 2d are, for the TE even case,

$$e_x(y) = \sqrt{\frac{2}{\pi}} \frac{1}{C} \cos \sigma y, \qquad |y| < d \qquad (4.42)$$

$$C = \sqrt{1 + \left(\frac{\nu}{\rho}\right)^2 \sin^2 \sigma d}$$
 (4.43)

where $\rho = -j\gamma_c$ is the wavenumber in the cover region, ranging from $0 < \rho < \infty$. Also, $\sigma^2 = v^2 + \rho^2$ and $v^2 = k_0^2 (n_f^2 - n_c^2)$. Note that the form given in (4.42) assumes the waveguide is centered about the origin in y. An eigenmode expansion for the excitation of a line-source located at y_0 is simple; the total radiation field is

$$E_x^R(y,z) = \frac{k_0 \eta_0 I_0}{2\pi} \int_0^z \frac{\cos[\sigma(y-t/2)] \cos[\sigma(y_0-t/2)]}{C^2 \zeta(\rho)} e^{j\zeta(\rho)|z-z'|} d\rho \qquad (4.44)$$

where the origin has been shifted to the center of the previously mentioned waveguide.

To excite even eigenmodes in the planar waveguide, the impressed field must be supported by an line source current in the transform domain of

$$j_x^e(y,z,\zeta) = I_0 \delta(y-t/2)e^{-j\zeta z'}$$

located at the center of the waveguide $(y_0 = t/2)$. This leads to the MoM implementation of the impressed field

$$e_x^i(y_m) = I_0 e^{-j\zeta x'} \frac{-j\eta_0 k_0}{2\gamma_c} \left[e^{-\gamma_c|y_m-t/2|} + R_T e^{-\gamma_c(y_m+t/2)} \right]$$
(4.45)

Because of the symmetry of the background environment, only one branch cut in the axial transform plane is implicated. From Chapter 3, the total spatial radiation field for the symmetric planar waveguide is constructed from the solutions to the EFIE as

$$E_x^R(y,z) = \frac{1}{2\pi} \int_{k_c}^{-jm} \left[e_x(y,\zeta^i) - e_x(y,\zeta^o) \right] e^{j\zeta|z-z'|} d\zeta$$
 (4.46)

For the case of limiting low-loss dielectrics, γ_c exhibits conjugate behavior on either side of the branch cut. When this conjugate behavior is considered in equations (4.23),

(4.24), (4.28), (4.30), and (4.41); it becomes obvious that the radiation spectral mode fields possess conjugate behavior as well, namely

$$e_x(y,\zeta^i) = jk_0\eta_0I_0\psi_x(y,\zeta)$$

$$e_x(y,\zeta^o) = jk_o \eta_0 I_0 \psi_x^{\bullet}(y,\zeta)$$

Here, ζ without any superscripting is assumed to be the interior side of the branch cut.

The EFIE-determined radiation field then can be constructed as

$$E_x^R(y,z) = \frac{-jk_0\eta_0I_0}{2\pi}\int_0^{\infty} \left[\psi_x(y,\zeta) - \psi_x^{\bullet}(y,\zeta)\right] e^{j\zeta|z-z'|} \frac{\rho}{\zeta} d\rho \qquad (4.47)$$

where the integration has been parameterized upon the wavenumber in the cover and where $-j\gamma_c = \rho$.

The integral-operator technique is now applied to a symmetric planar waveguide where $n_f = 1.5$, $n_c = 1.0$, and $t = 0.25\lambda$. Results are given in Figure 4.4, where the integrands of equations (4.44) and (4.47) are compared for various spatial frequencies in the cover ρ (normalized to k_0). This corresponds to an axial wavenumber ζ on the branch cut of

$$\zeta = \begin{cases} k_0 \sqrt{n_c^2 - \rho^2} & ; & 0 < \rho < n_c \\ -jk_0 \sqrt{\rho^2 - n_c^2} & ; & n_c < \rho < \infty \end{cases}$$
 (4.48)

It is evident that agreement between the two techniques is very good. Both methods show that the field periodicity within the waveguide increases as spectral frequency increases. The spectral peaking associated with these radiation modes is also exhibited. For the symmetric planar waveguide, the agreement between the integral-operator analysis and classical differential operator theory is very good.

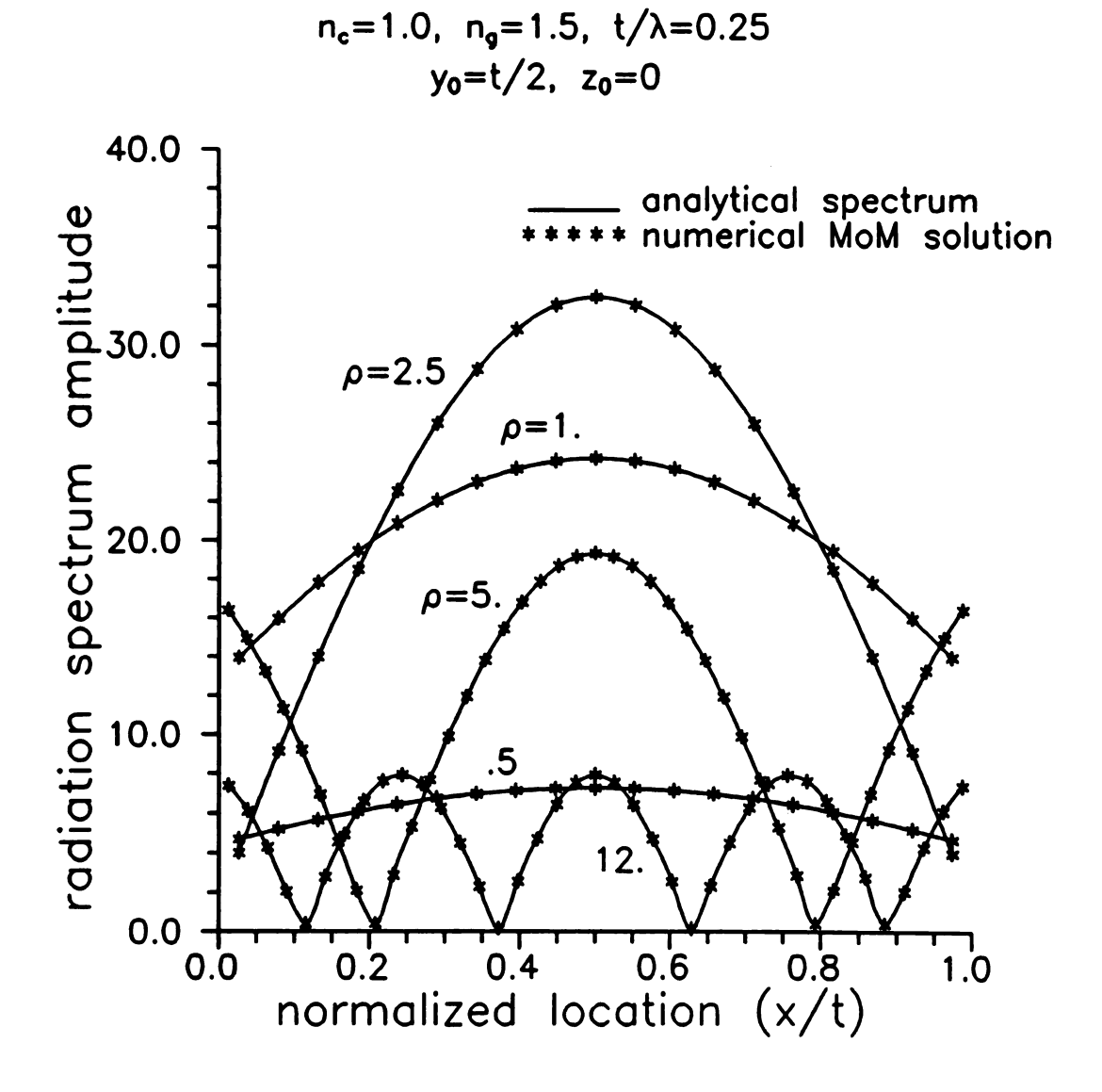


Figure 4.4 Spectral radiation mode amplitudes of a symmetric planar waveguide obtained by the integral-operator method compared to Rozzi's analytical closed-form results.

This same integral equation is now applied to an asymmetric planar waveguide. This waveguide under consideration has the same physical characteristics as the symmetric planar waveguide considered, save that now $n_s \neq n_c$. This introduces another branch cut in the axial transform plane associated with k_s . In the low-loss limit, the branch cuts coalesce as shown in Figure 4.5, where an upper half-plane closure has been chosen (case of z > z'). It is obvious that there are two distinct regimes of the radiation spectrum. The substrate radiation regime is associated with branch cut S, where $n_c < \zeta_r/k_o < n_s$. In this regime, γ_s is imaginary and possesses conjugate behavior on S while γ_c is still real (or ρ is imaginary). The cover, or full, radiation regime is associated with branch cut S. In this regime, both γ_s and γ_c are imaginary and possess conjugate behavior.

Figure 4.6 shows the amplitudes of various radiation regime spectral modes as defined in (3.47) for an asymmetric planar waveguide with $n_f = 1.5$, $n_c = 1.0$, $t = 0.25\lambda$, and $n_s = 1.2$ (so $n_s/n_c = 1.2$). The excitation remains a line current at $y_0 = t/2$, the center of the guiding region. The values of ζ correspond to z > z' closure as in Figure 4.5. It is obvious that the amplitudes associated with the substrate radiation regime $(-1.2 < \zeta < -1.0)$ are small compared to those in the full radiation regime, indicating that the full radiation regime dominates the non-evanescent portion of the radiation spectrum. As ζ moves deeper into the full radiation regime, the field periodicity increases as expected.

Figure 4.7 and Figure 4.8 both show the effect of asymmetry in the background environment (moderate asymmetry $n_s/n_c=1.2$ for Figure 4.7 and small asymmetry $n_s/n_c=1.05$ for Figure 4.8) on the radiation spectral modes by comparing to those

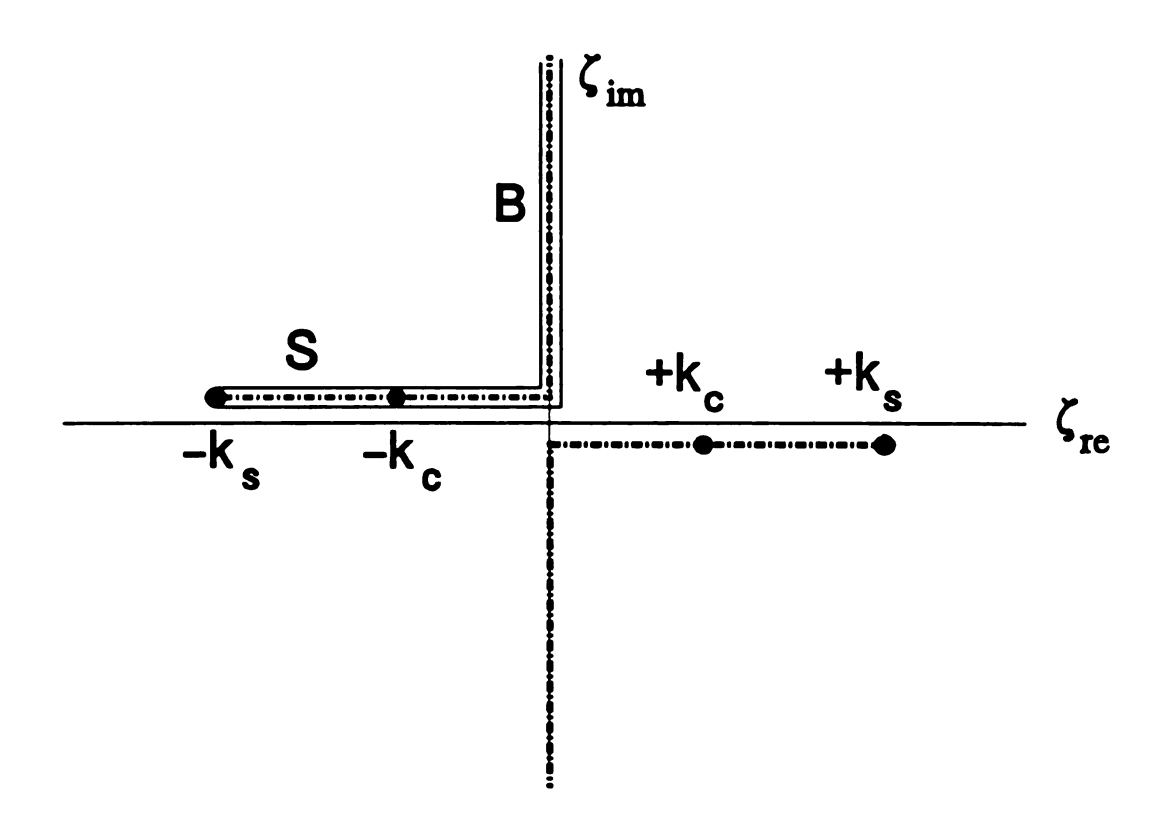


Figure 4.5 Axial-wavenumber plane (complex 5-plane) branch cuts for a typical asymmetric planar waveguide.

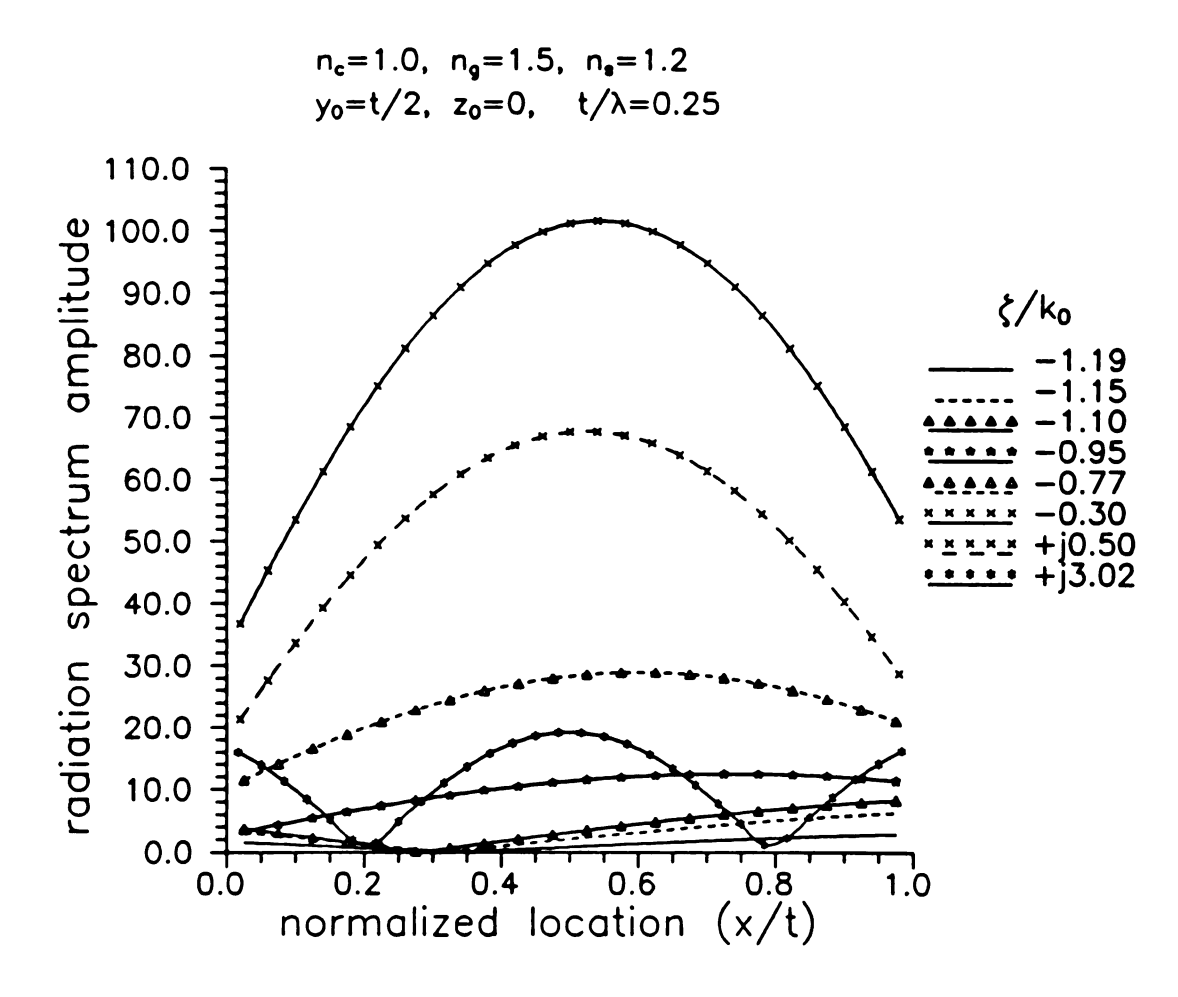


Figure 4.6 Spectral radiation modes in guiding region of asymmetric planar waveguide for both substrate and full radiation regimes.

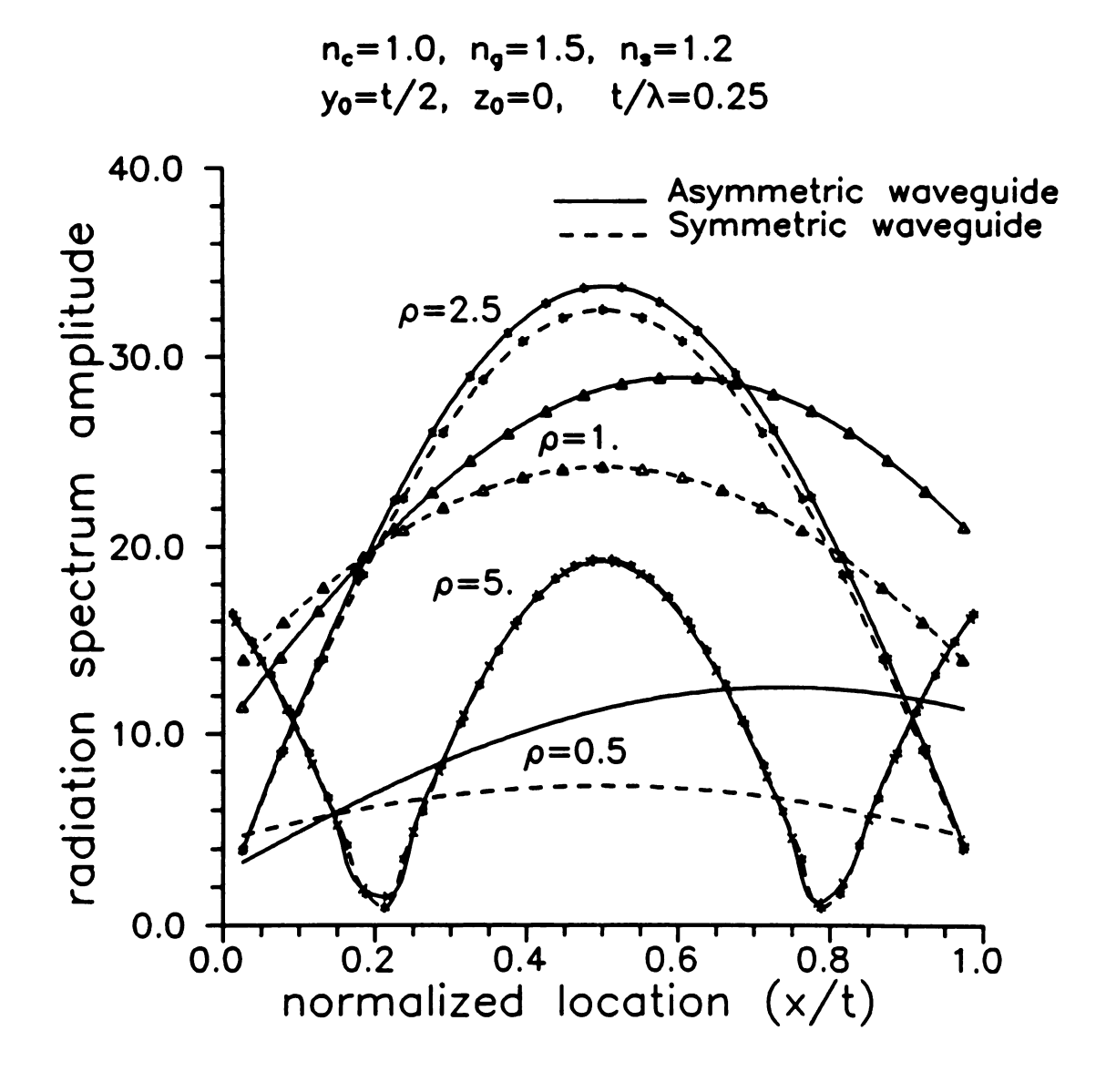


Figure 4.7 Effect of asymmetry $(n_r/n_c = 1.2)$ on the radiation mode field distributions, compared to the symmetric planar waveguide.

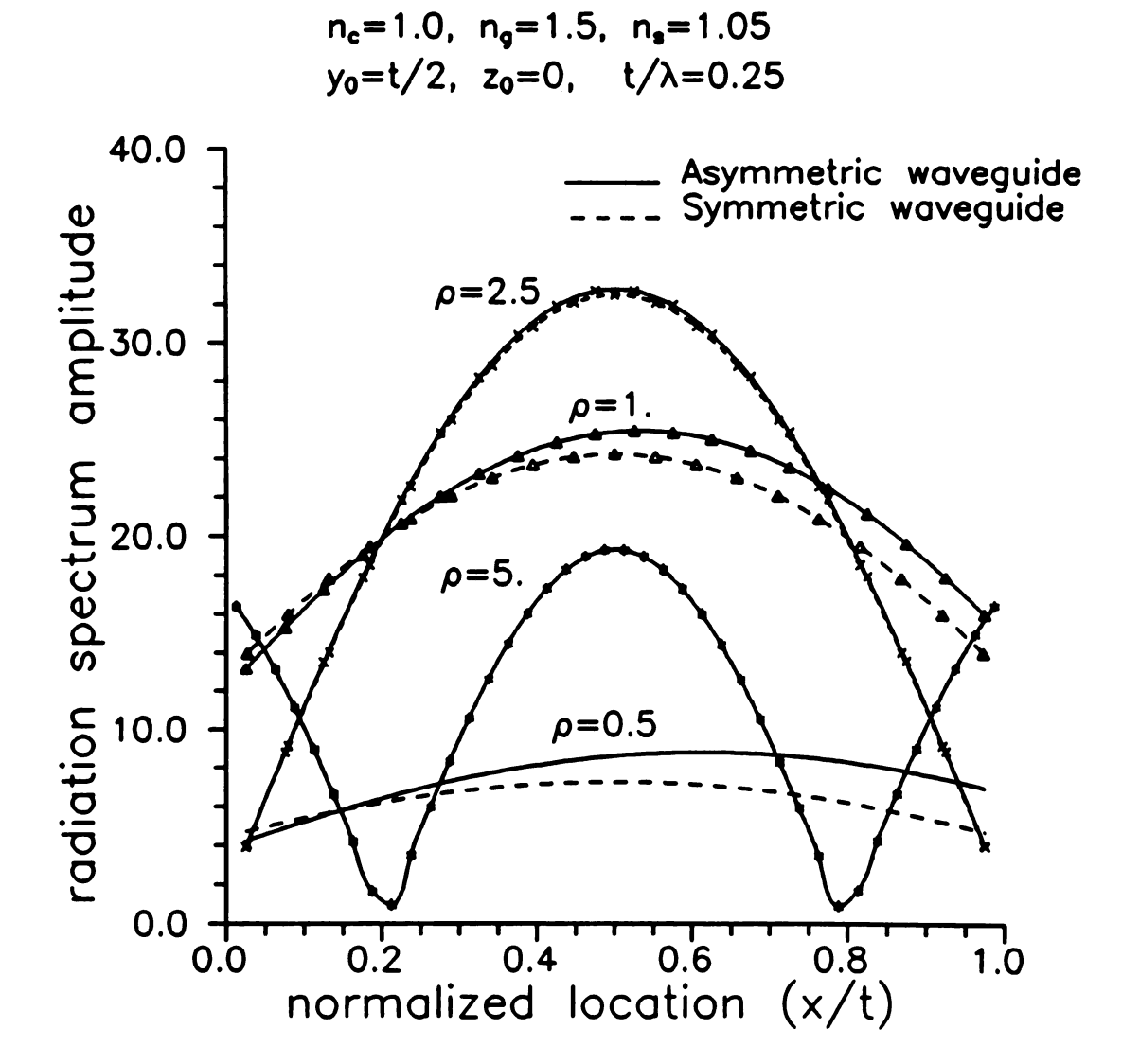


Figure 4.8 Effect of small amount of asymmetry $(n_r/n_c = 1.05)$ on the radiation mode field distributions, compared to symmetric planar waveguide.

spectral modes of a symmetric environment. This comparison is only made over the full radiation regime for normalized cover spectral frequency ρ (relation (4.48) still is valid), as there is no substrate regime for the symmetric case. A noticeable shift in the location of the guiding region maximum towards the cover is observed over the propagating portion of the full radiation spectrum $(0 < \zeta_r/k_0 < n_c \text{ or } n_c > \rho > 0)$ for the asymmetric case. The amplitudes increase as well. Both effects are more significant at low spectral frequencies. Furthermore, these shifts are more pronounced when strongly asymmetric.

As ρ moves deeper into the full radiation regime and the modes become evanescent, the maximum shift and amplitude difference disappear as seen in both Figure 4.7 and in Figure 4.8. Deep into the radiation regime, $\rho \approx \zeta/k_0$, meaning that $\gamma_s \rightarrow \gamma_c \rightarrow j\zeta$. At high spectral frequencies, ζ dominates both k_c , k_s , and the background environment is a slight perturbation effect on the impressed field. This indicates that iterative techniques can be quite effective in determining the radiation spectral modes at high spectral frequencies.

Summary

This chapter has demonstrated the implementation of the integral-operator technique in determining the continuous radiation spectrum for planar waveguides. The symmetric TE planar waveguide is a canonical problem for which closed-form analytical solutions are readily available. The integral-operator technique was found to be accurate and effective for determining the spectral radiation modes of these canonical problems.

Chapter 5

Continuous Radiation Spectrum for Microstrip Transmission Line

Having established that the transform-domain integral equation recovers the correct radiation spectrum for a canonical planar waveguide structure, it can now be applied to more common open-boundary waveguiding structures. This chapter applies the theory to the case of an isolated microstrip transmission line. In this chapter, numerical solution of the EFIE for a single microstrip line is implemented by Galerkin's method of moments with Chebyshev polynomial basis functions. Radiation-regime current distributions are presented.

5.1 Application of the EFIE

A typical microstrip line is shown in Figure 5.1. In this case, the strip is assumed to be a perfect conductor with infinitesimal thickness and a width of 2w, located at the film/cover interface. The film layer is of thickness t, and may in general be a lossy dielectric. This film layer is backed by a perfect conductor at y=-t and immersed in an air cover region.

Radiation spectrum surface currents of the microstrip line are determined by solving the EFIE for microstrip devices (2.43) under excitation; for the present case, the appropriate EFIE becomes

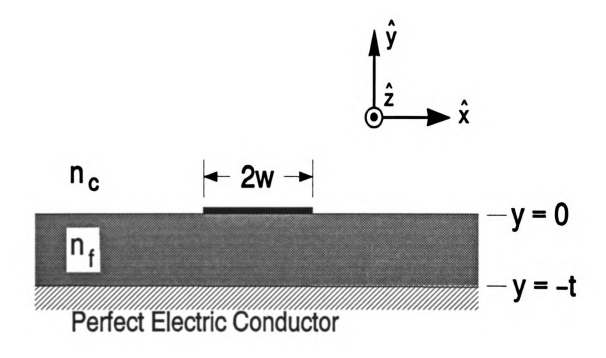


Figure 5.1 Configuration of microstrip transmission line.

$$\lim_{y\to 0} \hat{t} \cdot \int_{-w}^{w} \vec{g}^{e}(x | x'; y | y'=0; \zeta) \cdot \vec{k}(x', \zeta) dx' = -\hat{t} \cdot \vec{e}^{i}(x, y=0, \zeta)$$
 (5.1)

in the limit where $y \to 0$ on the surface of the strip and where the electric Green's dyad is used for notational compactness. Exchange of the limit $y \to 0$ with the source point integration is permissible under the condition that the integral remains convergent. When the source point and the observation point coincide, special consideration may be needed; convergence properties will be examined later. The same observation applies to the impressed field; however, it is of significance only if the source for the impressed field is at y = 0.

The surface current on the infinitely thin strip has only tangential components in the axial (z) and transverse (x) directions, namely

$$\vec{k}(x,\zeta) = \hat{x} k_x(x,\zeta) + \hat{z} k_y(x,\zeta) \tag{5.2}$$

One immediate consequence arising from this current distribution is the observation that the depolarizing dyad for the electric Green's dyadic is not necessary. Direct substitution of (5.2) into (5.1) and enforcing the tangential boundary conditions results in a pair of coupled scalar integral equations

$$\int_{-w}^{w} \left\{ g_{xx}^{e}(x \mid x'; y \mid 0; \zeta) k_{x}(x') + g_{xx}^{e}(x \mid x'; y \mid 0; \zeta) k_{z}(x') \right\} dx' = -e_{x}^{i}(x, y = 0)$$

$$\int_{-w}^{w} \left\{ g_{zx}^{e}(x \mid x'; y \mid 0; \zeta) k_{x}(x') + g_{zz}^{e}(x \mid x'; y \mid 0; \zeta) k_{z}(x') \right\} dx' = -e_{z}^{i}(x, y = 0)$$
(5.3)

It should be noted that even though (5.3) does not involve normal (9) electric field component this does not mean there are no normal electric fields. The scalar components of the electric dyadic Green's function are given as

$$g_{\alpha\beta}^{e}(x|x',y|0) = \frac{1}{2\pi} \int_{-\infty}^{\infty} C_{\alpha\beta}(\xi,\zeta) e^{j\xi(x-x')} e^{-p_{c}y} d\xi \qquad (5.4)$$

where α , β assume values of x and z. The coefficients $C_{\alpha\beta}$ are functions of ξ and ζ , taking the specific forms of

$$C_{xx}(\xi,\zeta) = \frac{(N_k^2 - 1)\xi^2 p_c}{Z^h(\xi)Z^e(\xi)} + \frac{(k_c^2 - \xi^2)}{Z^h(\xi)},$$
 (5.5)

$$C_{xx}(\xi,\zeta) = C_{zx}(\xi,\zeta) = \frac{(N_{fc}^2 - 1)\zeta\xi p_c}{Z^h(\xi)Z^a(\xi)} - \frac{\zeta\xi}{Z^h(\xi)},$$
 (5.6)

$$C_{zz}(\xi,\zeta) = \frac{(N_k^2 - 1)\zeta^2 p_c}{Z^h(\xi)Z^e(\xi)} + \frac{(k_c^2 - \zeta^2)}{Z^h(\xi)}.$$
 (5.7)

and where Z^a and Z^b are defined in Appendix B.

As the microstrip line is symmetric about x = 0, invoking parity about this point can simplify the problem. For the microstrip, the parity states depend upon the surface current and surface charge density. The surface charge density in terms of $\vec{k}(x)$ is

$$\rho_s(x) = \frac{\partial}{\partial x} k_x(x) + j \zeta k_z(x)$$

which can be decomposed into even and odd behavior in x. Looking at the dependence of the surface charge upon $\vec{k}(x)$, it is readily apparent that *even* axial surface currents and *odd* transverse surface currents generate an *even* charge distribution; this will be considered an even mode of the microstrip transmission line. Consequently, the appropriate parity states are then

even mode:
$$k_z(-x) = k_z(x)$$
; $k_x(-x) = -k_x(x)$
odd mode: $k_z(-x) = -k_z(x)$; $k_z(-x) = k_z(x)$ (5.8)

5.2 Method-of-Moments Solution

As with the planar waveguide, there are two issues to resolve at this point – method of solution for the EFIE and choice of excitation. Solution of integral equation (5.3) is accomplished with Galerkin's method of moments utilizing entire-domain basis functions. These basis functions are chosen to explicitly accommodate the edge singularity in axial current. Entire-domain basis functions are preferred in this situation primarily because the current is represented in a compact form with a relatively small number of unknown expansion coefficients.

The transverse and axial current components are expanded as

$$k_x(x) = \sum_{n=0}^{N} k_{xn} u_{xn}(x)$$
 $k_z(x) = \sum_{n=0}^{N} k_{zn} u_{zn}(x)$ (5.9)

where the $u_{an}(x)$'s exist over the entire domain $-w \le x \le w$ and have the axial current edge singularity built in. Substitution of MoM expansion (5.9) into (5.3) results in

$$\sum_{n=1}^{N} k_{xx} I_{xxn}^{e}(x) + \sum_{n=1}^{N} k_{xx} I_{xxn}^{e}(x) = -e_{x}^{i}(x)$$

$$\sum_{n=1}^{N} k_{xx} I_{xxn}^{e}(x) + \sum_{n=1}^{N} k_{xx} I_{xxn}^{e}(x) = -e_{x}^{i}(x)$$
(5.10)

to be enforced on the domain $-w \le x \le w$, and where

$$I_{\alpha\beta n}^{e}(x) = \lim_{y \to 0} \int_{-\infty}^{\infty} g_{\alpha\beta}^{e}(x | x'; y | 0; \zeta) u_{\beta n}(x') dx'$$
 (5.11)

In Galerkin's method, the expansion basis functions are used as the testing functions, resulting in a testing operator of

$$\int_{-\infty}^{\infty} dx \, u_{\alpha,m}(x) \{ \dots \} \qquad \dots \quad \alpha = x, z$$

which leads to a set of 2N by 2N linear equations that can be written in matrix form as

$$\begin{bmatrix} A_{xx}^{mn} & A_{xz}^{mn} \\ A_{zx}^{mn} & A_{zx}^{mn} \end{bmatrix} \begin{bmatrix} k_{xn} \\ k_{zn} \end{bmatrix} = \begin{bmatrix} B_{x}^{m} \\ B_{z}^{m} \end{bmatrix} \qquad \dots m, n = 0, 1, \dots N$$

$$(5.12)$$

The matrix elements are

$$A_{\alpha\beta}^{mn} = \int_{-w}^{w} u_{\alpha m}(x) I_{\alpha\beta n}^{e}(x) dx \qquad (5.13)$$

$$B_{\alpha}^{m} = \int_{-w}^{w} u_{\alpha m}(x) e_{\alpha}^{i}(x) dx \qquad (5.14)$$

where α , β take the values of x or z and where $I_{\alpha\beta n}^{e}$ is defined in (5.11). This MoM matrix equation is inhomogeneous, and is easily solved for a given excitation.

5.2.1 MoM expansions

Implementation of the method of moments solutions to develop the matrix elements given by (5.13) and (5.14) is straightforward. In this implementation, the spatial integrations over the basis functions will be exchanged with the spectral integration defining the Green's functions. Consequently, (5.13) becomes

$$A_{\alpha\beta}^{mn} = \lim_{\gamma \to 0} \int_{-\infty}^{\infty} e^{-p_c \gamma} C_{\alpha\beta}(\xi) g_{\alpha m}(\xi) f_{\beta n}(\xi) d\xi \qquad \cdots \quad \alpha, \beta = x, z.$$
 (5.15)

where

$$f_{\beta n}(\xi) = \int_{-\infty}^{\infty} u_{\beta n}(x') e^{-j\xi x'} dx'$$
 ... $\beta = x, z$. (5.16)

$$g_{\alpha m}(\xi) = \int_{-w}^{w} u_{\alpha m}(x) e^{j\xi x} dx \qquad \cdots \quad \alpha = x, z.$$
 (5.17)

Matrix element (5.14) cannot be dealt with until a source excitation is chosen.

In this solution, Chebyshev polynomials with square-root edge factors are utilized as basis functions where

$$u_{xx}(x) = T_{x}(x/w)\sqrt{1 - (x/w)^{2}}$$

$$... -w \le x \le w$$

$$u_{xx}(x) = T_{x}(x/w)/\sqrt{1 - (x/w)^{2}}$$
(5.18)

where $T_n(x/w)$ is a Chebyshev polynomial of order n of the first kind and k_{xn} and k_{zn} are unknown expansion coefficients. One advantage of using Chebyshev polynomials as basis functions is that the spatial integrals can be evaluated analytically in closed form. Noticing the fact that Chebyshev polynomials of even order are even functions and odd order are odd functions, the spatial integrals reduce to the following four generic types and are evaluated as

$$\int_{0}^{w} \frac{T_{2n}(x/w)}{\sqrt{1-(x/w)^{2}}} \cos(\xi x) dx = (-1)^{n} \frac{\pi w}{2} J_{2n}(\xi w)$$
 (5.19)

$$\int_{0}^{w} \frac{T_{2n+1}(x/w)}{\sqrt{1-(x/w)^{2}}} \sin(\xi x) dx = (-1)^{n} \frac{\pi w}{2} J_{2n+1}(\xi w)$$
 (5.20)

$$\int_{0}^{w} T_{2n}(x/w) \sqrt{1 - (x/w)^{2}} \cos(\xi x) dx$$

$$= (-1)^{n} \frac{\pi w}{4} \left[J_{2n}(\xi w) + \frac{1}{2} J_{2(n+1)}(\xi w) + \frac{1}{2} J_{2(n-1)}(\xi w) \right]$$
(5.21)

$$\int_{0}^{w} T_{2n+1}(x/w) \sqrt{1 - (x/w)^{2}} \sin(\xi x) dx$$

$$= (-1)^{n} \frac{\pi w}{4} \left[J_{2n+1}(\xi w) + \frac{1}{2} J_{2(n+1)+1}(\xi w) + \frac{1}{2} J_{2(n-1)+1}(\xi w) \right]$$
(5.22)

where $J_{\mathbf{n}}(x)$ is the Bessel function of first kind.

5.2.2 Excitation considerations

Choice of an excitation will be made in the sense of Chapter 3; that is, point sources will be used to identify basic behavior of the radiation spectral components. The field supported by a point source within the layered background of the microstrip transmission line is given by

$$\vec{e}(\vec{r}) = -j\eta_0 k_0 \int \vec{g}^{\,e}(\vec{\rho} \mid \vec{\rho}'; \zeta) \cdot \vec{j}^{\,i}(\vec{\rho}') ds'$$

For a point source current at $\vec{\rho} = \vec{\rho}_0$ flowing in the \hat{x}_a direction,

$$\vec{j}^{i}(\vec{\rho}) = I_0 \delta(\vec{\rho} - \vec{\rho}_0) \hat{x}_a$$

The appropriate fields incident upon the microstrip transmission line then become

$$e_x^i(\vec{\rho}) = e_0 \hat{x} \cdot \vec{g}^e(\vec{\rho} \mid \vec{\rho}_0; \zeta) \cdot \hat{x}_{\alpha}$$

$$e_z^i(\vec{\rho}) = e_0 \hat{z} \cdot \vec{g}^e(\vec{\rho} \mid \vec{\rho}_0; \zeta) \cdot \hat{x}_{\alpha}$$
(5.23)

where $e_0 = -j\eta_c k_c I_0$.

An arbitrary current density can be decomposed into its even and odd contributions. This fact can be exploited to reduce problem complexity. It is desirable to excite the even and odd parity radiation-mode surface currents on the microstrip using a point source excitation. For *even* parity on the microstrip line, axial surface current is even, transverse current is odd, and the surface charge distribution is even about x=0. How does the surface current parity affect electric field parity? Consider that $\hat{n} \cdot (\epsilon_e \vec{e}(x)) = -\rho_s(x)$ at the surface of a perfect conductor, of which the microstrip transmission line is assumed to consist. Since $\hat{n} = \hat{y}$, obviously, $e_y(x)$ is even in x for even microstrip modes. An analysis of Maxwell's equations (6.3),(6.4) indicates that $e_z(x)$ will be even while $e_x(x)$ will be odd in x. Obviously, the opposite situation prevails for odd microstrip parity state.

Based on the above analysis, a point source excitation current within the system must take on the form

even:
$$\vec{j}(x_0, y_0) = \hat{z}\delta(y - y_0)$$
 at $x_0 = 0$
odd: $\vec{j}(x_0, y_0) = \hat{x}\delta(y - y_0)$ at $x_0 = 0$ (5.24)

to excite even/odd modes of the microstrip. Figure 5.2 and Figure 5.3 show this set of currents. Consequently, this results in an impressed field within the layered background of

$$e_x^{even}(x,y) = \hat{x} \cdot \ddot{\mathbf{g}}^{\circ}(x|0;y|y_0) \cdot \hat{z}$$

$$e_z^{even}(x,y) = \hat{z} \cdot \ddot{\mathbf{g}}^{\circ}(x|0;y|y_0) \cdot \hat{z}$$

$$e_x^{odd}(x,y) = \hat{x} \cdot \ddot{\mathbf{g}}^{\circ}(x|0;y|y_0) \cdot \hat{x}$$

$$e_z^{odd}(x,y) = \hat{z} \cdot \ddot{\mathbf{g}}^{\circ}(x|0;y|y_0) \cdot \hat{x}$$

Once the source excitation has been chosen, the impressed field is then worked into the Method-of-Moments expansion. Manipulating the forcing function matrix element (5.14) in the same fashion as (5.13) results in

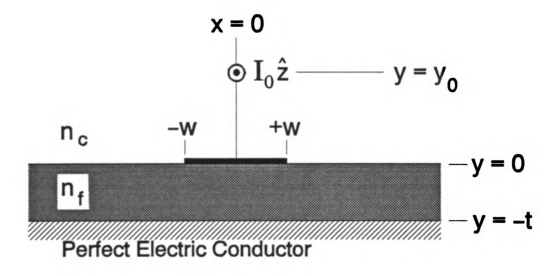


Figure 5.2 Excitation of even radiation spectral modes for microstrip line.

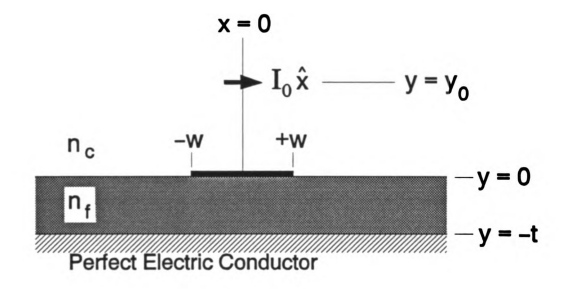


Figure 5.3 Excitation of odd radiation spectral modes for microstrip line.

$$B_{\alpha}^{m} = \int_{-\infty}^{\infty} e^{-p_{c}y_{0}} e^{-j\xi x_{0}} C_{\alpha y}(\xi) g_{\alpha m}(\xi) d\xi \qquad \cdots \quad \alpha, = x, z; \qquad (5.29)$$

where ν is the excitation current orientation and $x_0 = 0$ for parity state excitation.

One final point of interest involves the MoM form of the forcing function B_a^m . Whenever the excitation source is distant $(y_a | \text{large})$, or whenever the axial wavenumber ζ is far into the evanescent radiation spectrum $(\zeta = j\zeta_i, \zeta_i | \text{large})$, the $e^{-p_e y_0}$ term becomes highly oscillatory as $\xi \to \xi_{bc}$. This situation is amenable to evaluation by asymptotic methods about the saddle point.

Performing an asymptotic evaluation involves casting B_a^m in the form

$$B_{\alpha}^{m} = \int_{-\infty}^{\infty} F_{\alpha}^{m}(\xi) e^{\alpha f(\xi)} d\xi$$

where $\alpha = -y_0$ and $f(\xi) = p_c = \sqrt{\xi^2 - \xi_{bc}^2}$. The saddle point occurs when $f'(\xi_0) = 0$; this is at $\xi = 0$. Deforming the integration into the steepest-descents contour in the complex ξ -plane results in

$$B_{\alpha}^{m} = 2e^{-jq(\xi_{B}y_{0}-\pi/4)} \int_{-\infty}^{\infty} F_{\alpha}^{m}(jq\xi_{B},R) e^{-y_{0}R^{2}/2\xi_{B}^{2}} dR$$
 (5.30)

where a change of variables shows that

$$B_{\alpha}^{m} = 2\sqrt{\frac{2\xi_{B}}{y_{0}}}e^{-jq(\xi_{B}y_{0}-\pi/4)}\int_{-\infty}^{\infty}F_{\alpha}^{m}(jq\xi_{B},P)e^{-P^{2}}dP \qquad (5.31)$$

This could be indicative of problems as 5 becomes large.

5.3 Results

The method-of-moments analysis was implemented numerically. The results presented here are typical. The physical parameters of the low-loss microstrip transmission line under question are: film refractive index $n_f=3.13$, cover index of $n_c=1$, film thickness of $t=0.0635\lambda$, and a strip half-width w=2.85t. Even modes were excited by a \hat{z} directed unit current source at x=0 (Figure 5.2), while odd modes were excited by a unit current at x=0 flowing in the \hat{z} direction (Figure 5.3). All results were determined assuming an upper half-plane closure (z>z'). The radiation regimes for this problem are seen in Figure 5.4.

Figure 5.5 and Figure 5.6 show the normalized current distributions for the axial and transverse surface currents within the full radiation regime (branch cut *B*). It is obvious that as axial wavenumber \(\) moves deeper into the full radiation regime that the periodicity of the induced current on the microstrip increases. The amplitude appears to have no discernable pattern at this time. Figure 5.7 compares the effects of differences in excitation current location in \(y \) upon the radiation mode surface current density. It is apparent that as the excitation source approaches the microstrip, the transverse currents are strongly excited. This is because, near the microstrip, the \(x \)-directed electric field dominates. This has significance for microstrip excitation problems by near-proximity sources, as it shows that any quasi-TEM analysis, or analysis ignoring the transverse current, will not be sufficient because of the dominant effect of that electric field.

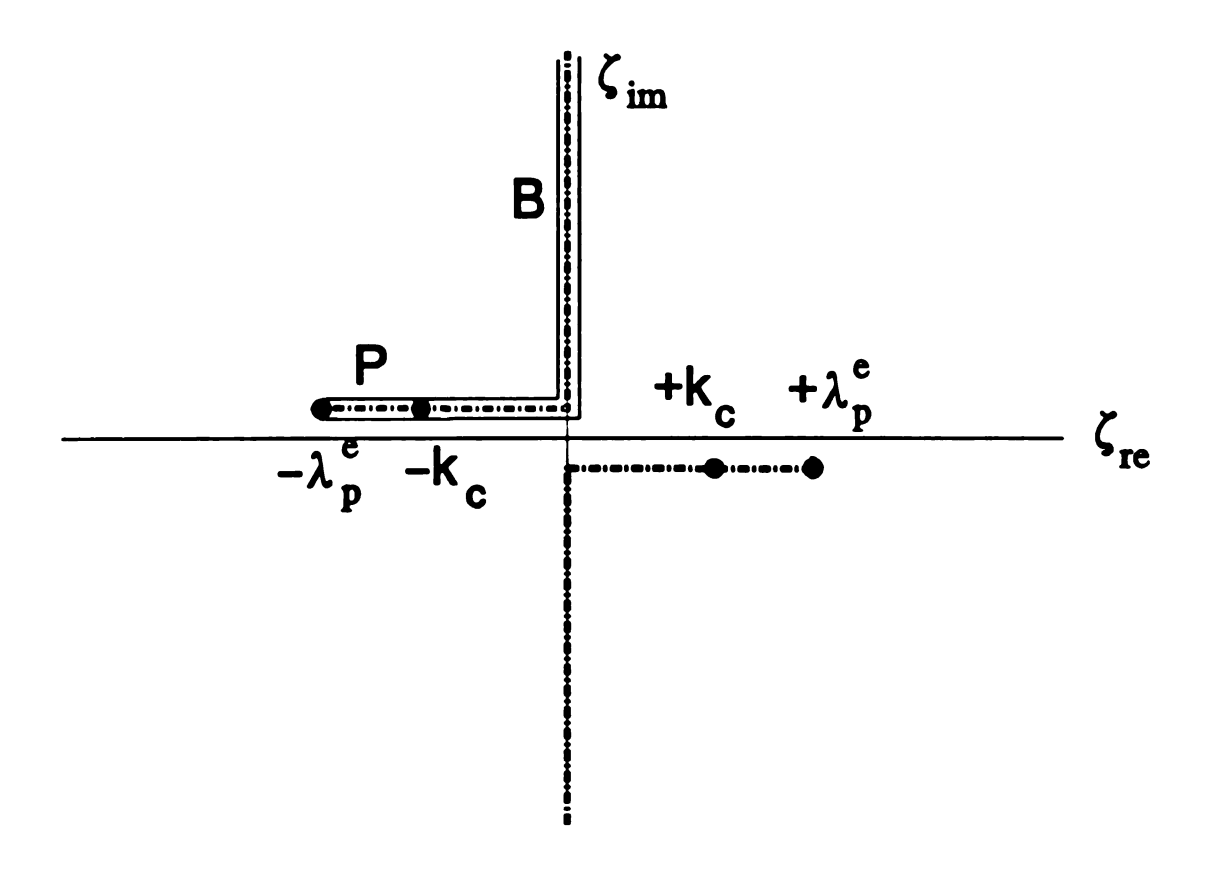


Figure 5.4 Axial wavenumber plane (complex 5-plane) branch cuts for low-loss microstrip transmission line.

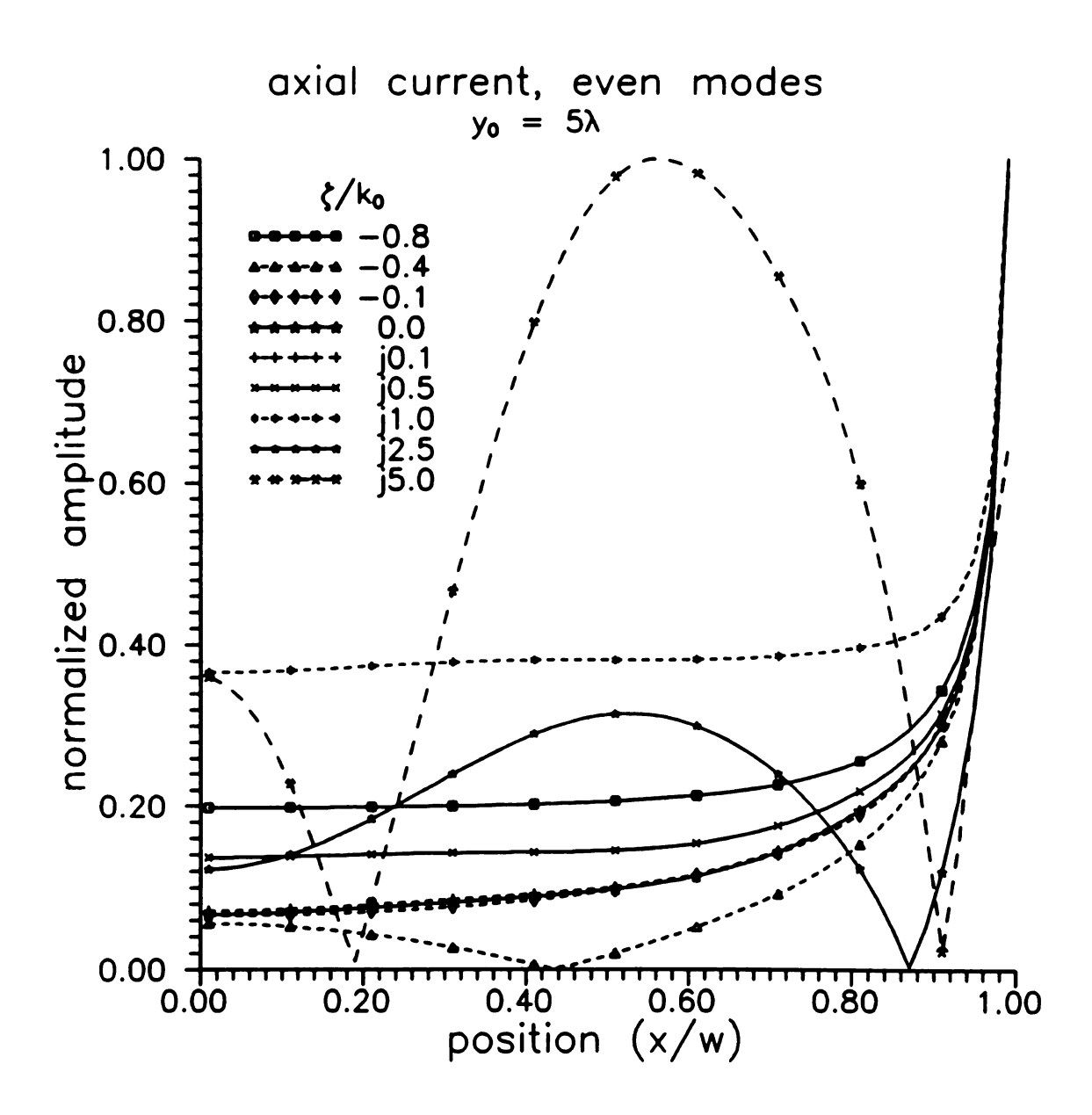


Figure 5.5 Normalized radiation regime axial surface current density, even parity. Excitation is 5λ above microstrip line.

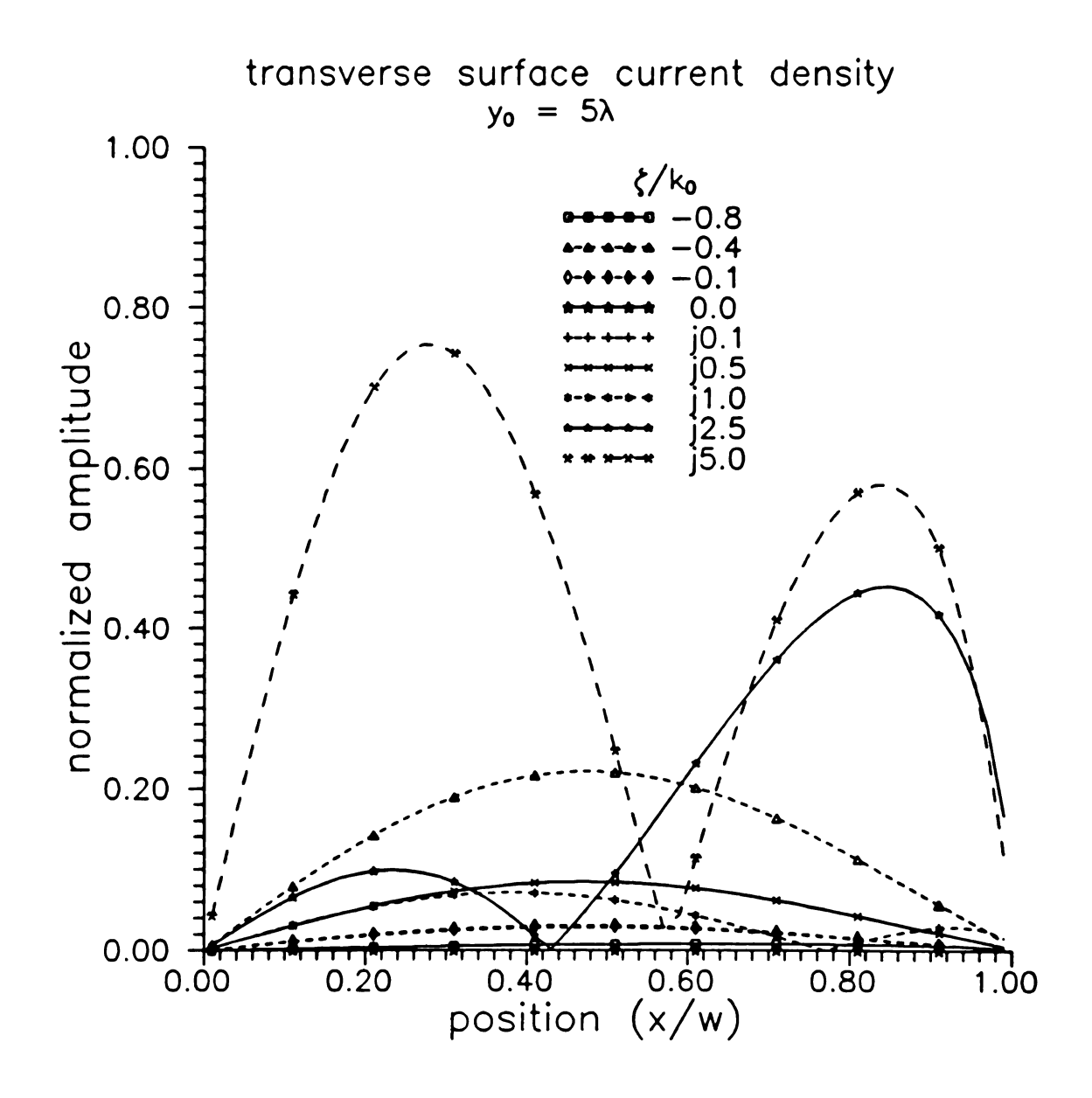


Figure 5.6 Normalized radiation regime transverse surface current density, even parity. Excitation is 5λ above microstrip line.

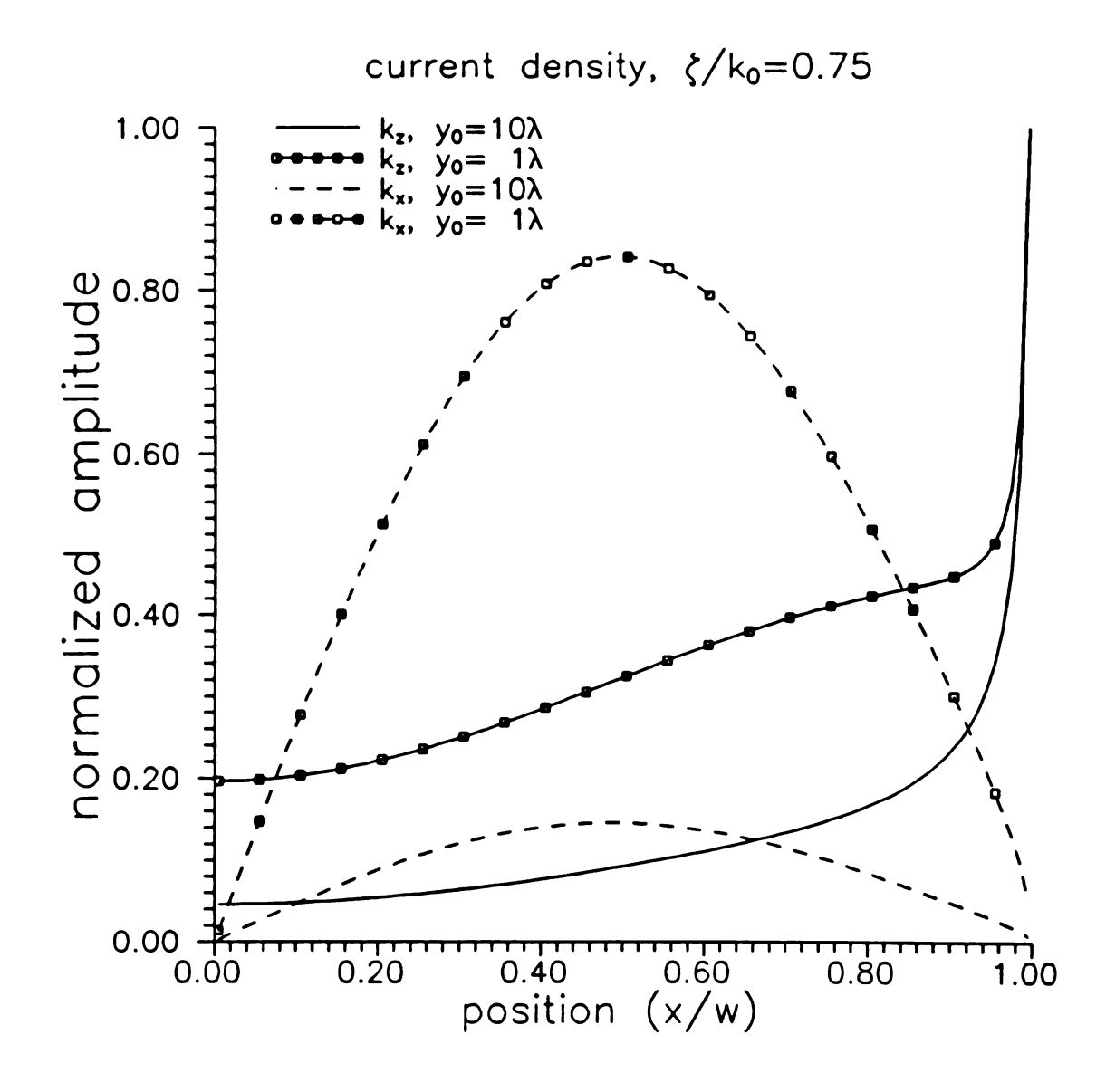


Figure 5.7 Effect of source excitation distance on radiation regime surface current amplitudes.

Figure 5.8 through Figure 5.11 display the actual current amplitudes for the axial and transverse radiation-regime surface currents in both even and odd parity states. From these results, it is obvious that the radiation-regime surface currents acquire an increasing periodicity across the strip width as ζ becomes more imaginary (deeper into the radiation regime, farther out the branch cut).

The observed increasing amplitude behavior in Figure 5.8 through Figure 5.11 is troubling, as these surface currents do not seem be converging in spectral frequency. This behavior is also completely contrary to the observed behavior in Chapter 4. This observed behavior may not present a problem however.

This increasing amplitude behavior seems to be associated primarily with the computation of the impressed field MoM elements from (5.29) as observed in the asymptotic form of (5.31). An increasing amplitude trend as ζ increases is obvious from inspection of (5.31). Yet, this impressed field exists in the space-domain. It is believed then that the form of (5.29) is unstable.

There are other possible explanations for the surface current amplitude trend. Recall from Chapter 4 that only TE modes of the planar waveguide were considered; those TE modes did not depend upon charges within the waveguiding structure. This spectral amplitude behavior may be caused by the charges involved in this microstrip transmission line.

Even so, this data trend is probably not serious. The amplitude behavior occurs in the evanescent portion of the radiation regime. When $z \neq z'$, the radiation spectrum superposition over radiation spectral components, identified by contour-closure in the complex ζ -plane, decays exponentially, which will annul any increasing amplitude trend.

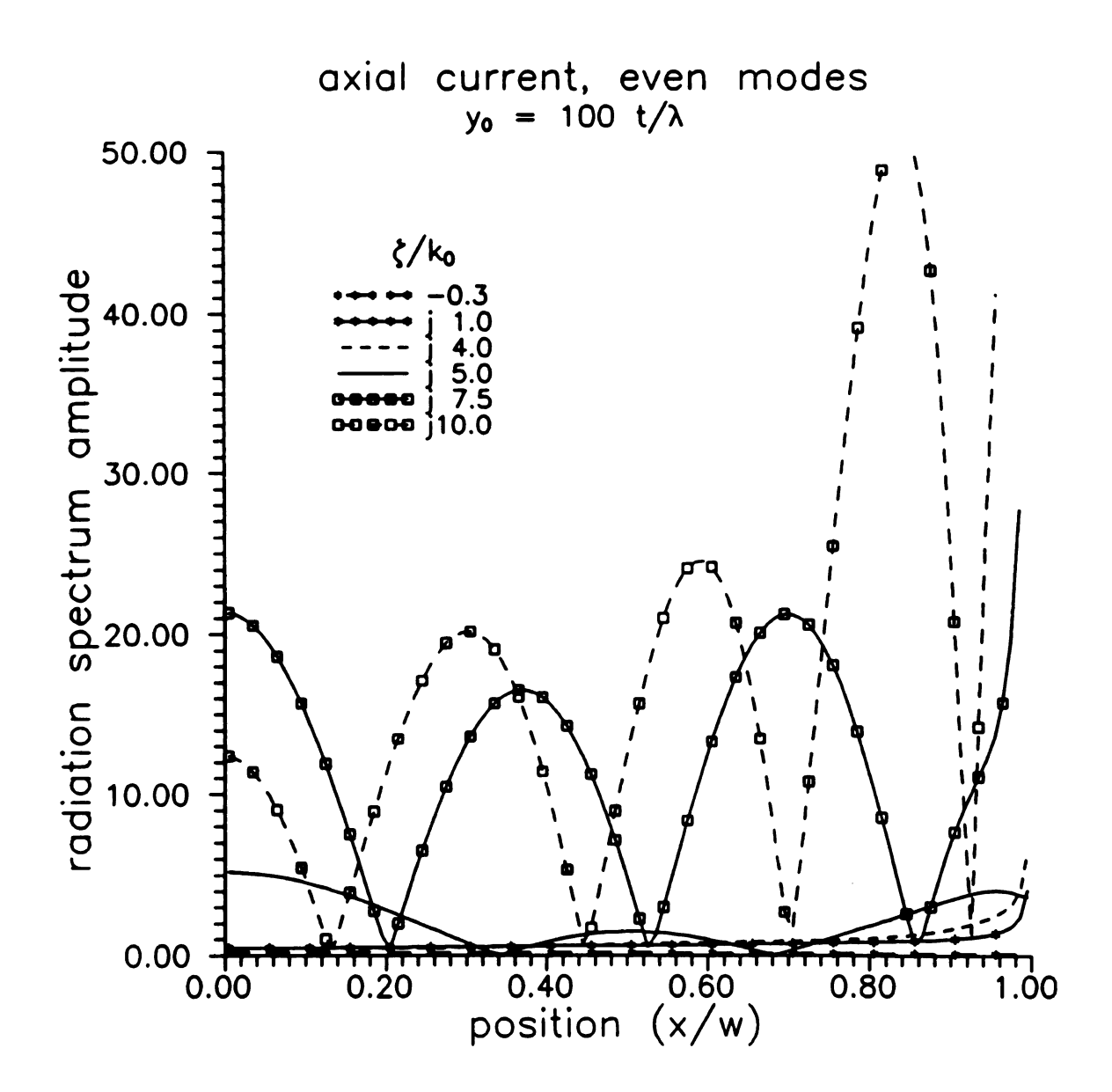


Figure 5.8 Radiation regime axial surface current amplitude, even parity.

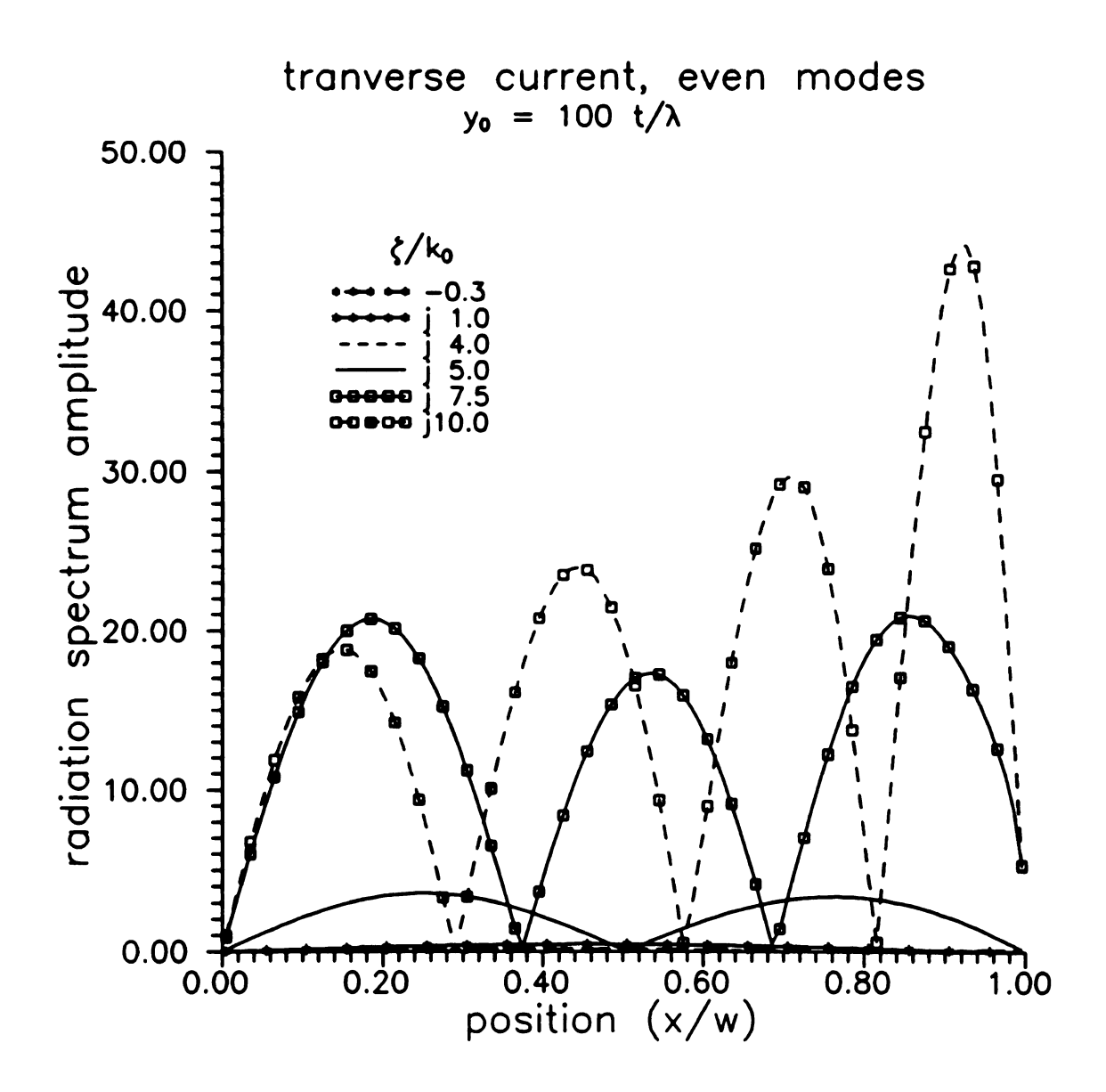


Figure 5.9 Radiation regime transverse surface current amplitude, even parity.

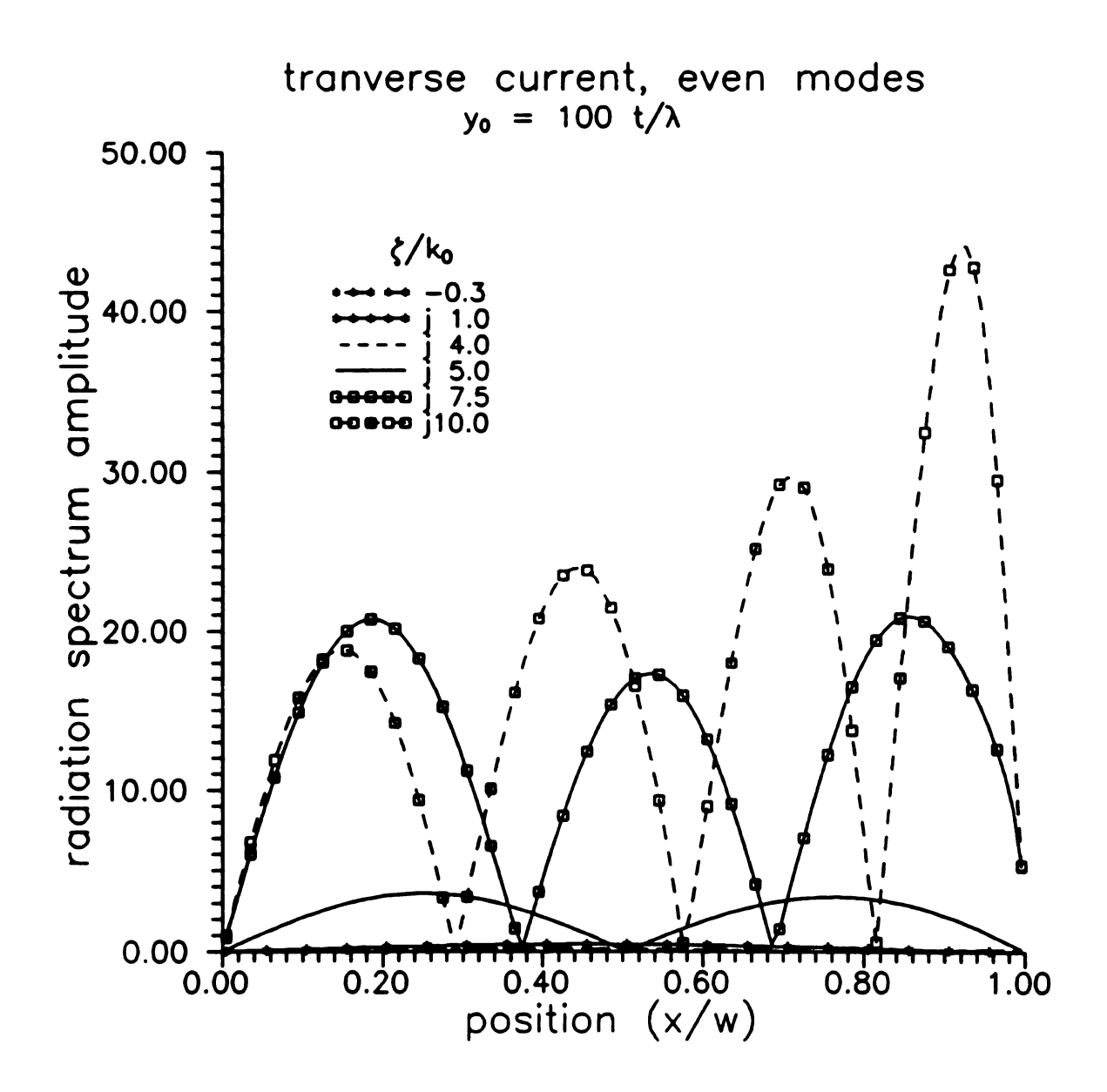


Figure 5.9 Radiation regime transverse surface current amplitude, even parity.

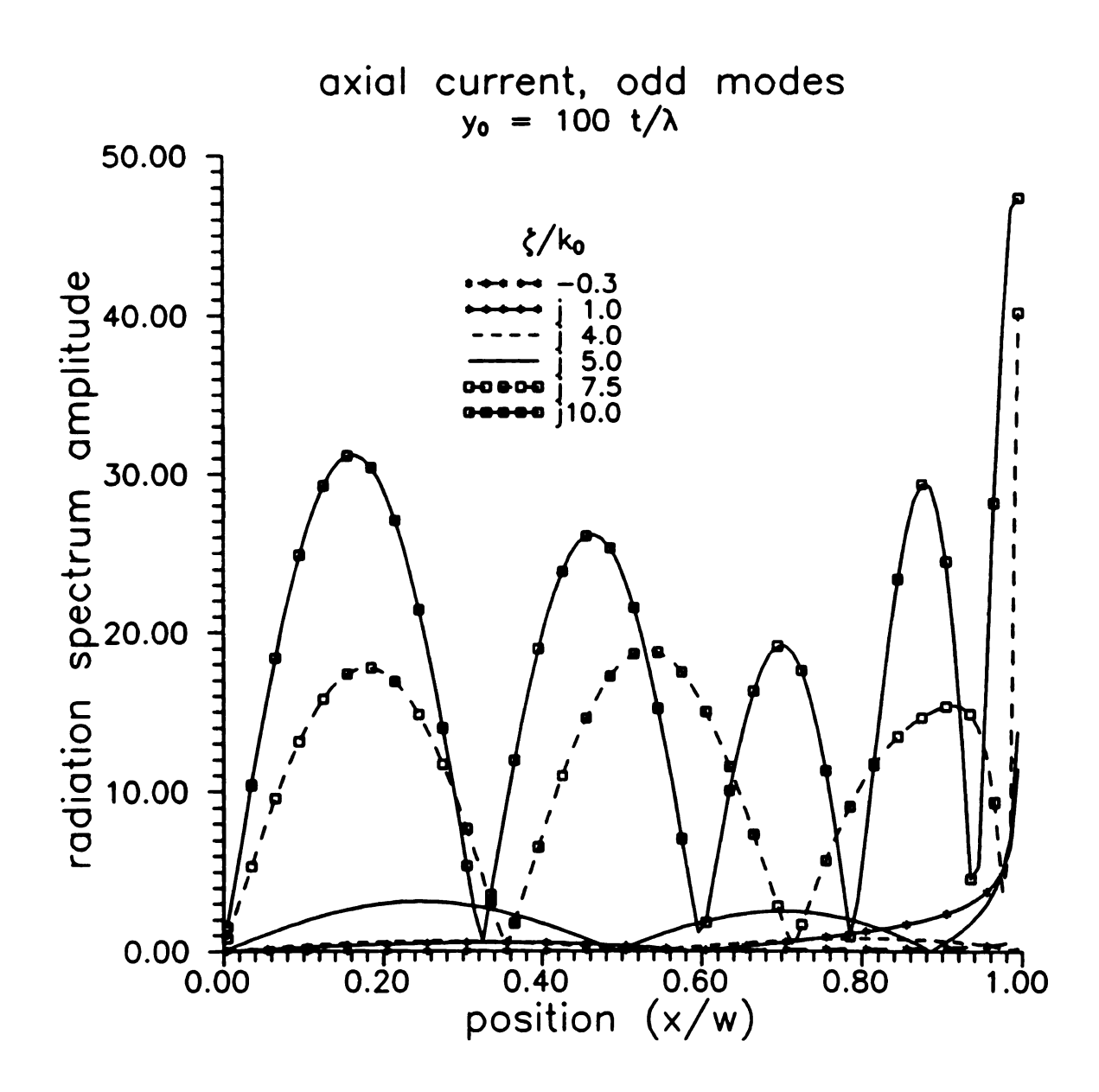


Figure 5.10 Radiation regime axial surface current amplitude, odd parity.

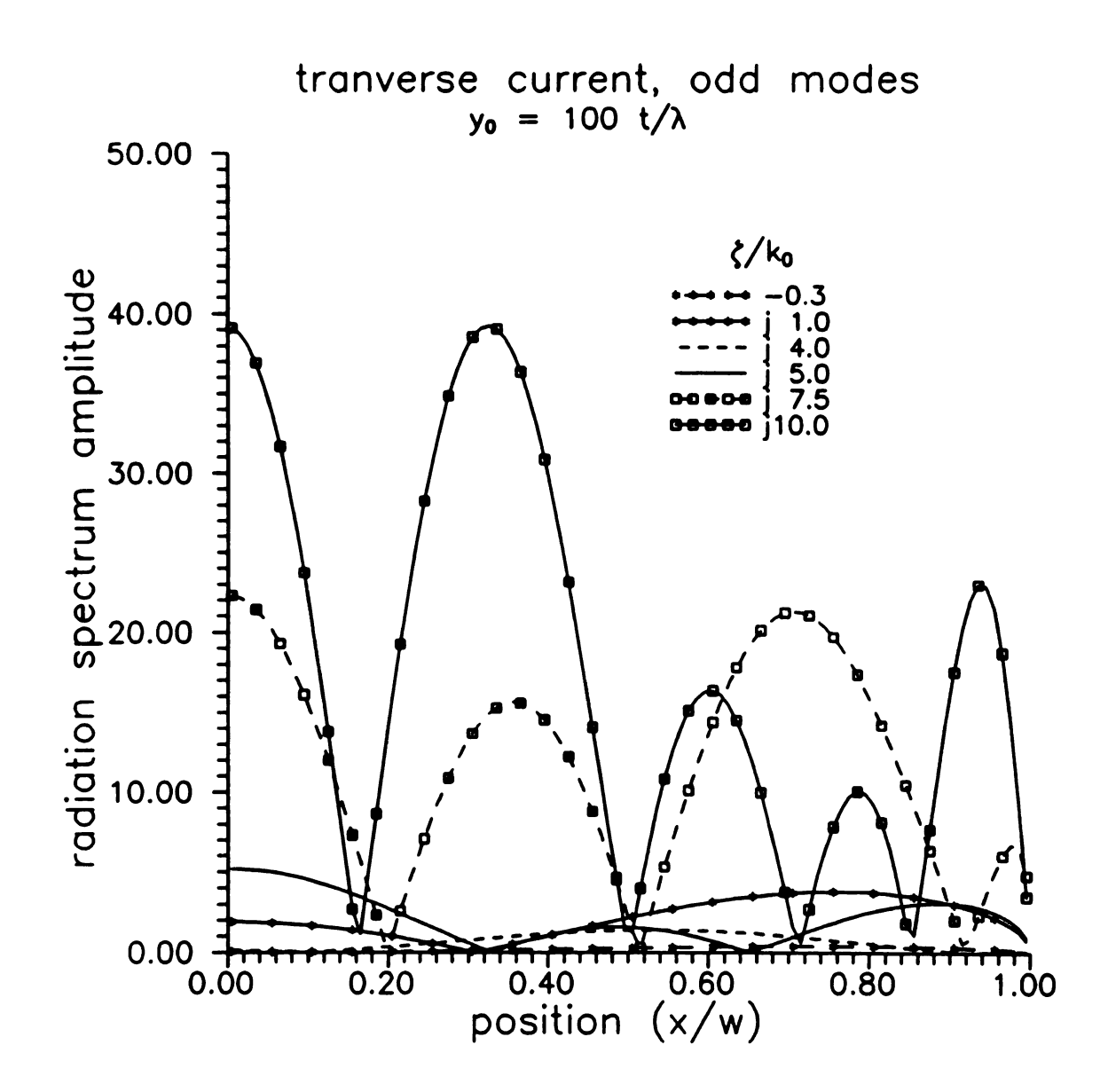


Figure 5.11 Radiation regime axial surface current amplitude, odd parity.

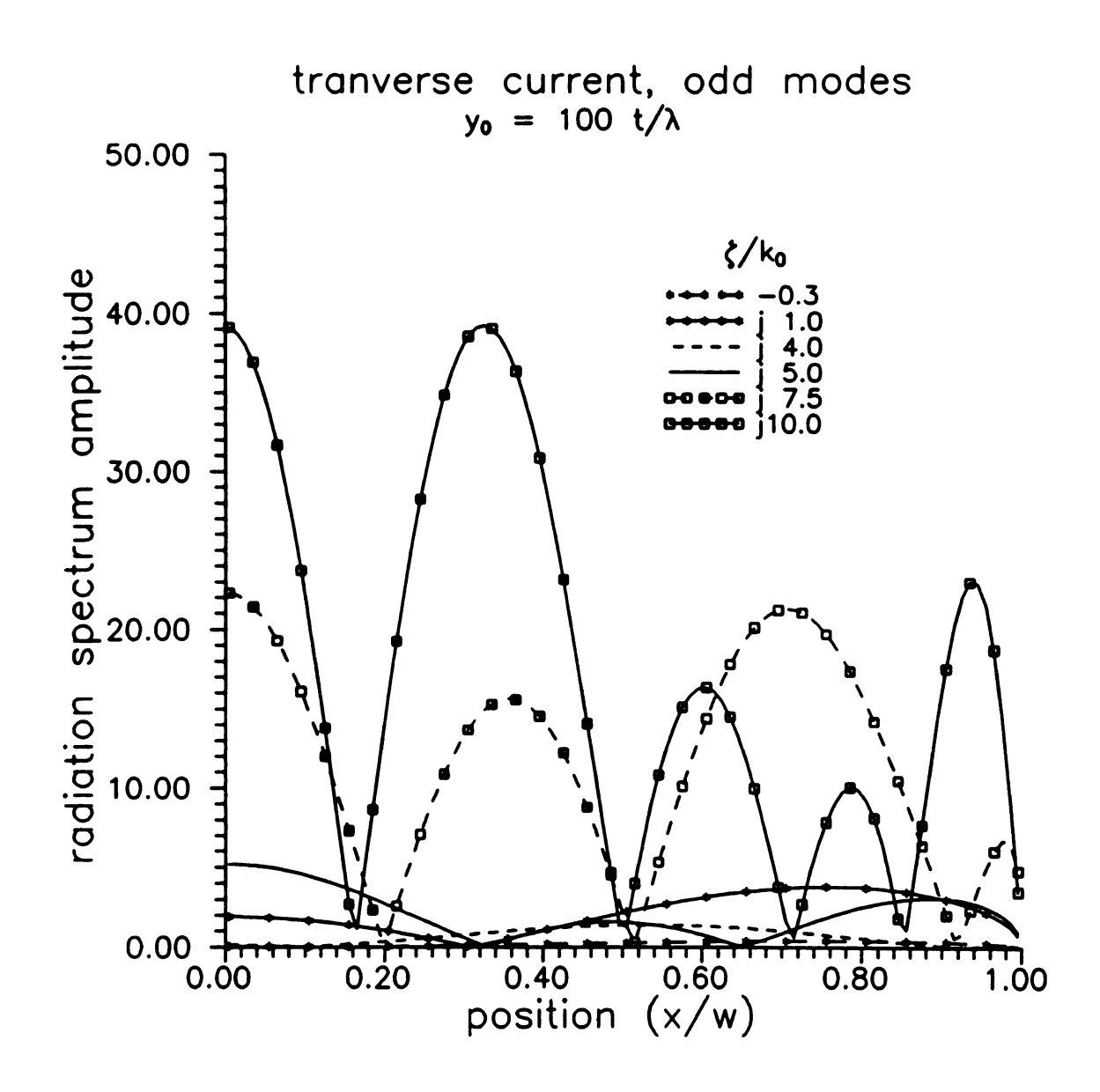


Figure 5.11 Radiation regime axial surface current amplitude, odd parity.

Finally, the current distributions within the surface-wave only radiation regimes were looked at. This is the limited portion of the radiation regime denoted P in Figure 5.4. Figure 5.12 and Figure 5.13 give typical surface current distributions where $\zeta = k_c$, the limiting edge of the transverse-only radiation regime. These currents are the dominant magnitude currents in the transverse-only regime, and are considerably smaller in amplitude than their counterparts in the full radiation regime. Other components within the transverse-radiation regime have much smaller amplitudes than this limiting case. As the current amplitudes within this regime are so small, it is conjectured that for a thin-film layer, power propagated away from the guide carried only within the film layer is small.

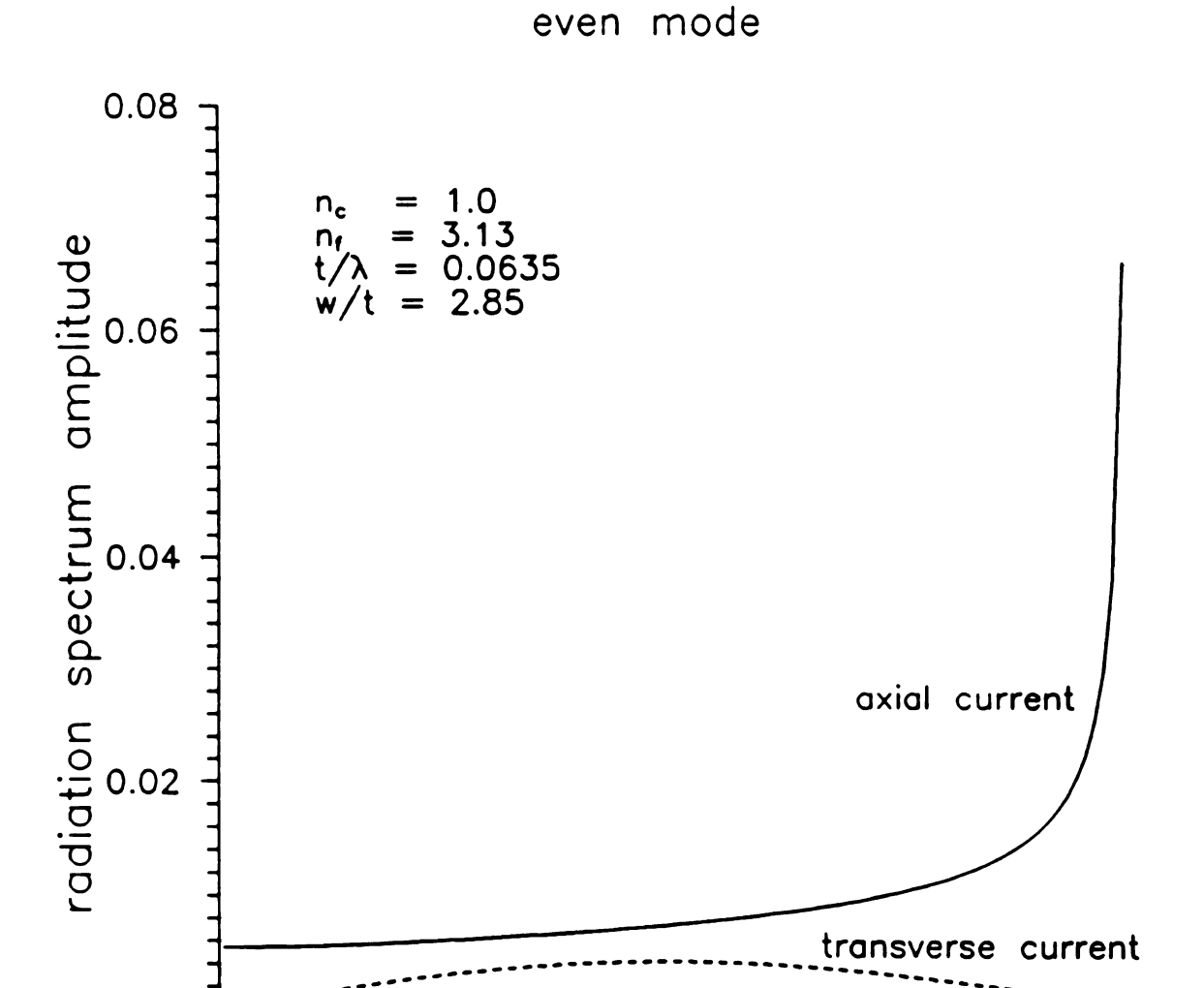


Figure 5.12 Typical surface current distribution within surface-wave radiation regime, even parity. Excitation source 5λ above microstrip, $\zeta = k_c$.

0.40 0.60 position (x/w)

0.80

1.00

0.00

0.00

0.20

odd mode

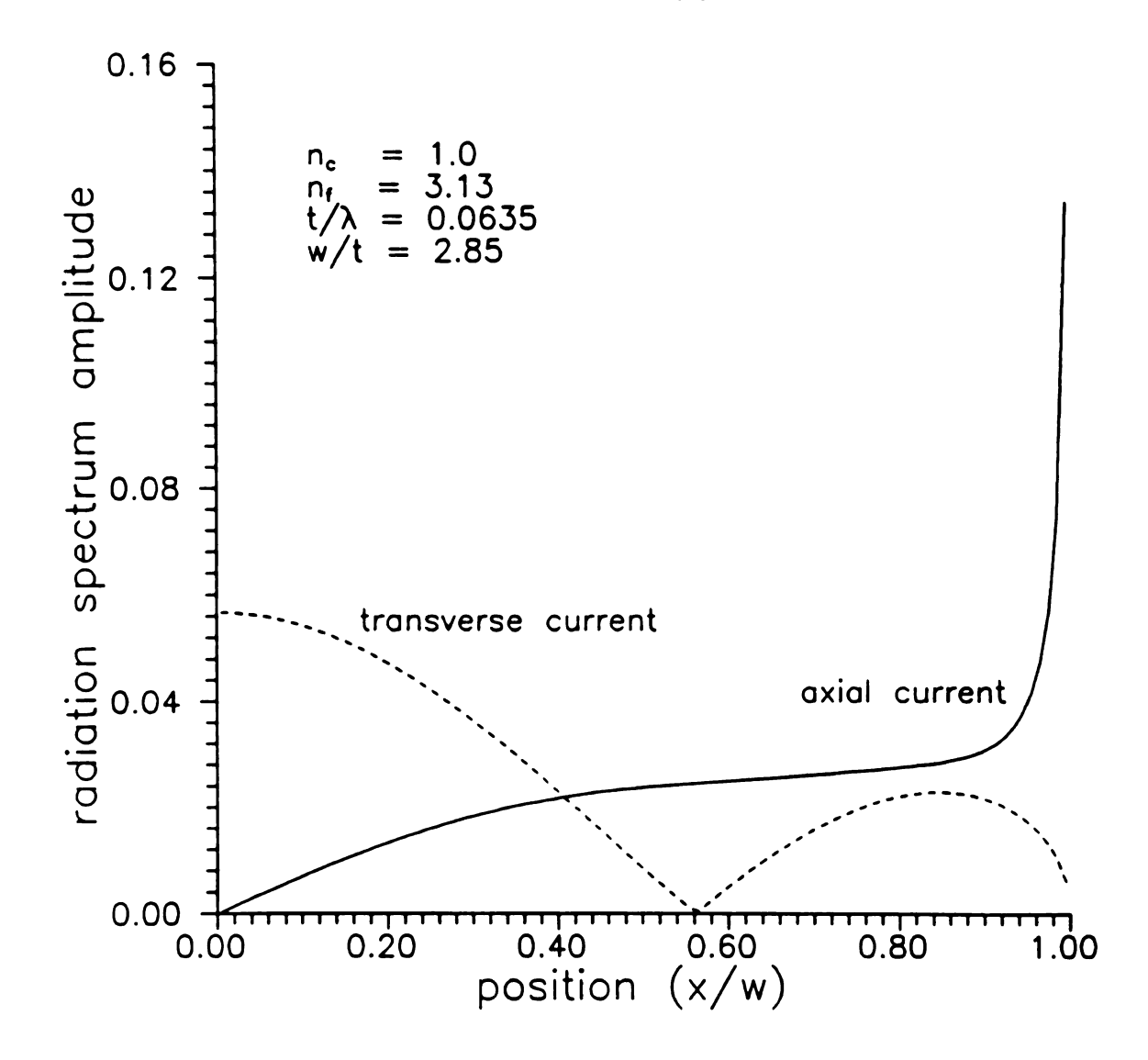


Figure 5.13 Typical surface current distribution within surface-wave radiation regime, odd parity. Excitation source 5λ above microstrip, $\zeta = k_c$.

Chapter 6

Leaky-wave Modes for the Dielectric Rib Waveguide

The integrated rib dielectric waveguide is a common structure used in integrated optics. While common and useful, the analysis of this waveguide is exceedingly difficult. Simple approximate techniques, such as Marcatilli's method [54], work well for electrically-large rib waveguides, but fail as these waveguides become small and approach cut-off.

Leaky-wave modes are used to model radiation loss via the method of steepest descents. These modes describe the waveguide operating in cutoff. As approximate techniques fail near cutoff, they cannot be used to determine leaky-wave modes. In addition to modeling radiation loss, leaky-wave modes of the rib dielectric waveguide may be important for coupling problems as well.

6.1 Application of the EFIE

Consider the optical dielectric waveguide as depicted in Figure 6.1. The background environment is that of a conductor/film/cover, which is the same environment as the microstrip transmission line in Chapter 5. The waveguide cross-section geometry is assumed to have symmetry about x = 0. Other than that, the EFIE as developed in (2.40) is applicable in general until a solution is needed for a specific cross-

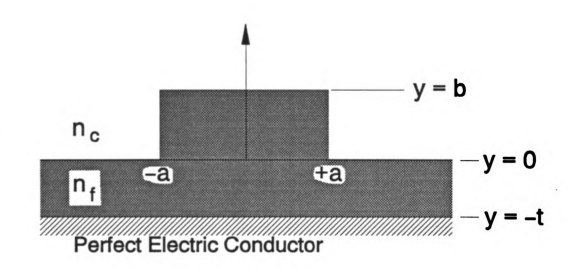


Figure 6.1 Configuration of a rib dielectric optical waveguide.

section. For the rib waveguide, the guiding region cross-section is rectangular.

The EFIE chosen to implement will be the original EFIE developed in (2.40), namely,

$$\vec{e}(\vec{\rho}) - (k_c^2 + \nabla \nabla \cdot) \int_{CS} \vec{g}(\vec{\rho} | \vec{\rho}'; \zeta) \cdot \frac{\delta n^2(\vec{\rho}') \vec{e}(\vec{\rho}'; \zeta)}{n_c^2} ds' = \vec{e}^i(\vec{\rho}; \zeta), \quad ... \forall \vec{\rho} \in CS$$

This integral equation is notationally more cumbersome; yet, it avoids having to deal with the source-point singularity problem and the necessary depolarizing dyad. Leakywave modes and bound modes are discrete modes, thus requiring that the homogeneous EFIE be solved. Then, the EFIE in (2.40) is

$$\vec{e}(\vec{\rho}) - (k_{\epsilon}^2 + \tilde{\nabla}\tilde{\nabla} \cdot) \vec{\pi}(\vec{\rho}) = 0$$
 (6.1)

where the Hertzian potential $\vec{\pi}$ is handled separately, taking the form

$$\vec{\pi}(\vec{r}) = \int_{CS} \frac{\delta n^2(x,y)}{n_c^2} \vec{g}(x|x';y|y';\zeta) \cdot \vec{e}(x',y',\zeta) ds' \qquad (6.2)$$

wherein an explicit dependence upon x and y has been shown.

6.1.1 Parity considerations

Parity considerations arise from previous analyses of the uniformly-clad rectangular waveguide. Because of the symmetry in the geometry and the uniform surround, the guiding modes are nearly degenerate. By pre-selecting a parity state, only that parity mode of a degenerate set will be determined. Reasons to analytically consider parity for the rib waveguide are not as overwhelmingly obvious as with the uniformly-clad waveguide, as the background introduces a measure of asymmetry into the problem. If the background is removed, however, the rib waveguide becomes the uniformly clad

rectangular fiber. Consequently, parity will be considered, so that this analysis can recover solutions in the specialization to the uniformly-clad waveguide (in which the reflected dyadic Green's function vanishes).

Parity considerations exploit field symmetry about x = 0. For graded, non-uniform guiding regions, this symmetry consideration assumes that the refractive index is even in x, namely, n(x,y) = n(-x,y). The symmetry effects can be ascertained by using the following equations obtained from the transform-domain Maxwell's equations:

$$\vec{e}_t = \frac{1}{k_c^2(x,y)} \left[\hat{x} \left(j\zeta \frac{\partial}{\partial x} e_z - j\omega \mu_0 \frac{\partial}{\partial y} h_z \right) + \hat{y} \left(j\zeta \frac{\partial}{\partial y} e_z + j\omega \mu_0 \frac{\partial}{\partial x} h_z \right) \right]$$
 (6.3)

$$\frac{\partial e_z}{\partial y} - \frac{\partial e_y}{\partial x} = -j\omega \mu_0 h_z \tag{6.4}$$

First, symmetry of the guiding region refractive index symmetry means that $k_c^2(x,y) = \omega^2 \mu_0 n^2(x,y) - \zeta^2$ is even in x. From an inspection of (6.3), it is readily observed that if e_x is to be even in x, then e_z must be odd in x while h_z is even in x. But, if h_z is to be even, then from (6.4) is obvious that e_y must be odd in x. This bears out when considering e_y as defined in (6.3). Since e_y should be odd, e_z must be odd, which it is; while h_z must be even, which it is. The symmetry states for this optical waveguide can then be defined as

state
$$e_x$$
 e_y e_z

1 even odd odd

2 odd even even

from which the electric field can be viewed as $\vec{e}(-x) = \vec{o} \cdot \vec{e}(x)$, where

$$\ddot{\sigma} = \pm [\hat{x}\hat{x} - \hat{y}\hat{y} - \hat{z}\hat{z}] \tag{6.5}$$

is defined as a symmetry dyad.

Application of parity to the EFIE necessitates decomposing the integral over the waveguide cross-section into

$$\int_{CS} (\cdots) = \int_{CS^+} (\cdots) ds^+ + \int_{CS^-} (\cdots) ds^-$$

where CS^+ is defined for the cross-section of the waveguide with x > 0, while CS^- is defined for the x < 0 portion of the waveguide. Making the variable change of $x' \rightarrow -x'$ in the CS^- integral mirrors the limits of integration in x, that is

$$\int_{CS^{-}} (\cdots, x') ds^{-} = \int_{CS^{+}} (\cdots, -x') ds^{+}$$

Consequently, under parity considerations, the Hertzian potential in (6.2) can be constructed as

$$\vec{\pi}(\vec{\rho}) = \int_{CS} \frac{\delta n^2(x,y)}{n_c^2} \left[\vec{g}(x|x') \cdot \vec{e}(x') + \vec{g}(x|-x') \cdot \vec{e}(-x') \right] ds'$$
 (6.6)

Making use of the symmetry dyadic as defined in (6.5) allows (6.5) to be written as

$$\vec{\pi}(\vec{\rho}) = \int_{C_s} \frac{\delta n^2(x,y)}{n_c^2} \vec{g}^s(x|x';y|y';\zeta) \cdot \vec{e}(x',y',\zeta) ds' \qquad (6.7)$$

where CS^+ is the x>0 cross-section of the waveguide, and $g^*(x|x';y|y';\zeta)$ is the symmetric Green's dyad, explicitly expressed as

$$\ddot{g}^* = \ddot{g}(x|x';y|y';\zeta) + \ddot{g}(x|-x';y|y';\zeta) \cdot \ddot{\sigma}$$
 (6.8)

The symmetry dyadic $\ddot{\sigma}$ is diagonal; consequently, no directional change in the scalar components of $\ddot{g}^{*}(x|x';y|y';\zeta)$ occurs.

6.1.2 EFIE for integrated dielectric waveguide

Upon recognition of the symmetry dyad, work can begin upon specializing the EFIE to the integrated dielectric waveguide. In this development, explicit dependence upon x and y will be suppressed unless necessary for clarity. Tensor notation will be used for the dyadic $(\ddot{g} = \sum_{\alpha} \sum_{\beta} g_{\alpha\beta} \hat{x}_{\alpha} \hat{x}_{\beta})$ and vector $(\ddot{f} = \sum_{\alpha} f_{\alpha} \hat{x}_{\alpha})$ components to generate compact expressions for the field components. Within this tensor notation, summation indices α are assumed to take on the values of x, y, z.

In tensor notation then, the EFIE becomes

$$\sum_{\alpha=x,y,z} \hat{x}_{\alpha} \left\{ e_{\alpha} - k_{c}^{2} \pi_{\alpha}^{z} \right\} - \tilde{\nabla} \tilde{\nabla} \cdot \vec{\pi}^{z} = 0$$
 (6.9)

The differential operator $\tilde{\nabla}\tilde{\nabla}\cdot$ takes the form

$$\tilde{\nabla}\tilde{\nabla}\cdot\vec{\pi} = \sum_{\alpha} \hat{x}_{\alpha} \sum_{\beta} \frac{\partial^{2} \pi_{\beta}}{\partial x_{\alpha} \partial x_{\beta}}$$

under tensor notation; consequently, (6.9) becomes

$$e_{\alpha} - k_{c}^{2} \pi_{\alpha}^{s} - \sum_{\beta = x, y, z} \frac{\partial^{2} \pi_{\beta}^{s}}{\partial x_{\alpha} \partial x_{\beta}} = 0$$
 (6.10)

for $\alpha = x, y, z$. The scattered Hertzian potential is supported by equivalent sources induced by the electric field; thus, the scattered Hertzian potential can be constructed in tensor form as

$$\vec{\pi}^z = \sum_{\alpha} \hat{x}_{\alpha} \left\{ \sum_{\nu = x, y, z} \pi^z_{\alpha \nu} \right\} \tag{6.11}$$

where

$$\pi_{\alpha \nu}^{s} = \int_{C_{s}} \frac{\delta n^{2}(x', y')}{n_{c}^{2}} g_{\alpha \nu}^{s} e_{\nu} ds' \qquad (6.12)$$

This renders the EFIE in (6.10) into

$$e_{\alpha} - k_c^2 \sum_{\mathbf{v}} \pi_{\alpha \mathbf{v}}^{s} - \sum_{\beta} \sum_{\mathbf{v}} \frac{\partial^2 \pi_{\beta \mathbf{v}}^{s}}{\partial x_{\alpha} \partial x_{\beta}} = 0$$
 (6.13)

for $\alpha = x, y, z$.

The subsequent substitution of (6.12) into (6.13) will obtain an integral equation for e_{ν} ; before this is done, it is desirable to obtain the tensor form of the symmetric dyadic Green's function. The symmetric dyadic Green's function is composed of a principle and reflected part, namely

$$\ddot{\mathbf{g}}^{g} = \ddot{\mathbf{g}}^{gp} + \ddot{\mathbf{g}}^{gr} = \ddot{\mathbf{I}}_{g}^{gp} + \ddot{\mathbf{g}}^{gr} \tag{6.14}$$

In tensor notation, the idemfactor $\ddot{I} = \sum_{\alpha} \sum_{\beta} \delta_{\alpha\beta}$; and the symmetric Green's dyad takes the form

$$\ddot{g}^{s} = \sum_{\alpha} \sum_{\nu} (g^{sp} \delta_{\alpha \nu} + g^{sr}_{\alpha \nu}) \qquad (6.15)$$

Note that four of the components $g_{ev}^{\#}$ are zero.

There is one final trick left. The leading term in (6.13), $e_a(\vec{\rho})$, needs to be cast in terms of the "source" $e_v(\vec{\rho}')$. Exploiting the unit vector \hat{x}_a in tensor notation results in $e_a = \sum_{v=1}^{n} \delta_{av} e_v$, while judicious use of the Dirac delta function allows $e_a(\vec{\rho})$ to become

$$e_{\alpha}(\vec{\rho}) = \int_{CS} \delta_{\alpha \nu} \delta(\vec{\rho} - \vec{\rho}') e_{\nu}(\vec{\rho}') ds' \qquad (6.16)$$

Finally, substitution of (6.12), (6.15) and (6.16) into (6.13) results in the desired EFIE of

$$\sum_{\nu=1}^{3} \int_{CS} \left\{ \delta_{\alpha\nu} \, \delta(\vec{\rho} - \vec{\rho}') - k_0^2 \delta n^2(p') (g^{\alpha\beta} \delta_{\alpha\nu} + g^{\alpha\nu}_{\alpha\nu}) \right.$$

$$\left. - \frac{\partial}{\partial x_{\alpha}} \sum_{\beta} \frac{\partial}{\partial x_{\beta}} (g^{\alpha\beta} \delta_{\beta\nu} + g^{\alpha\nu}_{\beta\nu}) \frac{\delta n^2(\vec{\rho}')}{n_c^2} \right\} e_{\nu}(\vec{\rho}') ds' = 0$$

$$(6.17)$$

for $\alpha = x, y, z$.

6.2 Method-of-Moments Solution

The EFIE developed in (6.17) is now in a form for which the method of moments is readily applicable. The method of moments has been applied elsewhere in this dissertation; this section will briefly touch on the significant differences in the application to this waveguide.

6.2.1 MoM expansions

Each component of the dielectric waveguide field (e_x, e_y, e_z) will be expanded in terms of subsectional basis functions,

$$e_{\nu}(x,y) = \sum_{n=1}^{N} e_{\nu n} p_{n}(x,y)$$
 (6.18)

The basis functions used are two-dimensional pulse functions with the characteristic of

$$p_{n}(x,y) = \begin{cases} 1; & (x,y) \in partition \ n \\ 0; & elsewhere \end{cases}$$

The pulse functions are centered at (x_n, y_n) and are non-zero for $\frac{-\Delta x}{2} < |x - x_n| < \frac{\Delta x}{2}$ and $\frac{-\Delta y}{2} < |y - y_n| < \frac{\Delta y}{2}$. There are N_x elements along x and N_y elements along y, leading to the relations

$$N = N_x N_y$$

$$\Delta x = \frac{a}{2N_x}; \quad \Delta y = \frac{b}{N_y}$$

The waveguide refractive index is assumed piecewise continuous, taking the form $n(\vec{\rho}') = \sum_{n=1}^{N} n_n p_n(x', y'). \text{ Recognition that } n_c^2 = n_c^2 p_n^2 \text{ suggests that}$ $\delta n^2(\vec{\rho}') = (n_n^2 - n_c^2) p_n^2 = \delta n_n^2 p_n(x', y'), \quad \forall \vec{\rho}' \in \Delta S_n$ (6.19)

$$on(\rho) = (n_n - n_c)p_n = on_n p_n(x, y), \quad \forall \rho \in \Delta S_n$$

Substitution of expansions (6.18) and (6.19) into the generic form for scattered potential in (6.12) results in

$$\pi_{ev}^{s} = \int_{CS} g_{ev}^{s} \sum_{n=1}^{N} \frac{\delta n_{n}^{2}}{n_{c}^{2}} p_{n}(x',y') \sum_{m=1}^{N} e_{vm} p_{m}(x',y') dx' dy'$$

This expression simplifies and becomes

$$\pi_{av}^{s} = \int_{CS} g_{av}^{s}(\vec{\rho} | \vec{\rho}') \sum_{n=1}^{N} \frac{\delta n_{n}^{2}}{n_{c}^{2}} e_{vn} p_{n}(x', y') dx' dy' \qquad (6.20)$$

because the pulse function product $p_n p_m$ is zero where the pulses do not overlap $(m \neq n)$.

Passage of the summation on n through the integration on CS^+ of (6.20) yields the result

$$\pi_{\alpha \nu}^{s} = \sum_{n=1}^{N} \frac{\delta n_{n}^{2}}{n_{c}^{2}} e_{\nu n} I_{\alpha \nu n}$$
 (6.21)

where the MoM integral I_{and} is given as

$$I_{\alpha\nu n} = \int_{S_n} g_{\alpha\nu}^{s}(\vec{\rho} | \vec{\rho}') p_n(\vec{\rho}') ds' \qquad (6.22)$$

Point-matching the MoM solution in two dimensions uses the testing operation

$$\int_{CS} \delta(x-x_m) \, \delta(y-y_m)(\cdots) \, dx \, dy \qquad m = 1, 2, \cdots N \tag{6.23}$$

where location (x_m, y_m) is the center of the pulse function p_m .

The ultimate result of this operation is to turn the original EFIE in (6.17) into a matrix equation. After some algebra, this matrix equation is

$$\begin{bmatrix} A_{xx}^{mn} & A_{xy}^{mn} & A_{xz}^{mn} \\ A_{yx}^{mn} & A_{yy}^{mn} & A_{yz}^{mn} \\ A_{zx}^{mn} & A_{zy}^{mn} & A_{zz}^{mn} \end{bmatrix} \begin{bmatrix} e_{xx} \\ e_{yx} \\ e_{zx} \end{bmatrix} = \begin{bmatrix} 0 \\ 0 \\ 0 \end{bmatrix}$$
(6.24)

The matrix elements take the form

$$A_{\alpha\nu}^{mn} = \left(A_{\alpha\nu}^{mn}\right)^p + \left(A_{\alpha\nu}^{mn}\right)^r \tag{6.25}$$

with principle matrix elements given as

$$\left(A_{\alpha\nu}^{mn}\right)^{p} = \delta_{\alpha\nu}\delta_{mn} - \frac{\delta n_{n}^{2}}{n_{c}^{2}} \left[k_{c}^{2}I_{\alpha\nu n}^{p}(x_{m},y_{m}) + \sum_{\beta} \frac{\partial^{2}}{\partial x_{\alpha}\partial x_{\beta}}I_{\beta\nu n}^{p}\right|_{(x_{m},y_{m})}$$
(6.26)

and reflected matrix elements given as

$$\left(A_{\alpha\nu}^{mn}\right)^{r} = -\frac{\delta n_{n}^{2}}{n_{c}^{2}} \left[k_{c}^{2} I_{\alpha\nu n}^{r}(x_{m}, y_{m}) + \sum_{\beta} \frac{\partial^{2}}{\partial x_{\alpha} \partial x_{\beta}} I_{\beta\nu n}^{r} \Big|_{(x_{m}, y_{m})}\right]$$
(6.27)

The reflected matrix elements vanish in the case of a uniform surround. The MoM integrals within (6.26) and (6.27) are given as

$$I_{avn}^{p} = \delta_{av} \int_{CS^{+}} \left[g^{p}(x|x';y|y';\zeta) + \sigma_{v} g^{p}(x|-x';y|y';\zeta) \right] p_{n}(x',y') dx' dy'$$
 (6.28)

$$I_{\text{avr}}^{r} = \int_{CS^{*}} \left[g_{\text{av}}^{r}(x|x';y|y';\zeta) + \sigma_{y}g_{\text{av}}^{r}(x|-x';y|y';\zeta) \right] p_{n}(x',y') dx'dy' \qquad (6.29)$$

Application of the method of moments has converted the EFIE to a system 3N by 3N homogeneous linear equations. This system has a unique, non-zero solution only if $\det[A(\zeta)] = 0$. Any value of ζ that renders the determinant of (6.25) zero is the propagation constant of the corresponding discrete mode. The field distribution of the mode is then determined by finding the nullspace of the matrix in (6.25).

6.2.2 Special considerations for the MOM expansion

In the numerical implementation of (6.24)-(6.29), certain tricks can be employed to greatly improve computational efficiency. These tricks will be detailed in this section.

The first trick is to recognize that the MOM integrals of (6.28) and (6.29) decompose into

$$I_{\text{gyn}}^{p,r} = I_{\text{gyn}}^{(p,r)+} + \sigma_{\nu} I_{\text{gyn}}^{(p,r)-} \tag{6.30}$$

because x-symmetry has been implemented. The principle MOM integral can then be considered as $I_{avn}^{pz} = \delta_{av} I_n^{pz}$, where

$$I_n^{p\pm} = \int_{\Delta S_n} g^p(x|\pm x', y|y') dx' dy'$$
 (6.31)

and ΔS_n is the area of the pulse. The reflected MoM integrals take the form

$$I_{n}^{r^{\pm}} = \int_{\Delta S_{n}} g_{\alpha \nu}^{r}(x|\pm x',y|y') dx'dy'$$
 (6.32)

The Green's functions will be cast into their spectral form in ξ as in (2.44). Exchange of the spectral and spatial integrals results in

$$I_n^{p_{\pm}} = \int_0^{\infty} \frac{f_n^{\pm}(x,\xi)h_n^{p}(y,\xi,\zeta)}{2\pi p_c(\xi)} d\xi$$
 (6.33)

$$I_{\text{ava}}^{rz} = \int_{0}^{\infty} R_{\text{av}}(\xi) \frac{f_{\text{a}}^{z}(x,\xi)h_{\text{a}}^{r}(y,\xi,\zeta)}{2\pi p_{c}(\xi)} d\xi$$
 (6.34)

where the even behavior of the Green's function integrands in ξ has been exploited. The MOM function expansions are

$$f_n^{\pm}(x,\xi) = e^{j\xi x} \int_{-\Delta x/2}^{\Delta x/2} e^{zj\xi(x'-x_n)} dx'$$

$$h_n^P(y,\xi,\zeta) = \int_{\Delta y/2}^{\Delta y/2} e^{-p_c|y-(y'-y_n)|} dy'$$

$$h_n''(y,\xi,\zeta) = \int_{\Delta y/2}^{\Delta y/2} e^{-p_c(y+(y'-y_n))} dy'$$

and take specific forms of

$$f_n^{\pm}(x,\xi) = \frac{1}{\xi} \sin\left(\xi \frac{\Delta x}{2}\right) \cos \xi (x \pm x_n)$$
 (6.35)

$$h_n^{p}(y,\xi,\zeta) = \frac{2}{p_c} \begin{cases} e^{-p_c|y-y_n|} \sinh\left(\frac{p_c\Delta y}{2}\right) & \text{... for } |y-y_n| > \frac{\Delta y}{2} \\ 1 - e^{\frac{-p_c\Delta y}{2}} \cosh p_c(y-y_n) & \text{... for } |y-y_n| < \frac{\Delta y}{2} \end{cases}$$

$$(6.36)$$

$$h_n^r(y,\xi,\zeta) = \frac{2}{p_c} \sinh\left(p_c \frac{\Delta y}{2}\right) e^{-p_c(y+y_n)}$$
 (6.37)

Specific forms for the reflection coefficients $R_{ev}(\xi)$ can be found in Appendix B.

The other trick is implemented to improve convergence of the principle MoM integral $I_n^{p\pm}$ on ξ ; the reflected MoM integrals all have exponential decay in y, as evidenced by h_n^r in (6.29), (6.37). While most of the $I_n^{p\pm}$ terms possess exponential decay in y and ξ , the MoM expansion of h^p when $|y_m - y_n| < \Delta y/2$ decays as only ξ^{-1}

in its asymptotic form. For some matrix elements, the convergence may only be as ξ^{-1} due to the effects of spatial derivatives. This slow convergence can be analytically handled by adding and subtracting the asymptotic form of $I_n^{p\pm}$. This method is useful only if the asymptotic form has a closed-form integral on ξ . If this is indeed the case, then the asymptotic extraction yields

$$I_n^P = \int_0^{\pi} [\psi(\xi) - \psi_a(\xi)] d\xi + \int_0^{\pi} \psi_a(\xi) d\xi$$
 (6.38)

The asymptotic form of I_n^{pz} as $\xi \to \infty$ is easily recognized as

$$\psi_{a}(\xi) = -\frac{2}{\pi \xi} \sin(\xi \Delta x/2) \cos \xi (x \pm x_{n})$$

$$= -\frac{1}{\pi \xi} \left[\sin \xi (x \pm x_{n} + \Delta x/2) - \sin \xi (x \pm x_{n} - \Delta x/2) \right]$$
(6.39)

of which a closed form integral does exist, namely

$$\int_0^{\pi} \frac{1}{\xi} \sin a \xi \, d\xi = \frac{\pi}{2} \operatorname{sgn}(a)$$

where sgn is the signum function. Application of this relationship to (6.39) gives

$$-\frac{1}{2}\left[sgn(x\pm x_n+\Delta x/2)-sgn(x\pm x_n-\Delta x/2)\right]$$

The only time the above sum is non-zero is when there is overlap; this only occurs when $|x-x_n| < \Delta x/2$. Consequently, the asymptotic integral evaluates to

$$\int_{0}^{\infty} \psi_{a}(\xi) d\xi = \begin{cases} -1 ; & (x,y) \in partition \ n \\ 0 ; & elsewhere \end{cases}$$
 (6.40)

6.3 Spectral Analysis Considerations

If the film thickness is restricted such that only the TM₀ background surface wave mode can propagate, then the axial transform plane has the branch cuts as depicted in Figure 3.14. There are consequently four Riemann sheets of interest, of which only the top sheet corresponds to spectral, bound waveguiding modes.

Obeying both branch cuts B and P restricts the axial wavenumber ζ to the top sheet; any solutions to the EFIE on this sheet are the bound guiding modes. No special attention needs to be paid to the spectral integrals on ξ , as all the singularities are located below the real-line contour.

The second sheet determines surface-wave leaky waves. This sheet is reached by violating the P branch cut. The corresponding situation in the complex ξ -plane is that the background surface wave pole controlled by that branch cut is now located above the real axis. The inversion contour to evaluate the spectral integral must still remain above the pole. Deforming the contour to the real axis, as in Figure 6.2, thus captures the now non-spectral pole. This contribution can easily be recognized as non-spectral, since $e^{j\xi x}|_{\xi_p} = e^{j\xi_p x}e^{-\xi_p x}$, which propagates in the -x direction but grows exponentially in -x instead of decaying.

Either of sheets (3) or (4) is reached by violating the B branch cut in the complex ζ -plane. In either of these cases, the branch point migrates across the real-axis. The difference is whether or not the surface-wave pole, controlled by P, migrates above the real axis. The necessary deformation of the integration contour to remain above the original singularities for each of these cases is given in Figure 6.3.

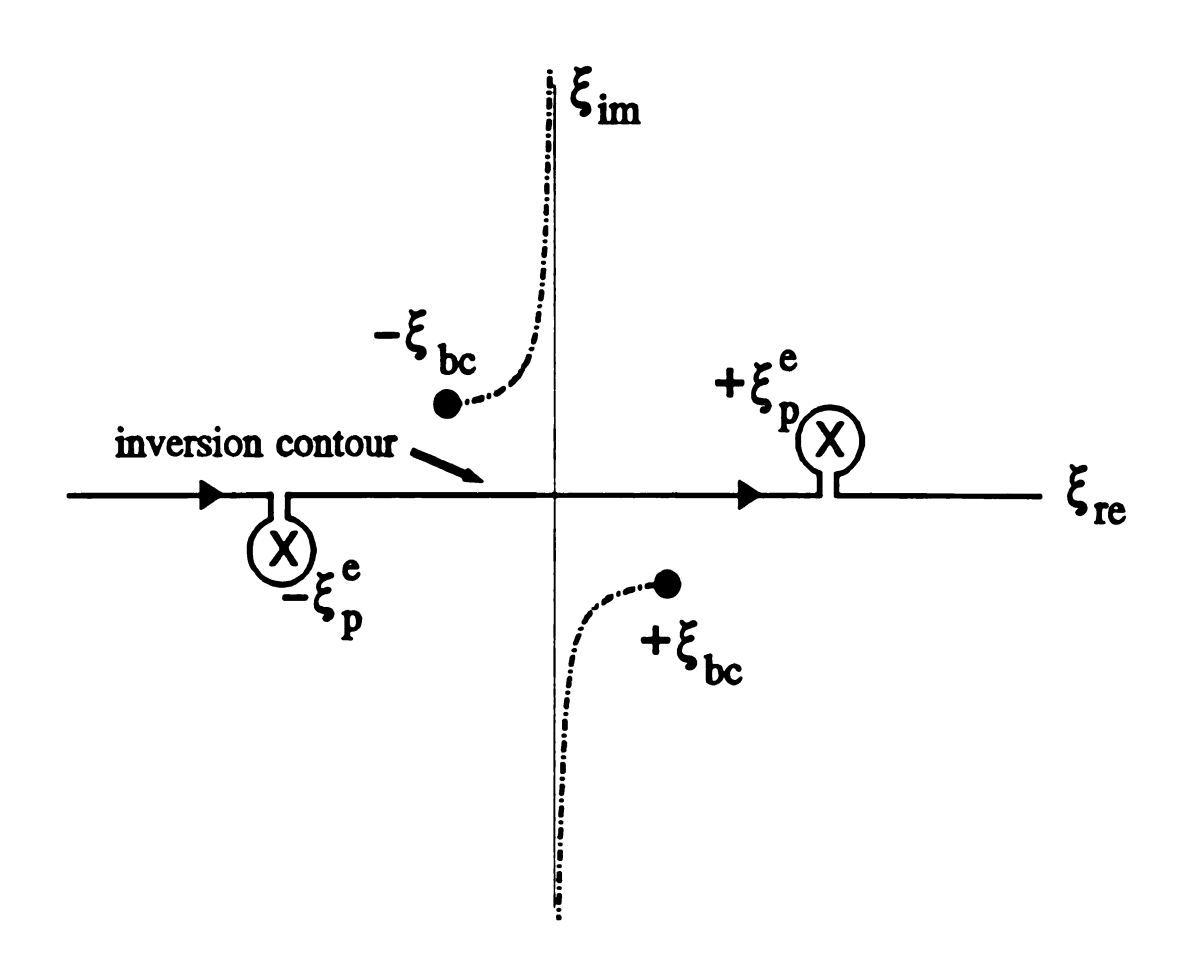


Figure 6.2 Complex ξ -plane singularities for surface-wave leakage.

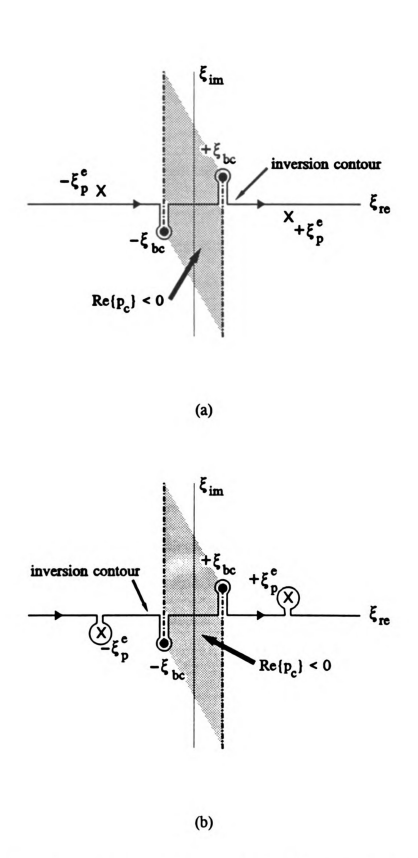


Figure 6.3 Singularities in the complex ξ -plane for: (a) space-wave leakage (sheet 3). (b) full (space/surface wave) leakage (sheet 4).

The choice of the branch cut in Figure 6.3 merits discussion. As observed in Chapter 3, the branch cut in the complex ξ -plane was specified to enforce the Sommerfeld radiation condition as $|y| \to \infty$. When the branch cut **B** is violated, this requirement is meaningless, as these will be leaky-wave modes. When ξ_{kc} migrates across the real axis, an attempt to enforce spectral behavior (the Sommerfeld radiation condition) on non-spectral modes results in a hyperbolic cut originating at ξ_{bc} that approaches infinity asymptotic to the imaginary axes but violates the deformed inversion contour; consequently, this is not permissible. The criteria for the branch cut in this case is less restrictive. Having discarded the idea of mapping the Sommerfeld-plane branch cut, any cutting in the ξ -plane can be chosen, as long as it: 1) maintains the continuity of the physical problem, and 2) does not violate the deformed inversion contour. These considerations taken together dictate the branch cut choice in Figure 6.3, starting at the branch point and passing through the real axis, approaching infinity asymptotically along the negative imaginary axis. Any branch cut obeying the above guidelines will not separate spectral (where $\Re(p_c) > 0$) from non-spectral (where $\Re(p_c) < 0$) sheets in the ξ -plane. In Figure 6.3, the improper region on the complex ξ -plane is denoted by the shaded area.

6.4 Results

A typical rib waveguide configuration was chosen for analysis. The waveguiding cross-section has dimensions of width 2a (-a < x < a) by height a (0 < y < a). The guiding region is homogeneous, with a refractive index of $n_f = 1.5$, the same as the film

layer refractive index. The cover medium has refractive index $n_e=1$, and the film layer has a thickness of t=0.2 wavelengths.

A dispersion curve of the dielectric rib waveguide modes is given in Figure 6.4. The bound modes are denoted as E_{mn}^{α} modes, where m and n designate the mode and α denotes the dominant component of electric field. Bound modes are found as solutions on sheet (1) of Figure 3.14. It is observed that the dominant mode for the rib waveguide is the principal E_{11}^{γ} mode. This E_{11}^{γ} has no lower frequency cut-off. At low frequencies it merges into the TM_0 surface wave pole of the conductor/film/cover background. Typical field distributions for the dominant and higher-order bound modes (1.23 < ζ/k_0 < 1.5) are given in Figure 6.5 to Figure 6.7. More periodicity is naturally observed for the higher-order modes.

Leaky-wave solutions have also been obtained by using the integral operator. These show up on the dispersion curve in Figure 6.4 over the range $\zeta/k_0 < 1.23$. These leaky-wave solutions can be of the three types mentioned previously. The ones shown on the dispersion curve as extensions to the E_{11}^x plot are solutions upon Sheet 2 in the complex ζ -plane, or surface-wave leaky waves. The attenuation constant for the modes is shown in Figure 6.8, while a plot of leaky-wave field distribution within the waveguide is displayed in Figure 6.9.

Two observations are apparent. First, the attenuation of the surface-wave only leaky waves is very small. This implies that the loss mechanism of surface waves propagating in the film layer does not carry much energy with respect to other loss mechanisms. This is consistent with observations on the small amplitude of the transverse-only radiation current amplitudes in Chapter 5. It is not correct to say that

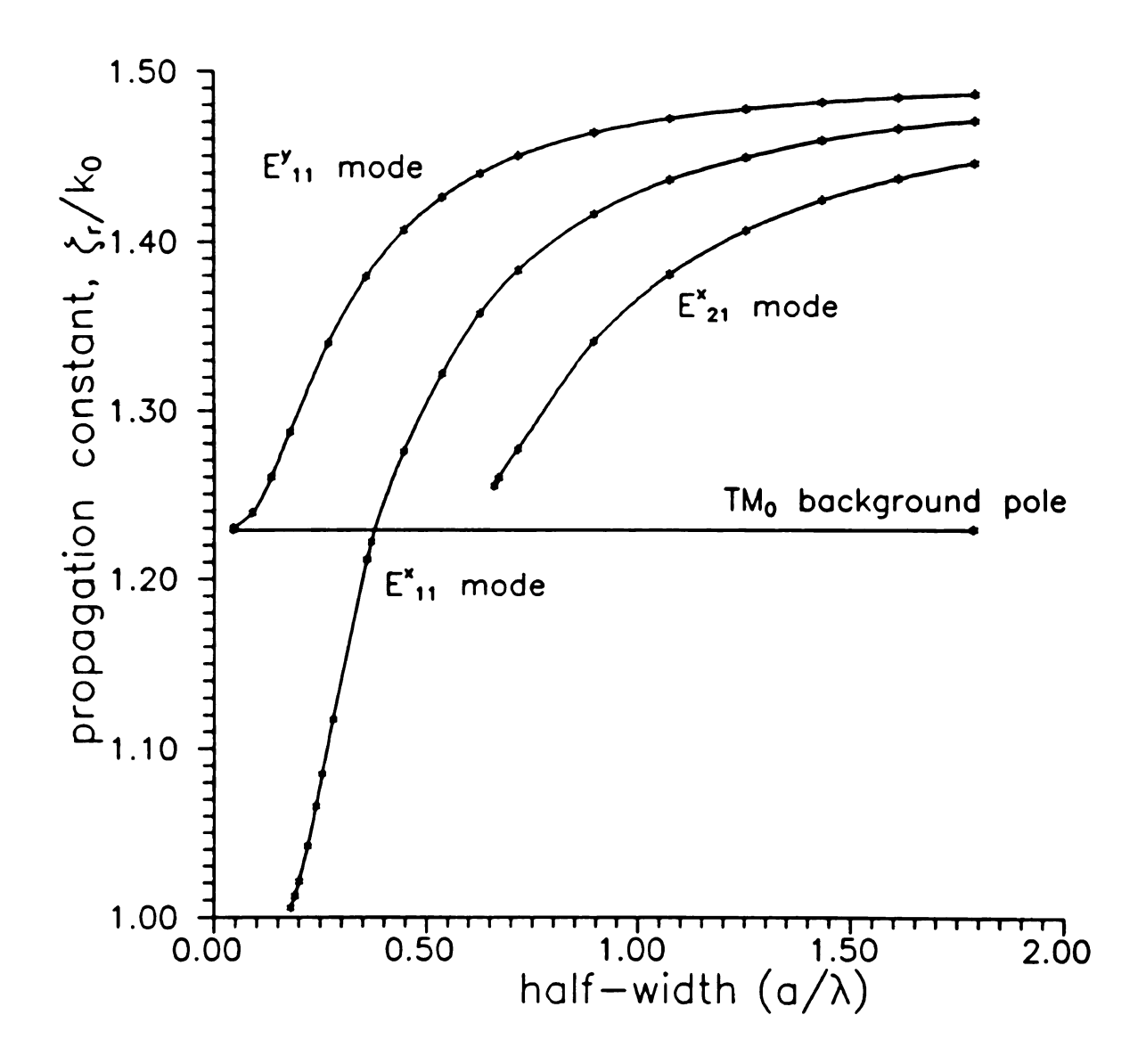


Figure 6.4 Dispersion curve for integrated dielectric rib waveguide.

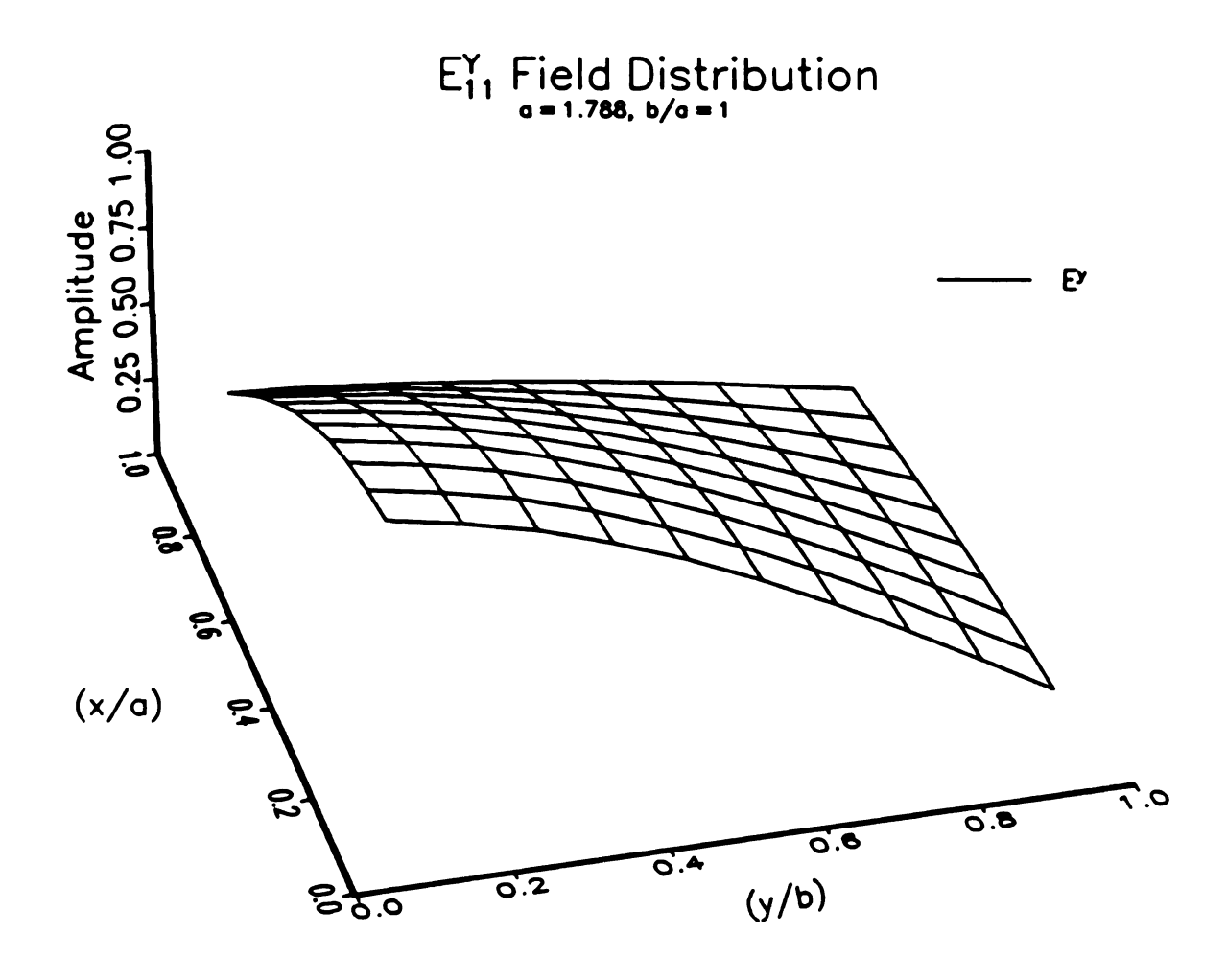


Figure 6.5 Field distribution for dominant E_{11}^y waveguide mode for guide half-width of $a=1.788\lambda$.

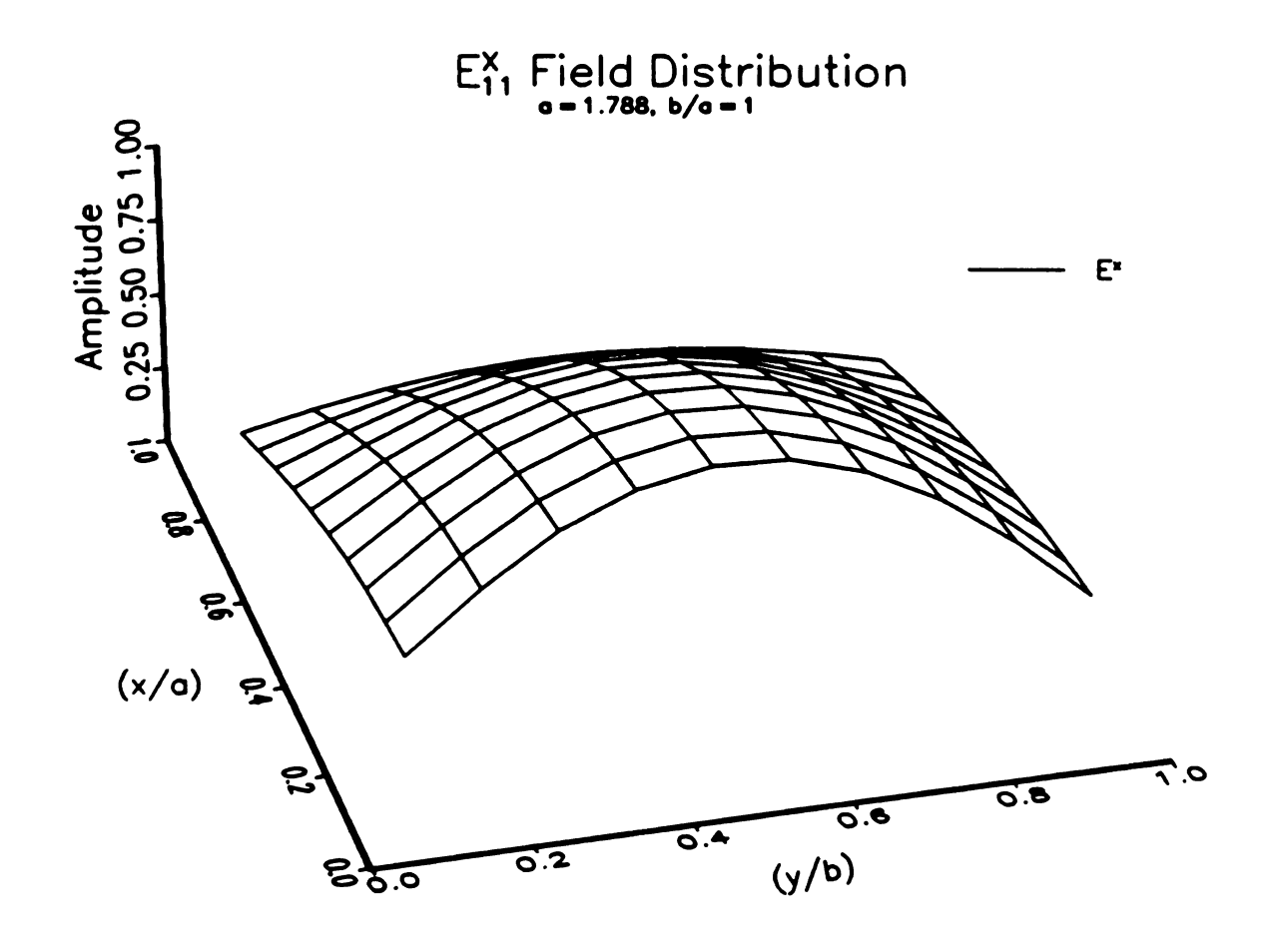


Figure 6.6 Field distribution for E_{11}^{x} waveguide mode for guide half-width of $a=1.788\lambda$.

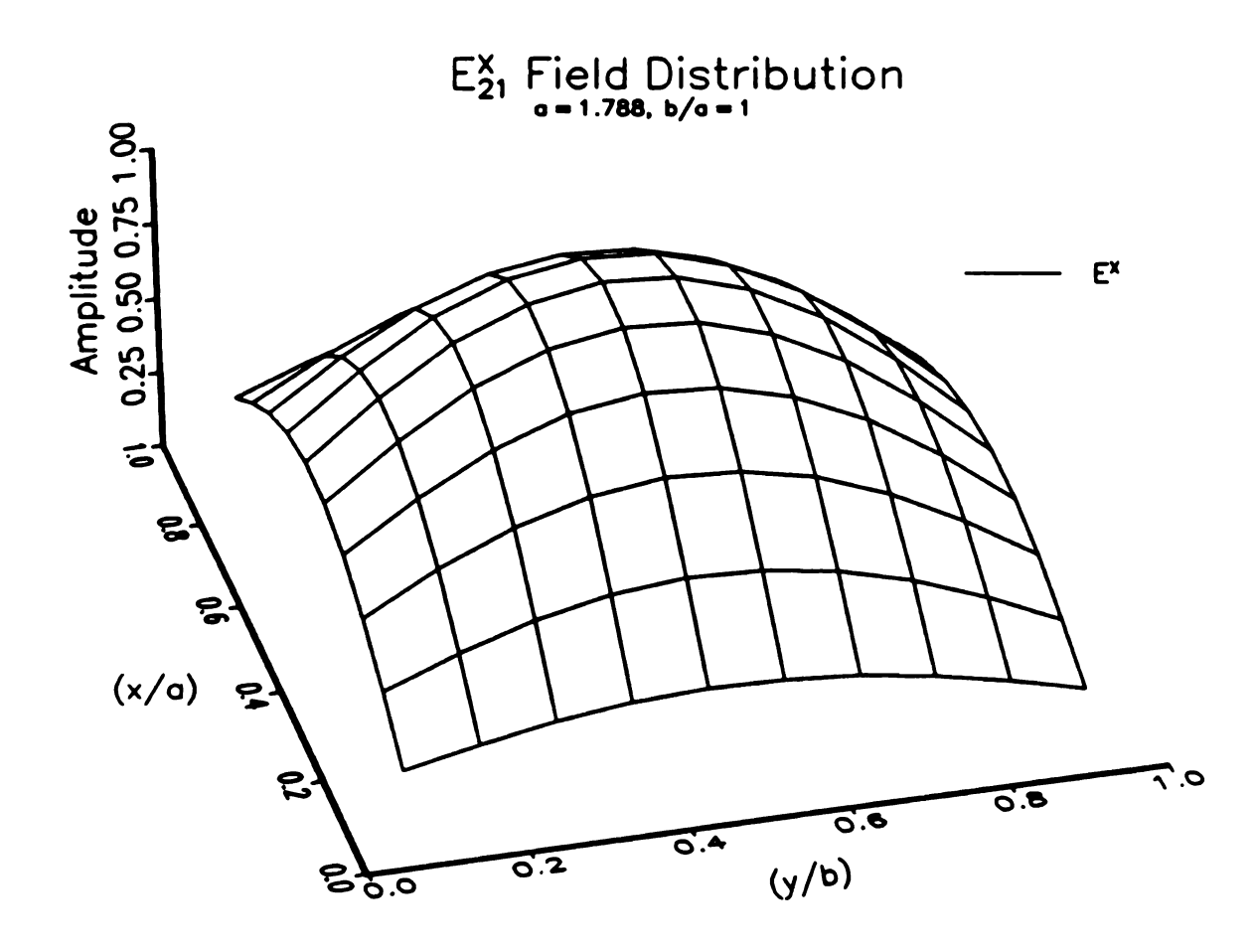


Figure 6.7 Field distribution for E_{21}^x waveguide mode for guide half-width of $a=1.788\lambda$.

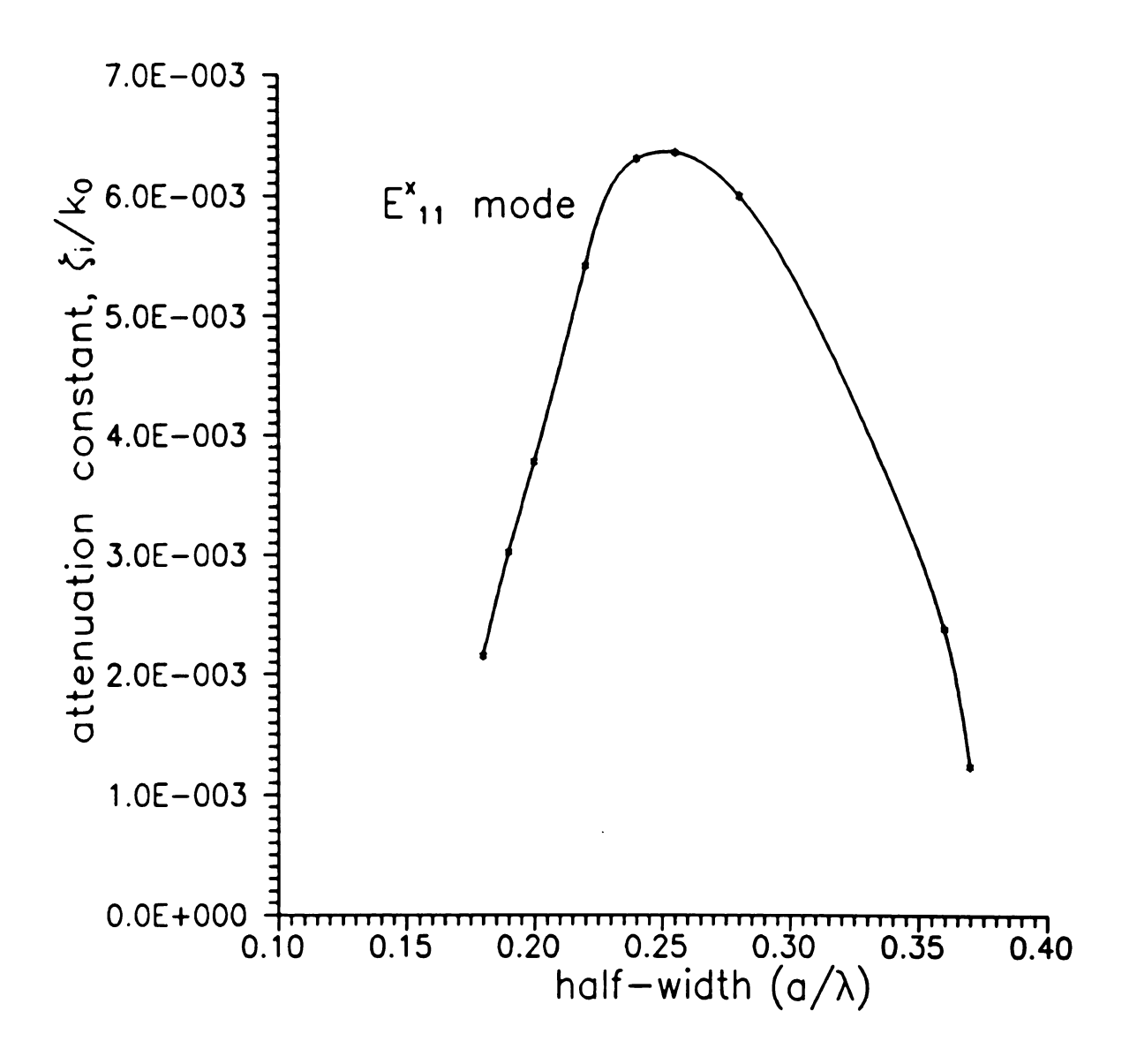


Figure 6.8 Attenuation plot for E₁₁ leaky-wave mode in surface-wave-leaky regime.

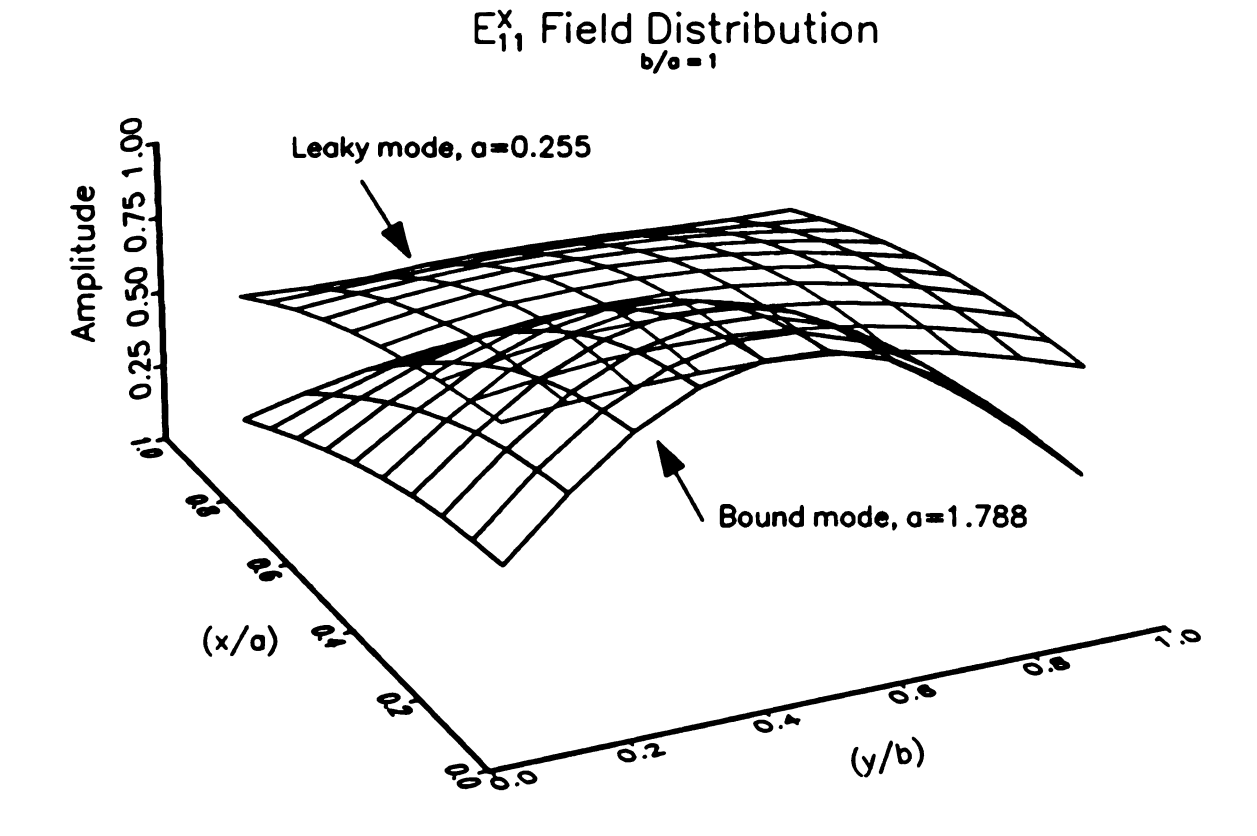


Figure 6.9 Field distribution for E^x₁₁ leaky-wave of rib waveguide compared to a bound guiding mode.

because a leaky-wave ζ_i is small that total loss is small; the ζ_i 's in Figure 6.8 are large losses when operating at optical frequencies. More striking is the loss of the confinement of the waveguide field for a leaky-wave mode.

Not many space-wave leaky modes (sheet 3 solutions) or full leaky modes (sheet 4 solutions) have been found. The following leaky wave poles have been determined and are tabulated below.

Table 6.1 Table of space-wave leaky wave poles (sheet 3) and full leaky wave (sheet 4) for the dielectric rib waveguide where b/a=1.

а	sheet 3 (space-wave) leaky mode, ζ ₃	sheet 4 (full) leaky mode, \$\xi_4\$	Δ, ζ, - ζ,	Δ
.5	0.86696 -j 0.17364	0.86969 -j 0.16913	-0.00273 +j 0.00461	0.00536
.49	0.85391 -ј 0.18829	0.85643 -j 0.18346	-0.00252 +j 0.00483	0.00545

A plot of their guiding region field distributions is shown in Figure 6.10. These leaky-wave poles are E_{22}^x leaky-waves based on their field distribution. Immediately obvious from Table 6.1 and Figure 6.10 is that there is very little difference between propagation constants and field distributions for a space-wave leaky mode or full-wave leaky mode solution at a given guide half-width a. This means the effect of the surface-wave pole on the field behavior is small. This is again consistent with observations about the thin-film surface-wave contributions throughout this dissertation.

E₂₂ Leaky Wave Field Distribution

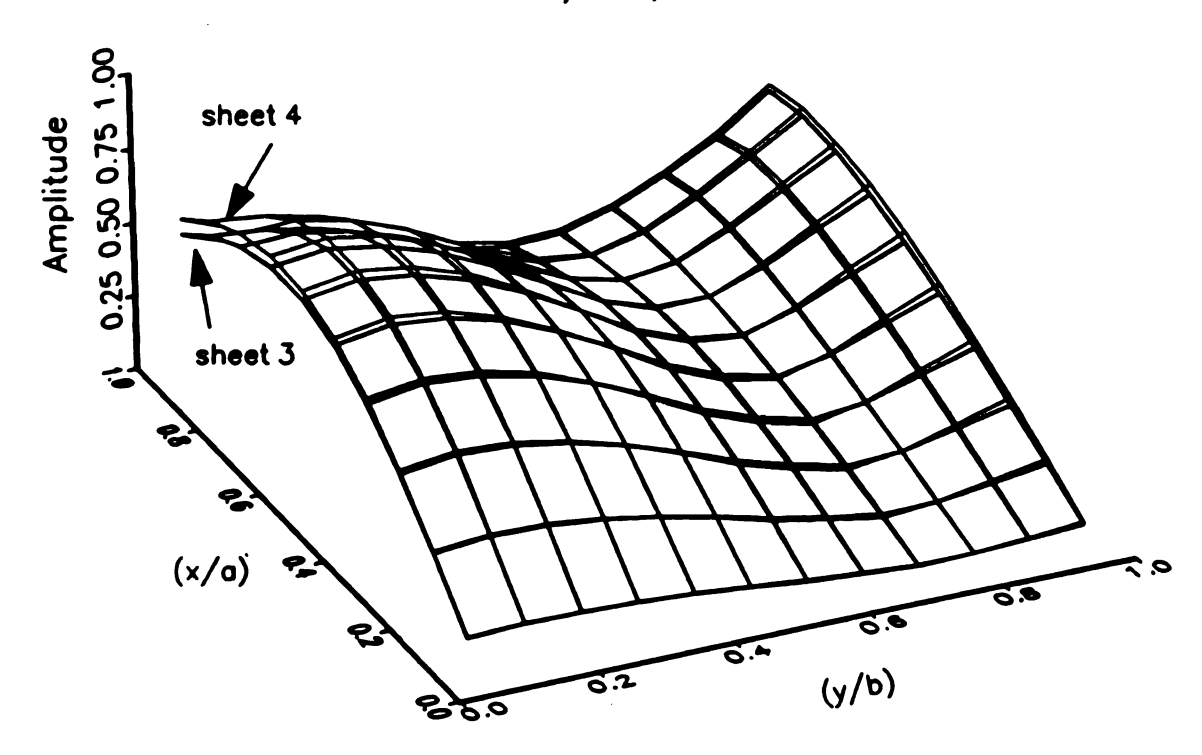


Figure 6.10 Comparison of field distributions of sheet 3 and sheet 4 leaky-wave modes.

Both space-wave leaky and full leaky waves can make significant contributions to the far-zone scattered field. The contribution of a given leaky-wave mode depends upon if it is intercepted by the steepest-descents contour. Given the similarity between the space-wave and full leaky mode, is it possible to use them interchangeably if only interested in the scattered-field above the rib waveguide. The usage of these leaky-wave modes on sheet (3) or sheet (4) to determine the scattered field is a good topic for future investigation.

Summary

The EFIE developed for dielectric waveguides in Chapter 2 has been applied to a integrated dielectric rib waveguide. Bound and leaky wave solutions were obtained. Of significant note is that the effect of the surface-wave pole of the background structure is very small. This is consistent with other observations throughout this thesis.

Chapter 7

Conclusions and Recommendations

A rigorous, full-wave integral-operator-based formulation to characterize the continuous radiation spectrum for a broad class of open-boundary waveguides has been presented. This formulation is capable of characterizing the complete propagation-mode spectrum for these open-boundary waveguides. Furthermore, this integral-operator formulation provides a conceptual, unifying treatment of the relation of leaky-wave modes to the propagation-mode spectrum and in particular the continuous radiation spectrum.

This formulation is based upon the rigorous dyadic Green's function describing the Hertzian vector potential supported by an arbitrary current source immersed in a planar layered background environment. This Green's function is identified via Fourier transform techniques; as a result, the Green's function scalar components obtained are inverse transforms of the Sommerfeld integral class. Knowledge of this Green's function allows determination of the associated electric and magnetic fields. The open-boundary waveguide is then recognized as a set of equivalent sources within the layered background; superposition over the set of equivalent sources then determines the appropriate electric-field integral equation describing the problem.

The afore-mentioned integral equation is solved in the axial-transform domain; recovery of the three-dimensional spatial waveguide fields from the determined transform-domain fields is accomplished by an inverse transform on axial wavenumber ζ . Evaluation of this transform by singularity expansion methods allows the identification of the propagation-mode spectrum. This spectrum is comprised of two distinct types of modes. There are a finite number of bound, hybrid waveguiding modes. These guiding mode fields are confined to the vicinity of the open-boundary waveguide and do not carry power transversely away from the waveguide. Such modes are associated with pole singularities of the transform-domain fields; a guiding mode satisfies the homogeneous transform-domain EFIE. Standard eigenfunction expansion theory can be applied to determine the expansion of an impressed field in terms of the guiding modes.

The other component to the propagation-mode spectrum is a continuum of radiation modes, which have field distributions that are not confined to the waveguide vicinity. The radiation modes provide the mechanism to carry power transversely away from the guiding structure, hence accounting for radiation losses. Radiation modes are associated with branch cuts within the axial transform domain; at these points, a radiation spectral mode satisfies the inhomogeneous transform-domain EFIE; consequently, solutions for the radiation spectral modes are dependent upon the impressed field. The total radiation field is the continuous superposition of EFIE solutions along the entire branch cut; this superposition satisfies the radiation condition at infinity. The nature of the Green's functions used by the EFIE, and their complicated dependence upon the axial wavenumber ξ and transverse spectral frequency ξ , obscure the regimes in which radiation modes would necessarily be continuous.

The regimes for the continuous radiation spectrum can be determined by enforcing the requirement that the Green's function scalar components must be spectral in nature; that is, bounded or vanishing as approaching infinity transversely. Enforcement of this behavior on the Green's functions requires that the forward Fourier transforms converge, in particular the transform on transverse coordinate x.

Mathematically, the forward transform must converge to an analytic function within a finite strip in the transverse spectral frequency plane which is parallel to the real-line axis; the inversion contour to evaluate the inverse transform lies parallel to the real axis within this strip of convergence. As the Fourier transform is an analytic function within its strip of convergence, no singularities of the Fourier transform can exist within this strip of convergence.

For the forward transform to model spectral behavior, the strip of convergence must minimally includes the real axis, upon which the inversion contour lies. Enforcing this requirement restricts any singularities within the transverse spectral-frequency plane to remain either within the lower- or upper- half-plane and not pass through the real axis from lower to upper and vice-versa. This provides the criteria for choosing the branch cuts within the axial wavenumber plane; consequently determining the regime for which the continuous radiation spectrum of the open-boundary waveguide is defined. Enforcing that the transform converge is the equivalent of enforcing the radiation condition.

For the limitingly low-loss case, the continuous radiation spectrum decomposes into a number of identifiable radiation regimes. There are any number of surface-wave radiation regimes, in which the radiation spectral components are propagating modes and have the characteristic of bounded oscillatory behavior in x but exponential decay in y.

These surface-wave regimes thus model the power carried transversely away from the open-boundary waveguide, within the interior (film) layers of the background structure, by excited surface-wave modes of that layered background. Each of these surface-wave regimes is associated with an excited surface-wave mode.

There are two other possible radiation regimes associated with the wavenumbers of the semi-infinite cover/substrate layers of the background environment. The substrate regime is typically comprised of propagating radiation modes with bounded, oscillatory fields in the transverse x coordinate and in the normal y coordinate within the substrate layer, but with exponential decay in y within the cover region. The other regime is the typical full radiation regime, in which the radiation mode has bounded oscillatory behavior both transversely in x and in y within both the cover and substrate. The radiation modes within the full-radiation regime can be either propagating or evanescent.

Substrate- and full-radiation regimes can be identified for open-boundary devices of arbitrary geometry in multi-layered backgrounds; the surface-wave radiaton modes as identified are new and specific to waveguiding applications.

The criterion defining the continuous radiation spectrum serves to define an n-sheeted Riemann surface for the axial transform domain. Proper spectral behavior is associated only with the top sheet; all other sheets are non-spectral. The transform-domain homogeneous EFIE possesses solutions on the other sheets; these solutions are the improper or leaky-wave modes of the open-boundary waveguide. This integral-operator formulation is therefore capable of identifying the leaky-wave modes of these open-boundary waveguides. Because of the branch cut choice, leaky-wave modes never influence the proper spectrum of the waveguide. As leaky waves are non-spectral, they

cannot exist over all of space, but rather have meaning only in specific restricted spatial regimes. Leaky waves are significant in the asymptotic evaluation (as in the method of steepest descents) of the scattered field for an excitation problem. Leaky waves augment the saddle-point contribution to the waveguide scattered field in a restricted spatial regime, defined wherever the SDC contour intercepts the leaky-wave pole. It is within this regime for which a leaky-wave solution has physical significance.

This theory was then applied to determine the radiation spectrum for planar dielectric waveguides. These planar waveguides possess canonical, closed-form solutions determinable by differential operator techniques. The integral-operator formulation agreed well with canonical results, giving confidence in its validity for more complicated problems. It was observed that the deeper into the radiation spectrum, the more periodic the waveguide field became. Asymmetric waveguides were also considered. The effect of the asymmetry was rather significant upon the propagating radiation spectral modes but insignificant upon the evanescent radiation modes.

The integral-operator formulation was then applied to determine the radiation spectrum of a simple practical waveguiding structure in MMIC design, the microstrip transmission line, for which no known results exist. Results for the spectral radiation mode surface currents were numerically obtained at relatively small spatial frequencies within the radiation regime. It was observed for a thin-film substrate that the surface current amplitudes in the transverse-only radiation regime are very small compared to the amplitudes within the full radiation regime. This indicates that the amount of transverse-power loss, carried away from the microstrip by the excited background surface wave, is very small. Again, increasing periodicity of the radiation modes was

observed deeper into the radiation regime. Deep into the evanescent portion of the full radiation regime (that is, $|\zeta_i| \to \infty$), a disturbing trend of increasing radiation mode surface current amplitudes was observed. This observed trend is most likely due to an artifact from the calculation of the impressed field. Even though disturbing, the effect of the increasing amplitudes is annulled when considering the total radiation field, as the modes in question are evanescent and exponentially decaying.

Finally, the integral-operator formulation was applied to the determination of leaky-wave modes of the integrated dielectric rib waveguide in a cover/film/conductor background. There are no published results for any leaky-wave modes of these structures. For a thin-film substrate, the axial wavenumber plane has four Riemann sheets. The top sheet (Sheet 1) solutions are the hybrid guided-wave modes. Leaky-wave solutions were found on each remaining sheet. Sheet 2 solutions are the surface-wave-only leaky waves. These leaky waves have small attenuation constants relative to the leaky-wave solutions on sheets 3 and 4. This indicates that power carried away only in the film layer is small with respect to other radiation loss mechanisms. This is consistent with results from the microstrip analysis. Finally, leaky-wave solutions on sheet 3 or 4 were observed to have similar eigenvalues for either sheet. The attenuation constants for these leaky-wave solutions indicate that radiation into the cover region dominates radiation loss mechanisms.

Having confirmed the validity of the integral-operator technique, many extensions to this research become obvious. First, more investigation as to the behavior of the impressed field in the transform-domain is needed. Electric charges have been suggested as a source for the increasing spectral amplitude deep into the radiation spectrum of the

microstrip transmission line. This can be investigated initially by applying the EFIE to determine the TM radiation spectrum for a symmetric planar waveguide, as TM mode behavior depends upon electric charge. As there are closed-form solutions for the symmetric planar waveguide TM radiation modes to compare results to, this can yield valuable insight into the behavior of the impressed field in the transform domain.

This integral-operator technique is easily applied to more complicated open-boundary waveguiding structures. For example, thick-film substrates or non-conductor-backed multi-layered environments are investigated by including all surface-wave poles of the background structure. The simplest of these extensions is investigating thick-film layers that support more than a single surface wave mode. Another simple extension is to investigate the continuous radiation spectrum for a pair of coupled microstrip transmission lines in a conductor/film/cover environment.

The preceding ideas can be accomplished without much effort. If one is willing to develop new Green's functions, many other possibilities open up. Dielectric channel waveguides can be easily analyzed by using a different dyadic Green's function kernel. The integral-operator technique can be applied to determine the leaky modes and continuous radiation spectrum of microstrip transmission lines on an anisotropic substrate. This necessitates developing a new set of Green's functions, and could bring to light new physical phenomena.

An intriguing application is an investigation of the effect of the propagating continuous radiation spectrum upon microstrip discontinuity measurements. This has potential benefits for applications such as microwave material characterization.

Finally, more investigation needs to be carried out as to the contributions of each type of leaky-wave mode to the total scattered field from a waveguide. This would involve determining a solid methodology for applying the method of Steepest Descents for three-dimensional problems. As mentioned before, the similarity of certain leaky-wave solutions on different sheets suggests that there is much left to understand.

In summary, this integral-operator technique shows promise to conceptually characterize the radiation spectrum for a wide variety of open-boundary waveguides. The technique includes the excitation in a natural, straightforward manner. The integral-operator technique also provides a methodology to identify leaky-wave modes of these structures. Finally, this technique shows how the radiation spectrum and leaky waves relate to each other, and consequently unifies both approaches.



Appendix A

Electric Hertzian Potentials

A.1 Electric Hertzian Potential

Maxwell's equations govern the behavior of the electromagnetic fields of an openboundary waveguides, and take the form

$$\nabla \times \vec{\mathbf{E}} = -j\omega \mu \vec{\mathbf{H}} \qquad \text{Faraday's Law}$$

$$\nabla \times \vec{\mathbf{H}} = j\omega \epsilon \vec{\mathbf{E}} + \vec{\mathbf{J}} \qquad \text{Ampere-Maxwell Law} \qquad (A.1)$$

$$\nabla \cdot \vec{\mathbf{E}} = \rho / \epsilon \qquad \text{Gauss's Law}$$

$$\nabla \cdot \vec{\mathbf{H}} = 0 \qquad \text{Magnetic Source Law}$$

for linear, isotropic, homogeneous media and time-harmonic fields. Maxwell's equations as given in (A.1) are a set of overspecified, coupled partial differential equations, with Gauss's Law and the Magnetic Source Law embedded within the Ampere-Maxwell Law and Faraday's Law respectively. A direct solution from (A.1) is possible; after some manipulation, the associated Helmholtz equations are found to be

$$\nabla^{2}\vec{\mathbf{E}} + k^{2}\vec{\mathbf{E}} = j\omega\mu\vec{\mathbf{J}} + \nabla(\frac{\rho}{\epsilon})$$

$$\nabla^{2}\vec{\mathbf{H}} + k^{2}\vec{\mathbf{H}} = -\nabla\times\vec{\mathbf{J}}$$
(A.2)

with $k^2 = \omega^2 \mu \epsilon$. The solutions obtained for equations (A.2) unfortunately possess a fairly complicated dependence upon the source terms; development and recognition of a Green's function for (A.2) is complicated and difficult.

There is a more satisfactory approach. From the observation that no magnetic sources exist, use of the standard vector identity $\nabla \cdot (\nabla \times \vec{A}) = 0$ allows the magnetic field to be formulated as the curl of an auxiliary vector potential. This is justified by Helmholtz's Theorem, which states that a vector field is uniquely specified to within a constant if both its curl and divergence are specified everywhere. Based upon historical precedence [55], the electric-type Hertzian vector potential $\vec{\Pi}(\vec{r})$ will be used. Consequently, the Hertzian vector potential is defined as a vector whose curl satisfies

$$\vec{\mathbf{H}} = i\boldsymbol{\omega} \boldsymbol{\epsilon} \nabla \times \vec{\mathbf{I}} . \tag{A.3}$$

Substitution of definition (A.3) into Faraday's Law reveals that

$$\nabla \times (\vec{E} - \omega^2 \mu \epsilon \vec{\Pi}) = 0 \tag{A.4}$$

and application of another standard vector identity, $\nabla \times \nabla V = 0$, allows the introduction of the electric-type Hertzian scalar potential Φ^e ; thus, the electric field is

$$\vec{\mathbf{E}} = k^2 \vec{\mathbf{\Pi}} - \nabla \Phi^e \tag{A.5}$$

with $k^2 = \omega^2 \mu \epsilon$. The sign of the potential is chosen for consistency with electrostatic convention. Substitution of (A.5) into Ampere-Maxwell's Law yields the wave equation

$$\nabla \times \nabla \times \vec{\Pi} - k^2 \vec{\Pi} = \frac{\vec{J}}{j\omega \epsilon} - \nabla \Phi^{\epsilon}$$
 (A.6)

which, by using the vector identity $\nabla \times \nabla \times \vec{\Pi} = \nabla \nabla \cdot \vec{\Pi} - \nabla^2 \vec{\Pi}$, can be cast into the more familiar form of

$$\nabla^2 \vec{\Pi} + k^2 \vec{\Pi} = -\frac{\vec{J}}{j\omega\epsilon} + \nabla(\nabla \cdot \vec{\Pi} + \Phi^e). \tag{A.7}$$

No divergence has yet been specified for $\vec{\mathbf{I}}$; by choosing to enforce the Lorentz gauge,

$$\Phi^e = -\nabla \cdot \vec{\Pi} \tag{A.8}$$

equation (A.7) simplifies to

$$\nabla^2 \vec{\Pi} + k^2 \vec{\Pi} = -\vec{J}/j\omega \epsilon. \tag{A.9}$$

Helmholtz's theorem is satisfied and the Hertzian vector potential is completely specified (though any choice for the divergence of $\vec{\mathbf{I}}$ will satisfy Helmholtz's theorem).

The Helmholtz equation for electric-type Hertzian potentials given in (A.9) has as a source term electric current density $\vec{J}(\vec{r})$; while useful for some applications, historically, the Hertzian vector potential has been supported by polarization currents $\vec{P}(\vec{r})$. A relationship between \vec{J} and \vec{P} is easily derived. Recalling that polarization charge density is $\rho_{pol} = -\nabla \cdot \vec{P}$, and that charge densities are related to current densities by $\nabla \cdot \vec{J}_{pol} = -j\omega \rho_{pol}$, it is easily recognized that $j\omega \vec{P} = \vec{J}_{pol}$. Thus, an equivalent equation to (A.9), with polarization sources, is

$$\nabla^2 \vec{\Pi} + k^2 \vec{\Pi} = \frac{-\vec{P}}{\epsilon}$$
 (A.10)

Regardless of which version of the Helmholtz equation is used, the electric field is found in terms of the Hertzian vector potential as

$$\vec{\mathbf{E}} = k^2 \vec{\mathbf{\Pi}} + \nabla \nabla \cdot \vec{\mathbf{\Pi}} \tag{A.11}$$

A.2 Hertzian Potential Boundary Conditions

An analysis of planarly-layered geometry, as depicted in Figure 2.2, could proceed without developing specific boundary conditions on the Hertzian potential. The electric and magnetic fields can be calculated from solutions to Helmholtz equation (A.10) by using equations (A.3) and (A.11), then matching tangential-field boundary conditions at a source-free interface,

$$\mathbf{\hat{n}} \times (\vec{E}_1 - \vec{E}_2) = 0$$

$$\mathbf{\hat{n}} \times (\vec{H}_1 - \vec{H}_2) = 0$$
(A.12)

an indirect technique at best. If boundary conditions for the Hertzian vector potential can be developed, then these can be applied directly to solutions of (A.10), and intermediate operations can be avoided. This becomes significant for multi-layered geometries.

Essentially, the Hertzian potential boundary conditions are a disguised version of the standard electric and magnetic field boundary conditions as given in (A.12). Using cartesian coordinates, the electric and magnetic fields in the i_{th} region, in terms of Hertzian vector potentials, are

$$E_{ix} = k_i^2 \Pi_{ix} + \frac{\partial}{\partial x} \nabla \cdot \Pi_i \qquad H_{ix} = j\omega \epsilon_i \left(\frac{\partial \Pi_{ix}}{\partial y} - \frac{\partial \Pi_{iy}}{\partial z} \right)$$

$$E_{iy} = k_i^2 \Pi_{iy} + \frac{\partial}{\partial y} \nabla \cdot \Pi_i \qquad H_{iy} = j\omega \epsilon_i \left(\frac{\partial \Pi_{ix}}{\partial z} - \frac{\partial \Pi_{ix}}{\partial x} \right)$$

$$E_{iz} = k_i^2 \Pi_{iz} + \frac{\partial}{\partial z} \nabla \cdot \Pi_i \qquad H_{iz} = j\omega \epsilon_i \left(\frac{\partial \Pi_{iy}}{\partial x} - \frac{\partial \Pi_{ix}}{\partial y} \right)$$
(A.13)

The interface is planar and source-free, while the regions on either side of the interface are homogenous, have the same permeability $\mu = \mu_0$, but possess dielectric contrast. The boundary conditions in equation (A.12) will be applied to the fields as given by equation (A.13), from which relations on the Hertzian potential will be deduced. This looks difficult, as all components of $\vec{\Pi}$ and their derivatives are involved. However, by choosing orthogonally directed polarization currents, and using linear superposition, the task can be accomplished. The results of this process are well-known in the literature [16,29], having been stated as

at a dielectric-dielectric interface, with $N_{21}^2 = \epsilon_2 / \epsilon_1$. The boundary conditions in (A.14) simplify at a dielectric-perfect electric conductor (PEC) interface, becoming

$$\frac{\Pi_{1a} = 0}{\frac{\partial \Pi_{1y}}{\partial y}} = 0 \tag{A.15}$$

for $\alpha = x, z$. For problems involving magnetic contrast, the boundary conditions of (A.14) need to be slightly modified; the results can be found in [56].

A.3 Interpretations and Considerations

Working through the process used to arrive at the boundary conditions in (A.14) and (A.15), while seemingly redundant, reveals insights into the analytical method being used, and the necessary form for solutions. For a vertical (normal to interface) excitation of $\vec{P} = \hat{y}P_0$, only vertical components of Hertzian potential ($\vec{\Pi} = \hat{y}\Pi_y$) are excited. Application of the boundary conditions (A.12) to the scalar field components in Cartesian coordinates gives

$$E_{\text{tan}}: \frac{\partial}{\partial x_{\alpha}} (\nabla \cdot \hat{y} \Pi_{1y}) = \frac{\partial}{\partial x_{\alpha}} (\nabla \cdot \hat{y} \Pi_{2y})$$

$$H_{\text{tan}}: \frac{\partial (\epsilon_{1} \Pi_{1y})}{\partial x_{6}} = \frac{\partial (\epsilon_{2} \Pi_{2y})}{\partial x_{6}}$$
(A.16)

where $\alpha = x,z$, $\beta = x,z$ and $\hat{x}_{\alpha} \perp \hat{x}_{\beta}$. Equality of tangential derivatives for any point (x,z) on the planar interface implies

$$\nabla \cdot \Pi_{1} = \nabla \cdot \Pi_{2} \implies \frac{\partial \Pi_{1y}}{\partial y} = \frac{\partial \Pi_{2y}}{\partial y}$$

$$\Pi_{1y} = N_{21}^{2} \Pi_{2y}$$
(A.17)

where $N_{21}^2 = \epsilon_2/\epsilon_1$. The conclusion about tangential derivatives that leads to (A.17) is intuitive; it is also mathematically rigorous. If tangential derivatives of two functions are equal at each point on the interface (consider the $E_{\rm tan}$ boundary condition in (A.16)), then the integrals of each tangential derivative over an arbitrary path on the interface will also be equal, namely

$$\int_{\Delta I} \frac{\partial (\nabla \cdot \vec{\Pi}_1)}{\partial x_a} dx_a = \int_{\Delta I} \frac{\partial (\nabla \cdot \vec{\Pi}_2)}{\partial x_a} dx_a$$

from which it is evident that the conclusion reached in (A.17) is valid. A similar procedure can be applied to the H_{total} relations.

Consider now a horizontal (tangential) excitation $\vec{P} = \hat{x} P_0$ over a planar interface. A naive assumption is that only horizontal components of Hertzian potential ($\vec{\Pi} = \hat{x} \Pi_x$) exist. Application of the electric field boundary conditions in (A.12) gives

$$E_{\alpha}: \quad \delta_{x\alpha} k_1^2 \Pi_{1x} + \frac{\partial}{\partial x_{\alpha}} (\nabla \cdot \hat{x} \Pi_{1x}) = \delta_{x\alpha} k_2^2 \Pi_{2x} + \frac{\partial}{\partial x_{\alpha}} (\nabla \cdot \hat{x} \Pi_{2x}) \quad (A.18)$$

for $\alpha = x, z$. Obviously, $\nabla \cdot \vec{\Pi}_1 = \nabla \cdot \vec{\Pi}_2 \rightarrow \Pi_{1x} = \Pi_{2x}$ satisfies the boundary conditions for $\alpha = z$. Satisfying the boundary conditions for $\alpha = x$ also requires that $k_1^2 \Pi_{1x} = k_2^2 \Pi_{2x}$ — an obvious contradiction. It is apparent that a horizontal source cannot excite only horizontal potentials over a planar interface, but should also excite vertical potentials as well. This excitation is actually intuitive if careful consideration is given to the electric

field maintained by Hertzian vector potentials. An interface with dielectric contrast has a net surface polarization charge density, implying a discontinuity of the electric fields normal (vertical) to the interface. As evidenced in equation (A.13), the electric field has a strong component in the direction of Hertzian potential; as a consequence, there must always be a vertical component of Hertzian potential at a planar interface. Another consequence of this excitation is that any Green's function satisfying the Helmholtz equation (A.10) in a layered background environment will be dyadic in nature.

With the horizontal (tangential) source exciting both horizontal and vertical components of Hertzian vector potential ($\vec{\Pi} = \hat{x}\Pi_x + \hat{y}\Pi_y$), application of (A.12) reveals

$$\hat{\mathbf{x}} - fields \qquad \hat{\mathbf{z}} - fields \\
\vec{\mathbf{E}} : \quad \mathbf{k}_{1}^{2} \Pi_{1x} + \frac{\partial}{\partial x} (\nabla \cdot \vec{\Pi}_{1}) = \mathbf{k}_{2}^{2} \Pi_{2x} + \frac{\partial}{\partial x} (\nabla \cdot \vec{\Pi}_{2}) \qquad \frac{\partial}{\partial z} (\nabla \cdot \vec{\Pi}_{1}) = \frac{\partial}{\partial z} (\nabla \cdot \vec{\Pi}_{2}) \qquad (\mathbf{A}.19) \\
\vec{\mathbf{H}} : \qquad \frac{\partial}{\partial z} (\boldsymbol{\epsilon}_{1} \Pi_{1y}) = \frac{\partial}{\partial z} (\boldsymbol{\epsilon}_{2} \Pi_{2y}) \qquad \boldsymbol{\epsilon}_{1} \frac{\partial \Pi_{1x}}{\partial y} - \boldsymbol{\epsilon}_{2} \frac{\partial \Pi_{2x}}{\partial y} = \frac{\partial}{\partial z} (\boldsymbol{\epsilon}_{1} \Pi_{1y} - \boldsymbol{\epsilon}_{2} \Pi_{2y})$$

where the first line is for electric fields and the second for magnetic fields. This implies the following Hertzian potential boundary conditions

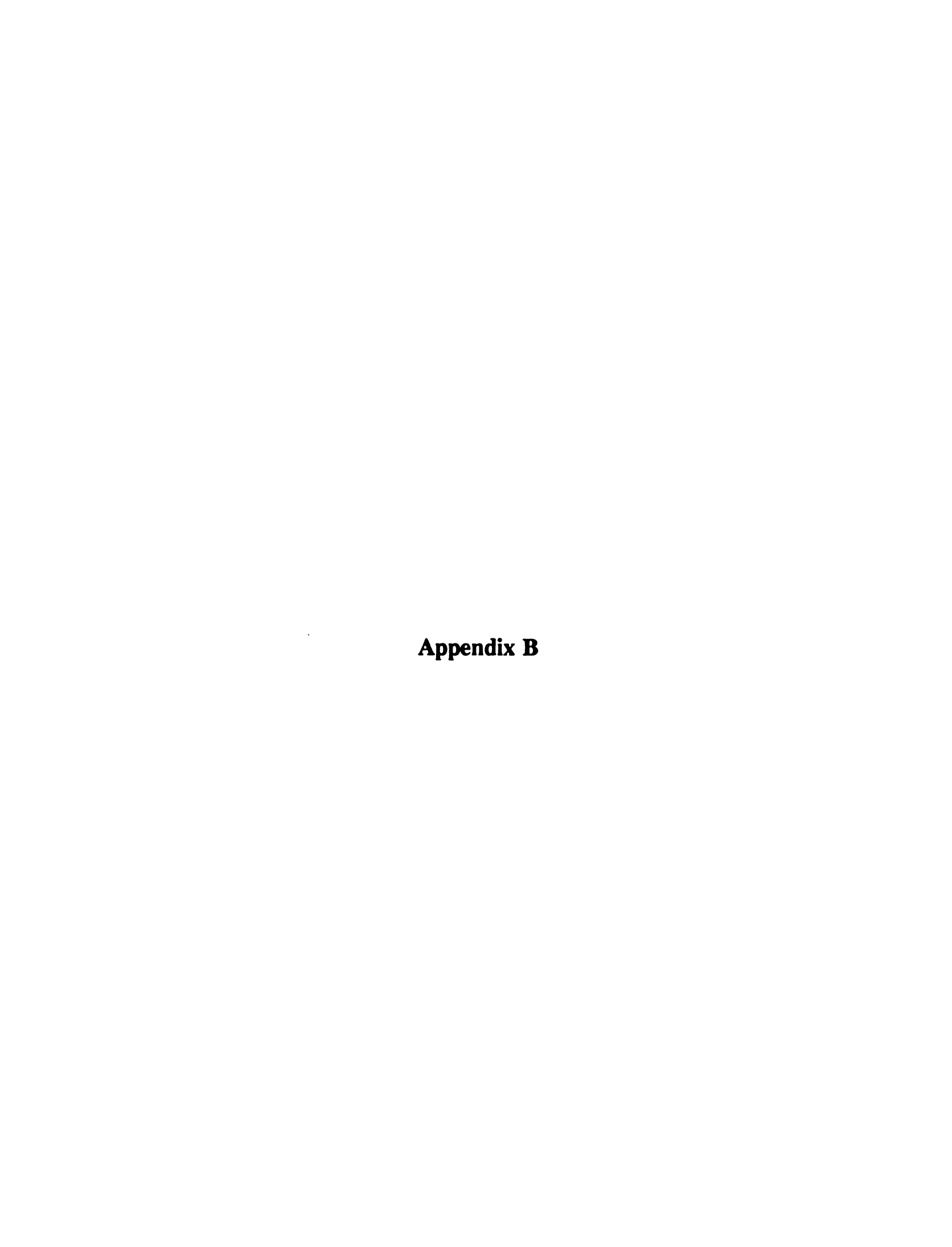
$$\Pi_{1x} = N_{21}^2 \Pi_{2x} \qquad \nabla \cdot \vec{\Pi}_1 = \nabla \cdot \vec{\Pi}_2
\Pi_{1y} = N_{21}^2 \Pi_{2y} \qquad \frac{\partial \Pi_{1x}}{\partial y} = N_{21}^2 \frac{\partial \Pi_{2x}}{\partial y}$$
(A.20)

Similar results arise for an excitation of $\vec{P} = \hat{z}P_0$. By superposition, the results in equations (A.17) and (A.20) generalize to the desired boundary conditions on Hertzian potentials presented in (A.14).

Note that the condition $\nabla \cdot \vec{\Pi}_1 = \nabla \cdot \vec{\Pi}_2$ shows up for both vertical (A.17) and horizontal (A.20) excitation boundary conditions. As $\nabla \cdot \vec{\Pi} = -\Phi^e$, this translates into continuity of the scalar potential, supported by polarization charges, across the interface

(a comforting result). Obviously, the continuity of scalar potentials is the mechanism that couples horizontal components of Hertzian vector potential to its vertical components.

Determining the boundary conditions on Hertzian potential with a perfect electric conductor in region 2 follows a similar process. Application of the appropriate boundary condition, $\mathbf{\hat{n}} \times \mathbf{\vec{E}_1} = \mathbf{0}$, results in the Hertzian potential boundary conditions of (A.15).



Appendix B

Spectral Representation of the Dyadic Green's Function

B.1 Principal Dyadic Green's Function

The principal Hertzian potential is the potential supported by a current radiating in unbounded space. This potential satisfies the Helmholtz equation (A.9), written in scalar form below ($\alpha = x, y, z$),

$$\nabla^2 \Pi_{\sigma}^{\rho} + k^2 \Pi_{\sigma}^{\rho} = -J_{\sigma}/j\omega \epsilon \tag{B.1}$$

subject to the boundary condition that the potential vanish at infinity (the radiation boundary condition). The Green's function for this equation satisfies (B.1) with the Dirac delta function as the excitation,

$$\nabla^2 G^p(\vec{r}|\vec{r}') + k^2 G^p(\vec{r}|\vec{r}') = -\delta(\vec{r} - \vec{r}')$$
 (B.2)

subject to the same boundary condition. Without loss of generality, a solution for $G^{p}(\vec{r}|\vec{r}'=0)$ will be sought, and the final result shifted to an arbitrary \vec{r}' .

From Chapter 2, the two-dimensional Fourier transform pair is,

$$G^{p}(\vec{\mathbf{r}}) = \frac{1}{(2\pi)^{2}} \int_{-\infty}^{\infty} \tilde{G}^{p}(\vec{\lambda}, y) e^{-ij\vec{\lambda}\cdot\vec{r}} d^{2}\lambda$$
 (B.3)

$$\tilde{G}^{p}(\vec{\lambda}, y) = \iint_{-\infty}^{\infty} G^{p}(\vec{\mathbf{r}}) e^{-j\vec{\lambda} \cdot \vec{r}} d^{2}r$$
 (B.4)

where $\vec{\lambda} = \hat{x}\xi + \hat{z}\zeta$ is the 2-D spatial frequency. Writing $G^{P}(\vec{r})$ as its inverse transform and exploiting the relationship

$$\frac{1}{(2\pi)^2} \int_{-\pi}^{\pi} e^{j\vec{\lambda}\cdot\vec{r}} d^2\lambda = \delta(x)\delta(z), \qquad (B.5)$$

equation (B.2) becomes

$$\frac{1}{(2\pi)^2} \int_{-\infty}^{\infty} \left\{ \left[\frac{\partial^2}{\partial y^2} + k^2 - \lambda^2 \right] \tilde{G}^p(\vec{\lambda}, y) + \delta(y) \right\} e^{j\vec{\lambda} \cdot \vec{r}} d^2\lambda = 0, \qquad (B.6)$$

where the $(\nabla^2 + k^2)$ operator has been passed under the double spectral integral. Since $\mathscr{F}^{-1}\{...\}=0 \rightarrow \{...\}=0$, it is clear that (B.2) becomes

$$\left[\frac{\partial^2}{\partial y^2} - p^2(\vec{\lambda})\right] \tilde{G}^p(\vec{\lambda}, y) = -\delta(y)$$
 (B.7)

in the transform domain, where $p(\lambda) = \sqrt{\lambda^2 - k^2}$. The solution of (B.7), \tilde{G}^p , solves the homogenous problem for $y \neq 0$, must vanish as $|y| \to \infty$, must be continuous across y=0, and must have a step discontinuity in the first derivative at y=0. This last statement can be confirmed by integrating (B.7) with respect to y about y=0, resulting in

$$\lim_{\epsilon \to 0} \frac{\partial \tilde{G}^p}{\partial y} \bigg|_{-\epsilon}^{\epsilon} = -1 + p(\vec{\lambda}) \int_{-\epsilon}^{\epsilon} \tilde{G}^p(\vec{\lambda}; y) dy$$

where the RHS integral vanishes as $\epsilon \rightarrow 0$ because it is continuous across y=0 (Midpoint theorem). When these boundary conditions are met, the solution for \tilde{G}^{P} is

$$\tilde{G}^{p}(\vec{\lambda},y) = \frac{e^{-p|y|}}{2p(\lambda)}.$$
 (B.8)

where $\Re\{p(\lambda)\}>0$ to insure (B.8) vanishes as $y\to\infty$. Inverse transforming equation (B.8) then results in, after shifting to an arbitrary \vec{r}' ,

$$G^{p}(\vec{r}|\vec{r}') = \int_{-\infty}^{\infty} \frac{e^{j\vec{\lambda}\cdot(\vec{r}-\vec{r}')} e^{-p(\lambda)|y-y'|}}{2(2\pi)^{2}p(\lambda)} d^{2}\lambda.$$
 (B.9)

the desired spectral representation of the principle Green's function.

B.2 Reflected Dyadic Green's Function

The reflected dyadic Green's function arises from matching the Hertzian potential boundary conditions in a planar layered background environment. This dissertation considers two different background environments: a two-layer interface, serving as the background for an asymmetric planar waveguide, and a tri-layered background environment, which is appropriate for both the microstrip and integrated dielectric rib waveguide analysis. The most general case of the background, a tri-layered configuration, will be developed in this appendix; from this, the appropriate specializations to simpler environments will be made.

The Hertzian potential boundary conditions are developed in Appendix A.

Enforcing these boundary conditions results in

$$\Pi_{1g} = N_{21}^2 \Pi_{2g}$$
 $\alpha = x, y, z$ (B.10)

$$\frac{\partial \Pi_{1\alpha}}{\partial y} = N_{21}^2 \frac{\partial \Pi_{2\alpha}}{\partial y} \qquad \alpha = x,z$$
 (B.11)

$$\frac{\partial \Pi_{1y}}{\partial y} - \frac{\partial \Pi_{2y}}{\partial y} = -(N_{21}^2 - 1) \left[\frac{\partial \Pi_{2x}}{\partial x} + \frac{\partial \Pi_{2z}}{\partial z} \right]$$
 (B.12)

for the y=0 interface and

$$\Pi_{2a} = N_{32}^2 \Pi_{3a}$$
 $\alpha = x, y, z$ (B.13)

$$\frac{\partial \Pi_{2\alpha}}{\partial y} = N_{32}^2 \frac{\partial \Pi_{3\alpha}}{\partial y} \qquad \alpha = x, z \qquad (B.14)$$

$$\frac{\partial \Pi_{2y}}{\partial y} - \frac{\partial \Pi_{3y}}{\partial y} = -(N_{32}^2 - 1) \left[\frac{\partial \Pi_{3x}}{\partial x} + \frac{\partial \Pi_{3z}}{\partial z} \right]$$
 (B.15)

for the y=-t interface, where $N_{ij}=n_i/n_j$ and n_i is the it layer refractive index.

Assuming the sources are in the cover (region 1), the Hertzian potential in each region, developed in Chapter 2, is written in scalar form as

$$\Pi_{1\alpha}(\vec{r}) = \frac{1}{(2\pi)^2} \int_{-\infty}^{\infty} e^{j\vec{\lambda}\cdot\vec{r}} \left[\int_{V} \frac{J_{\alpha}}{j\omega\epsilon_1} \frac{e^{-j\vec{\lambda}\cdot\vec{r}'}e^{-p_1(\lambda)|y-y'|}}{2p_1(\lambda)} dV' + W_{1\alpha}^{r}(\lambda)e^{-p_1(\lambda)y} \right] d^2\lambda \quad (B.16)$$

$$\Pi_{2\alpha}(\vec{r}) = \frac{1}{(2\pi)^2} \int_{-\alpha}^{\alpha} e^{j\vec{\lambda} \cdot \vec{r}} \left[W_{2\alpha}^t(\lambda) e^{p_2(\lambda)y} + W_{2\alpha}^r(\lambda) e^{-p_2(\lambda)y} \right] d^2\lambda.$$
(B.17)

$$\Pi_{3\alpha}(\vec{r}) = \frac{1}{(2\pi)^2} \int_{-\pi}^{\pi} e^{j\vec{\lambda}\cdot\vec{r}} \left[W_{3\alpha}^t(\lambda) e^{P_3(\lambda)y} \right] d^2\lambda. \tag{B.18}$$

for $\alpha = x,y,z$, and where $\Re \{p_i\} > 0$ is enforced to satisfy the radiation condition.

For tangential components of Hertzian potential ($\alpha = x, z$ in (B.16)-(B.18)), boundary conditions (B.10), (B.11), (B.14) and (B.15) are appropriate; these will be enforced at y=0 or y=-t for all x and z. If (B.16)-(B.18) are to satisfy the boundary conditions for an arbitrary x or z, then the bracketed inner quantities must satisfy the boundary conditions. This is equivalent to solving the entire problem in the transform domain. Regardless, matching boundary conditions leads to the linear system of equations

$$-W_{1\alpha}^{r} + N_{21}^{2}(W_{2\alpha}^{t} + W_{2\alpha}^{r}) = V_{\alpha}$$

$$W_{1\alpha}^{r} + \frac{N_{21}^{2}p_{2}}{p_{1}}(W_{2\alpha}^{t} - W_{2\alpha}^{r}) = V_{\alpha}$$

$$W_{2\alpha}^{t} e^{-p_{2}t} + W_{2\alpha}^{r} e^{p_{2}t} - N_{32}^{2}W_{3\alpha}^{t} e^{-p_{3}t} = 0$$

$$W_{2\alpha}^{t} e^{-p_{2}t} - W_{2\alpha}^{r} e^{p_{2}t} - \frac{N_{32}^{2}p_{3}}{p_{2}}W_{3\alpha}^{t} e^{-p_{3}t} = 0$$

$$(B.19)$$

where, as observed previously in Chapter 2,

$$V_{\alpha} = \int_{V} \frac{J_{\alpha}(\vec{\mathbf{I}}')}{j\omega\epsilon_{1}} \frac{e^{-j\vec{\lambda}\cdot\vec{\mathbf{P}}'}e^{-p_{i}y'}}{2p_{1}(\lambda)} dV' \qquad \alpha = x,z$$
 (B.20)

The system of equations (B.19) is solved to yield the following

$$W_{2\alpha}^{t} = \frac{T_{12}^{t}}{D^{t}} V_{\alpha}$$

$$W_{2\alpha}^{r} = \frac{T_{12}^{t} R_{32}^{t} e^{-2p_{2}t}}{D^{t}} V_{\alpha}$$

$$W_{1\alpha}^{r} = \left[R_{21}^{t} + \frac{T_{21}^{t} T_{12}^{t} R_{32}^{t} e^{-2p_{2}t}}{D^{t}} \right] V_{\alpha}$$

$$W_{3\alpha}^{t} = \frac{T_{12}^{t} T_{23}^{t} e^{(p_{3} - p_{2})t}}{D^{t}} V_{\alpha}$$
(B.21)

where the individual interfacial reflection and transmission coefficients are

$$R_{21}^{t} = \frac{p_{1} - p_{2}}{p_{1} + p_{2}}, \qquad R_{12}^{t} = \frac{p_{2} - p_{1}}{p_{1} + p_{2}}$$

$$T_{21}^{t} = \frac{2N_{21}^{2}p_{2}}{p_{1} + p_{2}}, \qquad T_{12}^{t} = \frac{2p_{1}}{N_{21}^{2}(p_{1} + p_{2})}$$

$$R_{32}^{t} = \frac{p_{2} - p_{3}}{p_{2} + p_{3}}, \qquad T_{23}^{t} = \frac{2p_{2}}{N_{32}^{2}(p_{2} + p_{3})}$$
(B.22)

and

$$D^{t} = 1 - R_{12}^{t} R_{32}^{t} e^{-2p_{2}t}$$
 (B.23)

Where (B.23) is zero, pole singularities occur in the solutions given in (B.21). These pole singularities correspond to the TE surface-wave modes of the background structure.

Enforcing boundary conditions (B.10), (B.12), (B.13) and (B.15) for normal components of potential will lead to the linear system of equations

$$-W_{1y}^{r} + N_{21}^{2}(W_{2y}^{t} + W_{2y}^{r}) = V_{y}$$

$$W_{1y}^{r} + \frac{P_{2}}{P_{1}}(W_{2y}^{t} - W_{2y}^{r}) = V_{y} + F \left[j\xi V_{x} + j\zeta V_{z} \right]$$

$$W_{2y}^{t} e^{-P_{2}t} + W_{2y}^{r} e^{P_{2}t} - N_{32}^{2} W_{3y}^{t} e^{-P_{3}t} = 0$$

$$W_{2y}^{t} e^{-P_{2}t} - W_{2y}^{r} e^{P_{2}t} - \frac{P_{3}}{P_{2}} W_{3y}^{t} e^{-P_{3}t} = -G \left[j\xi V_{x} + j\zeta V_{z} \right]$$
(B.24)

where

$$F = \frac{(N_{21}^2 - 1)}{p_1} \frac{T_{12}^t \left[1 + R_{32}^t e^{-2p_2 t} \right]}{D^t}$$

$$G = \frac{(N_{32}^2 - 1)}{p_2} \frac{T_{12}^t T_{23}^t e^{(p_3 - p_2)t}}{D^t} e^{-p_3 t}$$

$$V_y = \int_V \frac{J_y(\vec{t}')}{j\omega \epsilon_1} \frac{e^{-j\vec{\lambda} \cdot \vec{r}'} e^{-p_3 y'}}{2p_1(\lambda)} dV'$$
(B.25)

and D^t is defined previously. Note that the spatial derivative operators on x and z are passed under the spectral integration in (B.16)-(B.18), resulting in the $j\xi$ and $j\zeta$ terms respectively.

The system of equations (B.24) is solved to yield

$$W_{2y}^{r} = \frac{T_{12}^{n}R_{32}^{n}e^{-p_{2}t}}{D^{n}}V_{y} + \frac{\left[R_{32}^{n}N_{21}^{-2}C_{1} + C_{2}\right]}{D^{n}}e^{-2p_{2}t}\left[j\xi V_{x} + j\zeta V_{z}\right]$$

$$W_{2y}^{t} = \frac{T_{12}^{n}}{D^{n}}V_{y} + \frac{N_{21}^{-2}C_{1} - R_{21}^{n}C_{2}e^{-2p_{2}t}}{D^{n}}\left[j\xi V_{x} + j\zeta V_{z}\right]$$

$$W_{1y}^{r} = \left[R_{21}^{n} + \frac{T_{12}^{n}R_{32}^{n}T_{21}^{n}e^{-2p_{2}t}}{D^{n}}\right]V_{y} + \left[C_{1} + \frac{T_{21}^{n}(R_{32}^{n}N_{21}^{-2}C_{1} + C_{2})e^{-2p_{2}t}}{D^{n}}\right]\left[j\xi V_{x} + j\zeta V_{z}\right]$$

$$W_{3y}^{t} = \left\{\frac{T_{12}^{n}T_{23}^{n}}{D^{n}}V_{y} + \left[N_{32}^{-2}C_{2} + \frac{T_{23}^{n}(N_{21}^{-2}C_{1} - R_{21}^{n}C_{2}e^{-2p_{2}t})}{D^{n}}\right]\left[j\xi V_{x} + j\zeta V_{z}\right]\right\}e^{(p_{3} - p_{2})t}$$

where

$$R_{21}^{n} = \frac{N_{21}^{2}p_{1} - p_{2}}{n_{21}^{2}P_{1} + p_{2}}, \quad R_{32}^{n} = \frac{N_{32}^{2}p_{2} - p_{3}}{N_{32}^{2}p_{2} + p_{3}}$$

$$T_{21}^{n} = \frac{2p_{2}}{N_{12}^{2}p_{2} + p_{1}}, \quad T_{12}^{n} = \frac{2p_{1}}{N_{21}^{2}(p_{1} + p_{2})}$$

$$T_{23}^{n} = \frac{2p_{2}}{N_{32}^{2}p_{2} + p_{3}}$$

$$C_{1} = \frac{N_{21}^{2}(N_{21}^{2} - 1)T_{12}^{t}}{N_{21}^{2}p_{1} + p_{2}} \frac{1 + R_{32}^{t}e^{-2p_{2}t}}{D^{t}}$$

$$C_{2} = \frac{N_{32}^{2}(N_{32}^{2} - 1)}{N_{22}^{2}p_{2} + p_{3}} \frac{T_{12}^{t}T_{23}^{t}}{D^{t}}$$

and

$$D^{n} = 1 - R_{21}^{n} R_{32}^{n} e^{-2p_{2}t}$$
 (B.28)

Wherever (B.28) vanishes, pole singularities will occur in the solutions given in (B.26). These singularities correspond to the TM surface-wave modes of the background structure. Also, note that the coupling coefficients C_1 and C_2 also depend upon D^t ; obviously, solutions in (B.26) possesses TE surface-wave mode singularities as well.

Rewriting coefficients in region (1) in terms of the scalar components of the source excitation $\vec{V}(\vec{r}')$ gives

$$W_{1\alpha}^{r} = R_{t}V_{\alpha}$$

$$W_{1y}^{r} = R_{\alpha}V_{y} + C[j\xi V_{x} + j\zeta V_{z}]$$
(B.29)

where

$$R_{t} = R_{21}^{t} + \frac{T_{12}^{t} R_{32}^{t} T_{21}^{t}}{D^{t}} e^{-2p_{2}t}$$

$$R_{n} = R_{21}^{n} + \frac{T_{12}^{n} R_{32}^{n} T_{21}^{n}}{D^{n}} e^{-2p_{2}t}$$

$$C = C_{1} + \frac{T_{21}^{n} \left[R_{32}^{n} N_{21}^{-2} C_{1} + C_{2}\right]}{D^{n}} e^{-2p_{2}t}$$

$$(B.30)$$

The total space-domain potential may be written as

$$\vec{\Pi}_{1} = \vec{\Pi}_{1}^{p} + \vec{\Pi}_{1}^{r}. \tag{B.31}$$

Equation (B.29) is substituted into (B.16) to yield

$$\vec{\Pi}_{1}(\vec{r}) = \int_{V} \vec{G}(\vec{r}|\vec{r}') \cdot \frac{\vec{J}(\vec{r}')}{j\omega\epsilon_{1}} dV'$$
 (B.32)

where

$$\ddot{G}(\vec{\tau}|\vec{\tau}') = \ddot{G}^{p}(\vec{\tau}|\vec{\tau}') + \ddot{G}^{r}(\vec{\tau}|\vec{\tau}')$$
 (B.33)

$$\ddot{G}^{p}(\vec{r}|\vec{r}') = \ddot{I}G^{p}(\vec{r}|\vec{r}') \tag{B.34}$$

$$\ddot{\mathbf{G}}^{r}(\vec{\mathbf{r}}|\vec{\mathbf{r}}') = \hat{\mathbf{x}}G_{t}^{r}\hat{\mathbf{x}} + \hat{\mathbf{y}}\left[\frac{\partial G_{c}^{r}}{\partial x}\hat{\mathbf{x}} + G_{n}^{r}\hat{\mathbf{y}} + \frac{\partial G_{c}^{r}}{\partial z}\hat{\mathbf{z}}\right] + \hat{\mathbf{z}}G_{t}^{r}\hat{\mathbf{z}}$$
(B.35)

$$G^{p}(\vec{r}|\vec{r}') = \int_{-\infty}^{\infty} \frac{e^{j\vec{\lambda}\cdot(\vec{r}-\vec{r}')} e^{-p_{e}|y-y'|}}{2(2\pi)^{2}p_{e}} d^{2}\lambda$$
 (B.36)

$$\begin{cases}
G_t^r(\vec{r}|\vec{r}') \\
G_n^r(\vec{r}|\vec{r}') \\
G_c^r(\vec{r}|\vec{r}')
\end{cases} = \iint_{-\infty} \begin{cases}
R_t(\lambda) \\
R_n(\lambda) \\
C(\lambda)
\end{cases} \frac{e^{j\vec{\lambda}\cdot(\vec{r}-\vec{r}')}e^{-p_c(y+y')}}{2(2\pi)^2p_c}d^2\lambda. \tag{B.37}$$

Obviously, by returning to space domain, the multiplications by $j\xi$ and $j\zeta$ return to spatial derivatives on x and z, as seen in (B.35).

If region 3 (the substrate) happens to be a perfectly-conducting material, then $n_3^2 \rightarrow -j \infty$. Consequently, $p_3 \rightarrow j \infty$; in this limit, the following interfacial coefficients become

$$R_{32}^{t} \rightarrow -1$$
 $R_{32}^{n} \rightarrow +1$ (B.38)
 $T_{23}^{t} \rightarrow 0$ $T_{23}^{n} \rightarrow 0$

and the reflection and coupling coefficients become

$$R_{t}(\lambda) = \frac{p_{1} - p_{2} \coth(p_{2} t)}{Z^{h}(\lambda)}$$

$$R_{n}(\lambda) = \frac{N_{21}^{2} p_{1} - p_{2} \tanh(p_{2} t)}{Z^{e}(\lambda)}$$

$$C(\lambda) = \frac{2(N_{21}^{2} - 1)p_{1}}{Z^{h}(\lambda)Z^{e}(\lambda)}$$
(B.39)

where

$$Z^{e}(\lambda) = N_{21}^{2} p_{1} + p_{2} \tanh(p_{2}t)$$

 $Z^{h}(\lambda) = p_{1} + p_{2} \coth(p_{2}t).$

The coefficients given in (B.39) have been manipulated to provide a more stable form when implementing numerically. Still, whenever $Z^{\epsilon}(\lambda)$ or $Z^{h}(\lambda)$ vanish, pole singularities occur; these are associated with the TM even or TE odd surface-wave background modes respectively.

For a two-layer background environment, there is obviously no separate interface between region 2 and region 3. The reflection/transmission coefficients for the region 2-3 interface are

$$R_{32}^{t} = 0$$
 $R_{32}^{n} = 0$
 $C_{2} = 0$
(B.40)

and the coefficients (B.30) simplify dramatically, becoming

$$R_{1} = \frac{p_{1} - p_{2}}{p_{1} + p_{2}}$$

$$R_{21}^{n} = \frac{N_{21}^{2} p_{1} - p_{2}}{N_{21}^{2} p_{1} + p_{2}}$$

$$C_{1} = \frac{2p_{1}(N_{21}^{2} - 1)}{(p_{1} + p_{2})(N_{21}^{2} p_{1} + p_{2})}$$
(B.41)

If dealing with lossy materials, the term $N_{21}^2 p_1 + p_2$ can vanish; this corresponds to the famous and contentious Zenneck wave [35].

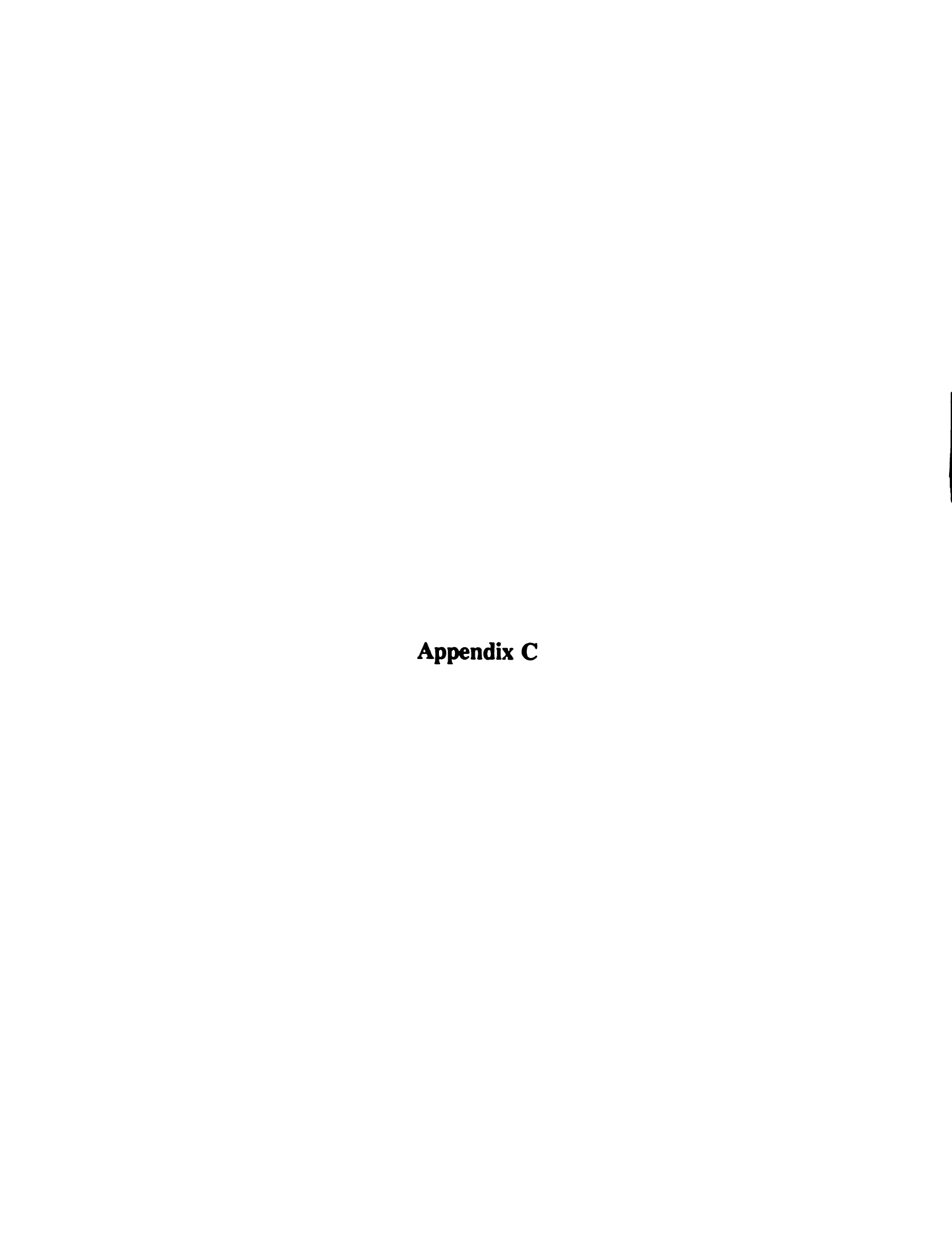
It has been stated without proof that the zeros of the denominator terms D^t from (B.23) and D^n from (B.28) correspond to surface-wave modes of the background structure. Noting that the tri-layer background structure is an asymmetric slab waveguide motivates the following definitions

$$\gamma = p_c = \sqrt{\lambda_p^2 - k_c^2}
\delta = p_s = \sqrt{\lambda_p^2 - k_s^2}
\kappa = -jp_f = \sqrt{k_f^2 - \lambda_p^2}$$
(B.42)

where γ , δ , and κ possess positive real parts. After algebraic manipulation, D^{ϵ} in (B.23) is seen to become

$$\tan \kappa t = \frac{\kappa(\gamma + \delta)}{\kappa^2 - \gamma \delta}$$
 (B.43)

the well-known eigenvalue equation for TE surface-wave modes of the background structure [11]. The solutions lie within the regime $\max\{k_c, k_s\} < \lambda_p < k_f$; these solutions are indeed surface-wave modes of the background, for the fields are oscillatory in the film $(p_f = j\kappa)$ and exponentially decaying in the cover $(p_c = \gamma)$ and substrate $(p_s = \delta)$. An analogous procedure can be carried out for D^n in (B.28); it is apparent that D^n will become the eigenvalue equation for TM surface-wave modes of the asymmetric planar waveguide.



Appendix C

Proof of the Analytic Function Definition Theorem of Chapter 3

Theorem I, the proof of which is presented in this appendix, is central to the development of convergence criteria for the Fourier transform pairs used in the analysis of open-boundary waveguides. While the proof of Theorem I does not warrant inclusion in the main text, it is of interest nevertheless.

C.1 Theorem and Definitions

The following theorem, taken from Titchmarsh [42], defines an analytic function by means of integration.

Theorem I: Let D be the region. Let f(z,w) be continuous in z and w where $z \in D$ and w lies on a smooth contour C, possibly unbounded. Let f(z,w) be an analytic function of z in D for each w on C. Let $\int_C f(z,w) dw$ be uniformly convergent. Then

$$F(z) = \int_C f(z, w) dw$$
 (C.1)

is an analytic function of z in D.

Before stating the proof of Theorem I, some preliminaries are needed. An analytic function is defined as: A complex function f(z) of a complex variable z is analytic at a point z_0 if it is differentiable at every point within a neighborhood of z_0 . An analytic

function satisfies the Cauchy-Riemann conditions; namely, an analytic function f(z) = u + jv of z = x + jy satisfies $u_x = v_y$ and $u_y = -v_x$ at each point where analytic. A function is analytic in a region D if analytic at all points of region D. Also important is Cauchy's Integral Formula:

Let f be analytic in a region D, and C be a closed contour within D. Then at a point z_0 inside contour C

$$f(z_0) = \frac{1}{2\pi j} \int_C \frac{f(z)}{z - z_0} dz$$
 (C.2)

C.2 Proof of Theorem I

Choose Γ as some contour in region D enclosing point α . As f(z,w) is analytic,

$$f(\alpha, w) = \frac{1}{2\pi i} \int_{\mathcal{D}} \frac{f(z, w)}{z - \alpha} dz$$
 (C.3)

by Cauchy's integral formula. Also, $f(\alpha, w)$ is analytic, since $\alpha \in D$.

First consider a finite (bounded) contour C. Thus

$$F(\alpha) = \int_C f(\alpha, w) dw = \int_C \frac{1}{2\pi j} \int_{\Gamma} \frac{f(z, w)}{z - \alpha} dz \ dw \ . \tag{C.4}$$

Interchange of integration order is valid, as the integrand is continuous over both z and w. Consequently,

$$F(\alpha) = \frac{1}{2\pi j} \int_{\Gamma} \left[\int_{C} f(z, w) dw \right] \frac{dz}{z - \alpha} . \tag{C.5}$$

But the bracketed quantity is just F(z), hence

$$F(\alpha) = \frac{1}{2\pi j} \int_{\Gamma} \frac{F(z)}{z - \alpha} dz . \qquad (C.6)$$

Since α is enclosed by Γ , and Γ lies within D, then (C.6) is Cauchy's Integral Formula. Since F(z) satisfies Cauchy's Integral Formula as given in (C.6), F(z) is an analytic function of z in D.

Consider contour C now becoming unbounded on the positive w axis. Choose C_n as that part of C within the circle |z| = n, and let

$$F_{n}(z) = \int_{C_{n}} f(z, w) dw \qquad (C.7)$$

From the prior result in (C.6), $F_n(z)$ is analytic. Furthermore, each $F_n(z)$ is analytic, and $F_n(z) \rightarrow F(z)$ uniformly as $n \rightarrow \infty$. Since F(z) is a uniform limit of analytic functions, F(z) is analytic.

A consequence of Theorem I is that F(z) is continuously differentiable, or that all higher order derivatives exist, at each point where F(z) is analytic. While the proof of this statement, and of Cauchy's Integral Formula (C.2), are important, they are not of immediate interest and can be found elsewhere [57].



Bibliography

- [1] T. G. Livernois and D. P. Nyquist, "Integral equation formulation for scattering by dielectric waveguides," J. Opt. Soc. Am-A, vol. 4, pp. 1289-1295, 1987.
- [2] G. Goubau, "On the excitation of surface waves," *Proc. IRE*, vol. 40, pp. 865-868, 1952.
- [3] D. P. Nyquist, D. R. Johnson, and S. V. Hsu, "Orthogonality and amplitude spectrum of radiation modes along open-boundary waveguides," *J. Opt. Soc. Am.*, vol 71, pp. 49-54, 1981.
- [4] C. Vasallo, "Orthogonality and amplitude spectrum of radiation modes along open-boundary waveguides: comment," J. Opt. Soc. Am, vol 71, p. 1282, 1981.
- [5] R. A. Sammut, "Orthogonality and normalization of radiation modes in dielectric waveguides," J. Opt. Soc. Am, vol. 72, pp. 1335-1337, 1982.
- [6] C. Vasallo, "Orthogonality and normalization of radiation modes in dielectric waveguides: an alternative derivation," *J. Opt. Soc. Am*, vol. 73, pp. 680-683, 1983.
- [7] A. W. Snyder and J. D. Love, Optical Waveguide Theory, New York: Chapman and Hall, 1983.
- [8] V. V. Shevchenko, <u>Continuous Transitions in Open Waveguides</u>, Boulder: Golem Press, 1971.
- [9] A. W. Snyder, "Continuous mode spectrum of a circular dielectric rod," *IEEE Trans. Microwave Theory Tech.*, vol. MTT-19, pp. 720-727, 1971.
- [10] T.E. Rozzi, "Rigorous analysis of the step discontinuity in a planar dielectric waveguide," *IEEE Trans. Microwave Theory Tech.*, vol. MTT-26, pp. 738-746, 1978.
- [11] D. Marcuse, <u>Theory of Dielectric Optical Waveguides</u>, New York, Academic Press, 1974.
- [12] T. E. Rozzi, L. Zappelli, and M. N. Husain, "Radiation from discontinuities in dielectric rib waveguide," *Proc. 1991 European Microwave Conf.*, Sept. 1991.

- [13] J. M. Grimm and D. P. Nyquist, "Spectral analysis considerations relevant to radiation and leaky modes of open-boundary microstrip transmission line," to appear in *IEEE Trans. Microwave Theory Tech.*, January 1993.
- [14] D. P. Nyquist and J. M. Grimm, "Integral-operator-based spectral analysis for radiation modes of open-boundary waveguides," *Proc. 1992 URSI Intl. Symp. EM Theory*, Sydney, Australia, pp. 13-15, Aug. 1992.
- [15] N. Fache, V. Hese, and D. De Zutter, "Generalized space domain Green's dyadic for multilayered media with special application to microwave interconnections," J. Electromagn. Waves and Appl., vol. 3, pp. 651-669, 1989.
- [16] J. S. Bagby, D. P. Nyquist, and B. Drachman, "Integral formulation for analysis of integrated dielectric waveguides," *IEEE Trans. Microwave Theory Tech.*, vol. MTT-33, pp. 906-915, 1985.
- [17] D. P. Nyquist, "Deduction of em phenomena in microstrip circuits from an integral-operator description of the system," *Proc. 1989 URSI Intl. Symp. EM Theory*, Stockholm, Sweden, pp. 533-535, Aug. 1989.
- [18] J. Kiang, S. M. Ali, and J. A. Kong, "Integral equation solution to the guidance and leakage properties of coupled dielectric strip waveguides," *IEEE Trans. Microwave Theory Tech.*, vol. MTT-38, pp. 193-203, 1990.
- [19] S. T. Peng and A. A. Oliner, "Guidance and leakage properties of a class of open dielectric waveguides: Part I mathematical formulation," *IEEE Trans. Microwave Theory Tech.*, vol. MTT-29, pp. 843-854, 1981.
- [20] T. Tamir and A. A. Oliner, "Guided complex waves part I: Fields at an interface," *Proc. IEE*, vol. 110, no. 2, pp 310-324, 1963.
- [21] T. Tamir and A. A. Oliner, "Guided complex waves part II: relation to radiation patterns," *Proc. IEE*, vol. 110, no. 2, pp 325-334, 1963.
- [22] H. Blok, J.M. Van Splunter and H.G. Janssen, "Leaky-wave modes and their role in the numerical evaluation of the field excited by a line source in a non-symmetric, inhomogeneously layered, slab waveguide," *Applied Scientific Research*, vol. 41, pp. 223-236, 1984.
- [23] M. Guglielmi and D. R. Jackson, "Low-frequency location of the leaky-wave poles for a dielectric layer," *IEEE Trans. Microwave Theory Tech.*, vol MTT-38, pp. 1743-1746, 1990.
- [24] T. Tamir and F. Y. Kou, "Varieties of leaky waves and their excitation along multilayered structures," *IEEE Journal of Quantum Electronics*, vol. QE-62, pp. 544-551, 1986.

- [25] A. A. Oliner, "Leakage from various waveguides in millimeter wave circuits," *Radio Science*, vol. 22, no. 6, pp. 866-872, 1987.
- [26] A. A. Oliner, "Leakage from higher modes on microstrip line with application to antennas," *Radio Science*, vol. 22, no. 6, pp. 907-912, 1987.
- [27] K. A. Michalski and D. Zheng, "Rigorous analysis of open microstrip lines of arbitrary cross section in bound and leaky regimes," *IEEE Trans. Microwave Theory Tech.*, vol. MTT-37, pp. 2005-2010, 1989.
- [28] D. Nghiem, J. T. Williams, D. R. Jackson and A. A. Oliner, "Dominant-mode leakage effects for inhomogeneous stripline." *Proc. 1992 URSI Intl. Symp. EM Theory*, Sydney, Australia, pp. 430-432, Aug. 1992.
- [29] J. S. Bagby and D. P. Nyquist, "Dyadic Green's functions for integrated electronic and optical circuits," *IEEE Trans. Microwave Theory Tech.*, vol. MTT-35, pp. 206-210, 1987.
- [30] D. R. Johnson and D. P. Nyquist, "Integral-operator analysis for dielectric waveguides theory and applications," Digest of National Radio Science (URSI) Meeting, Univ. of Colorado, Boulder, Co., p. 104, Nov. 1978.
- [31] M. S. Viola and D. P. Nyquist, "An observation on the Sommerfeld-integral representation of the electric dyadic Green's function for layered media," *IEEE Trans. Microwave Theory Tech.*, vol. 36, pp. 1289-1292, 1988.
- [32] M. S. Viola and D. P. Nyquist, "An electric-field integral equation for the transverse field components within integrated dielectric waveguides," J. Electromagn. Waves and Appl., vol. 5, no. 11, pp. 1283-1297, 1991.
- [33] A. Sommerfeld, <u>Partial Differential Equations in Physics</u>, New York: Academic Press, 1964. pp. 236-265.
- [34] K. M. Chen, "A simple physical picture of tensor Green's functions in source region," *Proc. IEEE*, vol. 65, pp. 1204-1206, 1977.
- [35] A. Baños, Jr., <u>Dipole Radiation in the Presence of a Conducting Half-Space</u>, Oxford: Pergamon Press, 1966. pp. 20-25.
- [36] M.S. Viola, An Integral-Operator Approach to the Electromagnetics of Integrated Optics, Ph.D. Dissertation, Michigan State Univ., 1988.
- [37] A. D. Yaghjian, "Electric dyadic Green's functions in the source region," *Proc. IEEE*, vol. 68, pp. 248-263, 1980.
- [38] A. Papoulis, The Fourier Integral and its Applications, New York: McGraw-Hill, 1962. Chapter 2.

- [39] W. R. LePage, Complex Variables and the Laplace Transform for Engineers, New York: McGraw-Hill, 1961. pp. 268-300.
- [40] E. C. Titchmarsh, <u>Introduction to the Theory of Fourier Integrals</u>, 3rd. Ed.; New York: Chelsea Publishing, 1986. Chapter 1.
- [41] R. C. Paley and N. Wiener. <u>Fourier Transforms in the Complex Domain</u>, New York: American Mathematical Society, 1934. Chapter 1.
- [42] E. C. Titchmarsh, <u>Theory of Functions</u>, 2nd Ed.; Oxford, England: Oxford University Press, 1939. pp. 99-100.
- [43] R. Mittra and S. W. Lee, <u>Analytical Techniques in the Theory of Guided Waves</u>, New York: MacMillan, 1971. Chapter 3.
- [44] W. C. Chew, <u>Waves and Fields in Inhomogeneous Media</u>, New York: Van Nostrand Reinhold, 1991. Chapter 2.
- [45] W. C. Chew and J. A. Kong, "Resonance of the Axial-Symmetric Modes in Microstrip Disk Resonators," J. Math. Phys., vol 21, pp. 582-591, 1979.
- [46] M. S. Viola, An Integral-Operator Approach to the Electromagnetics of Integrated Optics, Ph.D. Dissertation, Michigan State Univ. Chapter 4.
- [47] R. E. Collin, Field Theory of Guided Waves, New York: McGraw-Hill, 1960. Chapter 11.
- [48] Yuan, Y., and D. P. Nyquist, "Full-wave perturbation theory upon electric field integral equations for coupled microstrip transmission lines," *IEEE Trans. Microwave Theory Tech.*, vol. MTT-38, pp. 1576-1584, 1990.
- [49] V. V. Shevchenko, op. cit., pp. 12-14.
- [50] B. Drachman, personal communications.
- [51] R. E. Collin, op. cit., Chapter 11.
- [52] A. Baños, Jr., op. cit., Chapter 2.
- [53] J. Matthews and R. L. Walker, <u>Mathematical Methods of Physics</u>, New York: W. A. Benjamin, 1965. pp. 75-90.
- [54] E. A. J. Marcatilli, "Dielectric rectangular waveguide and direction coupler for integrated optics", *Bell Syst. Tech. Jrnl*, vol. 48, pp. 2071-2102, 1969.
- [55] A. Sommerfeld, "Über die Ausbreitung der Wellen in der drahtlosen Telegraphie," Annalen der Physik (4th Folge), vol. 28, pp. 665-736, 1909.

- [56] Y. Yuan, Integral-Operator Analysis of Layered Media and Integrated Microstrip Configurations, Ph.D. Dissertation, Michigan State Univ., 1991. Chapter 2.
- [57] E. C. Titchmarsh, <u>Theory of Functions</u>, op. cit., pp. 80-82.